

This electronic thesis or dissertation has been downloaded from the King's Research Portal at <https://kclpure.kcl.ac.uk/portal/>



An Evaluation Of UHPLC-MS Technology Encompassing Elevated Temperatures, Low Viscosity Operation and Recently Developed Stationary Phase Materials

Heaton, James

Awarding institution:
King's College London

The copyright of this thesis rests with the author and no quotation from it or information derived from it may be published without proper acknowledgement.

END USER LICENCE AGREEMENT



Unless another licence is stated on the immediately following page this work is licensed

under a Creative Commons Attribution-NonCommercial-NoDerivatives 4.0 International

licence. <https://creativecommons.org/licenses/by-nc-nd/4.0/>

You are free to copy, distribute and transmit the work

Under the following conditions:

- Attribution: You must attribute the work in the manner specified by the author (but not in any way that suggests that they endorse you or your use of the work).
- Non Commercial: You may not use this work for commercial purposes.
- No Derivative Works - You may not alter, transform, or build upon this work.

Any of these conditions can be waived if you receive permission from the author. Your fair dealings and other rights are in no way affected by the above.

Take down policy

If you believe that this document breaches copyright please contact librarypure@kcl.ac.uk providing details, and we will remove access to the work immediately and investigate your claim.

This electronic theses or dissertation has been downloaded from the King's Research Portal at <https://kclpure.kcl.ac.uk/portal/>

Title:An Evaluation Of UHPLC-MS Technology Encompassing Elevated Temperatures, Low Viscosity Operation and Recently Developed Stationary Phase Materials

Author:James Heaton

The copyright of this thesis rests with the author and no quotation from it or information derived from it may be published without proper acknowledgement.

END USER LICENSE AGREEMENT



This work is licensed under a Creative Commons Attribution-NonCommercial-NoDerivs 3.0 Unported License. <http://creativecommons.org/licenses/by-nc-nd/3.0/>

You are free to:

- Share: to copy, distribute and transmit the work

Under the following conditions:

- Attribution: You must attribute the work in the manner specified by the author (but not in any way that suggests that they endorse you or your use of the work).
- Non Commercial: You may not use this work for commercial purposes.
- No Derivative Works - You may not alter, transform, or build upon this work.

Any of these conditions can be waived if you receive permission from the author. Your fair dealings and other rights are in no way affected by the above.

Take down policy

If you believe that this document breaches copyright please contact librarypure@kcl.ac.uk providing details, and we will remove access to the work immediately and investigate your claim.

**AN EVALUATION OF UHPLC-MS TECHNOLOGY
ENCOMPASSING ELEVATED TEMPERATURES, LOW
VISCOSITY OPERATION
AND RECENTLY DEVELOPED STATIONARY PHASE
MATERIALS**

A thesis submitted in partial fulfillment of the requirements for the degree of

Doctor of Philosophy

By

James Christopher Heaton

BSc (Hons) MSc

April 2012

Analytical & Environmental Sciences

King's College London, UK

To Mum, Dad and Jonathan.

Thanks for all the love, support and encouragement!

Love, James.

Abstract

There are several approaches to reducing mobile phase viscosity in order to overcome high pressures related to stationary phase permeability. This can be achieved either by elevating column temperature and or by employing organic rich eluents. To begin with, a standard application of UHPLC-MS was developed for the high throughput quantification of quinine and its major metabolite. In attempting to expand the performance capabilities of ultra-pressure systems a high temperature column oven was evaluated. It was found to be mostly unsuitable for incorporating micro-bore columns due to excessive system volume necessary for installation, and due to the effects of frictional heating associated with operation at ultra-high pressures. An attempt to reduce the effect of frictional heating by modifying the column hardware was evaluated, however only slight improvements were observed. This system has benefits to operate at elevated temperatures, however reduced column performance was always observed as shown by the separation of anabolic steroids and neutral test substances. An evaluation of HILIC column efficiency was undertaken by assessing the performance merits of several commercially available packings using the Knox/van Deemter and kinetic plots approaches. This work centred on evaluation using realistic test substances on underivatized silica, highlighting that very high efficiencies could be achieved using these phases, otherwise not achievable with reversed-phase systems due to peak shape improvements. The justification of which was further addressed by comparing the performance merits of ephedrine-substances separated by both reversed-phase and HILIC noting that the latter was far superior. Arguably the biggest disadvantage with HILIC is the reliance on acetonitrile based mobile phases. An in-depth evaluation of acetone as an alternative, aprotic organic modifier for HILIC-ESI-MS was undertaken, showing that this may not be suitable for the analysis of small polar molecules in positive ion electrospray.

Table of Contents

Abstract.....	(3)
Table of Figures.....	(9)
Table of Tables.....	(13)
1. Introduction.....	(16)
1.1.1 Origins of liquid chromatography.....	(16)
1.1.2 Modern drivers for liquid chromatography.....	(16)
1.1.3 Chemical basis for separation.....	(18)
1.2 Stationary Phase Chemistry.....	(19)
1.3 Chromatography Theory.....	(20)
1.3.1 Resolution.....	(20)
1.3.2 Influence of plate number (N) on resolution.....	(20)
1.3.3 Influence of selectivity (α) on resolution.....	(22)
1.3.4 Influence of retention factor (k) on resolution.....	(23)
1.4 Column performance relationships.....	(25)
1.4.1 The van Deemter equation.....	(25)
1.4.2 The Knox equation.....	(32)
1.4.3 Poppe and Kinetic plot performance evaluation.....	(33)
1.4.4 Extra-column band broadening effects.....	(38)
1.5 Relationships in gradient elution liquid chromatography.....	(40)
1.6.1 Influence of temperature as a separation tool.....	(42)
1.6.2 Elevated temperature in liquid chromatography.....	(44)
1.7.1 Development of Ultra High-Performance Liquid Chromatography (UHPLC).....	(47)
1.7.2 Benefits of Ultra-High Performance Liquid Chromatography (UHPLC).....	(51)
1.8 Superficially porous materials.....	(52)
1.9 Hydrophilic Interaction Chromatography (HILIC).....	(55)
2.0 Hyphenation of liquid chromatography to mass spectrometry (LC-MS).....	(59)
2.1 Electrospray Ionisation (ESI).....	(59)
2.2 Mass Analysers.....	(62)

2. Rapid quantification of quinine and its major metabolite (3S)-3-hydroxyquinine in diluted urine by UPLC-MS/MS.....	(65)
2.1 Introduction.....	(66)
2.2 Experimental.....	(68)
2.2.1 Chemicals.....	(68)
2.2.2 Standard preparation.....	(68)
2.2.3 Sample treatment.....	(69)
2.2.4 Chromatographic conditions.....	(69)
2.2.5 Mass spectrometry.....	(70)
2.3 Results and discussion.....	(71)
2.3.1 LC-MS/MS method development.....	(71)
2.3.2 Fragmentation of quinine and (3S)-3-hydroxyquinine.....	(75)
2.3.3 Autosampler carryover and optimised LC-MS/MS separation.....	(80)
2.3.4 Performance of assay.....	(83)
2.4 Conclusion.....	(85)
3. Investigation into the use of a forced-air thermostat for performing elevated temperature UHPLC separations.....	(86)
3.1 Introduction.....	(87)
3.2 Experimental.....	(91)
3.2.1 Chemicals.....	(91)
3.2.2 Instrumentation and methodology.....	(91)
3.3 Results and discussion.....	(94)
3.3.1 Preliminary data comparing column thermostatic devices.....	(94)
3.3.2 Evaluation of wall thickness on column performance.....	(97)
3.3.2.1 Operation of 3 µm packed columns using the Polaratherm forced-air oven with MeOH as the organic modifier.....	(97)
3.3.2.2 Operation of 1.9 µm packed columns using ACN as the organic modifier.....	(101)
3.3.2.3 Effect of increasing flow rate on retention.....	(103)
3.4 Conclusions.....	(107)

4. Investigation into the use of shell, fully porous particles and elevated temperatures in UHPLC for the highly efficient analysis of anabolic steroids.....	(108)
4.1 Introduction.....	(109)
4.2 Experimental.....	(112)
4.2.1 Chemicals and reagents.....	(112)
4.2.2 Equipment.....	(112)
4.2.3 Methodology.....	(113)
4.3 Results and discussion.....	(116)
4.3.1 Flow study (Column Comparison).....	(116)
4.3.2 Kinetic plot representation (Column Comparison).....	(120)
4.3.3 Operation of sub-2 μm BEH particles at elevated temperatures.....	(124)
4.3.3.1 Flow study.....	(124)
4.3.3.2 Kinetic plot performance at elevated temperature.....	(127)
4.3.3.3 Alternative solvent use at elevated temperatures for steroidal test mix.....	(131)
4.4 Conclusion.....	(133)
5. Kinetic performance comparison of sub and supra- 2 μm bare silica phases for the HILIC separation of basic pharmaceutical solutes in short narrow bore columns.....	(134)
5.1 Introduction.....	(135)
5.2 Experimental.....	(139)
5.2.1 Materials and reagents.....	(139)
5.2.2 Instrumentation.....	(139)
5.2.3 Flow rate study methodology.....	(140)
5.3 Results and discussion.....	(142)
5.3.1 Permeability and flow resistance comparison.....	(142)
5.3.2 Chromatographic performance comparison using basic solutes.....	(146)
5.3.2.1 Effect of flow rate on efficiency (van Deemter analysis).....	(146)
5.3.2.2 Knox plot data (ambient temperature).....	(151)
5.3.2.3 Operation at moderate versus ambient temperatures.....	(156)
5.3.2.4 Kinetic plot representation of data.....	(158)
5.4 Conclusion.....	(166)

6. Comparison of reversed-phase and hydrophilic interaction liquid chromatography for the separation of ephedrines.....	(167)
6.1 Introduction.....	(168)
6.2 Experimental.....	(172)
6.2.1 Chemicals and reagents.....	(172)
6.2.2 Solutions.....	(172)
6.2.2.1 Reversed-phase mobile phase.....	(172)
6.2.2.2 HILIC mobile phase.....	(172)
6.2.2.3 Sample preparation.....	(173)
6.2.3 LC conditions.....	(173)
6.2.3.1 Reversed-phase conditions.....	(173)
6.2.3.2 HILIC conditions.....	(174)
6.2.4 Detection.....	(174)
6.2.5 Methodology for the construction of van Deemter plots.....	(175)
6.2.6 Methodology for the construction of kinetic plots.....	(176)
6.3 Results and discussion.....	(177)
6.3.1 Effect of CH ₃ CN composition on retention of phenylpropanolamine, ephedrine and methylephedrine.....	(177)
6.3.2 Dependence on retention of mobile phase pH.....	(178)
6.3.3 Effect of increasing temperature on retention.....	(180)
6.3.4 Performance comparison between reversed-phase and HILIC.....	(183)
6.3.4.1 Peak shape comparison between HILIC and reversed-phase approach.....	(183)
6.3.4.2 van Deemter flow study to compare HILIC and reversed-phase.....	(185)
6.3.4.3 Kinetic plots of HILIC and reversed-phase.....	(188)
6.3.5 Application: Analysis of ephedrines by LC-Q-TOF-MS.....	(191)
6.4 Conclusions.....	(192)
7. Systematic evaluation of Acetone and Acetonitrile for use in HILIC Coupled with ESI Mass Spectrometry of Basic Small Molecules.....	(193)
7.1 Introduction.....	(194)
7.2 Experimental.....	(197)

7.2.1 Chemicals.....	(197)
7.2.2 Preparation of solutions.....	(198)
7.2.3 Sample Preparations.....	(198)
7.2.4 Chromatographic Conditions.....	(198)
7.2.5 Mass spectrometry conditions.....	(199)
7.3 Results and discussion.....	(200)
7.3.1 Optimisation of source parameters.....	(200)
7.3.2 Influence of acetone organic modifier on retention.....	(212)
7.3.3 Column robustness metrics.....	(214)
7.4 Conclusion.....	(214)
8. Conclusion and further work.....	(215)
List of abbreviations.....	(218)
Bibliography.....	(219)
Presentations.....	(220)
References.....	(221)

Table of Figures

Figure 1.1. Schematic of simple HPLC apparatus.....	17
Figure 1.2. Differential partition between analytes X and Y.....	18
Figure 1.3. Silanol derivatisation with chlorosilane agent scheme.....	19
Figure 1.4. Visual representation of the <i>A</i> -term.....	26
Figure 1.5. Visual representation of the <i>B</i> -term.....	27
Figure 1.6. Visual representation of the <i>C</i> -term.....	28
Figure 1.7. Differential analyte adsorption and desorption.....	29
Figure 1.8. Hypothetical van Deemter plot.....	31
Figure 1.9. Example of kinetic plots of t_0/N^2 versus <i>N</i> and <i>L</i> versus <i>N</i>	35
Figure 1.10. Comparison between Acquity UPLC and Alliance system volumes.....	39
Figure 1.11. Hypothetical van't Hoff plot of 3 neutral analytes.....	42
Figure 1.12. Hypothetical van Deemter as a function of particle size.....	48
Figure 1.13. Superficially and totally porous particle diffusion behaviour.....	52
Figure 1.14. Hypothetical retention mechanism of phenylephrine on silica.....	56
Figure 1.15. General schematic of off-axis positive ion electrospray ionisation.....	60
Figure 1.16. Taylor cone formation and emission of positively charged droplets.....	61
Figure 1.17. Schematic of the Waters Quattro Premier XE triple quadrupole mass spectrometer.....	63
Figure 2.1. Schematic of quinine metabolism in man.....	66
Figure 2.2. Improvement in shape and increase in retention time as a function of pH for quinine.....	71
Figure 2.3. Resolution and retention of (3R)-3-hydroxyquinine and (3S)-3-hydroxyquinine diastereoisomers as a function of pH.....	72
Figure 2.4. Purity assay of (3S)-3-hydroxyquinine as donated by the group of Prof. James M Cook.....	73
Figure 2.5. ESI positive product ion spectra of quinine and (3S)-3-hydroxyquinine.....	75
Figure 2.6. Common fragment ions of quinine and (3S)-3-hydroxyquinine.....	76
Figure 2.7. Mechanism for the formation of 253 <i>m/z</i> product ion.....	76

Figure 2.8. Postulated mechanism for the formation of the 279 <i>m/z</i> ion and the 295 <i>m/z</i> ion for quinine and (3S)-3-hydroxyquinine.....	77
Figure 2.9. Accurate mass MS/MS spectra of quinine [M+H] ⁺ by infusion.....	78
Figure 2.10. Accurate mass MS/MS spectra of (3S)-3-hydroxyquinine [M+H] ⁺ by infusion.....	79
Figure 2.11. Final UPLC-MS/MS separation of quinine and (3S)-3-hydroxyquinine.....	82
Figure 3.1. Effect of thermal environment on the migrational linear velocities within a column..	89
Figure 3.2. Polaratherm 9000 forced-air column thermostat (near-isothermal conditions).....	92
Figure 3.3. Acquity Column Oven (ACO) for near-adiabatic column heating.....	93
Figure 3.4. Standard 0.084" Thermo column hardware and modified 0.026" hardware.....	93
Figure 3.3. Comparison between coiled and un-coiled stainless steel tubing inlet devices.....	94
Figure 3.4. Comparison between Polaratherm and ACO at 60 °C.....	95
Figure 3.5. Corrected van Deemter curves for 40 °C, 50 °C and 60 °C.....	98
Figure 3.6. Corrected van Deemter curves for naphthalene on 150 x 2.1 mm ID, 1.9 μm Hypersil GOLD in different column hardware.....	102
Figure 3.7. Retention factors as a function of linear velocity and thermal environment at 30 °C using 150 x 2.1 mm ID, 1.9 μm Hypersil GOLD.....	104
Figure 3.8. System corrected Pressure drop vs. Flow rate for 0.084" wall thickness column, 150 x 2.1 mm ID, 1.9 μm Hypersil GOLD in ACO and Polaratherm.....	105
Figure 3.9. Retention factors as a function of linear velocity and thermal environment at 30 °C using 150 x 2.1 mm ID, 3 μm Hypersil GOLD.....	109
Figure 4.1. Chemical structures of analytes in steroidal test mix.....	115
Figure 4.2. Performance comparison using reduced Knox parameters and interstitial linear velocities correlation of corrected pressure drop as a function of linear velocity.....	117
Figure 4.3. Kinetic plot performance analysis considering plate time separation impedance and column length.....	121
Figure 4.4. van Deemter and Knox curves for operation of BEH at 60 °C and 130 °C using the forced-air oven.....	125
Figure 4.5. Influence of extra-column volume on column performance at the optimum operating pressure.....	126
Figure 4.6. Kinetic plot comparison at 60 °C and 130 °C.....	128
Figure 4.7. Comparison between 60 °C and 130 °C operation using coupled 10 + 15 cm long BEH C18 1.7 μm x 2.1 mm ID columns.....	130

Figure 4.8. Comparison between using isopropyl alcohol and ethanol organic modifiers for the separation of steroidal test mixture at 130 °C.....	132
Figure 5.1. On column pressure drop versus linear velocity for the tested supports.....	143
Figure 5.2. van Deemter Knox curves constructed for procainamide.....	147
Figure 5.3. Separation of toluene, caffeine, benzylamine, nortriptyline and procainamide. Order of elution identical on each column. Columns operated to yield their respective optimum plate number.....	150
Figure 5.4. Comparison between observed and corrected column performance for procainamide and diphenhydramine at the optimum plate count achieved for each phase.....	155
Figure 5.5. t_0 versus N kinetic plots for benzylamine.....	160
Figure 5.6. t_0/N^2 versus N kinetic plots for benzylamine.....	164
Figure 6.1. HILIC retention behaviour of methylephedrine, phenylpropanolamine and ephedrine at 50 °C.....	178
Figure 6.2. Retention factors of ephedrines as a function of pH at 50 °C.....	179
Figure 6.3. Plot of $\log k$ vs $1/T$ using acetonitrile:200 mM ammonium acetate pH 5.0 (95:5 v/v) for ephedrines.....	180
Figure 6.4. Plot of $\log k$ vs $1/T$ using acetonitrile:100 mM ammonium acetate pH 5.0 (95:5 v/v) for ephedrines.....	182
Figure 6.5. Effect of increasing flow rate on peak asymmetry (measured at 10 % peak height) for ephedrine and phenylpropanolamine using reversed-phase conditions.....	184
Figure 6.6. van Deemter curves for reversed-phase and HILIC phenylpropanolamine, ephedrine and methylephedrine.....	186
Figure 6.7. Kinetic plot representation of pressure drop limited plate number based on van Deemter data.....	189
Figure 6.8. Chromatograms illustrating the separation of phenylpropanolamine, cathine, ephedrine, pseudoephedrine and methylephedrine under the reversed-phase and HILIC conditions.....	191
Figure 7.1. Signal-to-noise surface plots of cone vs. capillary voltage for diphenhydramine and cytosine.....	200
Figure 7.2. Combined overlay of acetone background, cytosine spectra as result of peak integration in Empower 2 CDS undergoing baseline correction and cytosine spectra combined at the baseline of the peak without baseline noise subtraction.....	204

Figure 7.3. Diacetone ion at 116 m/z monitored using various cone gas flow rates with a mobile phase at pH 9.0.....	205
Figure 7.4. Mean signal intensity data based on $n=10$ injections for pH 3 data and pH 9 data.....	208
Figure 7.5. Comparison between $(CH_3)_2CO$ and CH_3CN at pH 9.0 using SIM for test solutes ($n = 10$).....	209
Figure 7.6. Scatter plot encompassing mean signal-to-noise values for overall sample set.....	211
Figure 7.7. Chromatogram of cytosine, adenine, caffeine, procainamide, nicotine, nortriptyline and diphenhydramine using $(CH_3)_2CO$, pH 3.0 and CH_3CN , pH 3.0. Composition of solvent-buffer (90:10, v/v).....	213

Table of Tables

Table 1.1. FDA Chromatographic method validation requirements.....	21
Table 1.2. Possibilities and limitations of the use of elevated temperatures for LC.....	45
Table 1.3. Peak capacity as a function of particle size and column length.....	53
Table 2.1. Exact mass error table showing elemental compositions for quinine and fragmentation products.....	78
Table 2.2. Exact mass error table showing elemental compositions for (3S)-3-hydroxyquinine and fragmentation products.....	79
Table 2.3. Linearity of quinine and 3-hydroxyquinine from 0-20 ng/mL performed over 3 days.....	83
Table 2.4. Accuracy and precision for quinine (n=3 day, six replicate injections per day).....	84
Table 2.5. Accuracy and precision for 3-hydroxyquinine (n=3 day, six replicate injections per day).....	84
Table 2.6. Retention time robustness metrics based on QC injections.....	85
Table 2.7. Summary of 10 volunteers post-administration diluted urinary concentrations.....	85
Table 3.1. van Deemter curve analysis based on Figure 3.5.....	99
Table 3.2. Deemter curve analysis based on Figure 3.6.....	103
Table 4.1. Testosterone physiochemical data.....	115
Table 4.2. Knox parameters, van Deemter minima and retentions factors for each of the tested columns.....	118
Table 4.3. Hydrodynamic functions of kinetic performance for each column.....	120
Table 5.1. Physiochemical properties of test analytes.....	141
Table 5.2. Physical and kinetic characteristics of tested chromatographic supports.....	144
Table 5.3. Retention data and van Deemter curve fit coefficients.....	148
Table 5.4. Knox curve fit coefficients.....	152
Table 5.5. Knox C-terms determined at ambient and moderate temperatures.....	156
Table 5.6. Comparison of achievable plate counts at set analysis times and corresponding column length required at different maximum pressures.....	162
Table 6.1. Properties of the compounds considered in the present study.....	169
Table 6.2. Van Deemter coefficients determined for HILIC and reversed-phase conditions....	187

Table 6.3. Kinetic plot parameters determined for HILIC and reversed-phase systems.....	190
Table 7.1. Physiochemical properties of hydrophilic test probes from www.chemspider.com197
Table 7.2. Solvent physiochemical properties.....	197
Table 7.3. Optimal source voltages determined for each compound based on surface response plots determined by extracted ion data.....	202
Table 7.4. Comparison between acetonitrile and acetone at pH 3.0 determined at optimum source voltages (n = 10).....	207
Table 7.5. Comparison between acetonitrile and acetone at pH 9.0 determined at optimum source voltages (n = 10).....	207

Acknowledgements

I'm finding this the hardest part to write. Well, maybe. There are so many people to be grateful towards. I'd firstly like to thank my supervisor Dr. Norman W. Smith for giving me this wonderful opportunity as well as the necessary moral support, which has been unwavering throughout. It's been an absolute pleasure and massive life experience which I'll always remember fondly. Not many people are fortunate enough to carry out research in separation science in the UK and I'm extremely grateful to have found a project which appealed directly. This would not have been possible without Prof. Robert S. Plumb and Waters Corp., who have provided excellent financial and equipment support throughout. It's been tough going at times and my second supervisor Dr. Cristina Legido-Quigley has offered very complementary supervision to Norman's. Her encouragement and guidance has been absolutely necessary. I'd also like to thank Prof. Cowan and the Drug Control Centre here at KCL for collaborations and general scientific discussion. More importantly they have provided me with casual lab work during the writing-up period, which has kept me in beer and rent money. I'd like to say thank you to Drs. Kourosh Ahmadi and Nilufer Rahmioglu at St. Thomas' Hospital for the collaboration, guidance and friendship.

I'd also like to thank my friend and collaborator Michael D. Jones at Waters Corp., who has been another great inspiration for bouncing ideas around with and providing support to the projects at KCL. The folks in the office past and present, their friendship and help have been fantastic throughout - you know who you are. Particularly, Nicola Gray, Fred Warren and Luke Whiley with whom I've collaborated and/or moaned at/with during the tough times. I'd also like to thank Drs. Harry Ritchie and Tony Edge at ThermoFisher for providing columns for the wall thickness study. Likewise, I'd also like to thank everyone that has generously provided me with columns to examine. I'd like to mention Meghan Roche of the Christopher Kane design studio for drawing of figures used in this thesis.

A special mention to Gregg, Dave K, Dave S, Col, Reuben, Adam and Christian, my scouse pals and band friends in London.

Last, but not least. I'd like to thank my girlfriend Leanne who has been the rock on which I've stood during my PhD studies. Her constant support and encouragement has been essential to my wellbeing and successes. Love you lots.

Chapter 1. Introduction

1.1.1 Origins of liquid chromatography

The inception of liquid chromatography based chemical separations is attributed to Russian scientist Mikhail Tsvett in the early 1900s and was devised to separate chlorophyll plant pigments [1]. Using a glass column packed with calcium carbonate, inspired by the fractionation methodologies used in petrochemical processes, this adsorption based method yielded the separation of yellow, orange and green pigments. This work was largely overlooked for several decades until Martin and Synge became interested in developing liquid based chromatography further. Their contribution introduced the idea of partition chromatography and pioneered the use of columns packed with water saturated silica gel, over which a non-polar liquid would flow [2]. Separations between a pair of analytes would then take place due to differential partitioning governed by their respective degrees of interaction with the stationary phase. They jointly received the Nobel Prize for Chemistry in 1952 for their seminal work in applying partition chromatography to the separation of amino acids. Even in these primitive days of liquid chromatography, Martin and Synge postulated that more efficient analyses would be achieved by using smaller particles and higher pressures.

1.1.2 Modern drivers for liquid chromatography

The requirements for isolation, identification and quantification of chemical species within a given sample matrix have been the main driving forces for developments in the separation science arena. Clearly, the values of the early pioneers have been maintained, and applied to much broader analytical challenges. High Performance Liquid Chromatography (HPLC) is one of the most widely used techniques employed in analytical laboratories worldwide. Such are the economics of the pharmaceutical and fine chemical industries, these have been central to developing the technique further in order to achieve faster analyses whilst maintaining a high degree of separating power. Figure 1.1 depicts the main components of a typical liquid chromatograph. The mechanical process in HPLC generally involves a pumped liquid (mobile

phase) and a separating column containing packing materials (stationary phase). The packing materials found in modern HPLC columns are spherical in nature and mostly made of silica. This housing is typically 2.1 to 4.6 mm internal diameter and range between 5 and 30 cm in length for most conventional applications. Earlier columns were packed with irregular shaped silica particles. The sample is introduced into the liquid flow preceding the column and is detected following separation by a variety of techniques, the most common being the ultraviolet detector (U.V.).

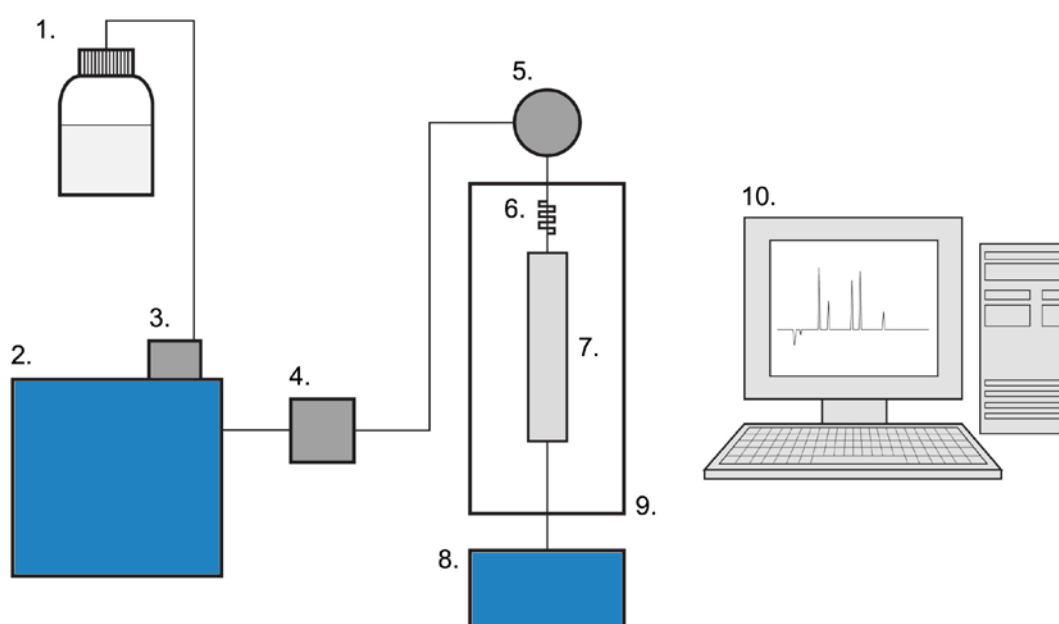


Figure 1.1. Schematic of simple HPLC apparatus: (1) mobile phase reservoir, (2) pump, (3) vacuum degasser, (4) in-line solvent filter, (5) sample injector, (6) eluent thermal stabiliser, (7) chromatographic column, (8) detector, (9) column heater, (10) computer for data handling and instrument control. Diagram redrawn based on reference [3].

1.1.3 Chemical basis for separation

There are two main separation mechanisms employed in liquid chromatography, normal and reversed-phase. In normal-phase chromatography the eluent travelling through the chromatographic column is said to be non-polar and the packing material polar, whereby adsorption between solutes and the stationary phase occurs. The most commonly used mechanism, reversed-phase, occurs due to the non-polar nature of the packing material and the polar characteristics of the mobile phase. The reversed-phase (RP) mechanism involves partitioning of the analyte into the non-polar surface of the stationary phase resulting in retention. Other chromatographic separation techniques include hydrophobic interaction, ion-exchange, size exclusion, hydrophilic interaction (HILIC), liquid-liquid partition and ion-pair [4]. Although outside the remit of this thesis, it is worth mentioning bioaffinity chromatography which employs immobilised antibody ligands that bind selectively to a protein, peptide or a small molecule of interest. The difference in retention observed between analytes and the degree to which this happens is referred to as selectivity, occurring due to differences in equilibrium distribution of analyte molecules. Figure 1.2 depicts the basis of retention between analytes X and Y on a single stationary phase particle and the interaction between the two phases, resulting in a differential migration. When a separation requires improvement, i.e. selectivity is not satisfactory, factors such as stationary phase functionality, mobile phase composition, pH and temperature can be varied [3].

Figure 1.2. Differential partition between analytes X and Y.

1.2 Stationary Phase Chemistry

The basis of most stationary phase packings in liquid chromatography is porous spherical silica. Silanol groups on the surface of the silica particles can be derivatised with a bonded functionality, typically a chlorosilane, which is reacted with the silanol groups resulting in a silicon ester as shown in Figure 1.3 [4].

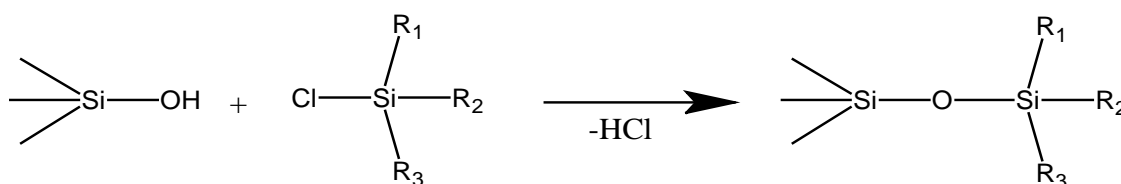


Figure 1.3. Silanol derivatisation with chlorosilane agent scheme.

R1 and R3 attached to the chlorosilane molecule are typically methyl groups, which exhibit the least steric hindrance on the silica surface, and are referred to as monofunctional bondings. These two groups can also be chlorinated allowing other derivatisation reactions with the silica surface yielding bifunctional and trifunctional bondings [4]. The main characteristic of bonded silanes is the functionality of R2 as this group can be varied depending on the type of selectivity and retention properties desired, the most common being hydrocarbon chains of increasing length such as C₈ and C₁₈.

1.3 Chromatography Theory

1.3.1 Resolution

The objective of developing any separation is to achieve the best possible resolution between analytes within a sample matrix in the shortest time; this can be achieved and optimised by understanding the parameters which influence the chromatographic process. The factors which influence a separation are the theoretical plate number, selectivity and retention factor and these are best described by the Purnell equation [5].

$$R_s = \frac{N^{1/2}}{4} \left(\frac{\alpha - 1}{\alpha} \right) \left(\frac{k_2}{1 + k_2} \right) \quad (1.01)$$

Where R_s is resolution, α is selectivity, N is the isocratic plate count and k_2 is the retention factor of the most retained of the two solutes. This fundamental equation depicts the parameters by which optimisation of resolution can be achieved by altering the selectivity, the retention factor, or the efficiency term. General requirements for method validation of each of these parameters are outlined in Table 1.1. Due to the efficiency term being a square root function, large values would be required to influence resolution and the selectivity parameter is much more powerful. According to guidelines outlined by the FDA on "Validation of Chromatographic Methods" the following criteria in Table 1.1 should be adhered to [6]. The tailing factor is important with regards to peak shape, especially in the analysis of basic amine containing solutes. The liquid chromatography of these solutes often result in poorly symmetrical peak shapes and offer an ongoing challenge to separation scientists, especially as many APIs (Active Pharmaceutical Ingredients) are amino-containing.

Parameter	Limit
Capacity Factor	$k > 2$
Injector Precision	RSD < 1% for $n \geq 5$
Resolution	$R_s > 2$
Tailing Factor	$T \leq 2$
Theoretical Plate	$N > 2000$

Table 1.1. FDA Chromatographic method validation requirements

Another way of expressing the degree of resolution between two analytes can be calculated simplistically by the following equation:

$$R_s = 1.18 \frac{t_{R_B} - t_{R_A}}{w_{B(0.5)} + w_{A(0.5)}} \quad (1.02)$$

Where t_R represents retention time (minutes) at the peak apex and thus the difference in separation of two analytes, which is subsequently divided by the sum of peak widths measured at half height $w_{0.5}$ (minutes) of the analyte pair.

1.3.2 Influence of plate number (N) on resolution

The number of theoretical plates can be estimated by the following equation:

$$N = 5.54 \left(\frac{t_R}{W_{(0.5)}} \right)^2 \quad (1.03)$$

Where t_R is the retention time of an analyte and $w_{(0.5)}$ is the peak width measured at half height. This parameter is dependent on physical elements such as particle size, length of the chromatographic column, and is a measurement of peak dispersion and hence the quality of the separation.

1.3.3 Influence of selectivity (α) on resolution

Selectivity is the contribution to resolution influenced by chemical and thermodynamic factors, shown below as the ratio between the partition coefficients of two analytes.

$$\alpha = \frac{k_B}{k_A} \quad (1.04)$$

Where, k_B and k_A are the retention factors of the stronger and less retained analytes respectively. The alpha value can be used to compare the variability of a separation between column chemistries [4]. Consideration of the packing chemistry used in reversed-phase separations is an important variable in the methods development process. Selectivity differences between two different packings may result in the resolution of critical pairs in a separation and is an important feature for method development. For example, phenyl bonded packings are said to induce increased retention of protonated amines and undergo π - π interactions with analytes having aromatic functionality; polar embedded phases offer retention with hydrogen-bond donors such as sulphonamides, unionised carboxylic acids and phenols [7].

There are several other features of polar embedded phases. Firstly, to shield silanol groups from amine groups contained within an analyte, secondly to offer hydrophilic characteristics to prevent stationary phase collapse in highly aqueous mobile phases and thirdly to offer retention for polar solutes by means of hydrogen bonding. Other bondings exist offering various selectivities for particular applications, particularly if geometric isomers or poor retention is encountered for example. Pentafluorophenyl-hexyl (hexyl denotes the spacer used between the ligand and the bonded silanol group) groups offer similar functionality to the phenyl phases except with added electronegativity for positively charged species and added shape selectivity. As mentioned previously with regards to the resolution equation, selectivity is the most powerful tool for optimising resolution and an understanding of the analytes physiochemical properties is essential for developing liquid chromatography methodologies. Nevertheless, the most common silica-based bonded phase is the C₁₈ (ODS) type for reversed-phase separations.

1.3.4 Influence of retention factor (*k*) on resolution

In order to determine the selectivity between a pair of analytes, the retention factor (*k*) needs to be determined. This parameter measures the degree of partition of an analyte between the stationary phase and the mobile phase with respect to an un-retained component, as depicted in equation 1.05.

$$k = \frac{t_R - t_0}{t_0} \quad (1.05)$$

The t_R value represents analyte retention time and t_0 indicates the column dead time in minutes, further defined by the following relationship of column dead volume (V_m) and the volumetric flow rate (F), equation 1.06. The column dead time is usually determined using a probe analyte with is not retained and permeates all the pores in the structure of the packing material. Typically for reversed-phase separations this is carried out with either uracil or thiourea due to their high hydrophilicity.

$$t_o = \frac{V_m}{F} \quad (1.06)$$

The degree of separation can be varied by influencing the degree of an analyte's interaction and therefore partitioning between the stationary and mobile phases. Depending on the presence of chemical functionalities on the analyte molecule, different degrees of interaction will be observed. Van der Waals (dispersive) forces occur between the hydrophobic regions of an analyte and the non-polar, hydrophobic stationary phase in reversed-phase systems. Hence the composition of organic modifier in the mobile phase is pertinent to the degree of partitioning. Mobile phases which are too rich in organic modifier will force the degree of partitioning into the bulk mobile phase and low retention will be observed. Controlling the degree of analyte ionisation is critical for reproducing retention times when ionisable functional groups are present; therefore varying the mobile phase pH is also a useful tool for manipulating resolution. Linear-solvent-strength theory [8] depicts a linear relationship between the logarithm of retention factor and the volume fraction of organic modifier in a binary isocratic mobile phase system. Linear-solvent-strength theory is expressed as [8]:

$$\ln(k) = \ln(k_w) - S_r \phi_B \quad (1.07)$$

Where k_w is the solute retention factor in pure water, ϕ_B the volume fraction of organic modifier and the S_r value corresponds to the eluotropic strength of the organic modifier used. Developed by Snyder and Dolan to expedite the process of optimising separations, this model forms the basis of Drylab and similar method development packages used extensively in the pharmaceutical and related industries.

1.4 Column performance relationships

1.4.1 The van Deemter equation

The refinement of liquid chromatography has largely been driven by the necessity to maximise theoretical plate count. Careful examination of the theoretical aspect of increasing column performance underpins many of the modern technical developments in liquid chromatography. The number of theoretical plates (N) obtained with a column is equivalent to the defined length in metres (L) divided by the 'Height Equivalent to a Theoretical Plate' or HETP, expressed by the following relationship:

$$N \equiv \frac{L}{H} \quad (1.08)$$

The van Deemter equation [9] shown below, expresses the HETP term as comprised by three distinct hydrodynamic functions. The A -, B - and C -terms will be discussed separately for their importance in achieving the optimum performance of any chromatographic column. Each component contributes to the degree of band broadening an analyte experiences as it passes through the chromatographic bed.

$$H = A + \frac{B}{u} + Cu \quad (1.09)$$

The A -term relates to the column packing density and particle size (d_p) which fundamentally results in varying degrees of Eddy diffusion an analyte band will experience during a separation. Eddy diffusion relates to the differential flow paths that an analyte can take through the structure of the packed bed. In the context of the van Deemter equation this term is deemed independent of the applied flow rate, as illustrated in equation 1.10 [4]. It should be noted however that this term may not be necessarily independent of flow [10].

$$A = \lambda_i d_p \quad (1.10)$$

λ_i is a packing factor and is generally expected to be between 1.5 and 2 for a well-packed bed, a lower value indicating higher structural uniformity throughout the column packing [4]. It is a measure of the flow inequality in a packed column and can be minimized by using small particle packings with a narrow particle size distribution. It is a measure of how well the column is packed as illustrated in Figure 1.4.

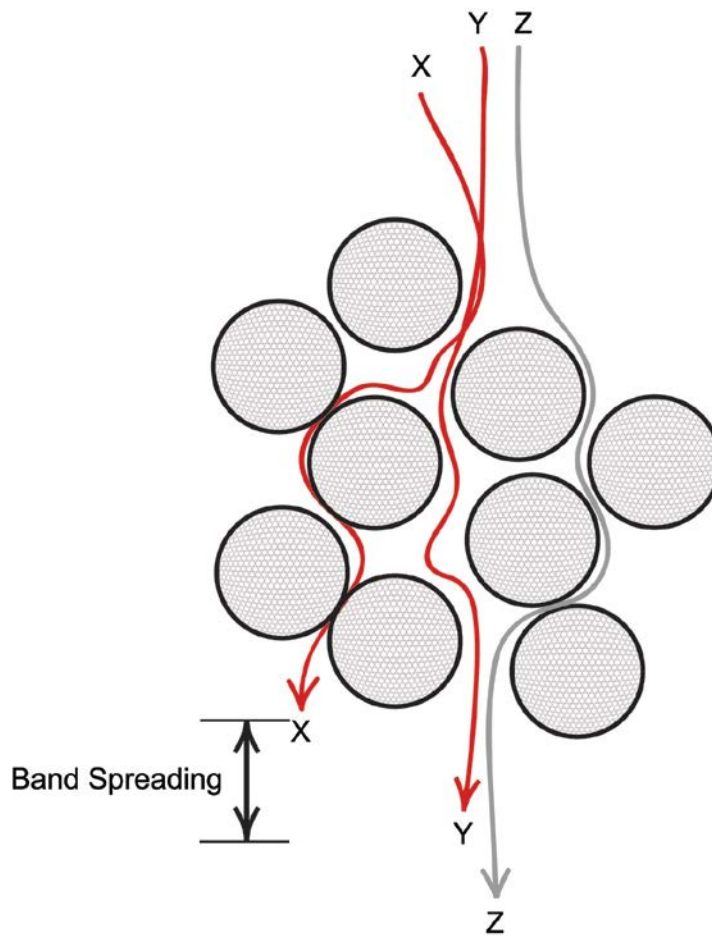


Figure 1.4. Visual representation of the A-term. Adapted from [11].

The B -term represents the contribution of longitudinal diffusion to the value of H which is dependent on the mobile phase linear velocity (μ) and the analyte diffusion coefficient (D_M) as shown by equation 1.11 [4].

$$B = 2\gamma \frac{D_M}{\mu} \quad (1.11)$$

The value for γ is a coefficient corresponding to the free movement of a molecule and any contributing obstructions in the migration path, and values of between 0.5 and 1 are usually representative for this obstruction factor, and allows for the diffusion by the impermeable skeleton of the packing material. This parameter is only of concern when working at high-temperatures, due its effect on the diffusion coefficient, and also at low flow rates when peak broadening may occur against or with the direction of the mobile phase.

Figure 1.5 illustrates that at higher linear velocities sharper peaks are observed due to the lower axial band diffusion in comparison to when slower flow is applied, giving rise to broader peaks.

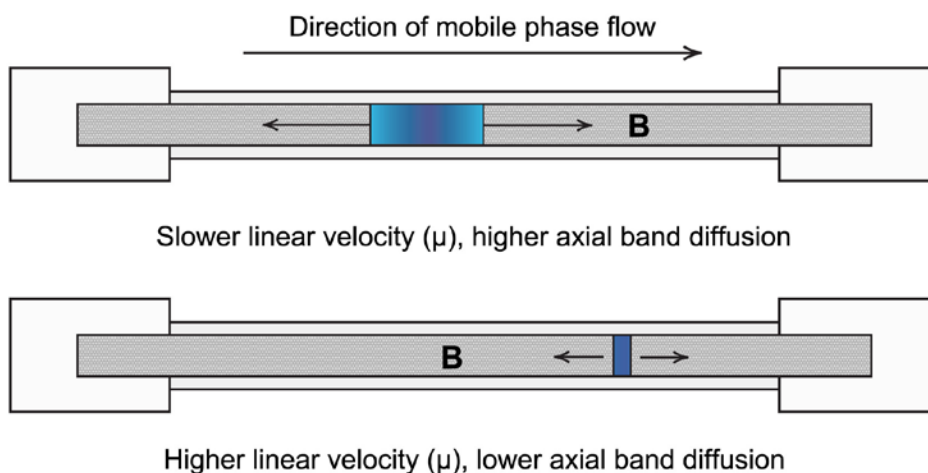


Figure 1.5. Visual representation of the B -term. Adapted from [11].

The C -term refers to the contribution to H by resistance to mass transfer of an analyte between the stationary and mobile phases. It is expressed by the following relationship [4]:

$$C = c \frac{d_p^2}{D_M} \mu \quad (1.12)$$

Where c is generally expected to range from 1/10 to 1/5 and μ is the mobile phase linear velocity.

This term is made up of two major contributing factors (H_M & H_S) which describe the process of analyte mass transfer in the mobile and stationary phases respectively. The resistance to mass transfer in the mobile phase can itself be further divided into two components; firstly from contributions due to differential migration of an analytes diffusion path within the flowing mobile phase, and secondly the disparity of analyte residence within the stagnant pores of the stationary phase structure, as shown collectively in Figure 1.6.

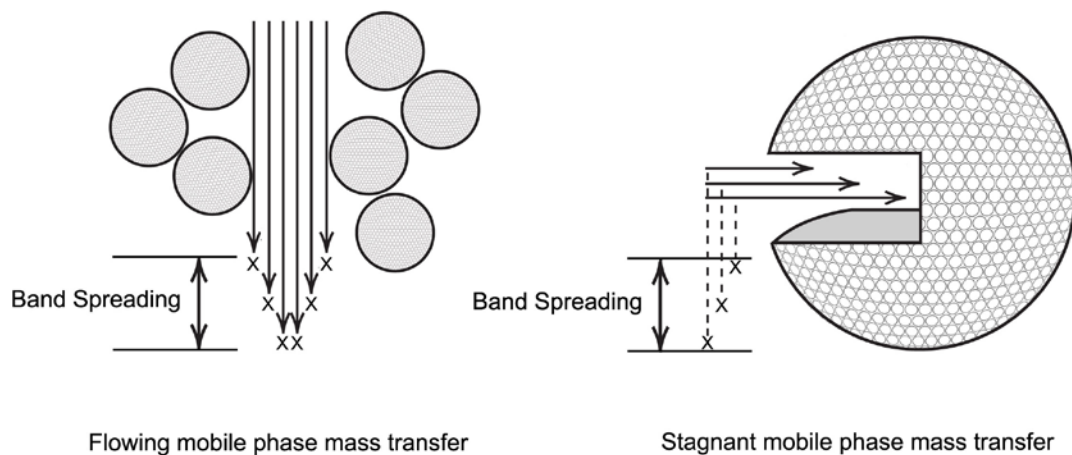


Figure 1.6. Visual representation of the C -term. Adapted from [11].

Flowing mobile phase mass transfer (H_M) can be expressed as per the equation developed by Golay [4, 12] and is best related to a packed bed in terms of a system of capillaries, expressed by the following:

$$H_M = \frac{1}{96} \frac{d_c^2}{D_M} \frac{11k + 6 \cdot k + 1}{(k + 1)^2} \mu \quad (1.13)$$

Where, d_c is the width of the channel the mobile phase is flowing through, and D_M is the diffusion coefficient. It can be seen that H_M is inversely proportional to the diffusion coefficient, D_M . Resistance to mass transfer in the stationary phase (H_S) can be determined as follows [4]:

$$H_S = \frac{2}{3} \frac{d_s^2}{D_S} \frac{k}{(k + 1)^2} \mu \quad (1.14)$$

Where d_s is the thickness of the stationary phase coating. Both these contributions increase linearly with increasing mobile phase linear velocity. Resistance to mass transfer in the stationary phase is proportional to the square of stationary phase layer thickness whilst H_S is inversely proportional to the diffusion coefficient D_S . Figure 1.7 illustrates the difference in adsorption and desorption of an analyte relative to the degree of interaction with the stationary phase layer, represented by H_S .

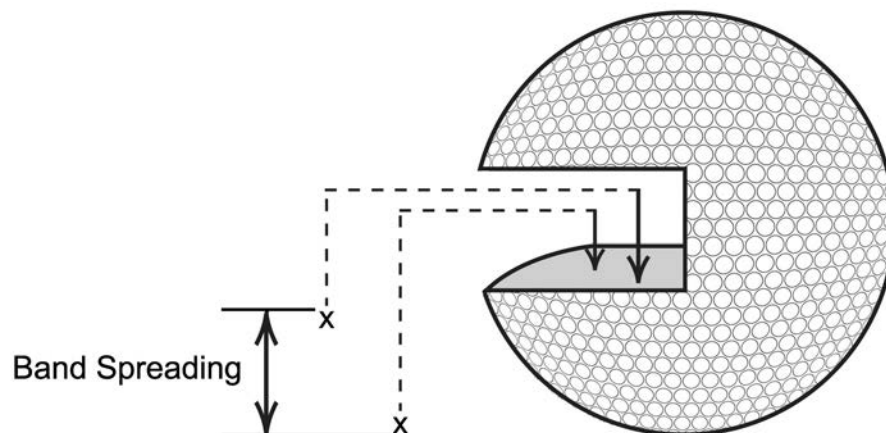


Figure 1.7. Differential analyte adsorption and desorption. Adapted from [11].

Mass transfer occurring in the stationary phase is dependent on the thickness (d) of the coating bonded onto the silica surface and the analyte diffusion coefficient (D_M), summarised in a general form by [4]:

$$C \propto \frac{d^2}{D_M} \quad (1.15)$$

The analyte diffusion coefficient value can be estimated using the empirical Wilke-Chang equation shown below [13]:

$$D_M = 7.4 \times 10^{-8} \frac{\sqrt{\psi_2 M_2 T}}{\eta V_1^{0.6}} \quad (1.16)$$

Where T is equal to temperature in Kelvin, M_2 is the molecular weight of the solvent, V_1 is the molar volume of the solute in millilitres, and η is the viscosity in centipoise and ψ_2 the association factor for the solvent.

The coefficients of the van Deemter equation can be displayed graphically as shown in Figure 1.8 below. Theoretical plate heights are determined over a range of linear velocities usually from very low to the maximum operating pressure of either the column packing or that deliverable by the chromatography pump. The sum of these terms is typically observed as a parabolic curve.

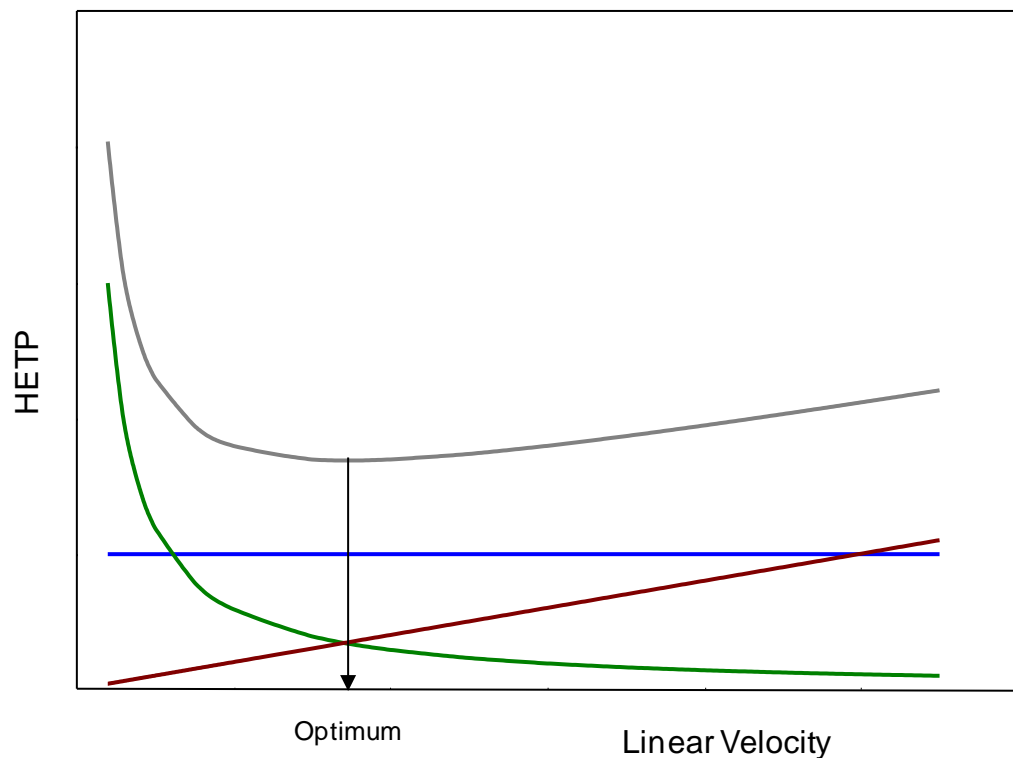


Figure 1.8. Hypothetical van Deemter plot constructed using the following coefficients $A = 5$, $B = 3$ and $C = 1$. Where A (Blue line), B (Green line), C (Red line) and HETP (Grey). The A -term may not necessarily be absolutely independent of flow.

The resulting van Deemter curve exhibits a minimum where the optimum linear velocity is found, this corresponds to the maximum number of theoretical plates achievable by the tested column. As the A -term is deemed independent of flow rate a constant value is observed across all velocities, whereas the B -term becomes negligible at higher linear flows. The C -term dominates at high linear velocities for reasons described by equations 1.12, 1.13 and 1.14.

1.4.2 The Knox equation

It was Giddings [14] that first proposed using dimensionless parameters in order to address band spreading due to the relationship between the convective and diffusive velocities. These relate to the velocities along the column and those relative to the packing particle diameter. Reduced parameters (h , ν) are shown below as a function of general plate height (H), particle diameter (d_p), linear velocity (μ) and diffusion coefficient (D_m).

Reduced linear velocity:
$$\nu = \mu d_p / D_m$$

Reduced plate height:
$$h = H / d_p$$

Knox then developed this idea further for comparing different supports and in determining the quality of packed columns for liquid chromatography. This is particularly relevant if the particle sizes of the compared columns are different and are perhaps of the same substrate silica i.e. BEH 5, 3.5 and 1.7 μm . The Knox equation [15] is shown below:

$$h = B/\nu + A\nu^{1/3} + C\nu \tag{1.17}$$

As in the van Deemter equation, there are three distinct functions of the Knox equation except they describe dispersion in the packed bed depending on the structure or quality of the packing. The A -term is usually around 1 and describes or is a measure of the “goodness of packing” and does not influence the gradient of the Knox curve. The B -term describes the axial molecular diffusion and the usual contribution to h is typically 2-4, whereas the C -term describes slow equilibration in the stationary zone and is approximately 0.1 in most cases. A well packed column should have a reduced plate height of around 2. In general, constructed Knox curves should overlay, however this is obviously not the case if well and poorly packed columns are compared. There are limitations to using the Knox equation however, since there is a dependence on the value used for the mean particle diameter and in the determination of the analyte diffusion coefficient. For the determination of particle size distribution, in most cases,

scanning electron microscopy (SEM) is utilised which can be prone to statistical error. Diffusion coefficients are usually estimated using the Wilke-Chang equation shown previously, by the Aris-Taylor open tubular method or by using capillary time-of-flight (CTOF) as recently proposed by Jorgenson *et al.* [16]. It was shown by Carr *et al.* [17] that empirical Wilke-Chang based estimations are subject to error when determined in organic rich mobile phases, thus employing the open tubular method for their work.

1.4.3 Poppe and Kinetic plot performance evaluation

The concept of separation time based performance was first described by Giddings [18] in a paper comparing the relative efficiency limits of gas and liquid chromatography. It outlines that the inlet pressure in liquid chromatography is the ultimate dictator of separation efficiency, as dictated in principle, by analyte diffusivity and eluent viscosity. The performance gains of gas over liquid chromatography at this time were ascribed to the C-term dominated region. Much faster and highly efficient analyses could be performed using gas chromatography, whereas if very high plate counts were required liquid chromatography would be favoured, but at the expense of analysis time (> 1 day).

Poppe [19] modified this approach further by plotting time equivalent to a theoretical plate (TETP) versus the plate number. Construction of so called "Poppe plots" incorporates the maximum deliverable system pressure and allows comparison in migrating to different particle sizes. It was highlighted here that very high plate counts could be achieved with larger particles, however this would be at the expense of analysis time. In progressing to smaller particle size diameters, these plots highlight the efficiencies achievable as imposed by the limitations of the chromatographic hardware. Tanaka *et al.* [20] used the Poppe plot to compare the benefits of monolithic columns versus particle packed columns. This concept was applied by Popovici *et al.* [21] for the application of size exclusion chromatography (SEC) providing an insight into the effect of inlet pressure using a fixed particle diameter.

Desmet *et al.* [22, 23] moved to simplify the approach of Poppe by redefining the mathematics involved in order to construct time based efficiency plots constrained by the limits imposed by the chromatographic hardware. This approach involved obtaining the permeability of the chromatographic support and incorporating this value into the kinetic calculation directly.

Column permeability is defined as the following [24, 25]:

$$K_{vo} = \frac{\mu \eta L}{\Delta P} \quad (1.18)$$

Where μ is the linear velocity, η is the mobile phase viscosity, L is the column length and ΔP is the pressure drop.

The approach of Desmet then allows for experimentally determined plate heights and linear velocities to be transformed using the following relationships, scaled as per the limiting pressure drop (ΔP_{\max}) of the instrumentation.

$$N = \frac{\Delta P_{\max}}{\eta} \left(\frac{K_{vo}}{\mu H} \right)_{\text{experimental}} \quad (1.19 \text{ a})$$

$$t_o = \frac{\Delta P_{\max}}{\eta} \left(\frac{K_{vo}}{\mu^2} \right)_{\text{experimental}} \quad (1.19 \text{ b})$$

The resulting kinetic plots allow for direct comparison between different support morphologies much like the approach of Poppe, constrained by the maximum pressure drop of the chromatographic instrument and the mechanical stability of the support. Figure 1.9 (a) shows kinetic plots of separation impedance time versus the plate count whereas Figure 1.9 (b) illustrates the length of column required to achieve the desired plate count at the maximum designated pressure drop.

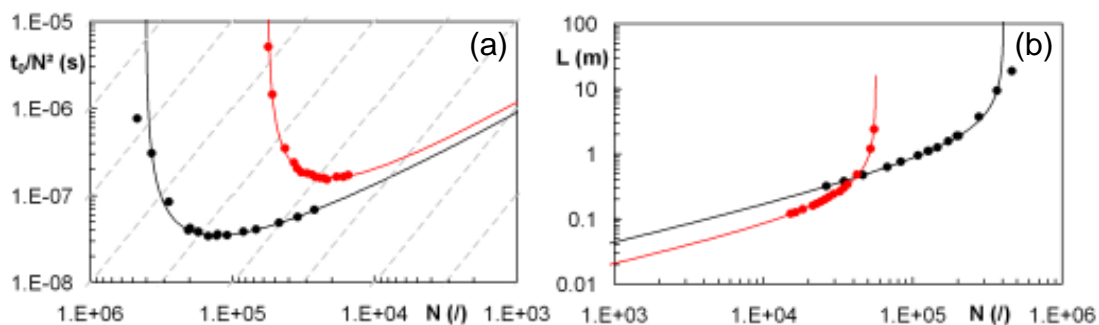


Figure 1.9. Example of kinetic plots of t_0/N^2 versus N and L versus N . Red and black data are for monolith and particle packed columns respectively [26].

Several authors have reported on the uses of kinetic plots and have found particular application in the ongoing evaluation of modern chromatographic materials. Initially, Desmet *et al.* [22, 23, 27] applied the Kinetic Plot Method (KPM) to evaluating monolithic versus several particle packed columns. Their work reiterated that due to the much higher permeability of silica monoliths that the available back pressure would allow the use of much longer columns, therefore achieving higher efficiencies otherwise unobtainable using particle packed columns. The concept of using monoliths has derived much attention, however as shown by McCalley [28] their lack of pH flexibility and poor performance for basic solutes as well as reproducibility problems have resulted in a diminishing interest in their application. Problems with fabricating radially homogeneous monolithic beds have been examined by Guiochon *et al.* [29, 30] indicating this characteristic is highly intrinsic to yielding good peak symmetry and high column efficiency.

Using thermally stable stationary phases, Desmet *et al.* [31] examined the use of high temperatures for exploring the kinetic advantages in operating at thermal extremes. Their work showed that by increasing temperature significant gains in analysis speed were due to reductions in mobile phase viscosity. In combination with higher inlet pressures even greater gains are achieved, however caution was heeded in terms of optimising system volume and detector acquisition speed so as to preserve the smaller peak volumes. Lestremau *et al.* [32] demonstrated that using very long columns (up to 200 cm) packed with 5 μm particles could yield approximately 200,000 plates per meter in around 120 minutes. This study was followed

up by Lestremau *et al.* [33] using the Poppe plot methodology, evaluating the possibilities of using conventional liquid chromatographs (≤ 400 bar, supra-2 μm particles) versus ultra-pressure systems (≤ 1000 bar, sub-2 μm particles). Cabooter *et al.* [31] evaluated the kinetic plot method to determine the optimum particle size for producing analysis times ≤ 30 minutes. This paper demonstrated that the benefits of sub-2 μm particles diminished at long analysis times due to the length of column required in order to achieve higher plate counts, a function of operating in the *B*-term dominated region of the van Deemter curve. They postulated using larger particle packed columns ($\sim 3 \mu\text{m}$) which were able to withstand ultra-high pressures (up to 1000 bar) as such formats would afford higher peak capacities than the corresponding sub-2 μm particles. Such advantages nevertheless require much longer columns, in the region of 44-88 cm, and analysis times from 30 to 120 minutes to be of any practical use. Cabooter *et al.* [34] used the KPM approach to designing a chromatographic system able to deliver 100,000 *N/m* in the shortest possible analysis time, comparing the use of sub-2 μm particles and superficially porous 2.7 μm reversed-phase systems (HALO). Due to the higher permeability of the (HALO) shell-particles ($1.42 \times 10^{-14} \text{ m}^2$) it was possible by coupling columns to achieve the objective plate count at lower pressures than with the system employing the sub-2 μm BEH silica packing ($5.21 \times 10^{-15} \text{ m}^2$). The respective column lengths were 60 and 40 cm respectively, however the approach of using the 1.7 μm particles with ultra-high pressure resulted in significantly shorter analysis times (46 versus 64 minutes with sub-2 μm versus 2.6 μm HALO respectively at 30 °C). Veuthey *et al.* [35] used the kinetic plot method to evaluate several commercially available sub-2 μm materials, noting kinetic differences were due to the relative permeabilities between manufacturers columns. Interestingly, the two Waters phases (C₁₈ and Shield RPC₁₈ chemistries) of the same underlying BEH silica, differed in performance, perhaps due to packing differences, with the latter performing best. In a further paper [36] the Veuthey group extended their kinetic evaluation of sub-2 μm phases to encompass their use with elevated temperatures (≤ 90 °C). This work highlighted that faster separations could be achieved when applying high temperature in order to overcome backpressure limitations due to reduced mobile phase viscosity. A separation of nine doping agents was performed in < 1 minute taking advantage of operation in the *C*-term dominated region whilst preserving column performance. Zhang *et al.* [37] conducted a thorough examination into the benefits of sub-2 μm versus superficially porous 2.7 μm at their relative pressure optima, this time using the Poppe plot approach. Their study concluded that similar performances between the two materials at $t_0 < 10$ s were observed due

to their comparable *C*-term coefficients. Whereas, at $t_0 > 1000$ s the latter considerably outperforms the sub-2 μm materials due to the benefits of the smaller *B*-term contribution to band broadening and also as a function of particle size. Using kinetic plots, Fountain *et al.* [38] showed the importance in minimising extra-column volume is essential for achieving the maximum performance of sub-2 μm particles. It was shown that capturing data for van Deemter studies at the appropriate detector speed settings (> 20 Hz) was essential for defining very small peak shapes at high linear velocities. Their study also highlighted the importance in operating at the optimum pressure, and that combining elevated temperature with pressures up to 1000 bar were beneficial for reducing analysis time using 1.7 μm BEH phases. Using an analyte (Levonorgestrel) from a pharmaceutical preparation, Fekete *et al.* [39] used the kinetic plot method to probe the performances of several sub-2 μm phases against a commercial monolith and a 2.7 μm fused-core material. Their study also indicated similar performances of the superficially porous material versus the sub-2 μm particles, echoing that similar plate counts were achieved except at lower pressures. Using the Poppe plot approach, Weber *et al.* [40] determined the optimal conditions for determining basal serotonin levels with analysis times < 1 minute using capillary UHPLC instrumentation.

Clearly, the kinetic plot visualisation of column performance offers many advantages, especially in designing chromatographic systems that afford the most efficient and or fastest analysis. These concepts have been used in this thesis to compare several column formats as shown in Chapters 4, 5 and 6.

1.4.4 Extra-column band broadening effects

The bandwidth and hence separation efficiency in liquid chromatography is highly dependent on the system volume of the instrument, as well as that obtained from an efficient chromatographic column. Therefore it is important when comparing chromatographic supports that data is corrected for extra-column dispersion contributions to plate height. Variation in the Gaussian elution profile from the contribution due to the column can be expressed as [41]:

$$\sigma_c^2 = \frac{[(\pi \cdot r \cdot L \cdot \varepsilon \cdot (1 + k))]^2}{N} \quad (1.20)$$

Where:

r = column radius

L = column length

ε = total porosity

k = capacity factor

N = plate number

Variance caused by contributing factors arising from instrument configuration is depicted by the following relationship:

$$\sigma_A^2 = \sigma_I^2 + \sigma_D^2 + \sigma_N^2 + \sigma_T^2 \quad (1.21)$$

Where:

σ_I^2 = variance due to geometry and volume of injector

σ_D^2 = variance due to geometry and volume of detector

σ_N^2 = variance due to unions, frits and connecting tubes

σ_T^2 = variance due to detector response

In order to preserve the efficiency of a separation, the contribution from the system variance should not exceed 10% to that accounted for by the packed column. This can result in a loss of efficiency of approximately 10% and a loss in resolution of 5% [41]. Extra-column effects are an important consideration when separating analytes with smaller k values, as well as when working with columns of small volume and high plate numbers [42], as shown by equation 1.20. An example of how extra-column band broadening can affect the observed performance of micro-bore columns is shown in Figure 1.10 [43]. The separation on the optimised Acquity UPLC system yielded 8,543 plates whereas the same column on the conventional HPLC instrument produced only 3,409 plates. In this example, the system volume for the Alliance HPLC was 876 μL whilst the Acquity UPLC was 105 μL .

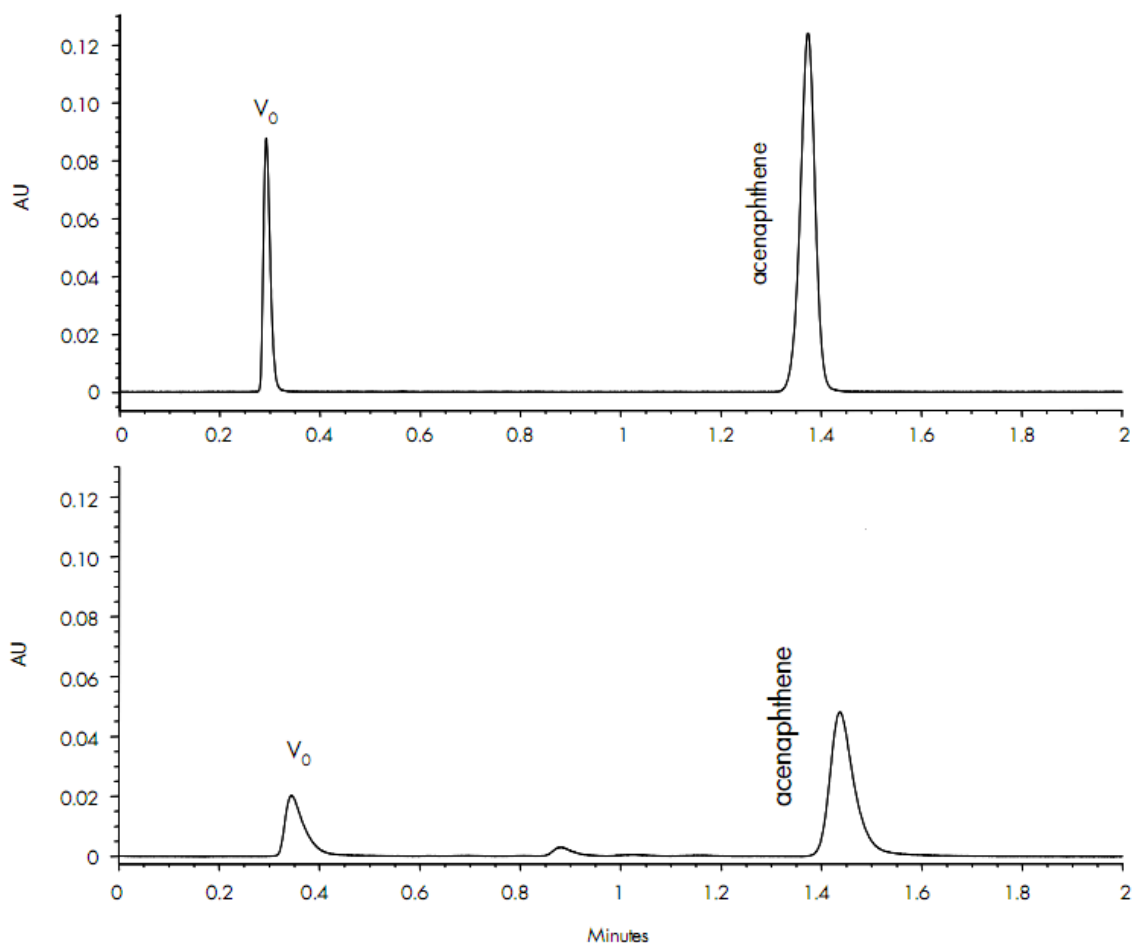


Figure 1.10. Comparison between Acquity UPLC (Top) and Alliance (Bottom) system volumes using a 1.7 μm BEH C18 2.1 x 50 mm column. Flow rate 0.4 mL/min.

1.5 Relationships in gradient elution liquid chromatography

Gradient elution chromatography is commonly employed in the analysis of samples containing analytes with wide ranging physiochemical properties. In order to evaluate the quality of the separation achieved in such analyses, the concept of HETP is not applicable, instead peak capacity is applied. This concept was initially developed by Giddings [44] and reworked by Snyder and co-workers [45] as the following:

$$n_c = \frac{t_{R,n} - t_{R,1}}{W} \quad (1.22)$$

Where $t_{R,n}$ represents the retention time of the last eluting peak in the gradient run and $t_{R,1}$ indicates the first eluted peak after the column dead time, and W is the peak width at baseline.

The early work of Snyder et al. [46, 47] outlined the theoretical and practical framework on the optimisation and use of gradient elution in reversed-phase liquid chromatography. They subsequently extended the understanding of gradient methodology to the separation of macromolecules [48]. Further work formed the foundation of computer assisted method development software Drylab as summarised in a review article [49] for gradient separations. Subsequent work involved combining temperature into gradient optimisation strategies for the analysis of complex samples [45, 50, 51]. An important relationship in gradient chromatography is the gradient-steepness parameter b and is expressed as [52]:

$$b = V_m \Delta\phi S / (t_G F) \quad (1.23)$$

Where V_m is the dead volume of the column, $\Delta\phi$ is the change in organic modifier concentration from the beginning to the end of the gradient time (t_G). The flow rate is depicted as F and the S value is derived from the linear solvent strength relationship in equation 1.07. This relationship is useful for maintaining chromatographic band spacing when migrating from conventional to micro-bore column formats.

According to Neue [53] the peak width (σ) under gradient elution for each peak is shown as follows:

$$\sigma = \frac{t_o}{\sqrt{N}} (k_e + 1) \quad (1.24)$$

Where, peak width (σ) is defined as a function of both the retention factor (k_e) and the column isocratic plate count. The derived value is then dependent on the inflection point upon which the peak width is measured from the determined isocratic plate count. The retention factor at the point of elution (k_e) is determined by the following relationship [54]:

$$k_e = \frac{k_o}{B \cdot \Delta c \cdot \left(\frac{t_o}{t_G} \right) \cdot k_o + 1} \quad (1.25)$$

The slope (G) due to the change in composition of the mobile over the course of a gradient analysis is expressed by the following [53]:

$$G = B \Delta c \frac{t_o}{t_G} \quad (1.26)$$

Therefore the retention factor under gradient elution can be shown as:

$$k_e = \frac{k_o}{G \cdot k_o + 1} \quad (1.27)$$

Where t_G is the gradient run time, Δc is the difference in solvent composition between the beginning and end of the gradient program. The B parameter is the compound specific slope determined from the logarithm of retention factor versus solvent composition as per Equation 1.07.

1.6.1 Influence of temperature as a separation tool

Temperature affects both the retention factor (k) and the selectivity parameter (α) in reversed-phase liquid chromatography, and for these reasons it can be employed as a separation tool when resolution requires optimisation. The van't Hoff equation describes the effect of temperature on retention factor (k):

$$\ln k = -\frac{\Delta H^{\circ}}{RT} + \frac{\Delta S^{\circ}}{R} + \ln \beta \quad (1.28)$$

The above equation depicts decreasing retention factor as a function of increasing temperature due to increased solute mass transfer between the mobile and stationary phases. The standard enthalpy change (ΔH°), standard entropy change (ΔS°), molar gas constant (R), absolute temperature in Kelvin (T) and the phase ratio of the column (β) are all contributory factors in this relationship [8]. By plotting $1/T$ vs. $\ln k$ as a van't Hoff plot the relationship between retention and temperature can be visualised. Figure 1.11 shows hypothetically the retention behaviour of three neutral analytes extrapolated from analyses at different temperatures.

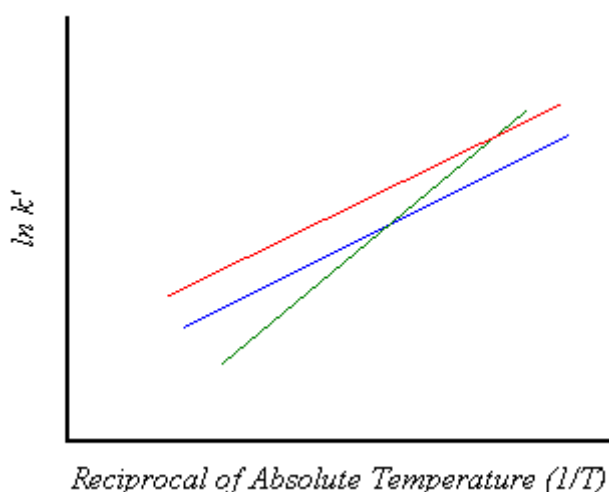


Figure 1.11. Hypothetical van't Hoff plot of 3 neutral analytes.

Temperature and retention can be related further in terms of selectivity, expressed by the following equation which considers the analysis of a solute at two different temperatures [55]:

$$\log k_T = \log k_R - \alpha(1/T_R - 1/T) \quad (1.29)$$

Where, k_R and T_R represent the retention factor and temperature from a reference analytical condition, while k_T and T are values from a different set temperature. As T is varied, and as long as the two compounds have different α values, resolution should change in accordance to Equation 1.01 [55]. Horváth established a rule which implies that a 5 °C change in temperature is equivalent to a 1 % change in mobile phase composition, this observation however being based on separations of small molecules using acetonitrile as the organic modifier [56]. In comparison to changing pH in order to induce a change in selectivity between two analytes, temperature can afford greater practical reproducibility. Dolan [57] suggests that a 1-2 °C change in temperature may be sufficient to improve the separation of a critical pair of analytes, rather than attempting to improve resolution with buffer adjustment when analysing ionisable species. The effect of temperature on the reversed-phase retention behaviour of basic analytes has been investigated by McCalley and co-workers. These investigations observed an increase in plate count and peak shape with increasing temperature both at acidic and neutral pHs. The most significant improvement was observed at pH 7.0 going from 30 to 60 °C in comparison to pH 3.0. These observations are thought to be attributed to a decrease in the pK_a of bases with temperature as well as increased rates of kinetic desorption associated with residual silanol group interactions [58]. Other work carried out examined quaternary amine compounds showing little change in efficiency due to increasing temperature. These studies concluded that at constant pH the pK_a of weaker bases changes considerably with increased temperature, causing a reduction in basic centre protonation, and hence analyte ionisation, giving rise to improved efficiencies, peak shape and increased retention [59].

1.6.2 Elevated temperature in liquid chromatography

The use of elevated temperatures in liquid chromatography is carried out in the region of 40 °C towards the super critical temperature of the eluting mobile phase. Effectively this leads to increased analysis speeds, lower resistance to mass transfer, and the opportunity to explore the use of more exotic and viscous eluents such as 2-propanol [60] and also 100 % subcritical water as the mobile phase [61, 62] for reversed-phase separations.

Increasing the column temperature decreases the mobile phase viscosity allowing for increased mobile phase linear velocities, decreasing analysis time through increased solute mass transfer kinetics. This increased temperature also allows the use of longer columns packed with small diameter particle sizes such as sub-2 µm materials, which would, otherwise require pumping pressure capabilities outside that of conventional equipment.

The following relationships dictate the improvements in using longer columns:

$$N \propto L \qquad R_s \propto \sqrt{N}$$

These concepts have been investigated by Plumb and co-workers [63] to achieve high plate counts using coupled columns containing sub-2 µm packing materials. In their investigations 79 000 plates were obtained by coupling two 15 cm long x 2.1 mm internal diameter columns operated at 90 °C with a flow rate of 0.5 mL/min. This setup was operated at 978 bar, close to the maximum of 1000 bar for their system. Later they added another 15 cm column operating at 0.32 mL/min furnishing 109 000 theoretical plates, however due to pressure limitations the optimum linear velocity was not achieved.

The possibilities and limitations of high temperature and temperature programmed HPLC was outlined by Vanhoenacker and Sandra [64], and are summarised in Table 1.2. Example references from the literature are listed for each of the postulated benefits.

Possibilities	Limitations
Increased speed [65-67]	Analyte stability [67]
Resolution improvements [63]	Column stability [68]
Selectivity changes in method development [55]	Equipment availability
Green chromatography [61, 62]	
Improved detectability [62, 69]	
Improved peak shape [58, 59, 69]	
Temperature programming [61, 70]	

Table 1.2. Possibilities and limitations of the use of elevated temperatures for LC.

An important feature of the equipment required to operate at elevated temperatures is that adequate pre-heating of the mobile phase occurs to prevent thermal mismatch with the temperature of the column. Thompson *et al.* [71] showed that a difference of only 5 °C could seriously affect the column efficiency. They also evaluated the length of tubing necessary to pre-heat the mobile phase, which is invariably dependent on the flow rate used. Teutenberg *et al.* [72] developed a programmable heating system incorporating a block heater to accurately control the temperature of the eluent, eliminating the necessity to use long lengths of pre-heating tubing.

The use of superheated water as an eluent for reversed-phase chromatography allows for elimination or large portions of the organic modifier. As temperature increases the dielectric constant of water decreases and the resulting eluent behaves more like a hydro-organic mobile phase, as summarised by Smith *et al.* [62].

Smith and co-workers [73] have investigated the use of a phenyl bonded hybrid (BEH) stationary phase with superheated water as the chromatographic eluent. In their studies they examined the retention properties and column efficiencies achieved using pure water in the temperature range of 40 to 200 °C using the oven from a gas chromatograph. These phases showed good thermal stability and yielded 45,740 plates/m at 130 °C for *p*-cresol and showed

that a homologous series of alkylphenones could be separated at 200 °C within 10 minutes using only superheated pure water.

Edge *et al.* [74] have investigated the use of thermally programmed gradients for metabolite profiling at fixed or isobaric pressure. This constant pressure operation was reported in an earlier paper [61]. The relationship for operating at constant pressure whilst varying the flow rate proportionally is as follows:

$$\ln P = \ln \left(\frac{\varphi \eta_o \mu L}{d_p^2} \right) + \frac{b}{T} \quad (1.30)$$

Where φ is a packing efficiency constant, μ is the mobile phase linear velocity, d_p is the stationary phase particle diameter and T is the temperature in Kelvin. The value η_o is the varying mobile phase viscosity as a function of temperature (T) and b is a constant, both derived from:

$$\eta T = \eta_o^e b / T \quad (1.31)$$

Edge *et al.* [75] used thermal gradient programming for the separation of a model pharmaceutical test mixture whilst Wilson *et al.* [76] investigated using an elevated temperature isobaric operation for the quantification of brominated metabolites affording detection using ICP-MS. In a later paper, Edge *et al.* [77] compared conventional HPLC, standard and elevated temperature UHPLC for metabolite identification concluding that the latter approach yielded the most favourable results.

1.7.1 Development of Ultra High-Performance Liquid Chromatography (UHPLC)

The advent of ultra-high pressure liquid chromatography systems has undoubtedly been of increasing interest since its commercial introduction by various instrument manufacturers. The development of these systems is driven by the increasing demands of sample through-put and resolving power, both of which can be achieved by using smaller diameter stationary phase particles. Sub 2- μm packing materials are now available with the necessary pumping equipment necessary to operate at their optimum operating linear velocities, achieving the highest possible separation efficiencies. Conventional high pressure liquid chromatographs capable of withstanding column pressure drops of approximately 400 bars are now surpassed by instruments able to achieve up to 1000-1500 bar.

The limitations of liquid chromatographic equipment can be explained by considering the concept of separation impedance (E) established by Bristow and Knox [15]:

$$E = \frac{t_R \Delta P}{N^2 \eta (1 + k)} \quad (1.32)$$

The retention time (t_R), pressure drop across the column (ΔP), number of theoretical plates (N), retention factor (k) and the viscosity (η) of the mobile phase are all considered by this relationship. The separation impedance implies that the higher the value for E the lower the column performance will be and hence the values in the equation have to be manipulated and exchanged correctly in order to achieve an optimum. For example, increasing the temperature reduces viscosity, therefore reducing pressure drop and analysis time [78].

Decreasing the particle size in order to achieve increased efficiencies requires the necessary pumping capacity as shown by the Darcy equation [3]:

$$\Delta P = \phi \eta L u / d_p^2 \quad (1.33)$$

Where, ΔP represents the pressure drop across the column, a result of the applied mobile phase linear velocity (u) being pumped through the packed bed. The column length (L), flow resistance factor (ϕ), solvent viscosity (η) and linear velocity are all directly relate to the pressure drop across the column. The particle diameter (d_p) is inversely proportional to the column pressure drop, and hence is the overall limiting factor due to the pressures required to provide optimum linear velocities, as shown below [3]:

$$\mu_{opt} \approx 3D_m / d_p \quad (1.34)$$

The following van Deemter plot illustrates the effect of decreasing stationary phase particle size resulting in a reduction in theoretical plate height:

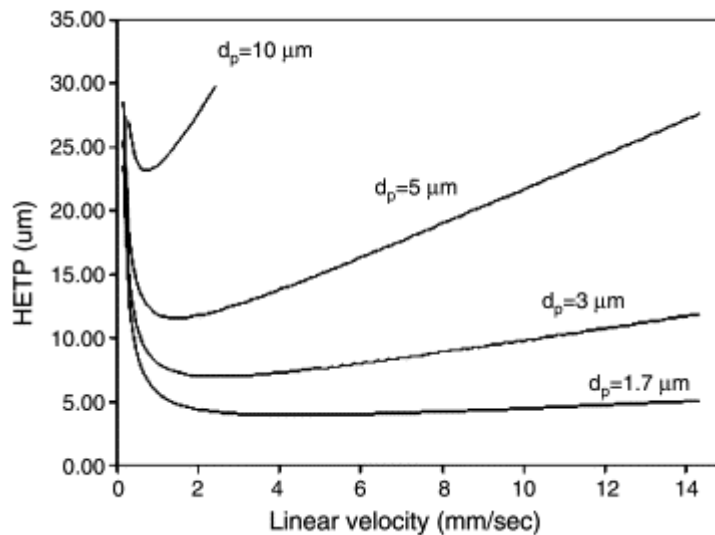


Figure 1.12. Hypothetical van Deemter as a function of particle size from [79].

Jorgenson and co-workers [80] took the theoretical relationships from equations 1.33 and 1.34 to develop a novel prototype ultra high-pressure reversed-phase system. In their initial work they reported the use of 50-70 cm long fused-silica capillary columns packed with 1.5 μm diameter non-porous particles operated at pressures up to 4,100 bar, or 60 000 psi. This system showed that for analytes with $k' \approx 2$ theoretical plate counts in excess of 200 000 could be achieved, translated into H_{min} values as low as 2.1 μm .

Further work by Jorgenson and co-workers [81] investigated the use of shorter 25-30 cm fused-silica capillary columns packed with 1 μm non-porous octadecylsilane-modified silica microspheres. Their work explored the use of both isocratic and gradient elution modes. Theoretical plates generated in the isocratic mode were again in the region of 200 000 at the optimum linear velocity (μ_{opt}) for analytes with values of $k' \approx 1$ with a 6 minute analytical run. In order to evaluate the peak capacity of the gradient program using this system, the peptides of a tryptic digest of ovalbumin were analysed on a 27-cm long capillary column. A peak capacity of 300 was observed for this sample in a 28.4 minute separation space, very significant in comparison to earlier work by Snyder and co-workers [82] using conventional HPLC equipment, where a value of 150 was obtained in 45 minutes.

Development and introduction by the Waters Corporation of the highly spherical, ethyl-bridged hybrid (BEH) silica organic/inorganic stationary phase support material by Wyndham and co-workers [83] has offered many advantages over contemporary silica-based supports. Problems associated with conventional silica supports include poor chemical stability outside of the pH range 2-8 due to hydrolysis of the bonded functionality under very acidic conditions, and dissolution in highly basic environments. Mechanical instability when operated at pressures above the conventional 400 bar has limited the application of contemporary porous silica-based materials to below 6000 psi (400 bar). To overcome this problem, non-porous, mechanically stable particles were employed in the early investigations of Jorgenson *et al.* [80, 81]. The problems associated with silica support breakdown result in losses in chromatographic efficiency and collapse of the packed bed. The main advantages of BEH based supports is that they overcome many of the problems associated with conventional based-silica supports, offering chemical stability over a pH range of 1-12, ultrahigh pressure mechanical strength and are available in many common surface bonding chemistries [83].

Jorgenson and co-workers [84] investigated the use of porous ethyl-bridged hybrid particles as a stationary phase support, making comparisons to the use of non-porous 1.0 μm materials. They used fused-silica capillaries up to 50 cm in length, packed with 1.5 μm BEH particles operated under isocratic conditions at pressures up to 4500 bar. Increased sample loading capacities in comparison to non-porous materials, along with the mechanical strength able to withstand high shear from high linear mobile phase velocities in ultrahigh pressure applications, were observed. Very high plate counts in the order of 200 000 near the optimum linear velocity at 1600 bar were achieved in a 9 minute isocratic separation on a 49.3 cm long capillary column.

Work carried out by Lee and co-workers [85] investigated the use of a pressure-balanced injection system for use with ultra-high pressure capillary chromatography, in order to enhance the practical application of this technique. In their investigations they evaluated the reproducibility, injection time, sample size required and pressure limitations of this injection system as applied to 100 μm x 30-33 cm fused silica capillaries packed with 1.5 μm isohexylsilane-modified (C_6) silica particles. By combining the principles of packing sub-2 μm material into capillary columns and performing analyses at elevated temperatures, Lee and co-workers [66] were able to achieve very fast separations with efficiencies up to 220 000 plates per meter. This was accomplished using 1.0 μm nonporous C_6 modified silica packed into 15 cm long capillaries operated at approximately 2000 bar; where the separation was achieved in under 30 seconds.

The impact in applying very high inlet pressures and volumetric flow rates when operating sub-2 μm particle packed columns can have consequences for column performance. Frictional heating takes place between the percolating mobile phase and the packing material resulting in the formation and subsequent dissipation of energy. This facet of ultra-pressure operation is dealt with in greater detail in Chapters 3 and 4.

1.7.2 Benefits of Ultra-High Performance Liquid Chromatography (UHPLC)

Since the developments of prototype ultra-high pressure liquid chromatographs there have been introductions of several commercial instruments, the first being by the Waters Corporation with their Acquity UPLC (Ultra Pressure Liquid Chromatography) system [86]. This instrument can operate at back pressures of up to 15 000 psi complemented by a very small system volume necessary for fully exploiting the highest possible efficiencies available from sub-2 μm stationary phase particles.

Practical assessment of gradient analysis performed by UPLC in the pharmaceutical arena was initially investigated by Wren [87], measuring peak capacity as a function of column length, gradient time and flow rate. This work concluded that peak capacity increased, up to a plateau, with increasing gradient time at fixed flow rates using columns packed with 1.7 μm materials. It was recommended, in terms of column length that for short analyses the smaller 50 mm column format is optimum. When higher peak capacities are required longer columns should be used in conjunction with long gradient times, at the discretion of available analysis time.

The benefits of UPLC were investigated further by Wren and co-workers [88] for use in pharmaceutical development. This work compared conventional and ultra pressure liquid chromatographic separations with respect to the drug development process. Improvements such as reduced solvent consumption, faster analyses and column equilibration times were shown. Comparisons between HPLC and UPLC using van Deemter plots showed the improvements in HETP when going from 5 μm to 1.7 μm particles, with the gains in efficiency being directly related to Equation 1.35. The optimum value of H can thus be determined as being directly proportional to particle diameter as long as the coefficients A-C are maintained:

$$H_{\min} = d_p \left(A + \sqrt{BC} \right) \quad (1.35)$$

1.8 Superficially porous materials

Horváth developed pellicular 50 μm glass bead packings coated with an ion-exchange functionalised divinyl-benzene based polymer for the analysis of nucleobases and nucleosides [89, 90]. Initially developed by Kirkland [91] commercially, superficially porous silica, or more recently fused-core particulates as stationary phase supports in liquid chromatography, offer an alternative to sub-2 μm technology. In order to reach the optimum linear velocity required by sub-2 μm materials users may not be able to achieve such operating conditions with conventional HPLC equipment. Superficially porous materials can however offer the chromatographer significantly improved efficiencies from conventional materials whilst still being able to operate using standard chromatographic equipment. Fused-core technology is based on the principle of a solid particle surrounded by a porous outer shell, of which the pores are 9 nm [92]. Figure 1.13 below is a schematic of analyte diffusion with respect to superficially porous and totally porous materials:

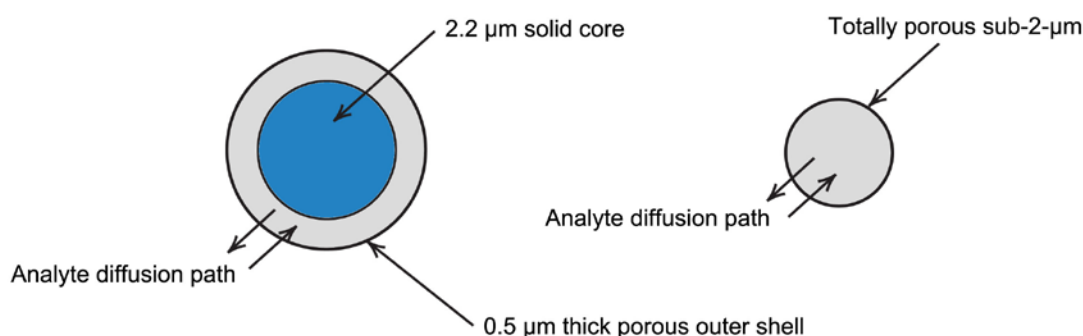


Figure 1.13. Superficially and totally porous particle diffusion behaviour.

The beneficial characteristics of superficially porous materials in comparison to totally porous materials and their applications has been outlined by DeStefano and co-workers [92]. Their work implied that the reduced analyte diffusion path of fused-core particles significantly improves the C-term in the van Deemter relationship, as mass transfer kinetics are increased, this observation being especially true for analytes with molecular weights higher than 600 Daltons. Guiochon and co-workers [93] modelled the mass-transfer-kinetics of columns packed

with fused-core particles. Their findings indicate that the decrease in the thickness of the porous shell is proportional to a decrease in the value for HETP, found to be only pertinent to larger molecular size analytes such as proteins and peptides and negligible for smaller molecules such as phenol. Carr and co-workers [94] have applied this approach to proteomics research by coupling columns packed with superficially porous particles to obtain very high peak capacities. They concluded that in order to achieve high peak capacities it is best approached using column formats exhibiting the highest isocratic efficiencies. Theoretical peak capacities (n_c) for an 11 peptide separation were calculated with respect to column length and particle size at the pressure limit of the system, shown below [94]:

d_p (μm)	L (cm)	t_G (min)	ΔP (MPa)	b^*	n_c	$n_c/(d_p^{0.5})$
1.8	7.5	60	39	0.08	377	281
3.5	28.5	228	39.2	0.08	543	290
5	58	464	39.1	0.08	603	270

* Gradient steepness calculated using S value of 40

Table 1.3. Peak capacity as a function of particle size and column length. The b parameter (Gradient steepness) in this table relates to that of Snyder and co-workers as shown in equation 1.23.

Hsieh and co-workers [95] compared the use of fused-core and sub-2 μm silica packed columns for determining Rimnabant in mouse plasma by LC-MS in both conventional and ultra pressure modes. It was noted that the respective optimum linear velocities of both materials were in a similar range, however the observed back pressure for the fused-core material was substantially lower and with no significant reduction in achieved plate heights. It was also observed that the C-term dominated region of the van Deemter plot for the fused-core material showed a flattening in comparison to the sub-2 μm phase, inferring improved analyte mass transfer kinetics.

The use of fused-core materials used in lower back pressure separations was investigated by Maloney and co-workers [96]. Their work showed that coupled columns (45 cm) packed with superficially porous materials could furnish peak efficiencies up to 92 750 plates/column (45 cm) with a backpressure of only 438 bar.

Mallett and co-workers [97] investigated the application of fused-core materials in the generic ballistic gradient analysis of biological samples in drug discovery, comparing them with sub-2 μm and supra-2 μm phases. Operated at 1.1 ml/min and run times of 1.05 minutes, their observations showed that no significant deterioration of the fused-core material occurred over approximately 4000 injections using a four component test mix. Under these conditions the sub-2 μm material was operating at \sim 700 bars in comparison to the fused-core material at \sim 400 bars. The operating flow rate yielded wider peaks with the sub-2 μm material explained as due to sub-optimal linear velocities used to exploit the efficiencies of this particle size.

Several superficially porous particles are now commercially available, namely the Ascentis Express 2.7 μm (Supelco), Poroshell 2.7 μm (Agilent) and Kinetex 2.6 μm (Phenomenex) being the most common. Yang *et al.* [98] evaluated these phases with regards to small molecule natural products using reversed-phase separations. Their investigations noted deterioration in the column performance when migrating from 4.6 mm to 2.1 mm ID column formats and differences in retentivity between different manufacturers materials. This work follows on from the work of McCalley [99] and Hooker *et al.* [100] on optimising system volumes for obtaining maximum performance of superficially porous materials, confirming that efforts must be made to reducing extra-column volume for preserving the performance of these columns using conventional equipment.

1.9 Hydrophilic Interaction Chromatography (HILIC)

Reversed-phase chromatography is the widely adopted retention mechanism for the majority of separations, however with respect to the analysis of small polar analytes this technique becomes difficult to apply. Martin and Synge [2] applied their normal phase technique to the separation of amino acids, in their work the silica used was saturated with water and the mobile phase was a mixture of chloroform and alcohol. This separation technique is regarded as a liquid-liquid partitioning separation mechanism due to the water bound onto the silica acting as an immobilised stationary phase. The utility of normal-phase systems in modern laboratories is seen as environmentally unfriendly and expensive, such are the means for disposing of toxic eluents. Moreover, the use of alkanes and apolar (e.g. chloroform, ethyl acetate) solvents can result in poor analyte solubility with hydrophilic compounds.

As an alternative to using normal-phase, Alpert [101] coined the term hydrophilic interaction chromatography. This work involved using a polar stationary phase, much like a normal phase system, except the mobile phase was an aqueous organic mixture, containing mainly higher proportions (>60%) of acetonitrile. Due to the more polar nature of the eluent, solubility issues associated with normal phase could be solved. The retention mechanism works on the basis that water adsorbs onto the stationary phase surface and becomes immobilised such that partitioning takes place between this and the bulk mobile phase. In reality the retention mechanism is more complex and many processes are taking place. The simplest stationary phase for HILIC is bare silica, where the underivatized silanol groups act as the functional group and are themselves both acidic and hydrophilic in nature. These groups are able to interact with, for example, basic analytes through hydrogen bonding and electrostatic interactions (ion-exchange). Figure 1.14 depicts the hypothetical retention mechanism for a basic solute on bare silica.

The extent of the tightly bound aqueous layer was investigated by McCalley *et al.* [102] indicating that significant proportions of the pore volume is occupied by molecules of water as inferred by the exclusion of benzene.

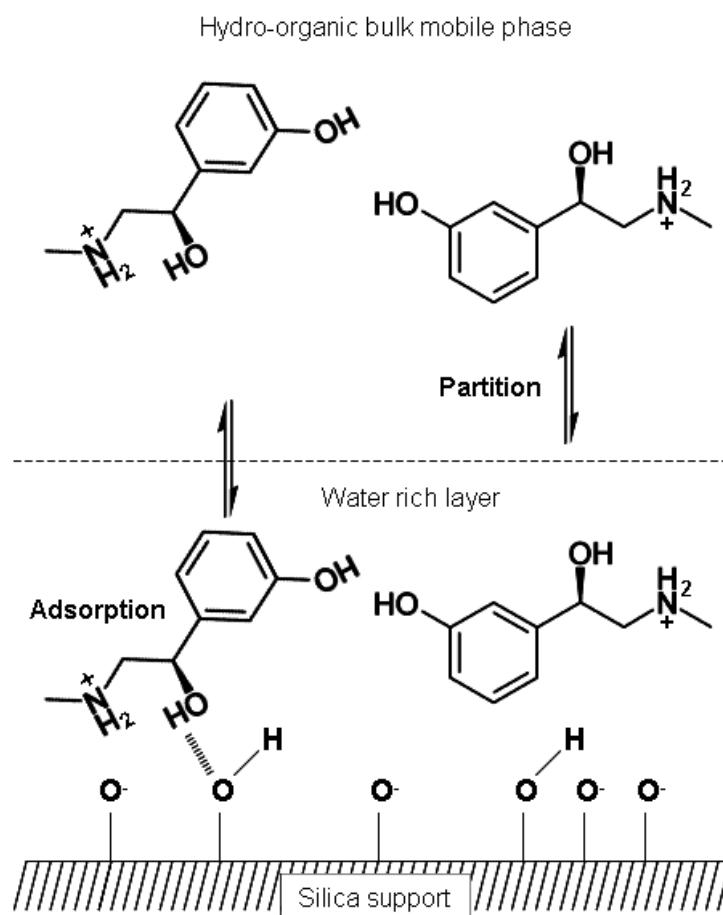


Figure 1.14. Hypothetical retention mechanism of phenylephrine on silica.

There are many advantages to using HILIC versus reversed or normal-phase methodologies. Firstly, the kinetic performance gains are due to the inherently organic rich mobile phase, affording increased analyte diffusivity. This can be shown by the following equation [103, 104]:

$$D_{m,T} = D_{m,303} \frac{\eta_{303}}{\eta_T} \frac{T}{303} \quad (1.36)$$

Where η_{303} and η_T are the mobile phase viscosities at 2 different temperatures, $D_{m,303}$ and $D_{m,T}$ are the diffusion coefficients at different temperatures (T in Kelvin). Typically, this allows for twice as fast diffusion in comparison to reversed-phase eluents thus enhancing mass transfer, and therefore lowering the C -term contribution as shown by McCalley [104].

Appelblad [105] showed that due to the effect of eluent viscosity on permeability extremely fast separations could be achieved, as well as the retention of very polar solutes using HILIC. This study further highlighted the kinetic advantages of using HILIC by means of kinetic plots, showing that much lower separation impedances are realised. Using the low viscosity mobile phases associated with HILIC the serial coupling of bare silica columns has been investigated by several workers. McCalley [106] showed that by serially coupling three 15 cm long 2.7 μm superficially porous (bare silica) packed columns, approximately 100,000 plates in around 15 minutes were obtained, using conventional instrumentation. Sandra *et al.* [107] generated around 130,000 plates by combining six 25 cm long 5 μm packed (bare silica) columns using < 350 bar back pressure in around 30 minutes. Grumbach *et al.* [108] showed that 1.7 μm BEH versus 3 μm Atlantis silica produced more efficient separations yielding sharper peak shapes increasing sensitivity for the former. Another advantage is the comparable loading capabilities for basic solutes over reversed-phase as shown by McCalley [104]. However since the injection solvent contains mainly acetonitrile, problems with solubility can be encountered with certain analytes and compromises must be made. Veuthey *et al.* [109] investigated the effect of injection solvent on peak shape in HILIC. They concluded that injection solvent polarity could be attenuated by displacing the water content with alcohols where lower concentrations of acetonitrile are necessary to enable the solubility of the analyte.

The main advantage of HILIC lies in the application of retaining polar solutes, particularly in the analysis of drug compounds and their metabolites as reviewed by Hseih [110]. Often drug metabolites are more hydrophilic than the parent compound, especially if conjugation to the glucuronide has taken place. Several applications have been developed using HILIC, in particular for the analysis of morphine and its major glucuronidated metabolites. Kolmonen *et al.* [111] developed a HILIC method for this application reporting that direct injection of the collected SPE eluent without requiring evaporation, hydrolysis or reconstitution could be performed. A reversed-phase method was published [112] for this application however the workers had to use a neutralising solvent to prevent degradation of the glucuronide due to the high pH used during extraction and chromatographed using a phase designed to offer retention of polar solutes. Nucleosides are extremely hydrophilic as they are sugar-conjugates of nucleobases and are extremely difficult to chromatograph by typical reversed-phase methodologies. Jansen *et al.* [113] reviewed the analysis of these conjugates depicting that

HILIC should be considered, having particular advantages over ion-pairing techniques particularly if detection by electrospray mass spectrometry is required.

Another advantage of the low viscosity HILIC eluent is the enhanced desolvation properties encountered with electrospray ionisation. This concept was shown by Mitchell *et al.* [114] in that up to 10 times greater signal was observed in HILIC mode versus reversed-phase. This affords greater sensitivity in comparison to more aqueous rich mobile phases, enhancing ion transfer from solution into the gas phase. This corresponds well with the use of ammonium formate/acetate based volatile buffers which are soluble in acetonitrile rich mobile phases. The use of such buffers were shown by McCalley [104] to be essential for achieving optimum peak shape, also illustrating that by simply using carboxylic additives alone was not suitable.

The main disadvantage in adopting HILIC is the reliance on acetonitrile, as outlined by Sandra *et al.* [115] during times of shortage of this solvent. They postulated using per aqueous retention which entails using water rich mobile phases (< 5% organic) to obtain retention, the opposite of conventional HILIC operation. Instead of acetonitrile, ethanol was adopted and shown to be useful for the separation of amino acids and biogenic amines. Fountain *et al.* [116] investigated using acetone as a direct replacement for acetonitrile in HILIC. They reported losses in signal when using acetone for certain analytes, moreover only generic electrospray voltages were applied in their study which may have not been optimal.

2.0 Hyphenation of liquid chromatography to mass spectrometry (LC-MS)

2.1 Electrospray Ionisation (ESI)

Electrospray ionisation mass spectrometry (ESI-MS) has no doubt been revolutionary in analytical chemistry. Initially reported by Dole *et al.* [117] as a means to generate polystyrene macroions from a dilute polymer solution via the application of an electrospray. This idea was developed further by Fenn *et al.* [118] for the analysis of intact proteins, the mechanism by which this occurs has since been interrogated and adapted by many workers. The main benefit of this technique is that little or no fragmentation of the analyte occurs and a singly charged or protonated molecule $[M+H]^+$ is produced. This is because unlike electron impact ionisation (EI), which is a destructive ionisation mechanism, electrospray is termed “soft” in comparison. With respect to proteins and peptides, where multiple charges can be adopted due to the presence of many interspersed amino groups, most drug molecules possess only a single amine functional group. In combining this technique with liquid chromatography many analytical challenges could be addressed and as such wide adoption of LC-MS in many research areas has been undertaken. Nevertheless, the early work of Vestal *et al.* [119, 120] investigated the use of thermospray ionisation as a means to connect liquid chromatography based separations to yield similar molecular ions. Many modern electrospray interfaces are a combination of these ionisation mechanisms as discussed below.

The enabling feature of an LC-MS instrument is the ion source. In order for ions to be detected within the mass spectrometer they must be transposed into the gas phase, after which they can be guided to the detector by the ion optics and quadrupoles within the instrument. In order for ions in solution to become ionised in the gas phase several processes are undertaken which are a complex function of the ion source parameters and the chemistry of the interfaced liquid. Modern ESI interfaces are generally made up of an electrospray needle/capillary held at high voltage ($\sim 0.5\text{-}4.5$ kV), whereby the eluent from the liquid chromatograph is interfaced, and a sampling cone (counter electrode). The sampling cone and the electrospray needle are held at opposing polarities, such that if positive ions $[M+H]^+$ are formed from the spray the negatively charged cone will sample the species which are positively charged. The converse of this is

negative ion electrospray which forms negatively charge ions $[M-H]^-$. Generally, the spraying needle and sample cone have a nebuliser gas which assists in the desolvation process.

The sampling cone also acts as a de-clustering potential to disrupt solvent clusters, enhancing ion transmission. These processes are all held at very high temperatures, with typical electrospray sources operating at between 300-800 °C and the sample cone at > 120 °C. The thermal and nebuliser conditions are a direct function of the eluent properties and applied chromatographic flow rate. The mechanism of electrospray is illustrated in the schematic below:

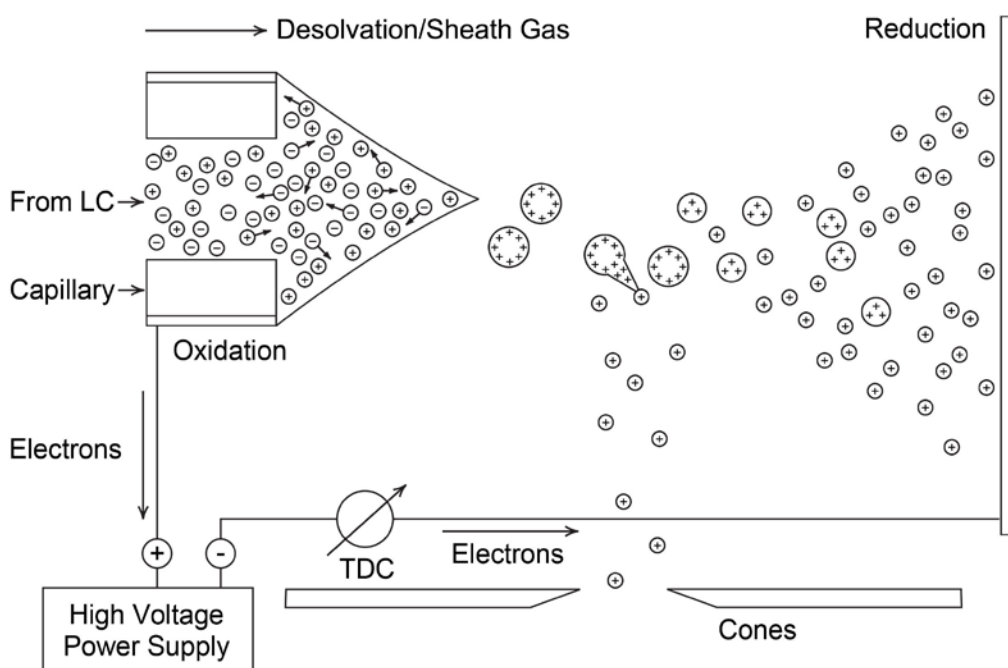


Figure 1.15. General schematic of off-axis positive ion electrospray ionisation [121].

Briefly, positively charged droplets are emitted from the spraying capillary (Taylor cone) which immediately undergo solvent evaporation resulting in ever decreasing droplet sizes until the 'Rayleigh' limit is reached. This limit is where the electrostatic repulsion between the molecules in the liquid droplet is exceeded causing fission events (Coulombic explosions) which form a jet of molecular ions. A schematic of the Taylor cone is shown in Figure 1.16. The molecular ions are then attracted by the sampling electrode and introduced into the ion optics. The degree by which solvent clusters are desorbed and the extent to which molecular ions are transferred into the mass spectrometer is termed electrospray ionisation efficiency [121]. In the opposing polarity, negative ion electrospray, the same principles apply as previously discussed. The two

main theories developed to describe the electrospray process are termed the 'Ion Evaporation Model' (IEM) of Thomson *et al.* [122] and 'Charge Residue Model' (CRM) from the initial work of Dole *et al.* [117, 123]. The IEM proposed evaporation of droplets due to electrostatic repulsion until the 'Raleigh' limit is reached, allowing for subsequent subdivisions to occur which result in yet smaller droplet formation. Conversely, the CRM depicts that successive droplet subdivisions would result in the formation of many very small droplets that would contain just one solute molecule.

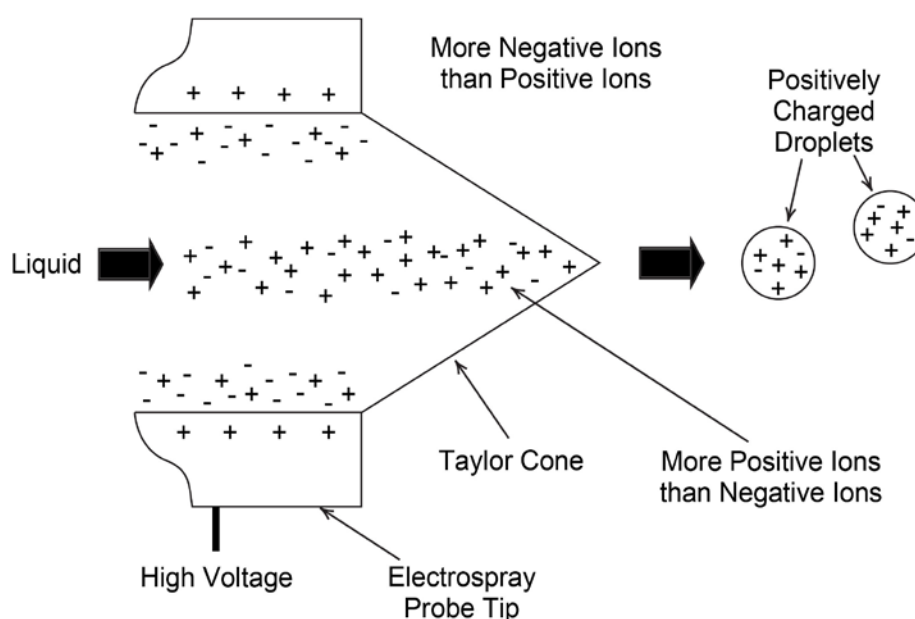


Figure 1.16. Taylor cone formation and emission of positively charged droplets [124].

Competition for protons in the electrospray source can be problematic particularly in the analysis of biological fluids or in the instance where analytes co-elute with each other. This is termed "ion suppression" and usually deteriorates or in some circumstances increases analyte signal intensity, resulting in poor analytical precision. These effects have been outlined and investigated by King *et al.* [125]. With respect to the analysis of drugs in biological fluids, the usual strategy to counteract this phenomenon is to use extraction methodologies such as solid phase (SPE) or liquid-liquid extraction (LLE). This allows for removal of much of the endogenous material associated with biological matrixes. Another technique is to manipulate the chromatography such that the interference is eluted in a different region of the chromatogram to that of the analytes of interest.

2.2 Mass Analysers

After ions are formed in the ion source they must be transferred towards the detector. This is usually an electron or photo-multiplier as is typically found in a triple quadrupole instrument, providing low resolution spectra, or a time-of-flight detector with a micro channel plate (MCP) providing high mass accuracy. Ion guides and quadrupoles are used to focus and select the ions of interest using radio (RF) frequency voltages. The quadrupoles effectively act a mass filter allowing selection of a particular m/z or scanning over a set mass range.

There are several functions of a triple quadrupole instrument summarised as follows. A schematic of a triple quadrupole instrument is shown in Figure 1.17. This illustrates the ion path through the instrument to the detector; the ions that reach the detector are a function of the scanning frequency the quadrupoles are operating in. In this particular example, a Waters Quattro Premier XE instrument was chosen which features an orthogonal Z-Spray electrospray interface. This type of ion source is termed off axis as the spray from the interfaced chromatography sprays across the sampling cone allowing for cleaner operation. For selected reaction monitoring (SRM) the first quadrupole (Q1) acts to select the m/z of the compound of interest, in Q2 a collision gas (typically Argon) is applied which fragments the precursor ion yielding product ions, Q3 is then used to select one or several of these products. This type of experiment yields high specificity for quantification of a substance. Product ion scanning experiments use Q1 to select the analyte m/z then applying collision energy in Q2 followed by Q3 selected to scan across a predetermined mass range. Precursor ion scanning selects an ion in Q3 and the masses which yielded this product are scanned over a mass range in Q1. The neutral loss experiment involves offsetting Q1 and Q3 to scan for products which have been fragmented in Q2 to be selectively recognised. Triple quadrupole instruments offer high selectivity and sensitivity and are used extensively in the quantification of drug substances, particularly biological matrices such as urine and plasma. They only offer nominal mass resolution and therefore cannot be used to yield elemental composition data.

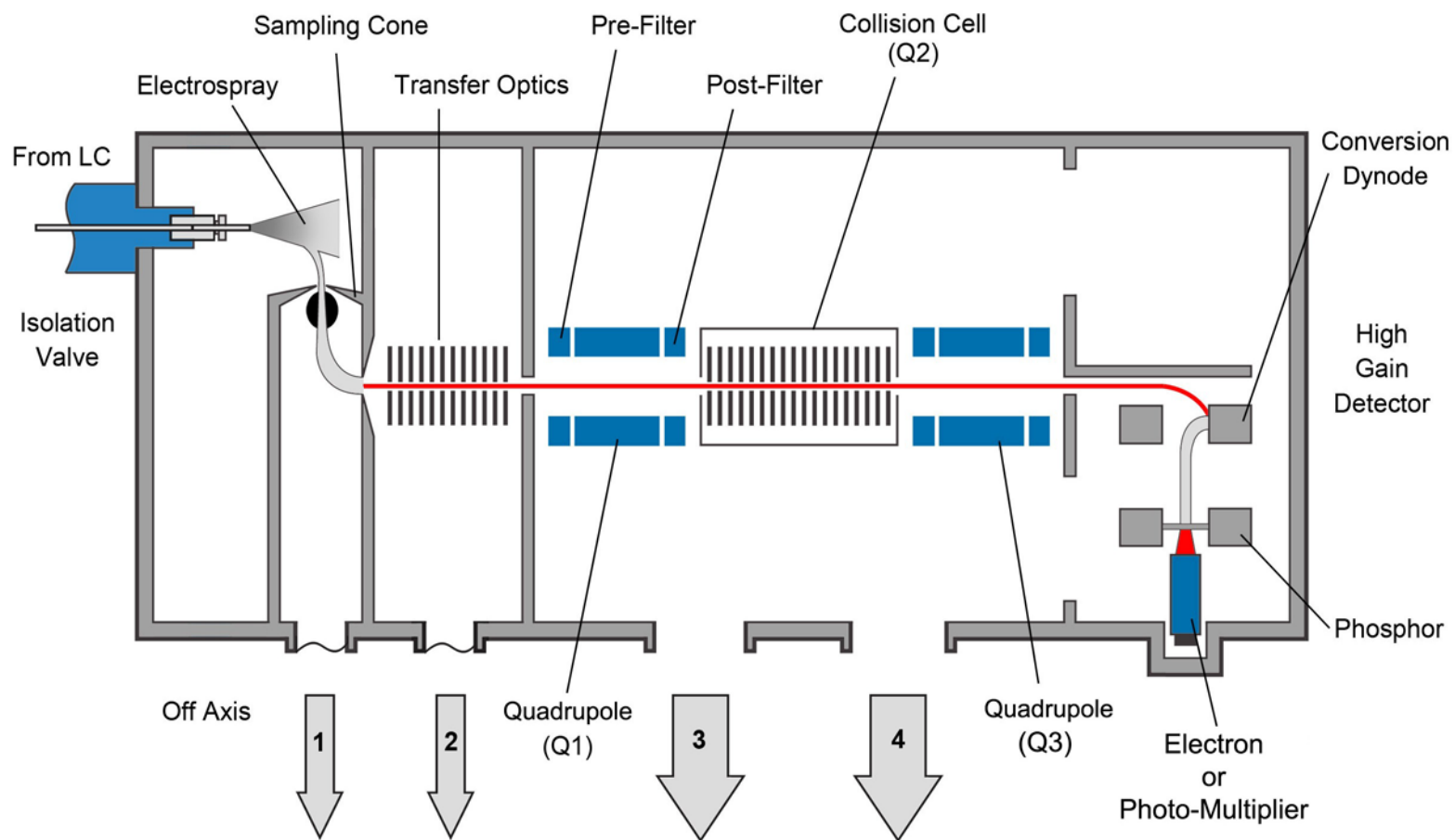


Figure 1.17. Schematic of the Waters Quattro Premier XE triple quadrupole mass spectrometer. Arrows 1, 2, 3 and 4 to vacuum pumps. Adapted from [124].

Alternatively, time-of-flight (TOF) instruments offer high mass resolution enabling determination of chemical compositions to within typically 5 ppm accuracy. These instruments can also be fitted with a quadrupole mass filter and collision cell, termed Q-TOF-MS. This allows for pre-selection of an ion and or fragmentation product akin to triple quadrupole systems, except the high mass accuracy of the detector allows for information rich spectra useful for structural elucidation. Such systems do not perform SRM experiments, instead any mass selected by the quadrupole followed by the application of collision energy results only in the measurement of product ions in the TOF across a predetermined mass range. These systems are growing in attention due to their fast scan speeds, enabling data capture over very small chromatographic peak widths now associated to UHPLC type separations. Owing to this function, these instruments are likely to become more prevalent as analysis speeds become increasingly important. One of the main advantages of Q-TOF instruments is their ability to impart high mass accuracy data, and as such have gained much notoriety in metabolite identification studies, where fast methodologies are required to screen and identify metabolites of a precursor drug. Similarly, metabonomic/metabolomic studies have benefitted from this technology as screening for potential biomarkers in large sample sets is becoming ever important to medical research.

In conclusion, there are a range of mass analysers now capable of being interfaced with chromatographic separations via electrospray ionisation. The selection and application of a mass spectrometer is highly dependent on the data which is required of the analytical challenge. In keeping with future developments in separation science, appropriate selection of the mass analyser is becoming even more important particularly as separation efficiencies yield yet smaller peak volumes. The seamless integration of liquid chromatography with mass spectrometry is undoubtedly going to become increasingly prevalent, particularly in the arena of phenotyping and “omics” type studies.

Chapter 2

Rapid quantification of quinine and its major metabolite (3S)-3-hydroxyquinine in diluted urine by UPLC-MS/MS

Abstract

A rapid UPLC-MS/MS quantitative assay for the quantification of quinine and (3S)-3-hydroxyquinine requiring minimal sample pre-treatment with a dilute-and-shoot type approach has been developed. The assay was run at 0.6 mL/min using gradient elution with 10 mM ammonium bicarbonate pH 10 and methanol with a total cycle time of 2.5 minutes on a 50 x 2.1 mm ID, 1.7 μ m Acquity BEH column. Peak shapes were highly symmetrical allowing for accurate peak integration. Calibration curves for both analytes were constructed from 1.00 to 20.00 ng/mL, yielding R^2 values > 0.995. Intra- and inter-batch assay precision and accuracy were evaluated using 6 injections of QC solutions on 3 separate days ($n = 18$) and were found to be within ± 10 % and 90 – 110 % respectively. The method was shown to be suitable for quantitatively determining the ratio of quinine to (3S)-3-hydroxyquinine for a cohort of samples from an epidemiological study. This chapter demonstrates an initial evaluation of UPLC technology integrated with ESI mass spectrometry for a high throughput application. The use of sub-2 μ m BEH (Bridged-Ethyl Hybrid) packed columns operated at high pH was shown to be robust. Initially, analyte carryover for quinine was found to be problematic, however this was overcome using a suitable autosampler wash step. This methodology showed superior throughput to previously reported conventional HPLC based methodologies for the co-analysis of quinine and the (3S)-3-hydroxylated metabolite. Some proposals on the fragmentation pathways of both analytes are also discussed, which have rarely been reported in the literature.

2.1 Introduction

Quinine can be mostly associated with the treatment of *plasmodium falciparum* induced malaria and has been applied as such an agent since the 17th century. The human hepatic metabolism of quinine has been well studied and is known to be specifically due to the family of Cytochrome P450 (CYP) 3A enzymes [126, 127]. The metabolic pathway of quinine to the corresponding Phase I metabolites is shown in Figure 2.1. CYP3A4 enzyme is the most abundant and important drug metabolising enzyme, thought to be responsible for the metabolism of more than 50% of the most commonly prescribed medicines. It is thought that many of the profound adverse reactions and poor therapeutic responses to xenobiotics can be ascribed to atypical CYP3A4 activity [128]. The primary metabolite of quinine is (3S)-3-hydroxyquinine, which is the product of CYP3A4 enzyme monooxygenases activity. The ratio of (3S)-3-hydroxyquinine to quinine is of interest as this can be used to measure CYP3A4 activity phenotype across a sample population by simple oral administration of the drug and subsequent collections of urine and/or plasma.

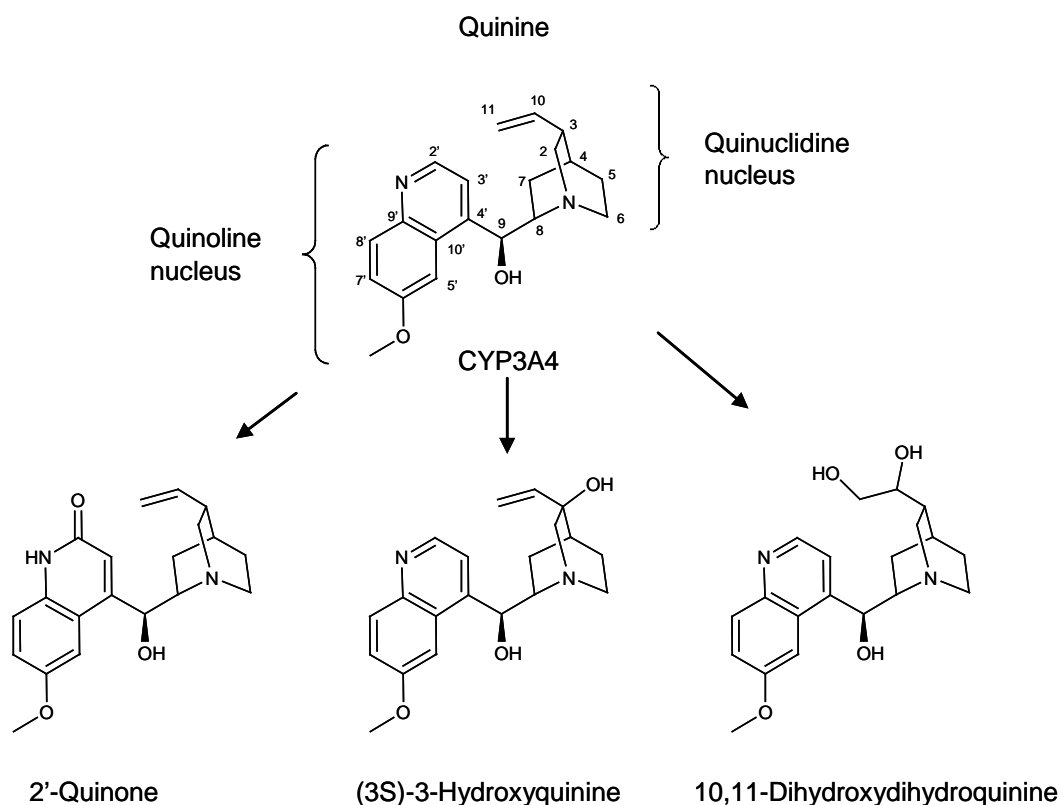


Figure 2.1. Schematic of quinine metabolism in man modified from [126].

The previously reported methodology used to quantify quinine and (3S)-3-hydroxyquinine was performed by GC-MS [129], HPLC-Fluorescence [130, 131] and more recently a method using HPLC-UV [132]. The newer UPLC-MS/MS technique represents higher throughput, and a faster and more accurate alternative. An earlier publication on the use of liquid chromatography interfaced with thermospray mass spectrometry [133] indicated the difficulty in obtaining suitable peak shapes for cinchona alkaloids in the context of drug development. McCalley *et al.* studied the chromatographic analysis of cinchona alkaloids, the family of compounds with which quinine is associated [134]. Quinine and several of its related metabolites possess two basic functional groups, hence it is of chromatographic importance to minimise interactions with acidic underivatized silanol groups associated with peak tailing. This can be achieved by running with an acidic mobile phase (~ pH 2.0) thereby suppressing free silanol ionisation or by reducing the extent of the basic group protonation by analysis in highly basic media. Interactions between amino groups and underivatized silanols can be negated using ion-pairing reagents; however this is usually avoided when interfacing such separations with mass spectrometry due to ion suppression. The introduction of pH stable bridged-ethylene hybrid stationary phase materials enables analysis at high pH [83]. This has been evaluated by several groups [135-137] who noted improved sensitivity when compared to classical formic acid based mobile phases and dubbed “wrong-way-round ionisation” [138].

The methodology reported here is intended for the analysis of samples inherently concentrated with quinine and (3S)-3-hydroxyquinine, since only the first pass of urine from volunteers was collected for analysis. The sensitivity of the mass spectrometer can be taken advantage of for their quantification in heavily diluted urine by UPLC-MS/MS without the requirement for extensive sample pre-treatment, such as solid-phase or liquid-liquid extraction methodologies. Although there are other known phase I and II metabolites of quinine the purpose of this study was to preserve and quantify only the primary drug and its major metabolite (3S)-3-hydroxyquinine. With this in mind the simplest sample treatment was pursued so as not to liberate any O-conjugated metabolites.

2.2 Experimental

2.2.1 Chemicals

Quinine free base (98% Pure) and Quinine-D₃ (Chemical Purity 97%, Isotopic Purity 99%) were purchased from Toronto Research Chemicals Inc. The single diastereoisomer (3S)-3-hydroxyquinine metabolite (Determined in-house to be 98% pure at King's College London by UPLC-UV) was not commercially available, however it was kindly donated by Prof. James M Cook of the University of Wisconsin, Milwaukee, USA via his published synthetic route [139]. HPLC gradient grade methanol, acetonitrile and trifluoroacetic acid (TFA) were purchased from Fisher Scientific Ltd. (Loughborough, UK). Isopropyl alcohol (IPA), Leucine enkephalin, ammonium bicarbonate, ammonium hydroxide and formic acid (all LC-MS grade) were purchased from Sigma-Aldrich (Dorset, UK). High purity water (18.2 MΩ) was provided in-house using a Milli-Q purification system (Millipore, UK). All buffer solutions were vacuum filtered through a 0.22 μm membrane filter (Sigma-Aldrich).

2.2.2 Standard preparation

Preparations of stock and QC quinine and (3S)-3-hydroxyquinine standards were prepared in methanol at a concentration of 0.1 mg/mL. A stock solution of the internal standard quinine-D₃ was prepared at a concentration of 0.1 mg/mL also in methanol and further diluted to a working concentration of 250 ng/mL. The working stock standard was diluted to 100 ng/mL inclusive of 250 ng/mL of the internal standard (Quinine-D₃) and was further diluted to yield the following calibration standards on each day of analysis: 0, 1, 2, 5, 10 and 20 ng/mL, all inclusive of 5 ng/mL internal standard. Working QC solutions were prepared once from stock QC and diluted to concentrations of 1, 5 and 20 ng/mL, inclusive of 5 ng/mL internal standard, and used fresh for each analysis. All working standards were prepared in methanol-water (50:50, v/v). All solutions were stored at -20 °C and used within two months of preparation with no observed deviation from QC concentrations during this time period.

2.2.3 Sample treatment

Fasting urine samples were collected from a total of 315 monozygotic and dizygotic twins from the TwinsUK adult registry (www.twinsUK.ac.uk) between 14-16 hours after administration of a 300 mg dose of quinine sulphate. Dilution of the samples was carried out using the following scheme: 50 μ L of urine was added to 50 μ L of internal standard followed by the addition of 900 μ L methanol-water (50:50, v/v). Samples were then vortexed and centrifuged for 10 minutes at 9,000 rpm and finally diluted by adding 50 μ L of the supernatant to 950 μ L methanol-water (50:50, v/v) ready for LC-MS analysis. Aliquots were collected and stored at -40 °C until analysed.

2.2.4 Chromatographic conditions

Liquid chromatography was carried out on a Waters Acquity Ultra Performance Liquid Chromatography system using a 50 x 2.1 mm ID column packed with an Acquity BEH C₁₈ 1.7 μ m phase (Waters Corporation, Milford, MA). The column was thermostatted at 40 °C and operated at a flow rate of 0.6 mL/min with a gradient program. During method development solutions of 10 mM ammonium bicarbonate (pH 4.0 and 10) were prepared by adjusting with formic acid. For the final method, mobile phase A consisted of 10 mM ammonium bicarbonate pH 10.0 adjusted with ammonium hydroxide solution. Mobile phase B was methanol. The gradient program was as follows: linear increase from 50% B to 100% B over 1 minute then held for 0.2 minutes and re-equilibrated for 1.3 minutes at 50% B before the next injection. Full loop injection mode was employed using a 20 μ L sample loop. Two separate needle wash programs were employed, a weak needle wash which was methanol-water (50:50, v/v) and a strong needle wash which was a mixture of isopropyl alcohol-acetonitrile-water-trifluoroacetic acid (60:30:10:0.1, v/v/v/v).

2.2.5 Mass spectrometry

The liquid chromatograph was interfaced to a Quattro Premier XE tandem mass spectrometer (Micromass, Manchester, UK). All analyses were performed in positive electrospray ionisation mode. Optimisation of selected-reaction monitoring (SRM) transitions for quinine and (3S)-3-hydroxyquinine was carried out by infusion of 1 µg/mL methanolic solutions in order to obtain the most intense fragment ions. Conditions for LC-MS/MS analyses were optimised manually by T-union infusion against the mobile phase flow and using a solvent composition at which the analytes eluted from the chromatographic column. Nitrogen desolvation gas was set at 900 L/hr and the cone gas at 50 L/hr. The capillary voltage was set at 0.8 kV, the cone voltage for quinine and (3S)-3-hydroxyquinine was set at 40 eV. Source and desolvation temperatures were maintained at 120 °C and 375 °C respectively. Collision energies (CE) were optimised for selected reaction monitoring (SRM) for quinine 325 > 160 (30 eV) and (3S)-3-hydroxyquinine 341 > 160 (35 eV), the acquisition mass window was set to 0.1 Da. and the collision gas (Argon) was maintained at 3.5×10^{-3} mbar. The dwell time was set at 5 ms, and inter-channel and inter-scan delays were set at 10 ms. For accurate mass experiments a Waters Xevo Q-TOF-MS (Waters Corp., Manchester, UK) system was used to collect spectra for quinine and (3S)-3-hydroxyquinine using Leucine enkephalin lock mass values at 120.0813 and 278.1141 Da. Analyte solutions for infusion were 1 µg/mL prepared in 50:50 v/v H₂O:ACN + 0.1% formic acid.

2.3. Results and discussion

2.3.1 LC-MS/MS method development

Initially, several pH conditions were evaluated in order to determine which pH would yield the optimum chromatographic peak shape as seen in Figure 2.2. Due to the ion suppression of the basic quinuclidine center with mobile phases of higher pH, quinine becomes more hydrophobic and as such its retention increases. Furthermore, peak symmetry improves allowing for accurate integration which is in turn beneficial to assay accuracy and precision.

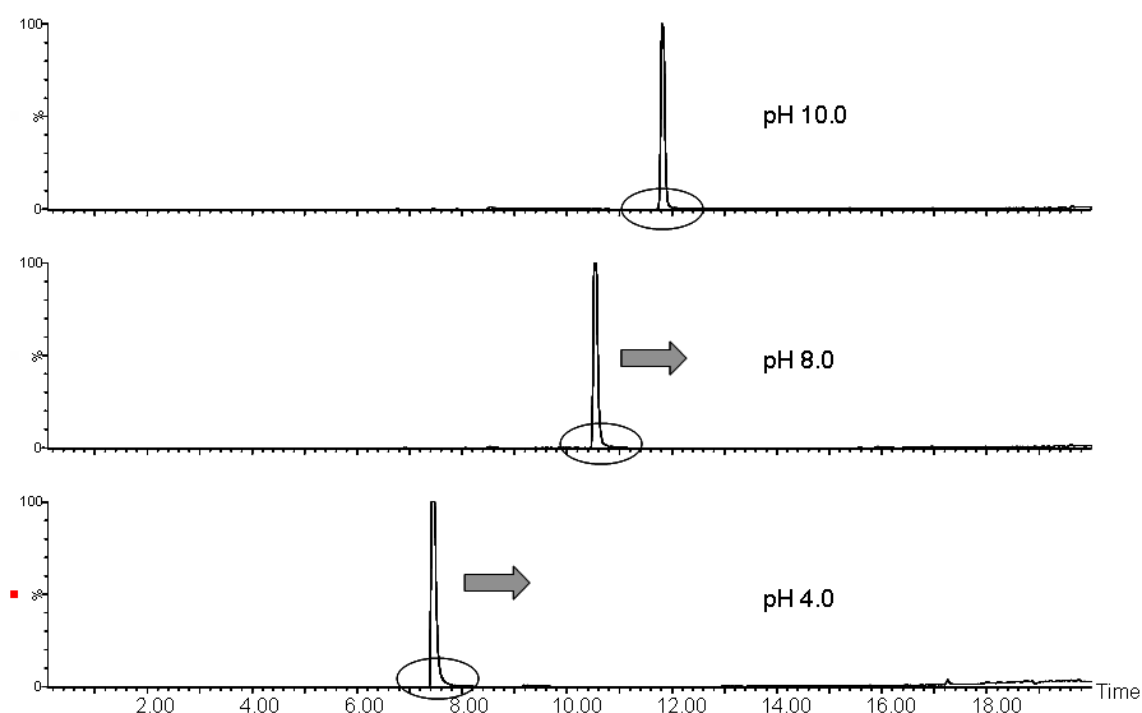


Figure 2.2. Improvement in shape and increase in retention time as a function of pH for quinine. Chromatographic conditions: 20 minute linear gradient from 0-100% methanol operated at 400 μ L/min with a temperature of 60 $^{\circ}$ C using a 1.7 μ m BEH C18 100 x 2.1 mm ID column.

The use of buffered pH manipulation for the separation of charged analytes is important for several reasons. Firstly, elution of analytes of interest from problematic matrix components in neat or partially diluted biological fluids may be achieved by mobile phase pH manipulation, which is important with the use of electrospray ionisation [136, 140]. Secondly, fine tuning of

analyte resolution can be achieved by simply altering the pH of the mobile phase. As an example, the in-house synthesis of 3-hydroxyquinine yielded the (3S) and (3R) diastereoisomeric products, the separation of which could be affected by simple alteration of the mobile phase pH as shown in Figure 2.3.

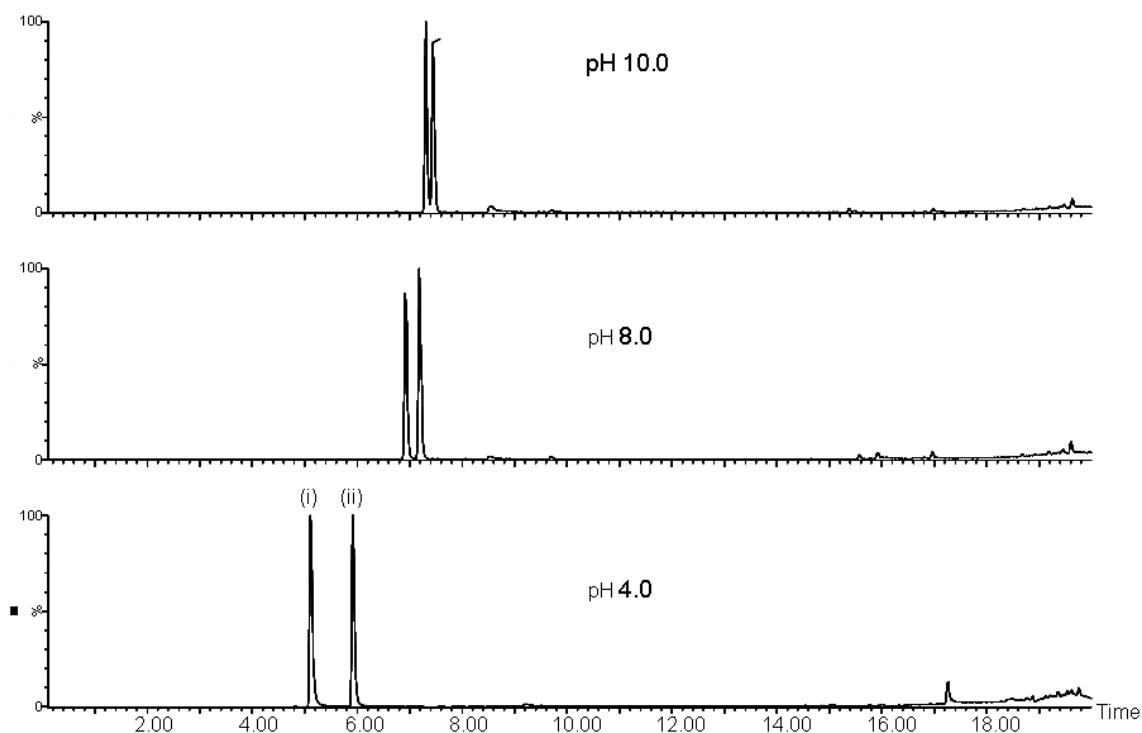


Figure 2.3. Resolution and retention of (3R)-3-hydroxyquinine (i) and (3S)-3-hydroxyquinine (ii) diastereoisomers as a function of pH. Conditions as in Figure 2.2.

Due to the high flow rate and fast gradient applied to this analysis, optimal source conditions were required of 900 L/hr and 50 L/hr for desolvation and source gas respectively in order to assist electrospray. The capillary voltage was optimally determined to be 0.8 kV by manual adjustment, and the signal intensity was found to deteriorate at higher applied voltages (Similar observations are reported later in Chapter 7). The reasons for the lower optimal capillary voltage are unknown and warrant investigation elsewhere. Similarly, cone voltages were determined by infusion against the mobile phase flow rate used and at the solvent composition under which the analytes eluted. Source and desolvation temperatures were optimised and maintained at 120 °C and 375 °C respectively in order to compensate for the higher flow rates used.

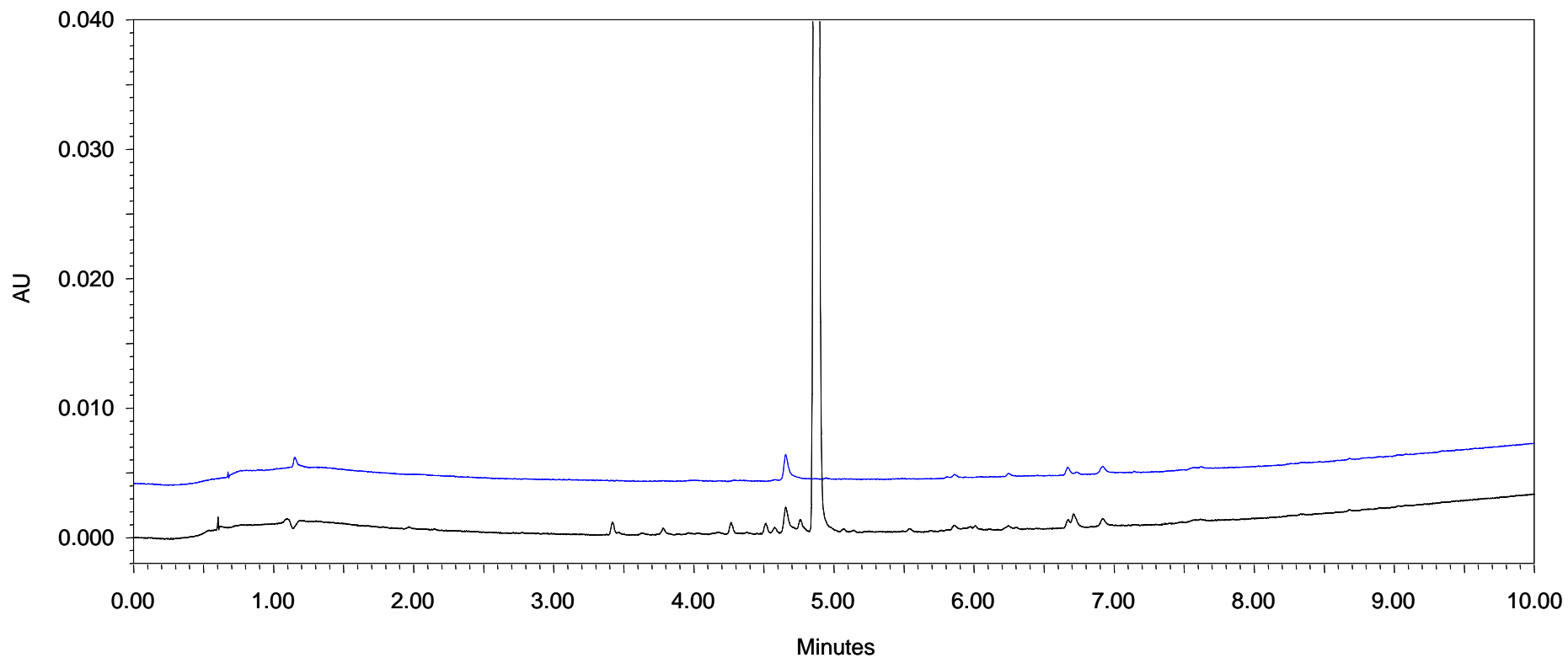


Figure 2.4. Purity assay of (3S)-3-hydroxyquinine as donated by the group of Prof. James M Cook. Conditions: 100 $\mu\text{g/mL}$ solution in initial mobile phase, 10 μL injection volume (Full loop), 400 $\mu\text{L/min}$ flow rate, 5-95 %B over 10 minutes, 60 $^{\circ}\text{C}$ column oven temperature. Data collected at 254 nm. Blue and black traces are mobile phase blank and (3S)-3-hydroxyquinine solutions respectively. Where, B was methanol and A was 10 mM ammonium bicarbonate pH 10.0 using 100 x 2.1 mm ID BEH C18 1.7 μm column.

Figure 2.4. shows the purity assay of the donated reference material for the quinine metabolite. This substance was difficult to obtain commercially and is not yet available as an analytical standard. Attempts were made in-house to synthesise this material however it proved vastly difficult and time consuming. The material was kindly donated by the group of Professor James M Cook, enabling this project to move forward and was of acceptable purity to develop the necessary assay. By subtracting the contribution of system and contamination peaks from those found in the chromatographed (3S)-3-hydroxyquinine solution an area percentage purity was calculated to be 98.4 %. Ideally the small peaks running before the main band would have been characterised, however this was deemed to too time consuming within the context of this project. Also any further purification may have resulted in losses of the precious material as only 100 mg were made available.

2.3.2 Fragmentation of quinine and (3S)-3-hydroxyquinine

Product ion spectra for quinine $[M+H]^+$ and (3S)-3-hydroxyquinine $[M+H]^+$ are shown in Figure 2.5. Collision energies for quinine and (3S)-3-hydroxyquinine were optimised empirically by infusion until the optimal fragmentation was determined. The most intense fragment ion was chosen by which to perform quantification and was determined to be common for both analytes at 160 m/z .

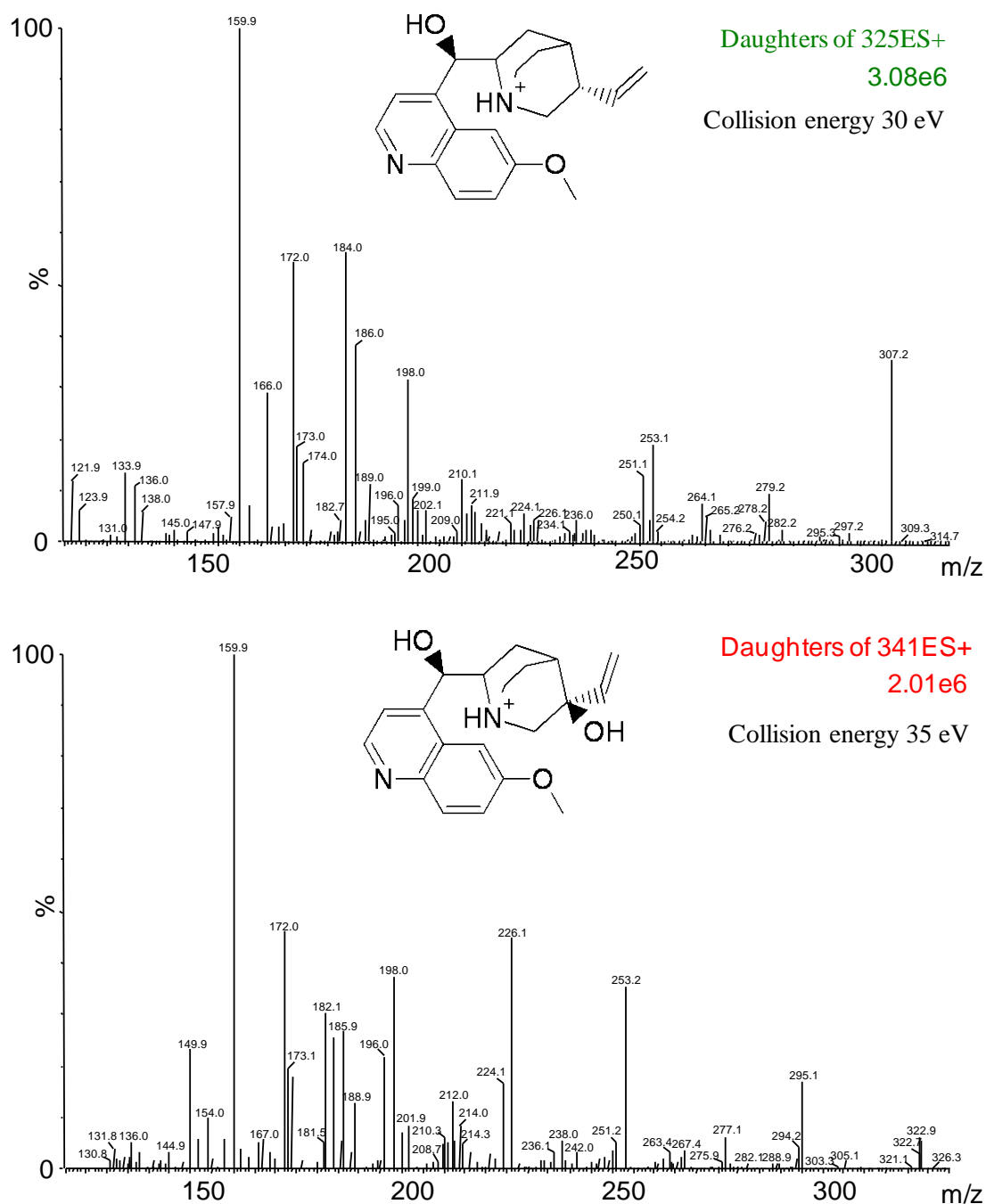


Figure 2.5. ESI positive product ion spectra of quinine (top) and (3S)-3-hydroxyquinine (bottom).

As is shown in Figure 2.5 it is unsurprising that quinine and (3S)-3-hydroxyquinine share some fragmentation products. The structures for these fragments are outlined in Figure 2.6 based on literature sources [141]. Both precursor ions exhibited a loss of water resulting in the formation of products at 323 m/z and 307 m/z for the metabolite and quinine respectively i.e. a loss of 18 Da. This loss is likely to occur at the 9 position on both analytes (See Figure 2.1 for analyte positions).

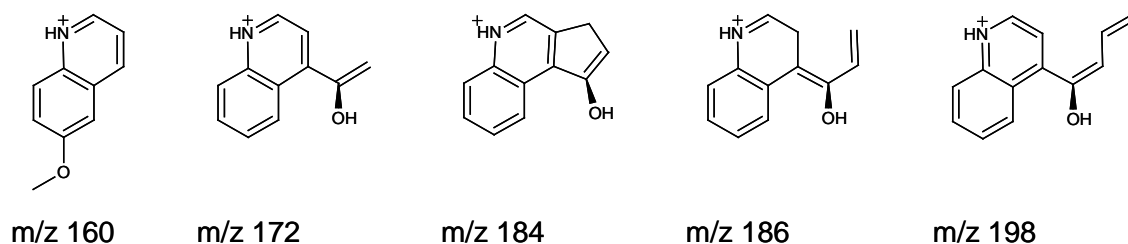


Figure 2.6. Common fragment ions of quinine and (3S)-3-hydroxyquinine based on ref [141].

The mechanism for the formation of the product ion at 253 m/z was suggested by Fujiwara *et al.* [142] and is also a common fragment of the hydroxylated metabolite of quinine. This is perhaps by analogy due to the formation of a double bond between positions 3 and 10 on the quinuclidine ring. On the (3S)-3-hydroxyquinine the formation of this bond will likely impact the loss of the hydroxyl group at the 3 position more readily, hence the higher signal for this ion in the metabolite spectra. The proposed mechanism for the formation of the 253 m/z product ion is shown in Figure 2.7 for quinine, accounted for by the loss of the methoxy group on the quinoline nucleus.

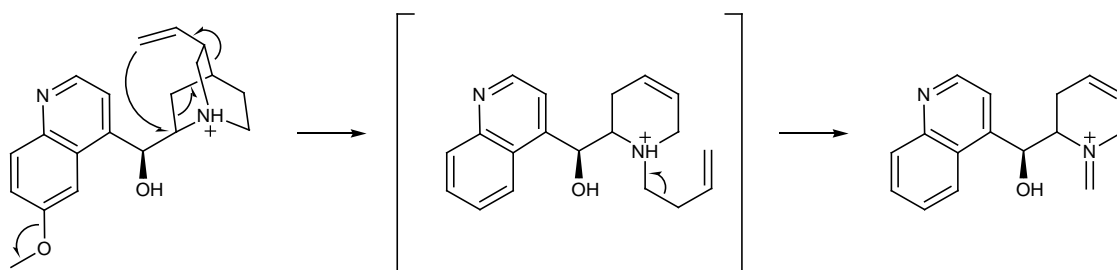


Figure 2.7. Mechanism for the formation of 253 m/z product ion based on Fujiwara *et al.* [142].

The rearrangement on the quinuclidine ring is due to cleavages at positions 3, 4, 7 and 8 which results in a new bond formation between carbons 8 and 11.

Likewise, the formation of product ions at 295 m/z and 279 m/z for (3S)-3-hydroxyquinine and quinine respectively are likely to be related due to a cleavage on the quinuclidine moiety at a different position. The presence of the hydroxyl group on the former indicates a mass difference of 16 Da indicating the sole difference to be oxygen. It could be considered therefore, that the fragmentation shares the same cleavage at positions 4 and 5 resulting in a double bond formation between the 7 and 4 centers. This is shown in Figure 2.8 and in both instances result in the initial common loss of the methoxy group from the quinoline nucleus as in Figure 2.7.

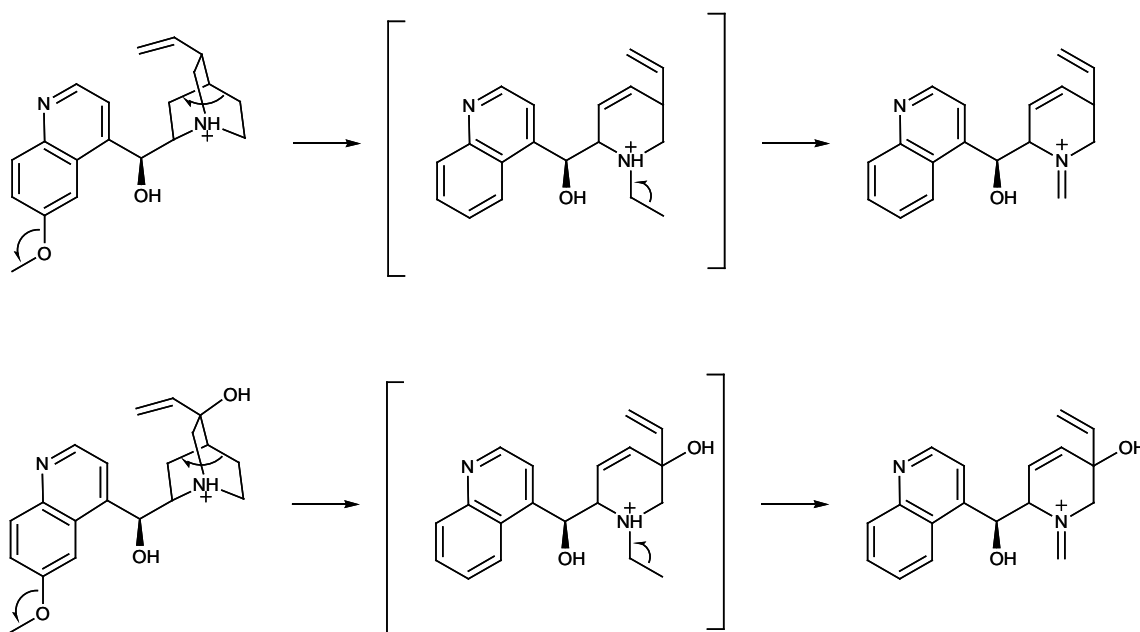


Figure 2.8. Postulated mechanism for the formation of the 279 m/z ion (top) and the 295 m/z ion (bottom) for quinine and (3S)-3-hydroxyquinine respectively.

In order to elucidate further the proposed fragments from literature and those found in our work, Q-TOF-MS/MS was used to confirm or add further evidence to their structure. Figures 2.9 and 2.10 show the accurate mass MS/MS spectra for quinine and (3S)-3-hydroxyquinine respectively. Tables 2.1 and 2.2 indicate the mass error and predicted elemental compositions for the respective analytes. For the smaller fragment ions between 160 – 198 Da, chemical formula matching those depicted in Figure 2.6 were found. Likewise, for the structures proposed in Figures 2.7 and 2.8 the predicted formula based on the exact mass MS/MS were observed. The mass accuracy data were acceptable and ranged between sub-1 ppm to approximately 15 ppm providing good confidence in the predicted elemental compositions of the fragment ions.

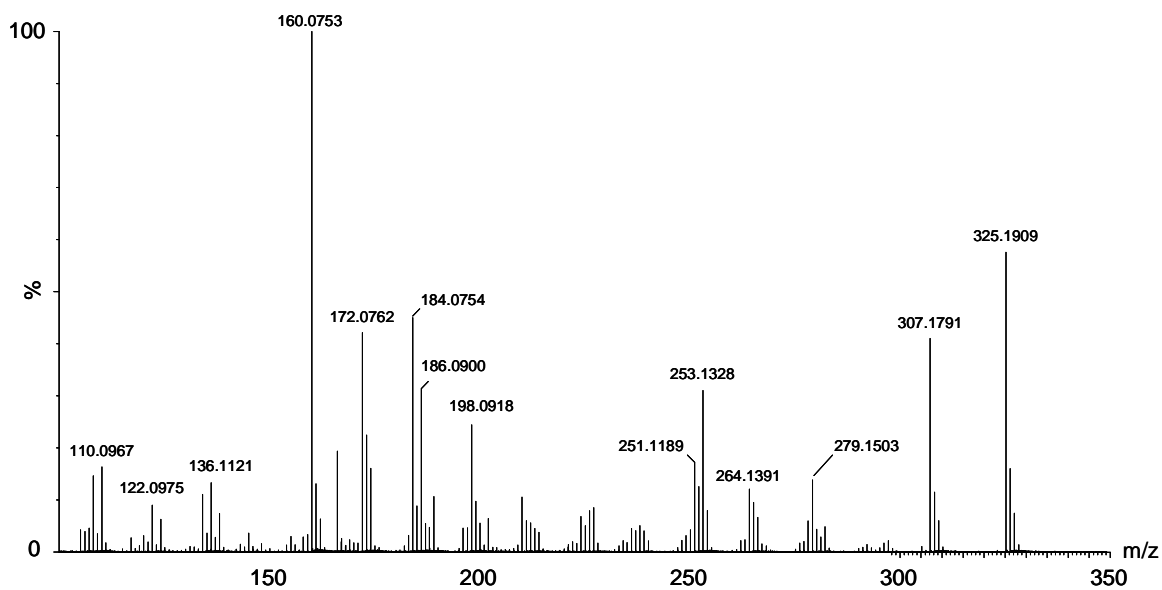


Figure 2.9. Accurate mass MS/MS spectra of quinine $[M+H]^+$ by infusion. Conditions: 10 $\mu\text{L}/\text{min}$, 3.5 kV capillary voltage, 15 eV cone voltage, 30 V collision energy, 325.19 Da set mass. Spectrum is 20 scans averaged, 0.1 second scan time.

Quinine

Mass $[M+H]^+$	Calc. Mass	mDa	PPM	Formula
325.1909	325.1916	-0.7	-2.2	C ₂₀ H ₂₅ N ₂ O ₂
279.1503	279.1497	0.6	2.1	C ₁₈ H ₁₉ N ₂ O
253.1328	253.1341	-1.3	-5.1	C ₁₆ H ₁₇ N ₂ O
198.0918	198.0919	-0.1	-0.5	C ₁₃ H ₁₂ N O
186.0900	186.0919	-1.9	-10.2	C ₁₂ H ₁₂ N O
184.0754	184.0762	-0.8	-4.3	C ₁₂ H ₁₀ N O
172.0762	172.0762	0.0	0.0	C ₁₁ H ₁₀ N O
160.0753	160.0762	-0.9	-5.6	C ₁₀ H ₁₀ N O

Table 2.1. Exact mass error table showing elemental compositions for quinine and fragmentation products.

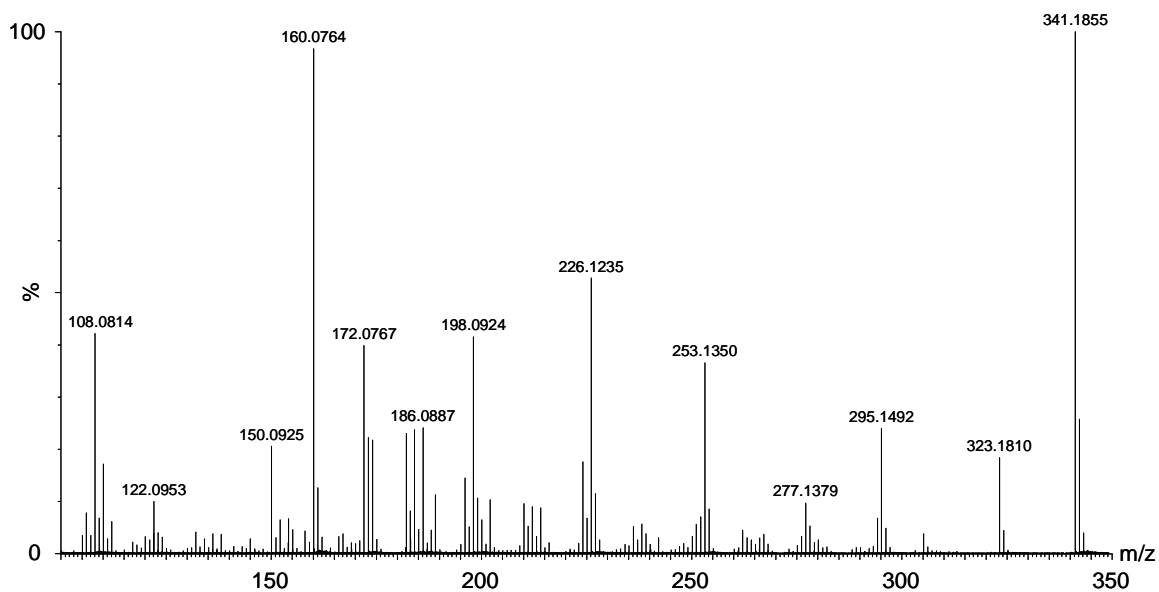


Figure 2.10. Accurate mass MS/MS spectra of (3S)-3-hydroxyquinine $[M+H]^+$ by infusion. Conditions: 10 $\mu\text{L}/\text{min}$, 3.5 kV capillary voltage, 45 eV cone voltage, 30 V collision energy, 341.19 Da set mass. Spectrum is 20 scans averaged, 0.1 second scan time.

(3S)-3-Hydroxyquinine

Mass $[M+H]^+$	Calc. Mass	mDa	PPM	Formula
341.1855	341.1865	-1.0	-2.9	C ₂₀ H ₂₅ N ₂ O ₃
295.1492	295.1447	4.5	15.2	C ₁₈ H ₁₉ N ₂ O ₂
253.1350	253.1341	0.9	3.6	C ₁₆ H ₁₇ N ₂ O
226.1235	226.1232	0.3	1.3	C ₁₅ H ₁₆ N O
198.0924	198.0919	0.5	2.5	C ₁₃ H ₁₂ N O
172.0767	172.0762	0.5	2.9	C ₁₁ H ₁₀ N O
160.0764	160.0762	0.2	1.2	C ₁₀ H ₁₀ N O

Table 2.2. Exact mass error table showing elemental compositions for (3S)-3-hydroxyquinine and fragmentation products.

2.3.3 Autosampler carryover and optimised LC-MS/MS separation

One of the more challenging aspects of developing this method was to eliminate analyte carryover. Due to the nature of the quinine in its hydrophobic state and the inherent sensitivity of the tandem mass spectrometer, significant carryover effects were observed in blank injections during method development. This can be analyte specific, i.e. the physicochemical nature of the analyte may incur an affinity for the chromatographic hardware. For instance, amines are known to chelate to metals which are present within the sampling device. Initially, weak and strong needle washes consisting of typical low and high organic strength solutions were implemented in the method, however carryover could not be avoided. By changing the sample needle to a Teflon coated type, the effect was minimised and then further eliminated by the introduction of isopropyl alcohol-acetonitrile-water-trifluoroacetic acid (60:30:10:0.1, v/v/v/v) as the strong needle wash solution. An excellent treatment of carryover prevention for the analysis of peptides and proteins by nano LC-MS was outlined by Mitulovic *et al.* [143]. A possible explanation for the elimination of sample carryover was that an ion-pairing mechanism between the quinine and TFA may have taken place. Including TFA in the strong needle wash may have altered quinine's strong affinity for surfaces within the fluidics of the autosampler, thereby dramatically reducing carryover. It should also be pointed out that the initial gradient conditions can cause solubility issues between the sample plug and the incoming mobile phase, resulting in smearing of the rotor stator upon turning from load to inject when it becomes in-line with the flowing eluent. Overall, the exact location and cause of sample carryover wasn't entirely discriminated. Nevertheless using slight modifications to the autosampler i.e. Teflon needle and a selective strong wash cycle this challenge was overcome.

The approach of using a short column under fast gradient conditions has been demonstrated by other workers for the high throughput analyses of biological samples [54, 144]. In the method reported here, short 50 x 2.1 mm ID columns packed with sub-2 μm materials gave the appropriate resolution and chromatographic performance required for rapid quantification using triple quadrupole mass spectrometry. Figure 2.11 shows an LC-MS chromatogram from the final separation and ESI conditions from the MRM transitions 341 > 160 for (3S)-3-hydroxyquinine and 325 > 160 for quinine. Clearly, there is potential to improve the throughput of this methodology i.e. by increasing flow rate and further adjustment of the gradient profile for

instance. However, this would have several implications. Firstly, desolvation parameters would have to increase to cope with higher solvent inlet and secondly peak widths would decrease. The latter would require increasing the mass spectrometer scan speed to improve peak definition; however this would likely impact undesirably on assay sensitivity. This demonstrates a limitation to the separations which can be hyphenated to this type of mass spectrometry. More appropriately, a fast scanning and sensitive Q-TOF-MS instrument would be more suited in the future where undoubtedly decreasing peak widths would be encountered. HILIC could also be perceived as a viable option to chromatograph these analytes, particularly as excellent peak shapes are achievable without the need to operate using such high pH mobile phases as was utilised here. Isocratic conditions could have been used; however this would have incurred use of a selective extraction methodology to ensure adequate removal of biologically endogenous material which can build up within the column. The major benefit of isocratic elution is the removal of a gradient re-equilibration step at the end of each analysis, which would contribute to reduced analysis times.

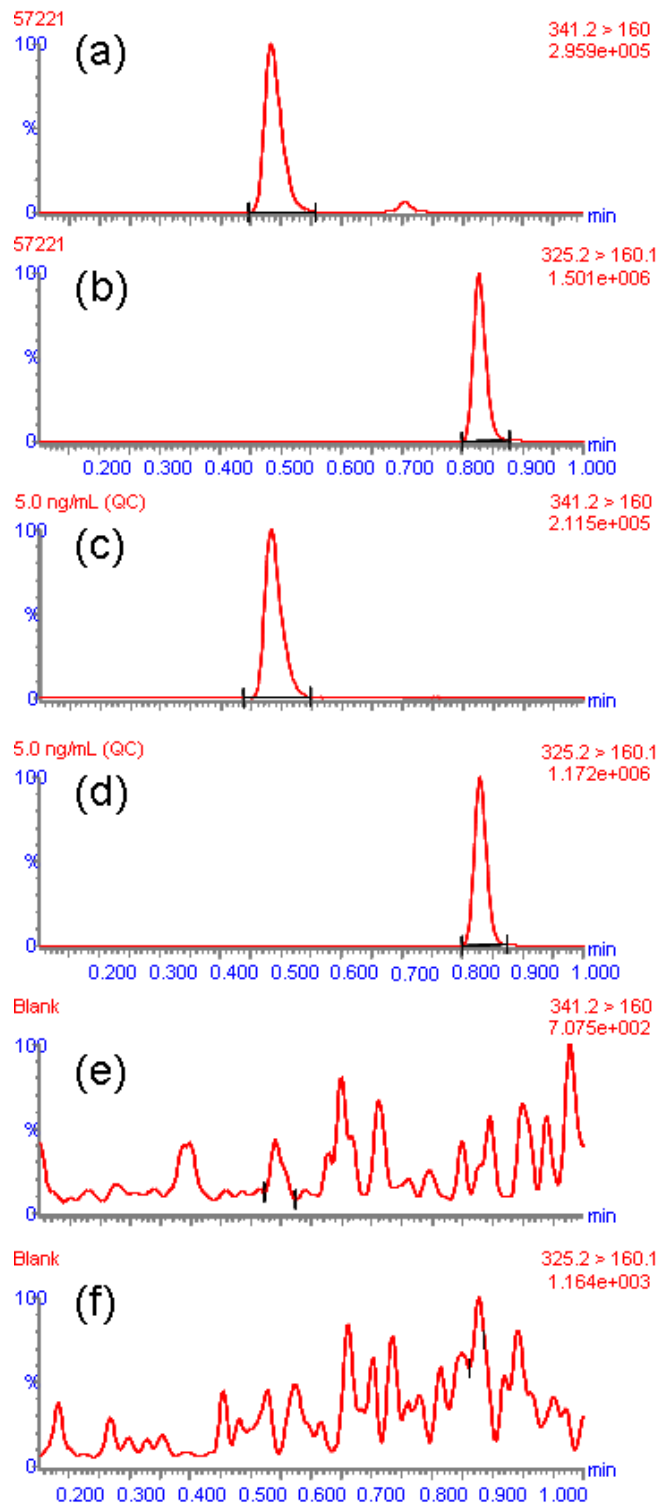


Figure 2.11. Final UPLC-MS/MS separation in: (a) volunteer quinine, (b) volunteer (3S)-3-hydroxyquinine, (c) 5 ng/mL QC quinine (d) 5 ng/mL (3S)-3-hydroxyquinine, (e) blank quinine trace (f) blank (3S)-3-hydroxyquinine trace.

2.3.4 Performance of assay

The method was evaluated in terms of accuracy, precision, linearity (Table 2.3) and specificity for both analytes. Tables 2.4 and 2.5 show the precision and accuracy for quinine and (3S)-3-hydroxyquinine respectively from QC samples analysed at three concentration levels over three different days. No extraction was deemed necessary due to the elevated concentrations of quinine and (3S)-3-hydroxyquinine present in the samples. This allows for matrix effects to be heavily diluted out in the devised dilution scheme removing the necessity for solid-phase or liquid-liquid extraction. Calibration curves were constructed based on the respective peak area ratios of quinine and (3S)-3-hydroxyquinine to quinine-D₃ versus their known concentrations providing a 1/concentration linear regression.

Table 2.3. Linearity of quinine and 3-hydroxyquinine from 0-20 ng/mL performed over 3 days.

Analyte	Calibration Equation ^(a)	r ² ^(b)	% RSD ^(b)
Quinine	y = 0.738(0.0160)x - 0.0415(0.00478)	0.9980	(± 0.178)
3(S)-3-hydroxyquinine	y = 0.187(0.00861)x - 0.0142(0.00441)	0.9977	(± 0.137)

(a) n = 3, data are mean (SD)

(b) n = 3, data are mean (%RSD)

Calibration curves were constructed from 0 to 20 ng/mL for quinine and (3S)-3-hydroxyquinine in order to assess the reproducibility and accuracy of the LC-MS method for quantitative purposes. Pooled QC solutions were prepared separately at 1 (LLOQ), 5 and 20 (ULOQ) ng/mL and assessed for deviation from the daily preparations of calibration curve performed over 3 days with 6 injections of each control injected per day. All solutions contained 5 ng/mL quinine-D₃ internal standard. Intra and inter batch accuracy and precision were found to be ≤ 10% for both quinine and (3S)-3-hydroxyquinine, and the data is summarised in Tables 2.4 and 2.5 respectively. Linearity coefficients (*r*²) were found to be ≥ 0.995 over the order of concentration required, as shown in Table 2.3. Also illustrated in Table 2.3 are mean intercept and slope data determined from 3 separate preparations of the calibration curve, notably intercepts for both analytes were very close to zero indicating carryover was indeed eliminated. Figure 2.11 (e) and (f) show a blank injection determined after the highest calibrant. All quoted LOQ data relate to diluted urinary sample concentrations. The method presented here provides rapid quantification of quinine and its major metabolite (3S)-3-hydroxyquinine accomplishing a sample throughput

of 25 per hour. This is a remarkable improvement to previously reported methodologies, which have run times of 22 minutes [130] and 20 minutes [132] respectively, affording measurements from a large cohort of samples to be realised in a short time frame.

Table 2.4. Accuracy and precision for quinine (n=3 day, six replicate injections per day)

Theoretical Conc. Of Quinine (ng/mL)	Intra Batch			Inter Batch
	Day 1	Day 2	Day 3	
1.0 (LLOQ)				
%CV (6 Injections)	7.20	4.29	8.35	6.61
%Accuracy	99.50%	106.57%	96.93%	101.00%
5.0				
%CV (6 Injections)	4.31	9.90	2.83	5.68
%Accuracy	102.49%	103.31%	97.43%	101.08%
20 (ULOQ)				
%CV (6 Injections)	2.95	4.74	3.89	3.86
%Accuracy	102.01%	103.23%	100.65%	101.97%

Table 2.5. Accuracy and precision for 3-hydroxyquinine (n=3 day, six replicate injections per day)

Theoretical Conc. Of (3S)-3-hydroxyquinine (ng/mL)	Intra Batch			Inter Batch
	Day 1	Day 2	Day 3	
1.0 (LLOQ)				
%CV (6 Injections)	6.50	8.57	5.14	6.74
%Accuracy	100.17%	98.68%	93.60%	97.48%
5.0				
%CV (6 Injections)	7.09	6.92	6.08	6.70
%Accuracy	98.55%	98.17%	97.75%	98.16%
20.0 (ULOQ)				
%CV (6 Injections)	2.95	5.72	4.03	4.23
%Accuracy	101.79%	95.80%	101.54%	99.71%

Chromatographic robustness was achieved throughout the course of running this method for a large number of samples from a phenotyping study. Table 2.6 highlights the retention time precision of each analyte determined from QC injections, the relative retention times are also shown as ratios of quinine / (3S)-3-hydroxyquinine. Reproducibility was found to be $< \pm 0.5\%$ RSD based on 58 injections for both retention time and relative retention of the analytes. Using a mobile phase buffer at pH 10.0 and a slightly elevated column temperature of 40 °C, approximately 1700 injections have been made on the same column without any appreciable shift in retention time or deterioration in peak shape.

Table 2.6. Retention time robustness metrics based on QC injections.

Analyte	Retention Time, mins ^(a)	% RSD
Quinine	0.835	(± 0.254)
(3S)-3-hydroxyquinine	0.487	(± 0.219)
Relative Retention ^(b)	1.715	(± 0.289)

(a) n = 58, data are mean (RSD)

(b) n = 58, data are mean (RSD) as (3S)-3-hydroxyquinine/quinine retention times

The method described here can be utilised to quantitatively assess the transformation of quinine to (3S)-3-hydroxyquinine as a specific marker for CYP 3A4 enzyme activity on a large sample size epidemiological study. A summary of diluted urinary concentrations determined from post-administration of quinine in volunteers are shown in Table 2.7.

Table 2.7. Summary of 10 volunteers post-administration diluted urinary concentrations.

	Quinine conc. (ng/mL)	(3S)-3-hydroxyquinine conc. (ng/mL)
Volunteer 1	3.0	3.4
Volunteer 2	6.6	8.3
Volunteer 3	6.3	6.6
Volunteer 4	3.1	3.1
Volunteer 5	4.4	3.8
Volunteer 6	4.3	15.1
Volunteer 7	6.3	11.9
Volunteer 8	2.4	5.1
Volunteer 9	7.7	10.7
Volunteer 10	3.9	4.7

2.4 Conclusion

A rapid and simple method was developed for the analysis of urine samples collected post-dose from the administration of the drug quinine. Quantification of quinine and (3S)-3-hydroxyquinine could be realised using a mobile phase at pH 10.0, resulting in highly symmetrical peak shapes. Heavy dilution of urine samples removed the necessity for sample clean-up or concentration by either liquid-liquid or solid-phase extraction. Accuracy, precision and linearity were all found to be acceptable. The findings on the application of this methodology to a large sample cohort have been reported elsewhere by Ahmadi *et al.* [145] for a genetic epidemiological study. It is clear that studies requiring such throughput would not have been achievable without the use of UPLC-MS technology.

Chapter 3

Investigation into the use of a forced-air thermostat for performing elevated temperature UHPLC separations

Abstract

This chapter deals with the integration of a thermostatic device for developing liquid chromatography separations at elevated temperatures, potentially up to 200 °C. As a control comparison, the standard Acquity oven was used to benchmark column/system performance. During this evaluation it was discovered through a set of experiments and articles in literature, that forced-air thermostats are perhaps not ideal for achieving the highest possible efficiency of a liquid chromatography column. As a means to alleviate this obstacle the hypothesis of using a column format which has a thinner wall was evaluated. This entailed comparing standard 2.1 mm ID column formats except the thick steel casing was reduced, thereby significantly decreasing the surface area available for heat transport to the surroundings to that of unmodified hardware. Data is presented which illustrates the impact of extra-column volume on observed chromatographic efficiency, the influence of thermostat-type on retention factor and the assessment of thin walled column hardware operated under forced-air conditions.

3.1 Introduction

The advent of ultra-pressure liquid chromatography has undoubtedly attracted significant interest since its inception by Jorgenson and co-workers [80, 81]. Subsequent commercialisation of appropriately robust instrumentation to succeed conventional pressure systems is fast becoming more prevalent [146]. The drive to do so is based on the well established theoretical framework of Saleem and Knox [147] published in 1969, whereby the decrease in particle size affords lower plate heights in accordance to the following relationship [148]:

$$h_{\min} = A + 2\sqrt{B C} \quad (3.1)$$

Where A is Eddy dispersion, B is axial diffusion and C is resistance to mass transfer. Not only is the drive to the smaller particle packed column challenging in terms of manufacturing packing materials with acceptable size distributions, but also the necessity to reduce system volumes when operating such columns [38]. It is essential that the smaller peak volumes are accommodated by appropriate connections before and after the separation in order to preserve the performance obtained using these modern ultra-high pressure liquid chromatographs.

The utility of sub-2 μm particles does indeed afford high efficiency separations in short analysis times, however migration linear velocities during the operation of columns packed with small particles can become disturbed by frictional heating effects. These effects are amplified depending on where the column is stored during operation and how well/poorly heat is transferred to the surroundings. The way in which heat is dissipated from a column is dependent on the thermal environment in which it is placed i.e. if a column is either insulated or placed under conditions where convection is promoted. There are two extremes which give rise to different column thermal behaviors, which impact directly on chromatographic performance.

Isothermal and adiabatic conditions give rise to different thermodynamic effects within a column and are outlined below:

- Isothermal conditions (temperature of the chromatographic system remains constant) lead to the formation of a radial temperature gradient (Δ_{RT}) that will result in significant contributions to band broadening due to exaggeration of the parabolic flow profile. This effect is a function of the volumetric flow rate (F_v), pressure drop (ΔP), heat conductivity of the packed bed (λ_p) and the length of the column (L) expressed as [149, 150]:

$$\Delta_R T = \frac{F_v \Delta P}{4\pi \lambda_p L} \quad (3.2)$$

- Adiabatic conditions (no heat loss to or from the system) on the other hand will provide an axial thermal gradient (Δ_{LT}) that contributes very little to any band broadening (assuming negligible contribution via backflow of heat along the column wall). This contribution is a function of the pressure drop (ΔP) and the specific heat capacity of the eluent per unit volume (C_p) [148]:

$$\Delta_L T = \Delta P / C_p \quad (3.3)$$

Disturbance of the linear velocities is exasperated depending on the degree of thermal insulation (Figure 3.1) of a column and as a result operating near to adiabatic conditions yields optimum performance [151]. In the case where good heat dissipation across the radial coordinate of the column takes place, retention factors are resultantly higher at the wall region than in the center of a solute band. On the contrary, if poor heat dissipation takes place, such as a column operated under adiabatic conditions (i.e. still-air thermostat) the opposite effects are observed. This phenomenon was initially investigated by Horvath [152] in an earlier paper and subsequently by Poppe [150, 153]. Recent evaluations by de Villiers [154], McCalley [155] and Cabooter [25] have illustrated how these effects become increasingly problematic with

decreasing particle sizes. Guiochon outlined the optimal thermal operating environment for increasingly finer particles, stating that if the power of frictional heating exceeds 4 W/m when operated under isothermal conditions the advantages of utilising such columns diminishes [156].

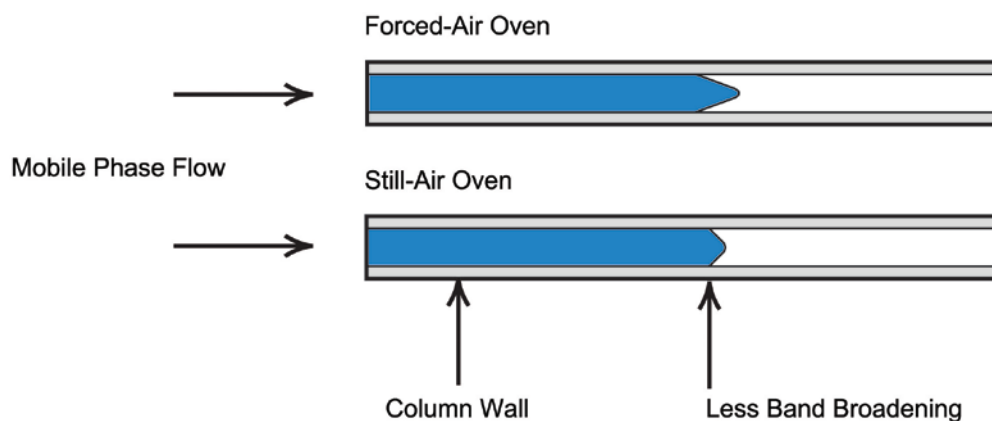


Figure 3.1. Effect of thermal environment on the migrational linear velocities within a column.

One way of achieving even higher separation efficiencies is to couple columns together in order to increase plate count [63, 157], however in doing so the pressure required to reach the optimum linear velocity increases. The result of this is an increase in heat generation since the power produced is dependent on the pressure drop (ΔP) across the column and the volumetric flow rate (F) as shown by the following equation [158]:

$$Power = \Delta PF \quad (3.4)$$

The constraint of pressure can somewhat be alleviated by operating at elevated temperatures which affords a decrease in the viscosity of the mobile phase, allowing flow rates otherwise inaccessible to be utilised. One of the main problems associated with practicing elevated temperature (i.e. 120-200 °C) is the lack of commercially available equipment and or inclusion of this facility into manufacturers' instruments. Obviously operating in this temperature range requires the stationary phase to be able to withstand such conditions. Furthermore, due to the frictional heating effect, increases in efficiencies gained with modern column technologies may be deteriorated by operation under inappropriate thermal environments.

The aims of this chapter were initially to evaluate the effectiveness of incorporating a high temperature column thermostat into the Waters Acquity UPLC setup. The limitation of the standard configuration being that the upper temperature limit of the Acquity Column Oven (ACO) was only 60 °C. However, due to the impact of the thermostat type on column performance several investigations were undertaken. Firstly, the influence of column wall thickness on chromatographic performance relative to the applied thermostatic environment was investigated. Secondly, determine changes in retention due to the occurrence of longitudinal temperature gradients within the column. Also, to emphasise on the importance of minimising the impact of extra-column band broadening on the operation of ≤ 2.1 mm ID column formats.

3.2 Experimental

3.2.1 Chemicals

Methanol and acetonitrile were of HPLC grade (Fisher Scientific, UK). Water was obtained from a MilliQ (Millipore, UK) system fitted with a 0.22 μm filter. Thiourea, naphthalene, acenaphthalene, nitrobenzene and octanophenone were purchased from Sigma-Aldrich (Poole, UK).

3.2.2 Instrumentation and methodology

Chromatography was performed on a Waters ACQUITY UPLC[®] system equipped with an ACQUITY UPLC[®] PDA detector module (Waters, Milford, MA). All data was collected at 254 nm at a data capture rate of 40 Hz in order to ensure adequate data points across the chromatographic peaks. Injections were performed in the full-loop mode using a 1 μL sample loop unless stated otherwise, with wash solvents of the same composition as the mobile phase used. Measurements were made based on at least duplicate injections. Curves for van Deemter plots were determined by increasing the applied flow rate from an initial 50 $\mu\text{L}/\text{min}$ to the maximum recommended operating pressure (≤ 400 bar for 3 μm and ≤ 1000 bar for 1.9 μm particles). Data was captured and integrated using Empower2 (Waters, Milford) acquisition software and peak widths measured at either half or 13.4% height. Corrections for extra-column dispersion were determined using a zero-dead volume union in place of the column with the same test solute used to construct the van Deemter curve. Mobile phases used in this study were premixed and compositions are as indicated in the relevant figures. All samples were prepared in the mobile phase at 10 $\mu\text{g}/\text{mL}$ unless stated otherwise. thiourea was used as the unretained marker.

- A Polaratherm Series 9000 column oven (SandraSelerity, Belgium) was configured with the active pre-heater and post-column cooling where specified (Figure 3.2).

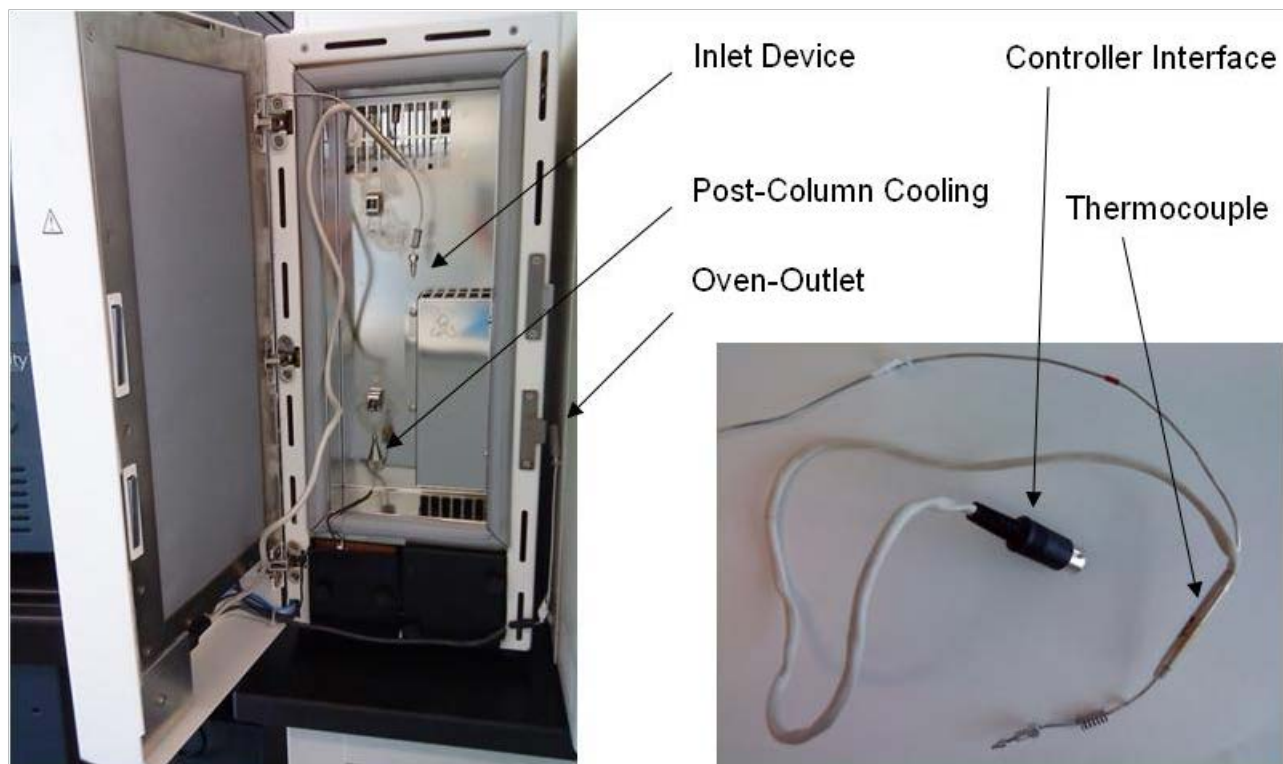


Figure 3.2. Polaratherm 9000 forced-air column thermostat (near-isothermal conditions).

- The Waters ACQUITY column oven was configured as the standard configuration inclusive of the pre-heating coil assembly unless stated otherwise (Figure 3.3).

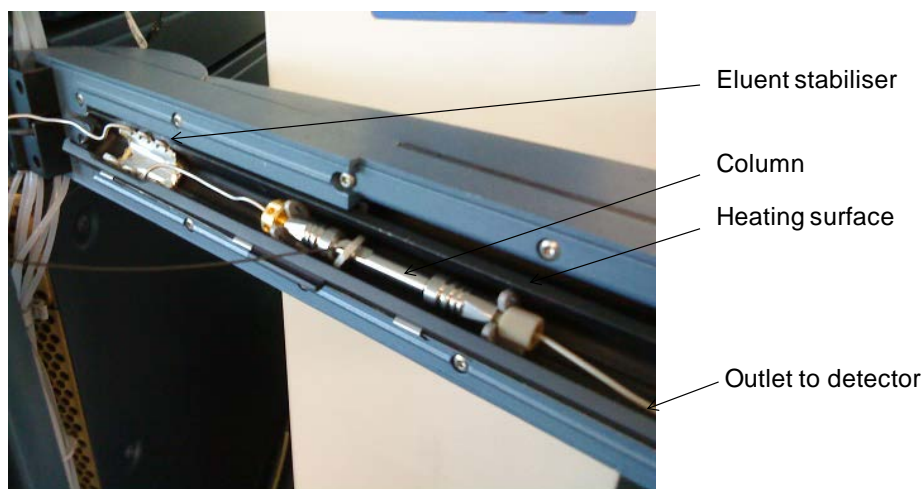


Figure 3.3. Acquity Column Oven (ACO) for near-adiabatic column heating.

Columns with a modified wall thickness (Figure 3.4) were supplied by Thermo Fisher Scientific (Runcorn, UK) as part of a collaborative research project into the effect of column hardware on chromatographic performance using elevated temperatures and forced-air thermostats. Wall thicknesses of 0.084" and 0.026" were used for this study. These were packed with either 3 μm or 1.9 μm Hypersil GOLD silica derivatised with a C18 alkyl bonded phase. Columns were 15 cm long with an internal diameter of 2.1 mm.



Figure 3.4. (Top) Standard 0.084" Thermo column hardware and (Bottom) modified 0.026" hardware.

3.3 Results and discussion

3.3.1 Preliminary data comparing column thermostatic devices

In order to determine the optimal configuration of the combined Acquity and Polaratherm set-up, experiments were conducted to compare the holistic efficiencies achieved with the standard UPLC operating arrangement. Firstly, van Deemter plots were constructed using a 100 mm x 2.1 mm i.d. 1.7 μm BEH C18 Acquity column in the standard instrument configuration at 60 $^{\circ}\text{C}$.

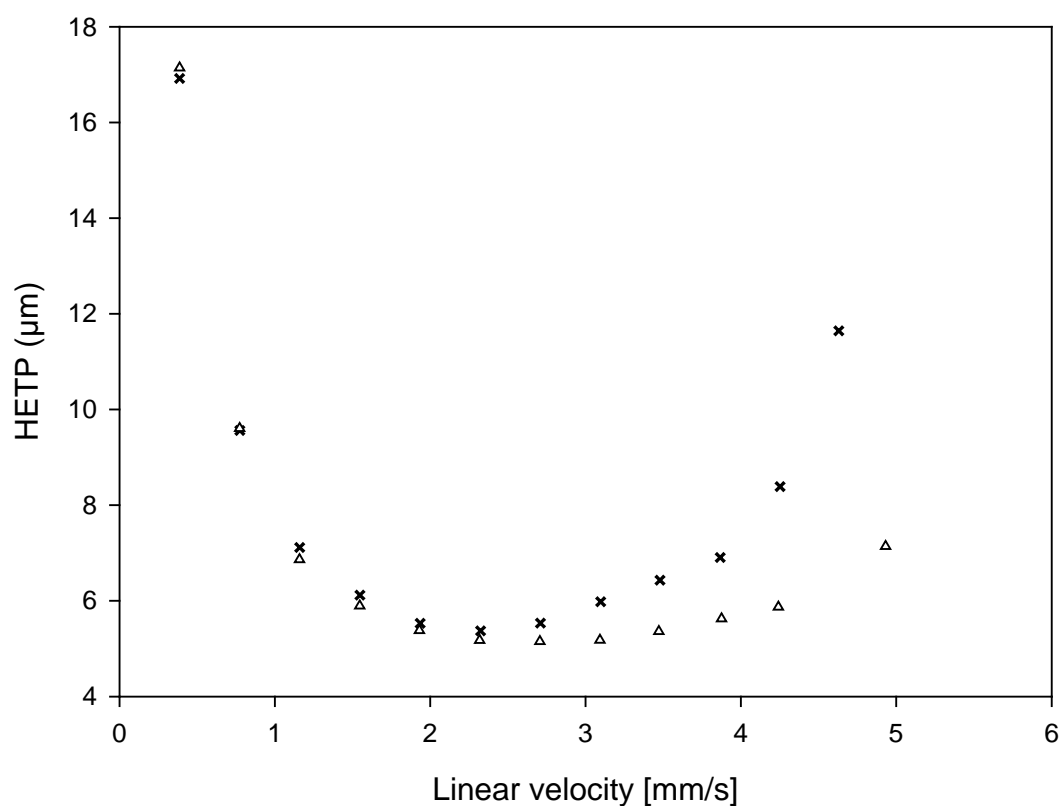


Figure 3.3. Comparison between coiled and un-coiled stainless steel tubing inlet devices. Where Δ is the coiled and x the uncoiled column inlet respectively.

The Acquity UPLC has two standard tubing configurations, depending on the requirement for mobile phase temperature stabilisation. Figure 3.3 shows a comparison between the inlet temperature stabiliser assembly and the standard steel inlet tubing. The temperature stabiliser is a piece of coiled tubing which is placed in direct contact with the heated surface of the Acquity

column oven. The van Deemter plot for naphthalene exhibits a distinct region at higher linear velocity (> 2 mm/s), a distinct divergence in the curves was observed when using the standard inlet tubing. This can be ascribed to insufficient mobile pre-heating. At low linear velocities, the differences in plate height are almost negligible between the two inlet configurations, implying that at these flows column performance is not dependent on pre-heating. The temperature stabiliser unit allows for operation at higher flow rates without drastically compromising the holistic system efficiency and therefore faster separation can thus be achieved.

The Polaratherm was configured with the UPLC incorporating the pre-heating assembly and the post-column cooling unit. This meant introducing further lengths of tubing into the system to incorporate the UV detector post-Polaratherm setup. Figure 3.4 shows the van Deemter experiment comparing the observed efficiencies (i.e. uncorrected for extra-column dispersion) when using the Polaratherm forced-air oven. In both instances the temperature was the same, heating the column and eluent to the desired 60 °C.

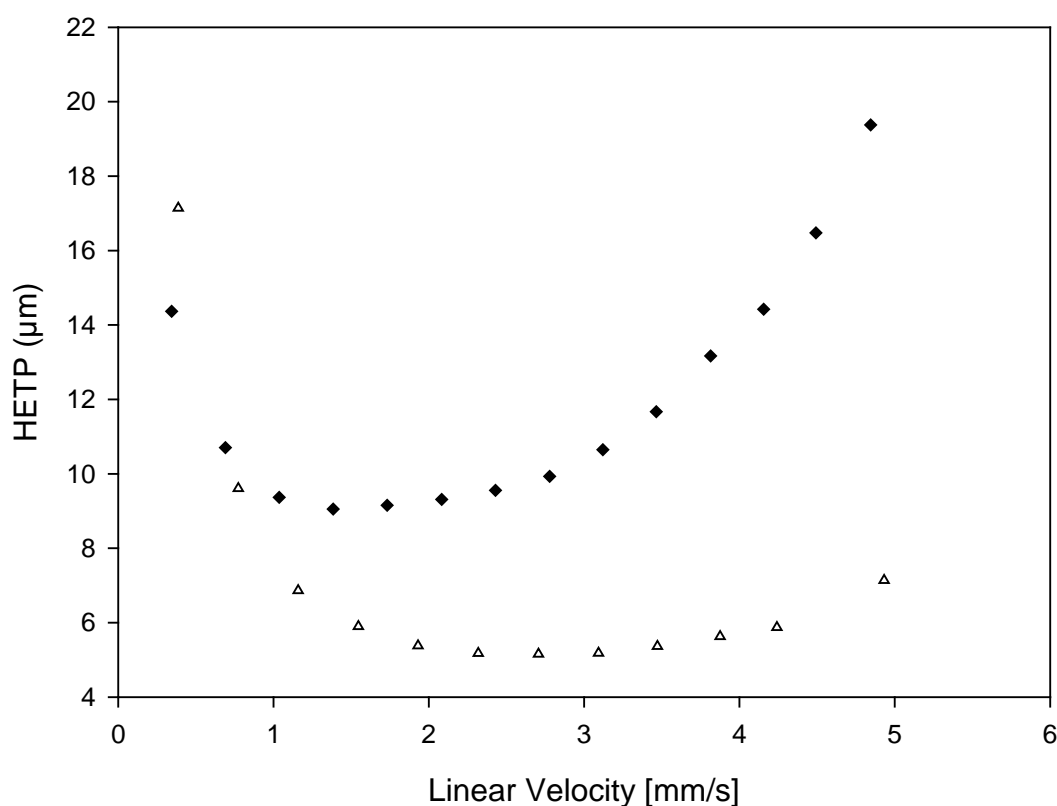


Figure 3.4. Comparison between Polaratherm (◆) and ACO (Δ) at 60 °C.

As shown in Figure 3.4, using the Polaratherm in its standard configuration with the Acquity UPLC a loss in efficiency for naphthalene of approximately 50% was found. Unsurprisingly, the tubing required to plumb the convection air oven for use in line with the chromatographic system drastically contributes to extra column band broadening effects. Clearly, the use of columns of ≤ 2.1 mm ID is not entirely suitable for operation with such extra-column volumes. Furthermore, the strong upturn in the van Deemter curve constructed using the Polaratherm setup implies that frictional heating effects are also contributing to losses in performance. Two facets of using the Polaratherm then needed to be addressed. Reduction in both the extra-column volume and the formation of radial temperature gradients was necessary. The former could be achieved by omission of the pre-heating and post-column cooling devices and replacing with minimal lengths of small bore tubing. The latter entailed developing a more subtle solution.

3.3.2 Evaluation of wall thickness on column performance

3.3.2.1 Operation of 3 μm packed columns using the Polaratherm forced-air oven with MeOH as the organic modifier.

Here the oven contains a fan that distributes the heat uniformly across the column compartment. It also contains an active mobile phase pre-heater which can adjust the incoming mobile phase to any desired temperature up to 200 °C. The post-column cooling function was omitted and replaced with a minimal length of 0.005" ID PEEK tubing so as to minimise extra-column volume. It has been shown by other workers [25, 154, 155] that transfer of the frictional heat generated within the column to the surrounding environment enhances radial thermal gradients which result in diminishing column performance. When the set temperature of the thermostat is conditioned by circulated air (Polaratherm), the column is said to operate near-isothermally; i.e. secondary heat which is formed due to frictional effects, will be predominantly lost through the column wall under these circumstances.

Ultimately the objective was to investigate the use of a commercially available forced-air thermostat (Polaratherm), the design of which is perhaps the most flexible in terms of use, heating, and cooling capacity. Employing thermal gradient programming, as in gas chromatography, would afford the liquid chromatographer an extra separation parameter and the possibility to eliminate the use of organic solvents. However, as shown by other workers [25, 154, 155] and by our data, it is the still-air conditions that are the most favorable for preserving column performance.

Figure 3.5 shows van Deemter curves constructed for columns of 0.026" and 0.084" wall thicknesses under forced-air conditions at 40, 50 and 60 °C. Different curve behavior was observed between the two evaluated housings. The modified column wall thickness is ~3 times thinner than the standard hardware, and this in essence would yield different heat flux behavior along the wall of the column towards the start of the packed bed. It is also interesting to note that the HETP minima appear to decrease and shift towards a higher linear velocity with increasing temperature in the forced air oven with the 0.084" (2.1 mm) wall thickness. However, this is a feature already described in the literature [63].

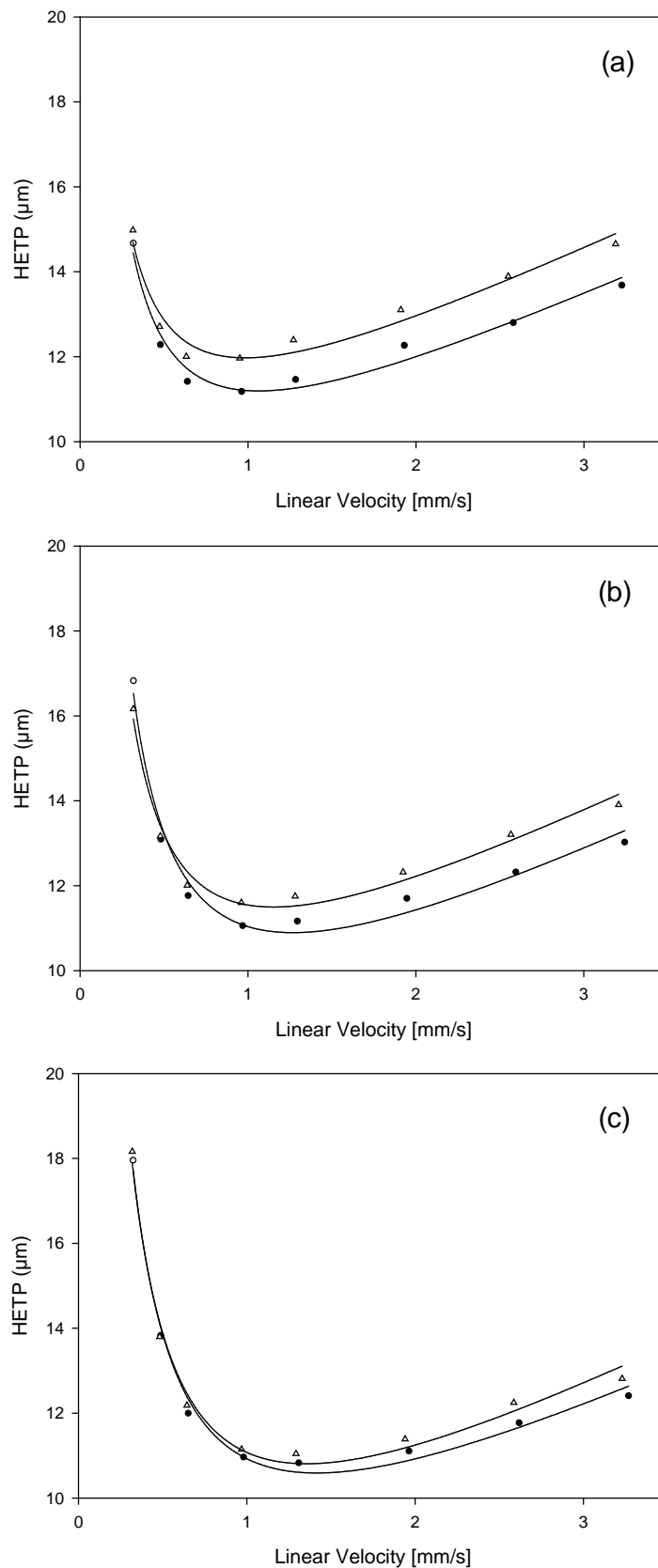


Figure 3.5. Corrected van Deemter curves for (a) 40 °C (b) 50 °C and (c) 60 °C. Columns (● 0.026" and Δ 0.084") 150 x 2.1 mm ID, 3 μm Hypersil GOLD 30:70 (H₂O:CH₃OH) mobile phase, 1 μL injection full loop (0.2 mg/mL naphthalene). Data was measure at 13.4% peak height.

A possible explanation for this observation is that at lower temperatures, effective heat transfer is not taking place. This may be due to a characteristic of the reduced surface area by which heat can be transferred to the surroundings in comparison to the standard hardware. The 0.026" wall thickness column performed optimally in comparison to the standard 0.084" under all investigated temperatures. No firm conclusions can be drawn here as there are doubts about the differences in the packing quality of both columns. Also the major differences between their performances should be apparent in the C-term region of the van Deemter curves. Table 3.1 shows the fitting coefficients determined for the van Deemter curves constructed in Figure 3.5.

Table 3.1. van Deemter curve analysis based on Figure 3.5 determined under forced-air conditions. Where (a) 40 °C (b) 50 °C and (c) 60 °C.

		Wall Thickness	
Term		0.026"	0.084"
a)	A (μm)	7.27	8.21
	B ($\times 10^{-4}$ mms^2/s)	2.09	1.85
	C (ms)	1.84	1.92
	H_{min} (Calc.)	11.19	11.98
	u_{opt}	1.06	0.98
b)	A (μm)	5.85	6.85
	B ($\times 10^{-4}$ mms^2/s)	3.20	2.68
	C (ms)	1.99	2.01
	H_{min} (Calc.)	10.90	11.50
	u_{opt}	1.27	1.15
c)	A (μm)	5.08	5.08
	B ($\times 10^{-4}$ mms^2/s)	3.91	3.88
	C (ms)	1.95	2.11
	H_{min} (Calc.)	10.59	10.81
	u_{opt}	1.42	1.35

Certainly, there are differences in the packing qualities of the two columns investigated here, as is shown by the A-term coefficients in Table 3.1. Carr *et al.* [159] postulated that increasing temperature might improve radial solute diffusion whilst also assisting laminar flow discrepancy, resulting in improved A-term coefficients. However, it is interesting that for each investigated temperature that the C-terms are slightly smaller with the thinner walled column and that the B-terms are also larger than those found with the standard hardware.

There are two types of radial thermal gradients possible; in the case of a negative type, the packed bed nearest the column wall is cooler than the center imposing differential retention across the radius of the column. The positive type of radial thermal gradient is the converse of the negative type; this comes about due to maximal heat being present towards the outlet which transfers back along the axis of the column towards the inlet by conduction through the steel wall. Under certain conditions both of these gradients compensate one another, therefore any deleterious effect on column performance may be reduced. This was implied by Kaczmarek and co-workers [160] however their conclusions were based on operation under natural convection (still-air) conditions. Likewise, this can be perceived as a similar effect noted earlier by Poppe *et al.* [153], whose experiments included mismatching the mobile phase influent to the column set temperature. This in effect was used to attenuate the sample plug retention profile as such to compensate for radial temperature gradient induced solute band distortion.

The quantity of heat (Q) that can be expected to be transported back to the column inlet is based on the thermal conductivity of the tube. This can be described by Fourier's law in the following equation [161]:

$$Q = -k * A * dT / L \quad (3.5)$$

Where k is the thermal conductivity of the column wall, L is the column length and A is the column wall cross section. The function dT is the measured axial temperature difference which should be expectantly similar between the two column formats. Therefore, with a thinner column wall a smaller backflow of heat would be found. Essentially this omits heat flux contributing to any sort of compensatory effect observed. It is more likely, given that the cross section of the thin wall column is three times smaller than the standard hardware, that reduced surface area is the feature which results in lessened heat loss. Moreover, the heat flux would be larger with the standard thicker-walled column and may impact more detrimentally on the complex thermal gradient behavior within these sorts of columns.

3.3.2.2 Operation of 1.9 μm packed columns using ACN as the organic modifier.

The effect of decreasing particle diameter in liquid chromatography is well documented. However, the resulting pressures and volumetric flow rates required to take advantage of the lower C-term dominated region of sub-2 μm materials results in much larger frictional heating. Following on from the investigation with the 3 μm phase using methanol as the organic modifier, the 1.9 μm variant was evaluated in the same column housing format as described previously. This was carried out using an aqueous-acetonitrile mobile phase in order to access to the highest possible volumetric flow rates. Decreasing particle diameter results in an increase in pressure drop (ΔP) according to the Darcy equation:

$$\Delta P = \phi \frac{\eta L u}{d_p^2} \quad (3.6)$$

Where η is the viscosity of the mobile phase, ϕ is the flow resistance of the packed bed, u linear velocity, L is the length of the packed bed and d_p is the particle diameter of the stationary phase material.

As shown in Figure 3.6, the adiabatic-type thermostat (ACO) preserves column performance and no deterioration in plate height was observed. At linear velocities greater than 2.0 mm/sec divergence in performance becomes apparent as a function of the column thermostat. The 0.026" walled column under adiabatic conditions (ACO) significantly outperforms the 0.026" walled column under isothermal conditions at higher linear velocities. This is due to the fact that the adiabatic conditions will only produce longitudinal thermal gradients (no loss in efficiency) whilst the isothermal conditions produce radial thermal gradient which yield significant losses in efficiency. Any differences in efficiency between the 0.026" and 0.084" walled columns under isothermal conditions at higher linear velocities are likely a function of the lower surface area of the former.

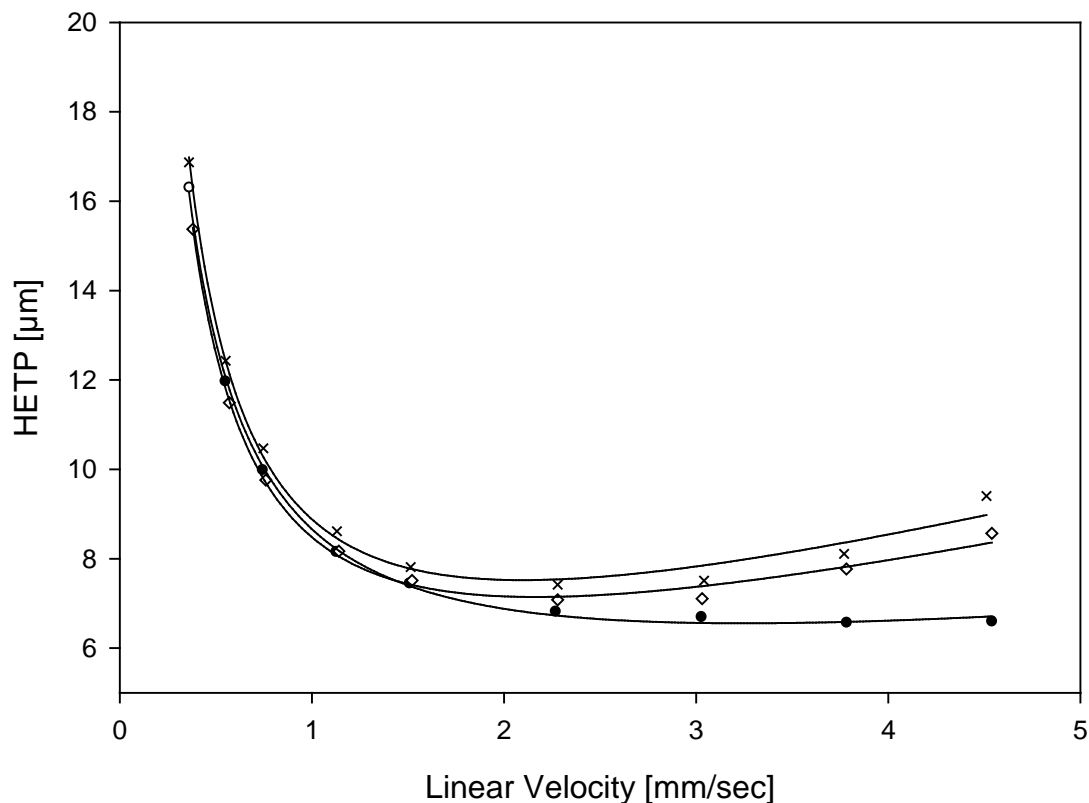


Figure 3.6. Corrected van Deemter curves for naphthalene ($k \sim 4$) on 150 x 2.1 mm ID, 1.9 μm Hypersil GOLD, 40:60 v/v $\text{H}_2\text{O}:\text{ACN}$ (30 $^\circ\text{C}$) in different column hardware • (0.026" ACO), x (0.084" POL), ◇ (0.026" POL) at 1000 bar ΔP_{max} .

Table 3.2 shows the determined van Deemter coefficients based on Figure 6. A smaller C -term was observed for the 0.026" wall thickness column however this was not necessarily significant. In comparison, using the modified column in the ACO the determined C -term coefficients were approximately 50% lower. Although using thin walled columns is an interesting hypothesis, it is unlikely that such column formats be implemented commercially unless safety concerns are addressed also. It should be postulated that more interrogative measurements be made in future studies, such as accurate monitoring of the temperature profiles across the column axis and of the emerging mobile phase post-column. Also, thermal imaging of the chromatographic system whilst in operation could also be of interest. Moreover, contributions to heat conductivity coming from the stationary and mobile phases should also be characterised. These features would certainly contribute to the differences in thermostat dependent chromatographic behavior. It would certainly be more interesting to observe chromatographic performance using more thermally conductive mobile and stationary phase materials in comparison to those used here.

Table 3.2. Deemter curve analysis based on Figure 3.6.

Term	(ACO) 0.026"	(Polaratherm) 0.026"	(Polaratherm) 0.084"
A (μm)	3.84	2.89	2.78
B (x10 ⁻⁴ mms ² /s)	4.40	4.62	4.97
C (ms)	0.42	0.98	1.13
H _{min} (Calc.)	6.56	7.15	7.52
U _{opt}	3.25	2.17	2.10

3.3.2.3 Effect of increasing flow rate on retention

As shown in Figure 3.7 retention is affected by the thermostat type for the 1.9 μm particle size using the standard column format. Several compounds of increasing hydrophobicity were chosen to probe how the residence time within the column would be influenced by the longitudinal thermal gradient. As is the case for the adiabatic situation a decrease in k was observed for all analytes across the linear velocity range which can be accounted for due to the increasing formation of a longitudinal thermal gradient. The increasing formation of a longitudinal thermal gradient results in losses in retention in accordance to the van't Hoff isotherm. Unusually, under isothermal-like conditions (Polaratherm forced air oven) the poorly retained nitrobenzene Figure 3.7 (a) exhibits almost constant k values across the linear velocity range, however the more strongly retained probe solutes showed an increase in retention with increasing linear velocity. This can be correlated to the observations of McCalley and co-workers [162, 163] who illustrated that an increase in pressure influences the difference in partial molar volume (ΔV) of the solute which allows further partitioning into the stationary phase, thereby increasing retention. If effective removal or re-distribution of the longitudinal thermal gradient occurs due to the forced-air thermostat and an increasingly isothermal environment results, then any resulting retention factor increase can be associated by the following:

$$\left[\frac{d(\ln k)}{dP} \right]_T = \frac{-\Delta V}{RT} + \left[\frac{d(\ln \beta)}{dP} \right]_T \quad (3.7)$$

Where ΔV is the change in the molar volume of the solute in the stationary and mobile phases and β is the phase ratio.

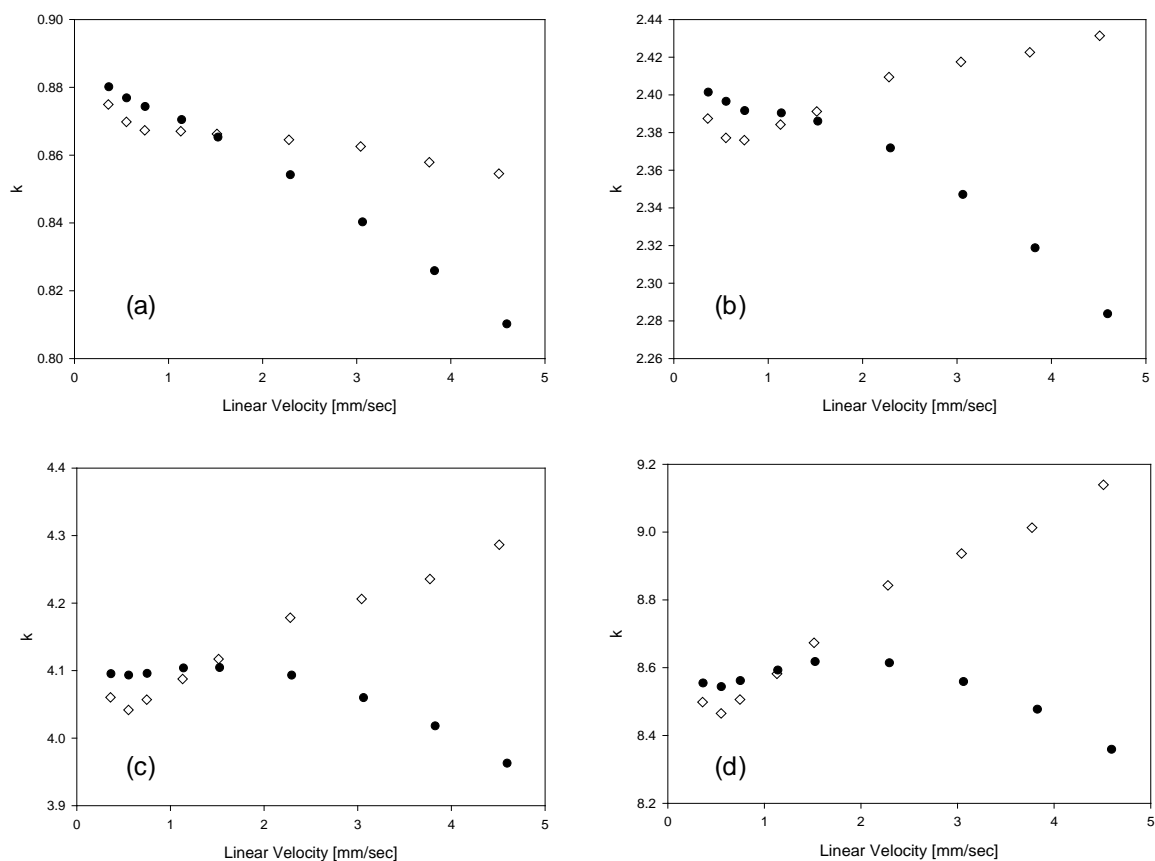


Figure 3.7. Retention factors as a function of linear velocity and thermal environment at 30 °C, (a) nitrobenzene, (b) naphthalene, (c) acenaphthene, (d) octanophenone. • (ACO), ◊ (POL) using 150 x 2.1 mm ID, 1.9 μ m Hypersil GOLD, 40:60 v/v (H₂O:ACN).

By correcting for the contribution made by the system tubing to the observed pressure-drop the resulting isolated column pressure-drop is shown in Figure 3.8. A divergence in the pressure drop for the same column operated in the different thermal environment was observed. In effect this different behavior can somewhat explain the increase in retention factor for solutes chromatographed under forced-air convection conditions. This type of effect may well contribute to explain issues in method transferability between instrument manufacturers with differing thermostat types.

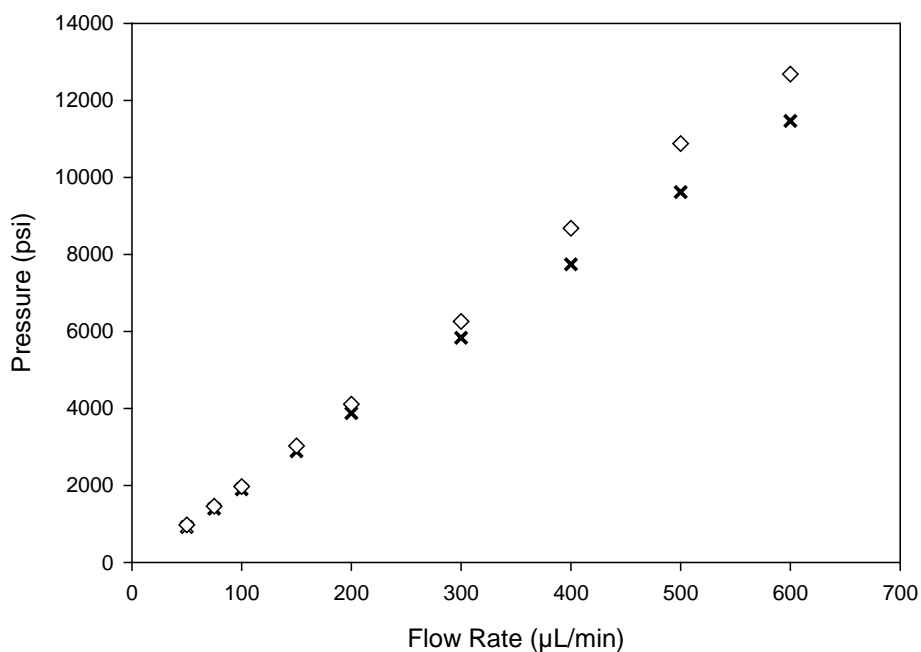


Figure 3.8. System corrected Pressure drop vs. Flow rate for 0.084" wall thickness column, 150 x 2.1 mm ID, 1.9 µm Hypersil GOLD, 40:60 v/v (H₂O:ACN) where x is ACO and ◇ is Polaratherm.

In comparison, the 3 µm data (Figure 3.9) showed similar trends to those observed by Cabooter [25] in that no significant increase in retention was observed under near-isothermal conditions, although marginal increases in retention were noted for analytes (c) and (d) in Figure 3.9 possibly owing itself to the slightly smaller particle size used in this study. This may be due to the lower power formation and distribution of thermal gradients which could directly influence pressure induced changes in retention. In the study of Cabooter and co-workers the active pre-heater was omitted from their Polaratherm based experiments, hence the difference in data presented here could be a function of this, as well as being due to the physiochemically different probe solutes.

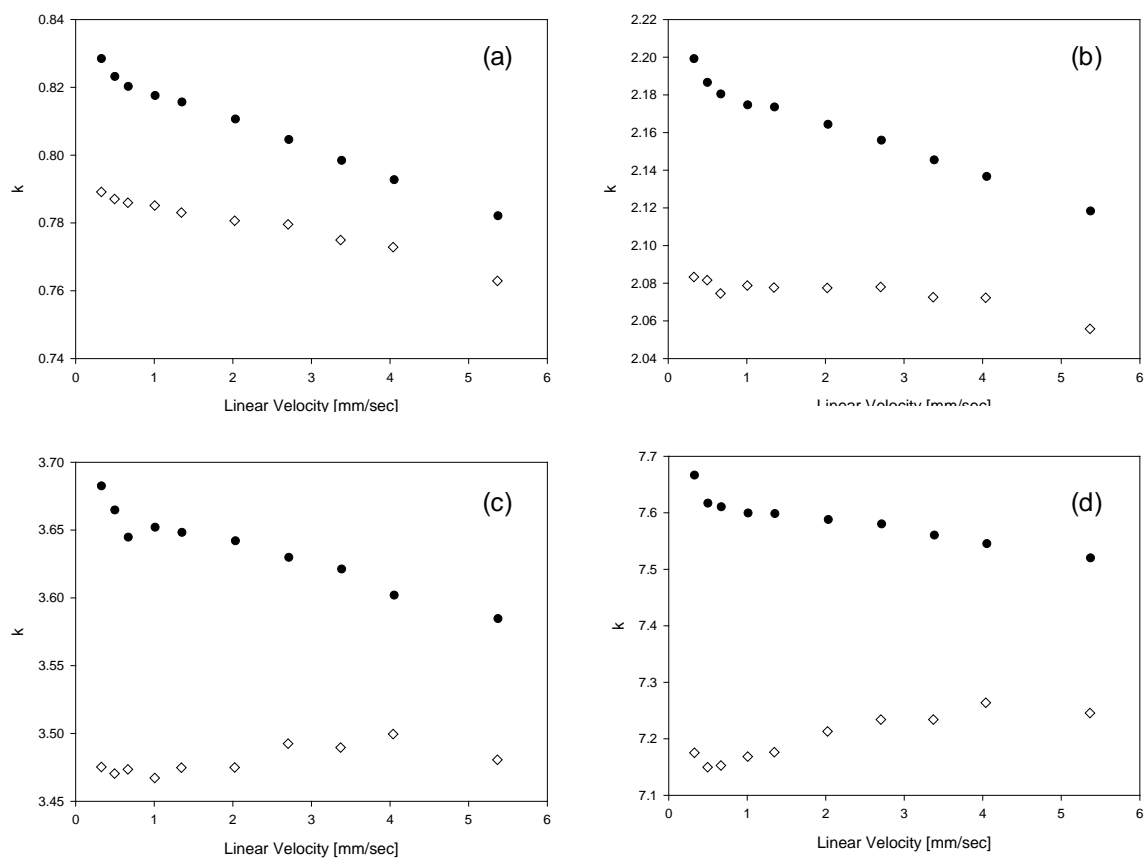


Figure 3.9. Retention factors as a function of linear velocity and thermal environment at 30 °C, (a) nitrobenzene, (b) naphthalene, (c) acenaphthene, (d) octanophenone. • (ACO), ◊ (POL) using 150 x 2.1 mm ID, 3 μ m Hypersil GOLD, 40:60 v/v (H₂O:ACN).

3.4 Conclusions

An evaluation of the performance of supra- and sub- 2 μm packed columns in two different wall thicknesses was performed. Similarly to other workers observations, it has been shown that operation of columns operated under forced-air convection conditions seriously compromises chromatographic performance due to the products of viscous frictional heating. The notion that column hardware with lower surface area characteristics may reduce losses in performance when operated further away from the near-adiabatic ideal requires further study. This should also entail columns of differing lengths and wall thicknesses as well hardware with much reduced end fittings. It is unlikely that smaller wall thicknesses than those used here could be used due to the risk of burst at pressures up to and exceeding 1000 bar. Furthermore, these results should be considered as preliminary since a larger set of sample columns of each wall thickness would help to further understand the hypothesis. Similarly, these should have approximately the same packing characteristics i.e. comparable *A*-term coefficients so as not to obscure any real effects due solely to the column hardware. It has been shown that the effect of radial thermal heterogeneity due to operating under near-isothermal conditions is less problematic working near the optimum linear velocity. Columns packed with sub-2 μm materials when operated in a forced-air thermostat were shown to give rise to an increase in their retention factor over the pressure range evaluated, with solutes of relatively higher retentivity showing the largest increases.

Clearly, if the drive to yet smaller diameter stationary phase materials is pursued, serious considerations on minimising system volumes for embracing smaller internal diameter columns must be anticipated. The use of 1 mm ID sub-2 μm packed columns was recently evaluated by Lestremau and co-workers [164] citing the necessity to operate under gradient conditions in order to overcome system volume dispersion. Intermediate cooling of the eluent between a series columns using integrated segments of active temperature modulation was developed by Broeckhoven and co-workers [165]. This was shown to alleviate the overall axial thermal gradient effect, which as implied to by Guiochon *et al.* [166] can potentially impinge on retention capacity.

Chapter 4

Investigation into the use of shell, fully porous particles and elevated temperatures in UHPLC for the highly efficient analysis of anabolic steroids

Abstract

Superficially and fully porous materials were evaluated in terms of separation performance based on Knox and kinetic plot approaches using testosterone as the probe analyte. These evaluations highlight the benefit of packing quality (lower Knox *A*-terms) and reduced axial diffusivity (lower Knox *B*-terms) in achieving the highest possible efficiency as limited by pressure. In expanding the efficiency domain and speed of analysis, elevated temperatures were also addressed using the bridged-ethylene hybrid (BEH) materials up to 130 °C. This work emphasises that in the fast analysis kinetic region that elevated temperatures are highly beneficial. In contrast, using moderate/lower temperatures was more important to adopt for longer and higher resolution separations due to the influence of temperature on axial diffusion. The elevated temperature approach also allowed for the use of ethanol/IPA as the organic modifier for reducing retention factors for steroidal substances.

4.1 Introduction

In liquid chromatography (LC) improvements in separation efficiency are usually a direct consequence of reducing the particle diameter at any fixed column length. Such improvements allow for greater chromatographic resolution, which is of particular importance for complex samples. As shown by Neue *et al.* [38] the migration to smaller particle sizes comes with it the need to operate the column at an optimum pressure which in turn yields the maximum plate number. However, as the particle size is reduced the pressure required to reach this optimum increases. The term ultra-high pressure liquid chromatography (UHPLC) was used to describe operation at ≥ 400 bar as described in the work of Jorgenson *et al.* [80, 84]. This technological advance was followed by a reduction in column internal diameter, so as to operate small particle packed columns with lower volumetric flow rates over the operating pressure range of an instrument. This minimises the effect of frictional heating which is detrimental to column performance, particularly in the C-term dominated region of the van Deemter curve. As well as shown previously in Chapter 3, several authors have reported on the operation of columns in different thermal environments. Guiochon *et al.* [156] and de Villiers *et al.* [154] strongly recommend operation of columns in as near to adiabatic conditions as possible in order to minimize the effect of radial thermal gradients prevalent at high inlet pressures e.g. at high volumetric flow rates. These observations were followed up by McCalley *et al.* [155] who compared several thermostats for use with conventional liquid chromatography. Although there are several benefits to reducing the column internal diameter such as lower solvent consumption, the packing qualities (Knox A-term) are significantly poorer than those of conventional dimensions (i.e. 4.6 mm I.D.) [30]. The advances in instrument design and small particle packed columns offer the possibility to perform analyses which are both faster and more efficient to those obtained with conventional equipment. Nevertheless, these advances are highly dependent on system volume as shown by several workers elsewhere [38, 99, 167].

Of particular interest is the adoption of superficially porous or pellicular materials as these have been shown to yield several advantages over more conventional materials. These materials were initially pioneered by Horvath *et al.* [90] and then by Kirkland *et al.* [91] however serious interest in these types of support remained dormant for several decades after their initial inception, mainly due to poor particle size distribution and limitations in loading capacity. More

recently, the group of Glennon reported [168, 169] the development of their own superficially porous stationary phases which exhibited comparable efficiencies to those available commercially. There are now a variety of marketed columns using this technology e.g. Kinetex (Phenomenex), Poroshell (Agilent) and HALO (AMT/Supelco). The synthesis of these materials results in the formation of highly monodisperse particles when compared to their fully porous counterparts. Their packing constants (Knox *A*-term) have also been found to be superior to those of fully porous nature when packed into conventional bore columns. Another advantage of these materials comes from the reduction in internal porosity resulting in smaller *B*-term coefficients [94, 170]. There are disadvantages however, particularly in that their chemical stability means pH manipulation range is inferior to that of hybrid particles. This is limiting especially for method development and also eliminates such silica based phases from operation at elevated temperatures, as they would almost certainly deteriorate rapidly under such conditions. Obviously, this is debatable depending on the presence and types of buffers used, solution pH and degree of organic fraction adopted for elution. Teutenberg *et al.* [68] compared several commercial stationary phase materials highlighting that hybrid-silicas are in fact very stable at thermal extremes relative to those based solely on silica, even when these are operated at neutral pH.

By introducing elevated temperatures (> 80 °C) analyses can become even faster and allow for the practical use of longer columns. Also, due to the impact of temperature on analyte diffusion coefficient (D_m) resistance to mass transfer is reduced and a flatter *C*-term contribution is generally observed. Antia and Horvath [171] demonstrated that reductions in viscosity and increased diffusion coefficient with temperature could lead to significant decreases in analysis time for large molecules. Similarly, the high temperature approach was shown to be useful for small molecules by Guillarme *et al.* [172] again showing advantages for decreasing analysis time. This offers a distinct advantage for large particle packed columns as faster separations can be achieved without significantly compromising efficiency. Lestremau *et al.* [32, 33] demonstrated this in an article involving conventional equipment and serially coupled columns to yield very high plate numbers. However, caution should be adopted in operating excessively long columns at such temperatures as operation below the optimum linear velocity results in increasingly inferior performance. This was referred to by Plumb *et al.* [63] operating serially coupled sub-2 μm packed columns with UHPLC equipment. The work of Smith *et al.* [62, 73,

173] have shown that the use of superheated water eluents can be useful for eliminating or reducing the amount of organic present in the mobile phase. Efficiency improvements have also been reported for basic solutes due to changes in their pK_a with temperature [58, 59]. Elsewhere, the benefits of high-temperature separations linked with electrospray mass spectrometry have been reported. There is however a generally perceived reluctance to operating at elevated temperatures in industrial applications, particularly in the pharmaceutical domain where hesitation is due to concerns over analyte stability on-column. Horvath *et al.* [171] showed that the Damköhler number (Da) can be used as a gauge to determine the potential of on-column degradation for a particular substance, and was shown to be dependent on linear velocity. de Villiers [174] demonstrated this further for the analysis of thermally labile wine anthocyanins illustrating that no degradation occurred even at analysis times of up to 2 hours. By combining both ultra-high pressures and small particles it is possible to achieve both efficient analyses and reduce analysis times significantly. This was demonstrated by Veuthey *et al.* [36] for a range of pharmaceutical drug substances at temperatures up to 90 °C.

The aim of this study was to compare several commercially available supports in order to identify the most appropriate phase for the application of anabolic steroid analysis, using testosterone as the probe analyte. Furthermore, to investigate the possibility of operating at elevated temperatures using the most thermally stable packing material for higher sample throughput. Clark [175] and Lee *et al.* [65] evaluated these principles using zirconia based phases separately, however these materials generally do not perform as efficiently as those based on silica. Moreover, it has been reported [176] that the bridged-ethyl hybrid (BEH) materials are robust up to 200 °C using pure water mobile phases so we chose to work with this phase for the elevated temperature work. Efficient separation of endogenous anabolic substances is important in doping control for instance, and serves as a suitable sample set to probe chromatographic performance. Likewise, due to the structural similarity of many anabolic steroid-type substances the highest possible efficiency is desirable.

4.2 Experimental

4.2.1 Chemicals and reagents

Acetonitrile, isopropyl alcohol and ethanol all HPLC grade were purchased from Fisher Scientific (UK, Loughborough). The water used here was from a Milli-Q purification unit (Millipore, UK). Thiourea, testosterone and other anabolic test substances were purchased from Sigma-Aldrich (UK). Stock solutions of testosterone were prepared in neat acetonitrile at a concentration of 1000 $\mu\text{g/mL}$, thiourea stock was 1000 $\mu\text{g/mL}$ in 40:60 v/v $\text{H}_2\text{O}:\text{ACN}$. This was diluted to a working concentration of 10 $\mu\text{g/mL}$ and 1 $\mu\text{g/mL}$ for testosterone and thiourea respectively for each mobile phase composition. Steroidal test mix was also at 10 $\mu\text{g/mL}$.

4.2.2 Equipment

All mobile phases were premixed to ensure solvent delivery was consistent at low flow rates as well as being degassed using an ultrasonic bath for 5 minutes. For all analyses at 60 °C the mobile phase composition was 65:35 v/v $\text{H}_2\text{O}:\text{ACN}$ and 75:25 v/v $\text{H}_2\text{O}:\text{ACN}$ for determinations at 130 °C. Chromatography was performed using an Acquity UPLC (Waters Corp., USA) which consisted of a binary solvent delivery system, sample manager and variable wavelength TUV detector with a 500 nL flow cell. Data was collected at 240 nm with an acquisition rate of 40 Hz (0.025 ms time constant) controlled using an Empower v2.0 (Waters Corp., USA) data station. The Acquity Column Oven (ACO) on this instrument had a temperature maximum of 65 °C and was fitted with an influent stabilizer tube to assist with mobile phase pre-heating. All injections were made in duplicate using partial loop needle overfill (PLUNO) mode at 0.5 μL using a 1 μL loop. For elevated temperature experiments an external Selerity Polaratherm 9000 (Selerity, USA) forced air thermostat was used, which consisted of active mobile phase pre-heating and post-column cooling components. The thermostat configuration is stated where applicable. The measured extra-column variance at 300 $\mu\text{L}/\text{min}$ was 31 μL^2 and 26 μL^2 using the Polaratherm configuration at 60 °C and 130 °C respectively. When configured with the ACO the extra-column variance at the same flow rate and at 60 °C was measured at 7 μL^2 .

4.2.3 Methodology

A flow study was conducted beginning at 50 $\mu\text{L}/\text{min}$ for all experiments at 60 $^{\circ}\text{C}$, increasing to 100 $\mu\text{L}/\text{min}$ for the experiment at 130 $^{\circ}\text{C}$ up to the maximum system pressure (~ 1000 bar). Thiourea was used as a marker for t_o and for determining linear velocity and solute retention factor. Experiments were carried out up to either or both of the maximum instrument operating pressures (~ 1000 bar) or that of the stationary phase mechanical stability i.e. 600 bar for shell-particles. In order to correct for extra-column retention time, dispersion and system pressure, the same experiment was performed except with a zero-dead volume union in place of the column. All data was corrected at half peak height. The corrected data was then used to determine kinetic plot parameters as devised by the methodology of Desmet *et al.* [22, 23] according to the following relationships:

$$N = \frac{\Delta P_{\max}}{\eta} \left(\frac{K_{vO}}{\mu_o H} \right)_{\text{experimental}} \quad (4.1)$$

$$t_o = \frac{\Delta P_{\max}}{\eta} \left(\frac{K_{vO}}{\mu_o^2} \right)_{\text{experimental}} \quad (4.2)$$

Permeability (K_{vO}) was calculated at the maximum pressure for each column:

$$K_{vO} = \frac{\mu_o \eta L}{\Delta P_{col}} \quad (4.3)$$

Curve fitting was carried out using Microsoft Excel, Sigma Plot or the kinetic plot analyser.

Viscosity (η) of binary aqueous-organic acetonitrile mixtures at each temperature was determined using the Chen-Horvath [103] correlation as follows:

$$\eta_{\phi,T} = \exp \left[\phi \left(-3.476 + \frac{726}{T} \right) + (1-\phi) \left(-5.414 + \frac{1566}{T} \right) + \phi(1-\phi) \left(-1.762 + \frac{929}{T} \right) \right] \quad (4.4)$$

Where, ϕ is the acetonitrile molar fraction and T is the temperature in Kelvin. This has a correlation of $\pm 20\%$ between 100 and 200 °C according to the investigations of Carr *et al.* [67]. Mobile phase viscosity was calculated to be 0.505 cP at 60 °C for 65:35 v/v H₂O:ACN solutions and 0.231 cP at 130 °C for 75:25 v/v H₂O:ACN solutions.

Diffusions coefficients used for fitting data to the Knox equation were determined using the Wilke-Chang correlation [13]:

$$D_m = 7.4 \times 10^{-8} \frac{\sqrt{x_{ACN} \psi_{ACN} M_{ACN} + x_{H_2O} \psi_{H_2O} M_{H_2O}}}{\eta V_A^{0.6}} T \quad (4.5)$$

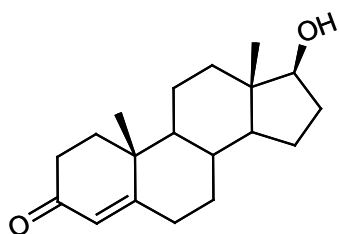
Where, x_{ACN} and x_{H_2O} are the molar fractions of each solvent respectively in a given mobile phase composition, ψ_{ACN} and ψ_{H_2O} are the association factors (ACN = 1, H₂O = 2.6), M_{ACN} and M_{H_2O} are the molecular weights of the solvents in g/mol respectively. The molar volume (V_A) for testosterone is 254.5 cm³/mole [177] and T is the temperature in Kelvin.

Calculated diffusion coefficients and physicochemical properties for testosterone are shown in Table 4.1.

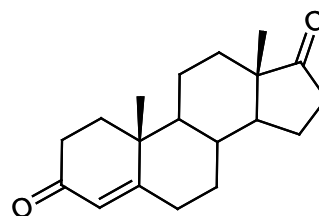
Compound	MW ^a	LogP ^a	D_m , 60 °C (cm ² /s)	D_m , 130 °C (cm ² /s)
Testosterone	288.2	3.179	1.18×10^{-5}	3.13×10^{-5}

^a from chemspider.com

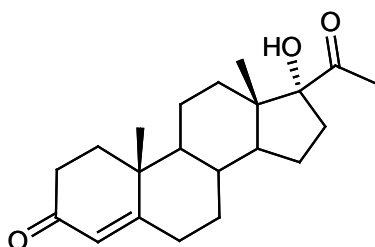
Table 4.1. Testosterone physicochemical data.



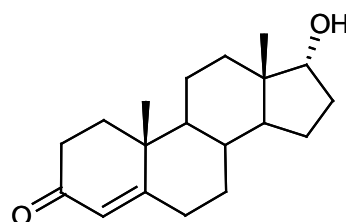
Testosterone



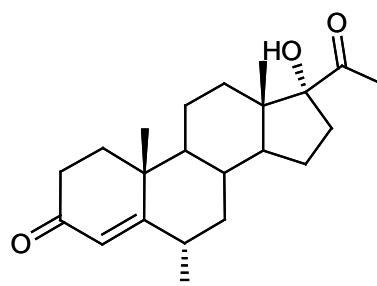
4-Androstene-3,17-Dione



17-a-hydroxyprogesterone



Epitestosterone



Medroxy-progesterone

Figure 4.1. Chemical structures of analytes in steroidal test mix.

4.3 Results and discussion

4.3.1 Flow study (Column Comparison)

Knox curves were constructed for each of the tested supports up to approximately their maximum operating pressure. The reduced plate height (h) and interstitial velocity parameters (v_e) were used to construct Knox plots for testosterone on each column as derived from plate height (H) data:

$$h = \frac{H}{d_p} \quad (4.6)$$

$$v_e = \frac{F d_p}{\pi r^2 \varepsilon_{ext} D_m} \quad (4.7)$$

Where r is the column radius, F is the volumetric flow rate, d_p is the particle diameter, D_m is the analyte diffusion coefficient (Table 4.1) and ε_{ext} is the external porosity (Table 4.2). Figure 4.2 (a) shows the Knox plots for each of the tested supports corrected for contributions from extra-column volume whereas Table 4.2 shows the derived curve fitting coefficients. From the plots it is clear that the fused-core HALO material outperforms all other phases significantly. This can be mostly attributed to the very low A -term seen for this column suggesting very good packing quality. Interestingly, it was the BEH material which gave the lowest packing coefficient out of all the evaluated columns. Both Kinetex superficially porous materials showed inferior packing coefficients in comparison. The two sub-2 μm phases yielded comparable performances at their van Deemter minima which is in agreement to the observations of Guiochon *et al.* [178]. In their work superior packing of the BEH material was noted as well as the difficulty in packing small superficially porous particles into ≤ 2.1 mm ID column formats.

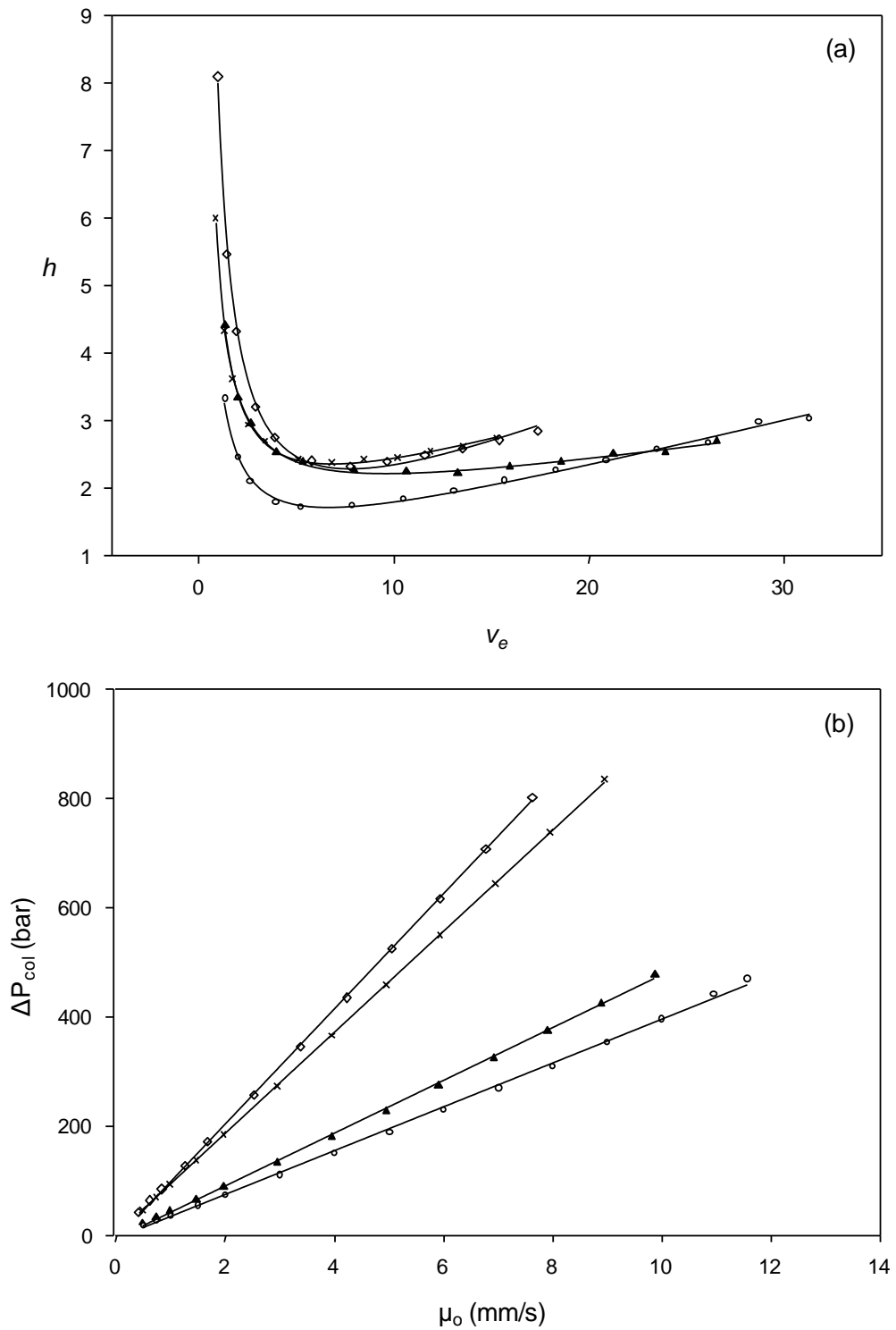


Figure 4.2. (a) Performance comparison using reduced Knox parameters and interstitial linear velocities (b) correlation of corrected pressure drop as a function of linear velocity. Where, \diamond (1.7 μm BEH), \times (1.7 μm Kinetex), \blacktriangle (2.6 μm Kinetex) and \circ (2.7 μm HALO).

Column ^a	d_p (μm) ^b	a	b	c	v_{opt}	h_{min}	H_{min}	k	ϵ_{ext}
1) BEH	1.7	0.43	7.19	0.120	7.75	2.33	3.97	5.2	0.360 ^c
2) Kinetex	1.7	1.20	3.95	0.085	6.80	2.38	4.05	6.4	0.410 ^d
3) Kinetex	2.6	1.42	3.85	0.042	9.60	2.23	5.80	6.5	0.400 ^c
4) HALO	2.7	0.77	3.15	0.071	6.63	1.72	4.65	5.2	0.423 ^c

^a all columns were 10 cm x 2.1 mm ID
^b as stated by the manufacturer
^c ref. [179]
^d ref. [169]

Table 4.2. Knox parameters, van Deemter minima and retentions factors for each of the tested columns.

The major benefit seen in this work and elsewhere [178] for core-shell materials was displayed in their relative B -terms, which were significantly smaller than those found with the fully porous BEH material. This is reflected in the optimum interstitial velocities between the two sub-2 μm phases, where the fully porous phase is required to be operated at higher pressures in order to achieve the maximum plate number. Unfortunately, the same cannot be said of the Kinetex 2.6 μm column as the h_{min} value as well as the Knox A -term recorded suggests this particular column was poorly packed. This was unexpected since the HALO column showed very low A -term values comparable to those reported by other workers. As suggested by Knox *et al.* [15], columns which exhibit long and flat minima with a relatively larger A -coefficient are usually a function of poor packing. Overall, the differences in the B -terms between fully and superficially porous materials are stark. It could therefore be suggested that operation of such columns at elevated temperatures should benefit from this feature; however from a practical point of view, this is unlikely given their poor chemical stability under such conditions.

The C -terms were found to be smaller for the core-shell phases in all cases when compared to the fully porous material. It has been shown elsewhere [178, 179] that the degree of thermal conductivity of the packing contributes to assisting heat transport, particularly important in the radial coordinate of the column. This occurs due to frictional heating of the percolating mobile phase through the packed bed. At high flow rates this effect becomes more prevalent and major contributions to the C -term take place. The higher thermal conductivity of the core-shell phases versus the hybrid silica may go some way to explaining the values obtained. However, the

severe divergence in *C*-term behaviour in the investigation of Guiochon *et al.* [178] of the same sub-2 μm materials was not observed in this study. This can be ascribed to those workers using high ACN content (78 and 100%) in order to construct Knox curves. As shown by McCalley [179] this solvent has poor thermal conductivity and in practical reversed-phase separations, such high organic fractions are seldom used isocratically.

Plots of linear velocity versus corrected column backpressure are presented in Figure 4.2 (b). When comparing the pressures generated by sub-2 μm versus supra-2 μm materials it is worth contrasting the performance of the BEH and the HALO material. When operated at their optimum pressures, the latter produced approximately 85% of the efficiency obtained with the 1.7 μm BEH column. This was achieved requiring only 26% of the pressure needed with the sub-2 μm column. Nevertheless, this resulted in about 2 minutes longer analysis time which for a high throughput application may be significant. Clearly, by operating a longer HALO column one could achieve higher plate counts within the limits of conventional operating pressures. However, this would be at the expense of analysis time. In order to better visualise the performance merits as a function of time it is more appropriate to use the kinetic plot method as explained in the next section.

4.3.2 Kinetic plot representation (Column Comparison)

Another way to compare stationary phase morphology is to utilise the plots outlined by Desmet *et al.* [22, 23]. Due to the differences in hydrodynamic permeability between the fully porous 1.7 μm BEH and the superficially porous 2.7 μm HALO columns it is useful to compare the performance merits using this approach. As these columns provided good packing coefficients and also the supra-2 μm material yielded very high efficiencies it is useful to know the limitations of these respective chromatographic systems. Furthermore, operating each system at the maximum available pressure drop allows for the operation of columns which are long enough to yield the highest possible plate count. In a previous report, Petersson *et al.* [37] showed that comparable efficiencies between 1.7 μm BEH and 2.6 μm HALO columns were obtainable although the latter was operated at much lower pressures. Similar conclusions were drawn by Cabooter *et al.* [34] and Maloney *et al.* [96]. As shown in Figure 4.3 the kinetic efficiency evaluation was undertaken as a function of plate time (t_0 versus N), separation impedance (t_0/N^2 versus N) and column length (L versus N) set at the maximum operating pressure for each phase. As shown in Table 4.3 the permeability (K_{VO}) of the HALO phase was significantly greater than the BEH phase. This feature results in there being a corresponding decrease in separation impedance (E) for the former material.

Column	K_{VO} (m^2)	E	φ
1)	4.80E-15	3275	602
2)	5.40E-15	3032	535
3)	1.05E-14	3217	647
4)	1.24E-14	1736	586

Table 4.3. Hydrodynamic functions of kinetic performance for each column.

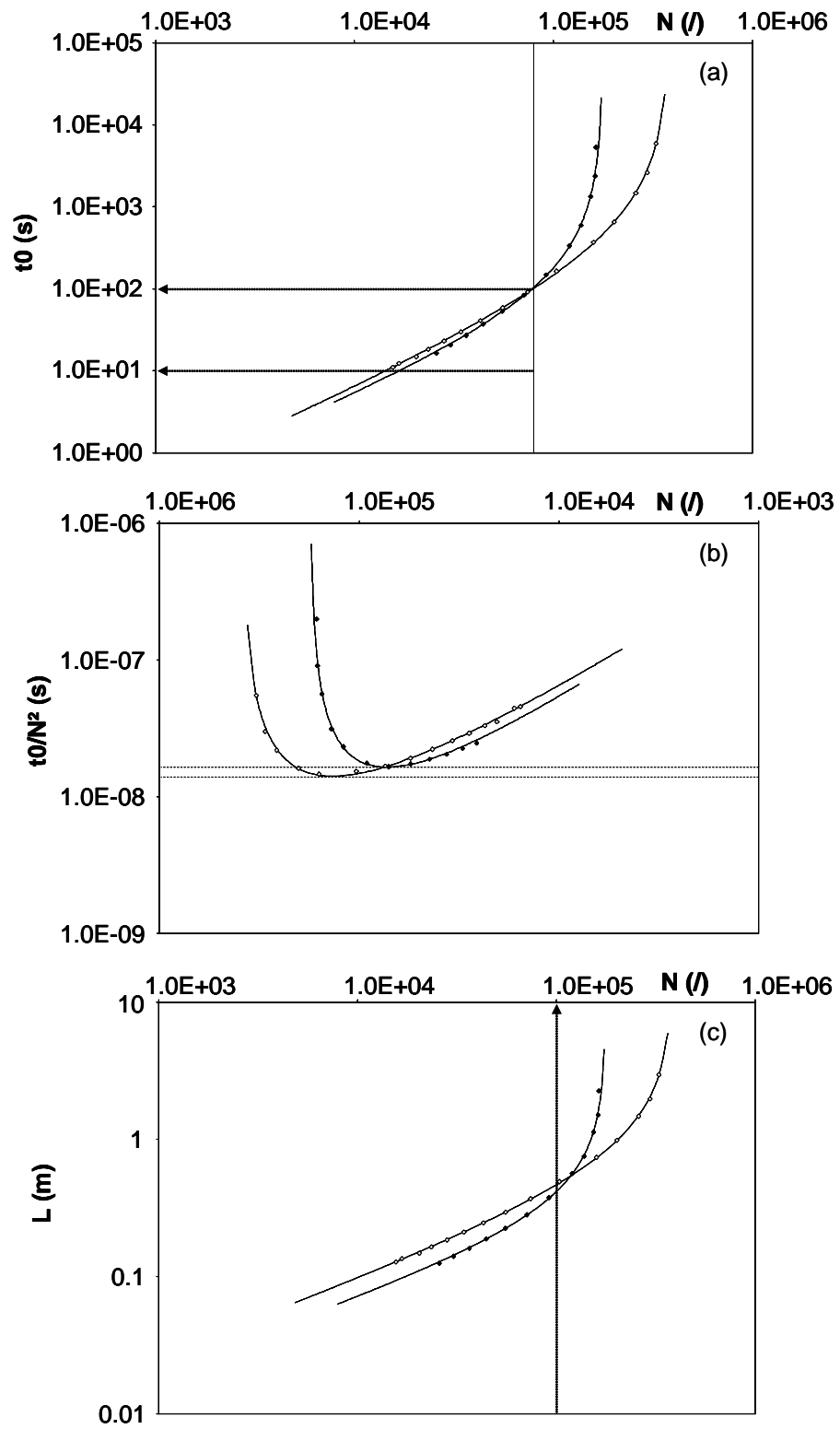


Figure 4.3. Kinetic plot performance analysis considering (a) plate time (b) separation impedance and (c) column length. Closed diamonds (1.7 μm BEH) and open diamonds (2.7 μm HALO).

Figure 4.3 (a) depicts the plate time curves for each phase plotted at their respective maximal pressures. In the high region of the curves, above the inscribed vertical line, very high efficiencies can be achieved using the fused-core particle. However, below the line the sub-2 μm phase exhibits higher plate counts across this entire range of plate times i.e. < 100 second plate time. For example, at plate times of 10, 50 and 100 seconds 171000, 246000 and 252000 N/m are achieved with the sub-2 μm particle respectively. Whereas, for the fused-core material the values are 117000, 182000 and 205000 N/m at the same plate times. Above 100 seconds a dramatic divergence in the kinetic curves is seen, which is due to the significantly smaller axial diffusion and the higher permeability of the fused-core column. Consequently, longer columns are permitted for the fused-core materials than with the sub-2 μm phase, enabling very high efficiency separations.

The plot in Figure 4.3 (b) resembles closely the curvature of a typical van Deemter curve, where the minima indicate the optimum plate number as well as the Knox-Saleem limit for each chromatographic system. The corresponding N_{opt} values were 73000 and 136000 for the 1.7 μm and 2.6 μm particles respectively. This corresponds exactly with the column length which when operated at the maximum pressure, would be operating at the optimum linear velocity.

Figure 4.3 (c) shows the length of column required to achieve a desired plate count when operating at the maximum pressure for each support. The lower asymptotes of the curves at lengths of 10 cm demonstrate that highest efficiencies are achieved with the sub-2 μm particle. This is due to the influence of the C-term on the HALO particle, as operating such a column at the maximum pressure entails operation above the optimum corresponding linear velocity. It is interesting to show that at lengths yielding up to 100000 plates, when operating at the maximum pressure for each system, that the sub-2 μm column significantly outperforms the HALO approach. Clearly, above the 100000 plate count mark the HALO particle yields far higher plate counts than with the sub-2 μm phase with equivalent lengths of column. However, columns begin to approach lengths that are practically unsuitable for most applications as well as extensive analysis times. Nevertheless, at plate times of 500 seconds using a column length approximately 90 cm long, the HALO column would yield around 182000 plates. In contrast, the sub-2 μm particle would yield approximately 132000 plates using a 70 cm long column. The

reason for the latter performing worse is solely due to such a column operating sub-optimally due to the impact of the axial diffusion term. Hence the maximum plate counts achievable with each system were 175000 and 380000 plates for the 1.7 μm and 2.6 μm particles respectively.

As shown by the work of others [180] these extrapolations can be open to conjecture, since differences in the quality of the columns used to determine the plate counts can result in erroneous kinetic predictions. Nevertheless, the two columns chosen here provided entirely acceptable plate counts at their optimum linear velocities. Fekete *et al.* [181] summarised the diversity in reported plate counts for fused-core and highly efficient fully porous particles in a thorough review. It appears on average that the efficiencies reported in this work are commensurate with those reported in their findings. In summary, sub-2 μm particles yielded faster and more efficient analyses in the short analysis time frame, whereas if high efficiencies are required then consideration of long columns packed with fused-core particles should be considered.

4.3.3 Operation of sub-2 μm BEH particles at elevated temperatures

4.3.3.1 Flow study

By applying elevated temperature to liquid chromatography several benefits can occur, in particular analysis time can be reduced by several factors. In terms of separation efficiency, applying higher temperatures does not increase the theoretical plate number of a column but instead assists in decreasing mobile phase viscosity which increases solute diffusivity. This feature allows for operation of linear velocities exceeding the optimum without severe deterioration in column performance. Also, the choice of thermostat is important as well as the need for adequate mobile phase pre-heating. Additional considerations, such as adequate data collection of the small peak volumes encountered with separations carried out at elevated temperatures should also be taken into account.

When increasing the temperature from 60 °C to 130 °C the diffusion coefficient for testosterone is increased by a factor of 2.7. Conversely, the eluent viscosity decreases by a factor of approximately 2.2. Figure 4.4 (a) and (b) show the impact of flow rate on column performance using the forced-air thermostat. Due to the effect of frictional heating, thermal gradients are formed in the radial coordinate of the column. These effects are enhanced when operated in near-isothermal conditions, as is performed here. At 60 °C the impact on the *C*-term for this column is highly significant, increasing from 0.12 in the previous analysis using the Acquity Column Oven (ACO) compared with 0.22 found using the forced-air thermostat. The Knox *B*-terms were also affected, changing from 7.19 in the ACO and rising to 8.49 with the forced-air oven. This may be a result of the effectiveness of the relative column thermostats at thermally conditioning both the column and also in pre-heating the mobile phase. Other more complicated features such as the impact of radial thermal gradients on retention factor should also be taken into consideration.

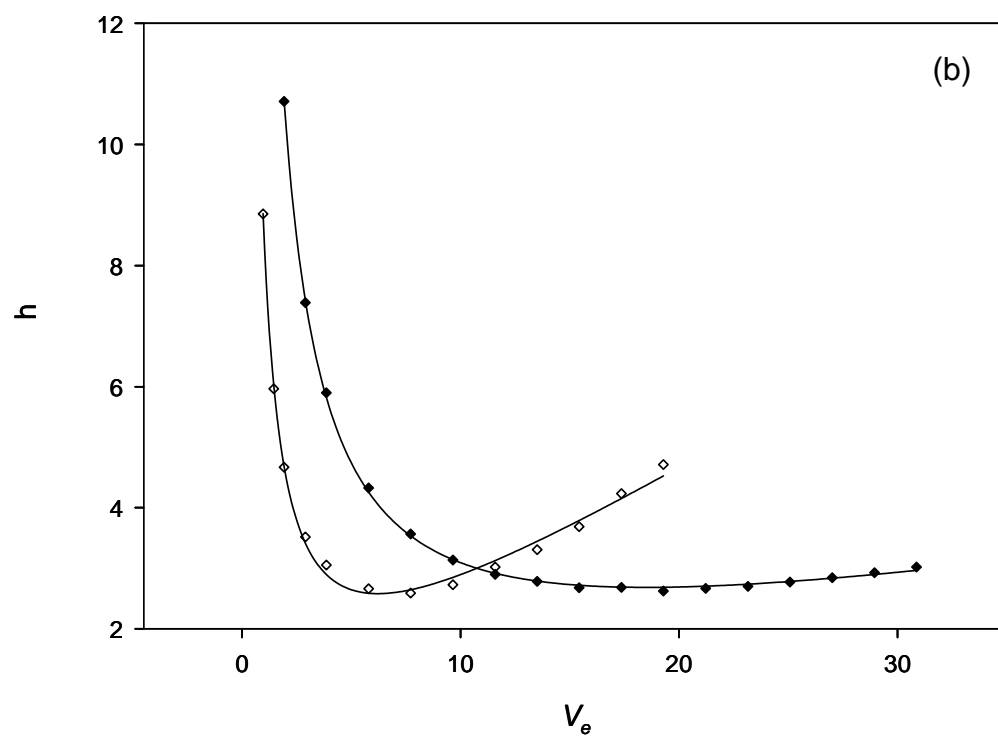
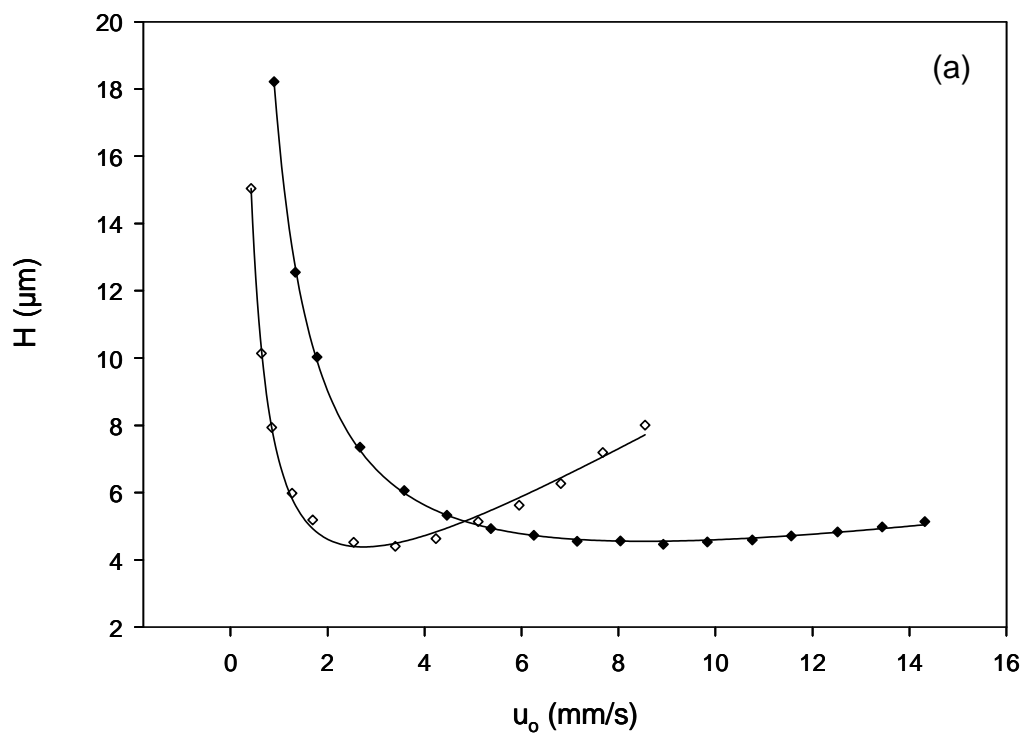


Figure 4.4. (a) van Deemter (b) Knox curves for operation of BEH at 60°C (open diamonds) and 130°C (close diamonds) using the forced-air oven. Data corrected for extra-column volume.

Surprisingly, at elevated temperatures the *C*-term region of the van Deemter/Knox curves was flat. This is in part due to the volumetric flow rate and pressure relationship on the power formation due to frictional heating under these conditions. However, it could be speculated that the effect of radial thermal gradients could be alleviated by a combination of increased diffusivity and the somewhat lower organic fraction (i.e. increased thermal conductivity of the mobile phase) used to maintain constant retention. The decrease in the *C*-term due to increased temperature was approximately 74% whereas the *B*-term was increased by around 128%. This resulted in a 3 times increase in the u_{opt} , which is in agreement with theory. That is, with fixed retention factors an increase in flow rate is required to reach the optimum linear velocity when temperature is raised. If analysis is carried out with u_{opt} at a lower temperature and the temperature is raised without changing u_{opt} then the efficiency ($> H$) will be greatly reduced. In order to compensate for this will require the analysis to be carried out at higher flow rates and increased pressure.

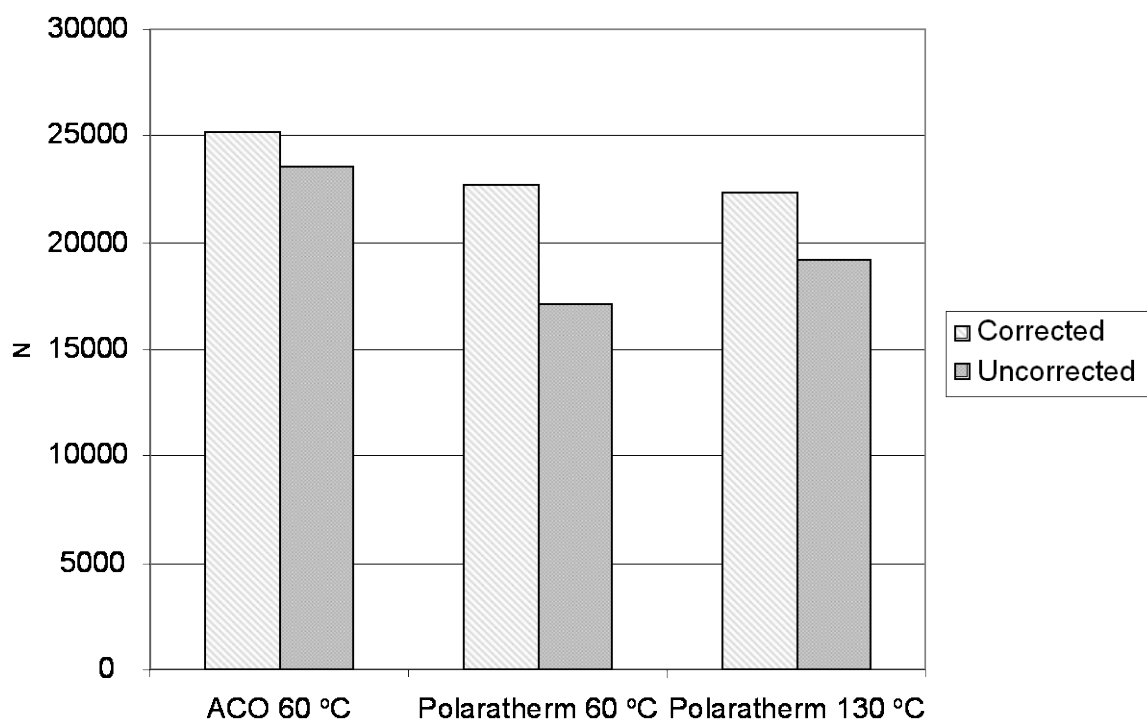


Figure 4.5. Influence of extra-column volume on column performance at the optimum operating pressure.

Another benefit of utilising elevated temperatures was that extra-column dispersion was reduced, and is in agreement with the observations of Neue *et al.* [38]. This is particularly important for accommodating the Polaratherm thermostat with 2.1 mm ID columns. Accordingly, the corrected plate values are essentially pointless in a practical sense due to the significant extra-column volume of the forced-air setup. The results are shown in Figure 4.5 and indicate clearly the dramatic losses in efficiency due to extra-column volume, which was around 6% for the ACO configuration at 60 °C. For the Polaratherm setup these figures were around 24% at 60 °C and 14% at 130 °C. A more detailed discussion on the use of forced-air versus still-air column thermostats is dealt with in Chapter 3.

4.3.3.2 Kinetic plot performance at elevated temperature

Due to the influence of elevated temperature on the B -term, operation of fully porous sub-2 μm particle packed columns can be adversely affected due to sub-optimal operation. This is apparent in Figure 4.6 (a) as a plot of t_0 versus N . It is in fact more beneficial to use lower rather than elevated temperatures for plate times > 500 seconds. The major benefit to operating using elevated temperature conditions is to reduce analysis time, which is shown in the lower asymptote of the kinetic curves. This is due to a significant decrease in the separation impedance as shown by the horizontal Knox-Saleem limit lines in Figure 4.6 (b). As mentioned previously, the minima of these curves corresponds to the column length which yields the optimal plate number for this particle, as operated at the maximum available pressure. The values were around 84000 and 58000 plates for the 60 and 130 °C systems respectively. Nevertheless, it is possible to obtain around 60000 plates with the latter in about 60% shorter analysis time than with the moderate conditions. The value of N_{opt} at 60 °C seems to be in conflict with the figure obtained in the study using the ACO thermostat. This is likely due to differences in experimentally determined column permeability values found between the thermostat types. Although not entirely dissimilar, differences in column thermal conditioning between the two systems may account for this observation due to subtle variations in temperature affecting viscosity.

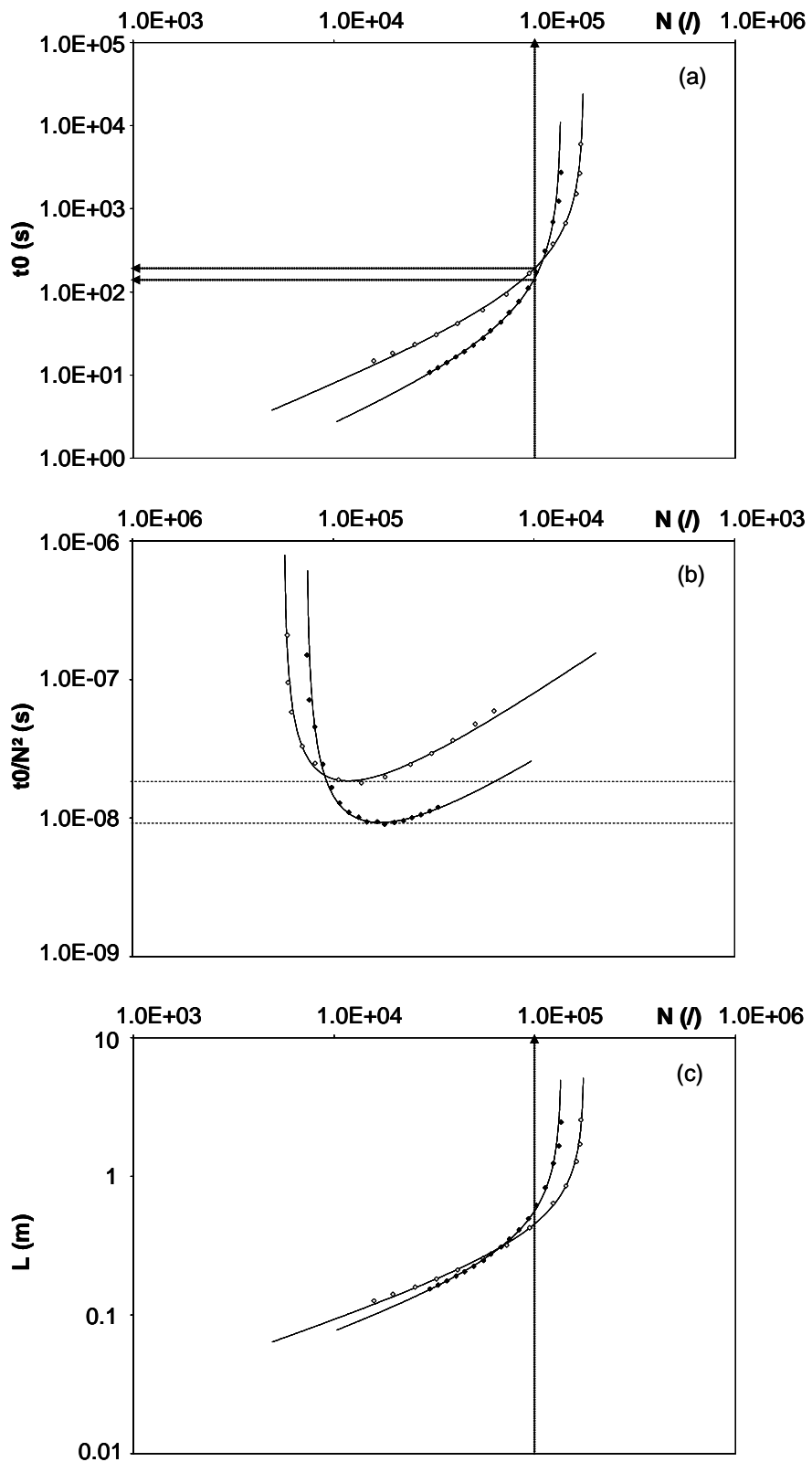


Figure 4.6. Kinetic plot comparison at 60 °C (open diamonds) and 130 °C (close diamonds). K_{vo} , 60 °C was $5.46 \times 10^{-15} \text{ m}^2$ and K_{vo} , 130 °C was $5.11 \times 10^{-15} \text{ m}^2$.

Figure 4.6 (c) shows the plate count achievable with different lengths of column. The divergence of the lower asymptotes can be ascribed to the influence of radial temperature gradients. When operating short column lengths isothermally at 60 °C and at the maximum pressure, the combined effect of the corresponding increase volumetric flow rate and pressure becomes increasingly detrimental. Usually for a fixed retention factor and column length temperature cannot yield higher plate numbers, however the use of elevated temperatures is shown to be beneficial in this instance i.e. for short columns operated at high flow rates. This is nevertheless already obvious from the van Deemter curves due to the compensation effect of elevated temperatures on the C-term. In order for the elevated temperature approach to yield around 100000 plates, a longer column (~ 53 cm) than the system operated at 60 °C ($L \sim 46$ cm) would need to be used. Although the former would be operating sub-optimally, estimated plate heights of 5.27 μm versus 4.56 μm at 130 and 60 °C respectively, using raised temperatures allows for around 34% faster analysis time.

As mentioned previously, the N_{opt} for the elevated temperature system is around 60000 plates. This can be realised at a plate time of approximately 28 seconds using a column length of 25 cm operated at the maximum pressure. In order for a similar plate count to be achieved with the moderate temperature system the plate time is significantly longer at 73 seconds. The calculated column length for the moderate temperature system was 28 cm which is a difficult dimension to approximate. Nevertheless, this still serves as a useful comparison to operating at elevated temperatures. Figure 4.7 shows the separation of the steroidal test mix at moderate and elevated temperatures both operated at the maximum pressure. The observed plate counts on each system were 52748 and 51262 measured for testosterone at 60 and 130 °C respectively. Moreover, the added benefit of operating at 130 °C was a 10% decrease in acetonitrile concentration which is useful for reducing solvent consumption and cost. Also highlighted is an observed change in selectivity, which is obviously a function of both the differences in solvent composition and temperature. Although the order of elution remains the same between the two sets of conditions it is certainly useful for method development purposes. Furthermore, an acceptable degree of resolution was maintained using the elevated temperature conditions.

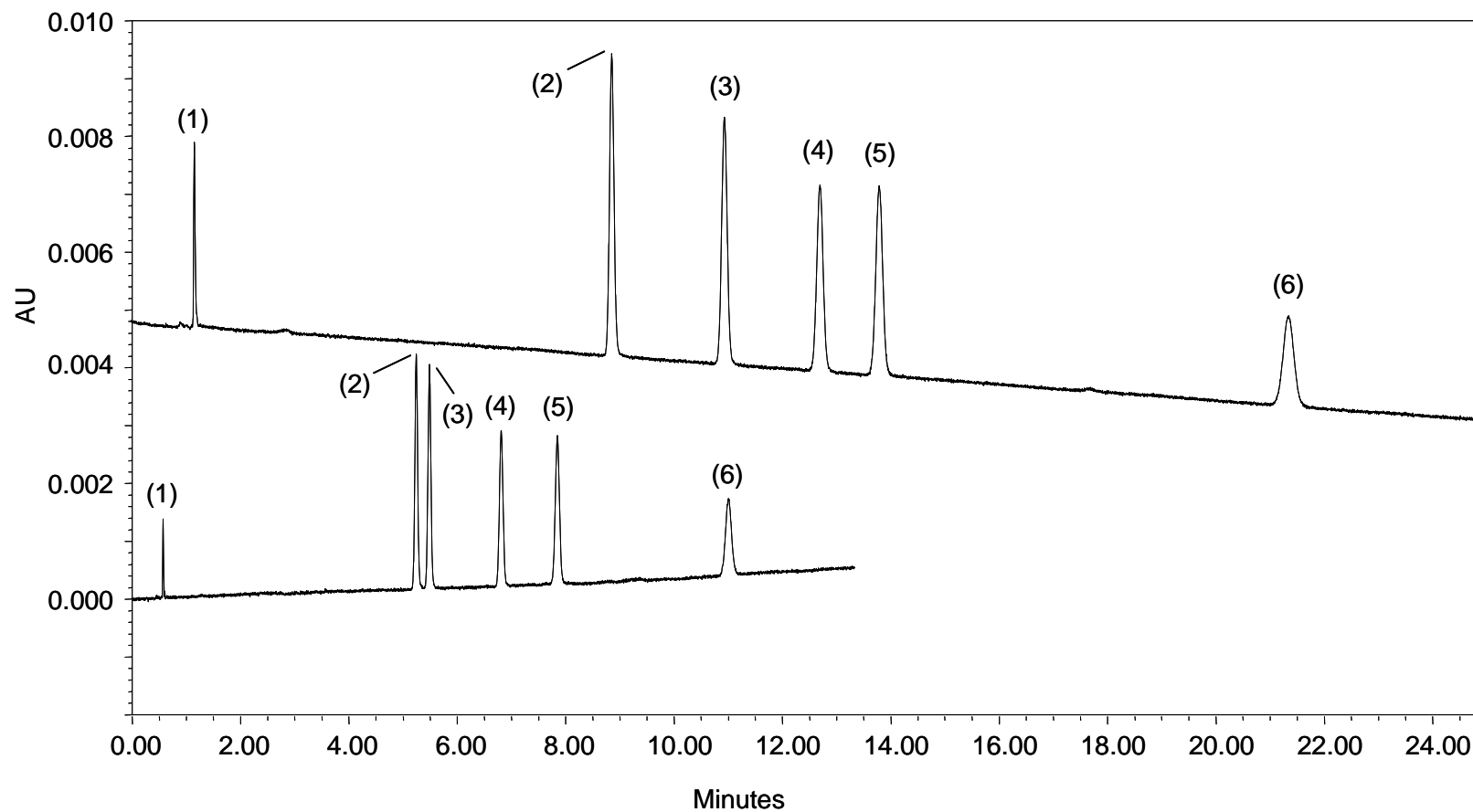


Figure 4.7. Comparison between (Top) 60 °C and (Bottom) 130 °C operation using coupled 10 + 15 cm long BEH C18 1.7 μ m x 2.1 mm ID columns. Analytes (1) Thiourea (2) Testosterone (3) 4-Androstene-3,17-Dione (4) 17- α -Hydroxyprogesterone (5) Epitestosterone (6) Medroxy-Progesterone. Flow rate and pressure (Top) 660 μ L/min, Δ P = 1014 bar (Bottom) 710 μ L/min, Δ P = 1002 bar.

4.3.3.3 Alternative solvent use at elevated temperatures for steroidal test mix

Elevated temperature allows for the use of solvents which are otherwise too viscous under moderate temperatures. Solvents such as IPA or ethanol are seldom used in reversed-phase chromatography due to their impractically high viscosity. However, such alternative solvents can be useful for expanding the selectivity domain available for optimising resolution, which is a more powerful approach than directly increasing separation efficiency. Moreover, greener approaches to solvent use are becoming more important to adopt and reducing use of acetonitrile is often sought. Figure 4.8 shows the separation of the steroidal test mix using IPA and ethanol. In both instances, owing to their higher solvent strength than acetonitrile, retention times are dramatically reduced increasing analysis speeds. This is an entirely chemical based reduction in analysis speed as opposed to a kinetically optimised approach. Interestingly, the order of elution between all three evaluated solvents the order of elution remained the same and usefully baselines resolution was achieved between all substances. The highest selectivity was found using ethanol as the organic modifier. Obviously, using an acetonitrile based mobile is more kinetically favorable due to the much lower viscosity afforded with those mixtures. The observed plate counts on each system were 36925 and 47974 measured for testosterone using IPA and ethanol respectively. The lower plate counts observed with the aqueous-alcohol mobile phase are due to their much higher viscosity than those found using acetonitrile mixtures, impacting negatively on analyte diffusion causing additional band broadening.

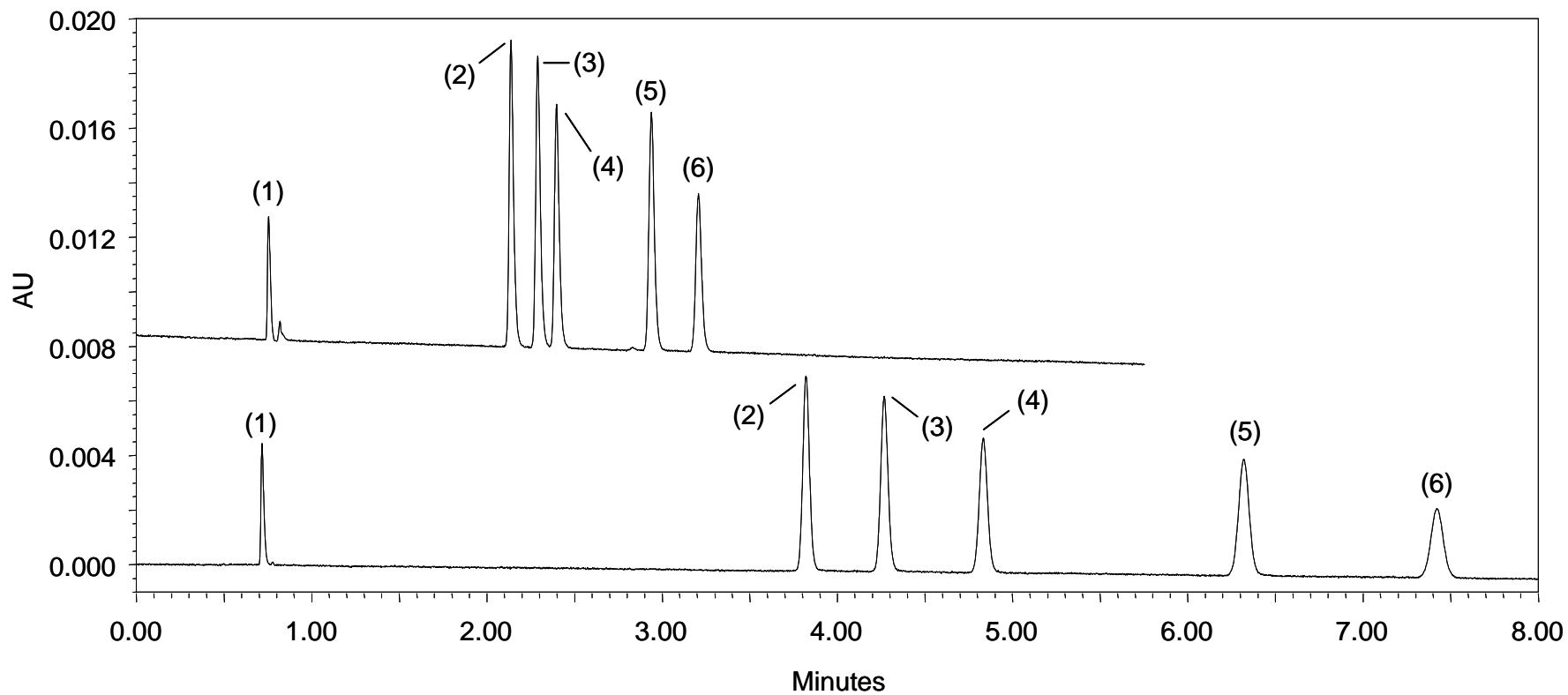


Figure 4.8. Comparison between using (Top) isopropyl alcohol and (Bottom) ethanol organic modifiers for the separation of steroidal test mixture at 130 °C. Both 75:25 v/v H₂O:Organic using coupled 10 + 15 cm long BEH C18 1.7 μm x 2.1 mm ID columns. Flow rate and pressure (Top) 660 μL/min, ΔP = 994 bar (Bottom) 710 μL/min, ΔP = 1004 bar. Analytes as in Figure 4.7.

4.4 Conclusion

Columns packed with different, recently developed reversed-phase stationary phase materials were compared in terms of their separation efficiency using testosterone as the probe analyte. By constructing Knox plots it was shown that the column packed with sub-2 μm BEH materials performed best overall. It was also shown that the column packed with this material had the lowest Knox *A*-term out of all the evaluated columns. The comparison of 1.7 μm BEH versus 2.7 μm HALO materials showed the former to be superior in the practically useful analysis range. These differences may have been obscured in literature several times by comparison of a poorly packed 1.7 μm BEH column with other superficially porous columns. It appears that there is no apparent advantage to superficially porous silicas with respect to their superior packing qualities directly. Instead, it can be perceived that it is the process which is used to pack columns rather than degree of stationary phase monodispersivity which contributes greatest to packing quality. Obviously this is open to debate; as investigations should be carried out using several columns from different production batches and manufacturers to make firm conclusions. This would nevertheless be difficult, and expensive, as column manufacturers have proprietary packing processes. The main advantage to superficially porous materials appears in their *B*-term behaviour and this feature may be useful at elevated temperature operation. Using 1.7 μm BEH materials at elevated temperatures (up to 130 $^{\circ}\text{C}$) afforded significant increases in analysis speed and the practical use of viscous solvents. Operation at elevated temperatures is certainly a useful avenue to explore, however it is essential that extra-column effects are minimised and still-air conditions are used. This work has provided useful information as to determining the maximum possible efficiency for the analysis of anabolic substances.

Chapter 5

Kinetic performance comparison of sub and supra- 2 μm bare silica phases for the HILIC separation of basic pharmaceutical solutes in short narrow bore columns

Abstract

Adequate retention and suitable peak shapes for many basic solutes can be somewhat difficult to obtain using conventional reversed-phase approaches. Despite the flexibility of RPLC, alternatives are often sought as complementary or orthogonal characteristics may also be required for complex separations. The term HILIC has been conjured to describe a mode of retention for which the analyses of difficult to retain polar solutes are best suited. Presented here are performance data on a range of short bare silica packed columns illustrating their kinetic differences. This work encompasses the evaluation of different particle morphologies showing the advantages to using small particle packed columns operated on an optimised modern chromatographic instrument. The evaluations were carried out using pharmaceutically relevant solutes which yield more realistic operating efficiencies.

5.1 Introduction

Column performance is constrained not only by the hardware of a chromatographic instrument but also the physiochemical properties of the eluent used to elute analytes of interest. This relationship often produces a dilemma as to which mode of chromatography is best employed for a particular separation, especially if fast and efficient analysis is desired. Bed permeability (K_{vo}) is an important measurement of the kinetic characteristics of a chromatographic column, and is directly proportional to solvent viscosity (η), and is defined as follows:

$$K_{vo} = \frac{\mu_o \eta L}{\Delta P_{col}} \quad (5.1)$$

Where, linear velocity (μ_o), column length (L) and the system corrected pressure drop (ΔP_{col}) denote the other constraints of column permeability. The drive towards smaller particles invariably increases the pressure drop required to achieve an optimum linear velocity (μ_{opt}). Therefore highly efficient separations using long columns packed with small particles are inherently more difficult to obtain without the necessary ability to deliver high pressures. Small particles and ultra high pressures are best suited to fast efficient analyses, as is desirable in high throughput applications. The group of Desmet have made strides to revise the approach of assessing the performance limitations of chromatographic supports under different operating conditions, namely using the Kinetic Plot Method (KPM) [22, 23]. This family of plots are a revision of the plate time curves devised by Poppe [19] that were preceded by the earlier work of Giddings [18] for comparing the respective performance limits of liquid and gas chromatography.

The two important equations derived for the KPM encompass the bed permeability parameter of the tested support, the linear velocity (μ_o) and theoretical plate height (H), shown as:

$$N = \frac{\Delta P_{\max}}{\eta} \left(\frac{K_{vO}}{\mu_o H} \right)_{\text{experimental}} \quad (5.2)$$

$$t_o = \frac{\Delta P_{\max}}{\eta} \left(\frac{K_{vO}}{\mu_o^2} \right)_{\text{experimental}} \quad (5.3)$$

Equations (5.2) and (5.3) allow scaling of van Deemter data (μ_o , H) making it possible to extrapolate the potential performance of a given support in terms of the maximum achievable pressure limitations imposed by the chromatographic system. Recently, several workers have investigated the kinetic performance characteristics of HILIC materials. Veuthey *et al.* [182] compared several sub-2 μm bare silica materials for the fast analysis of polar compounds, whereas Sandra and co-workers [107] investigated the use of long columns packed with 5 μm stationary phases for profiling of genotoxic manufacturing impurities, normally difficult to retain using reversed-phase methods. Plate counts in the order of 100,000/m have been reported [106] by serially coupling columns packed with 2.7 μm superficially porous bare silica using conventional pressures in around 15 minutes under HILIC conditions.

With respect to basic solutes, of which many therapeutic drug substances are classified, reversed-phase approaches are often fraught with challenges in optimising retention and peak shape. HILIC is essentially an aqueous normal phase separation technique [104] which in its simplest form utilises bare silica as the stationary phase with high acetonitrile (>70%) rich eluents, yielding retention via a number of physiochemical interactions between the solute and the sorbent. Manufacturers of stationary phases now offer a diverse range of bonded phases suitable for HILIC as recently studied by McCalley [183]. The difficulties in achieving suitable peak shapes for basic solutes has also been extensively reviewed and studied by McCalley [184] and clearly the use of the HILIC approach warrants consideration in this particular area of liquid chromatography. However, one incompatibility comes from the suitability of the injection

solvent since highly acetonitrile rich (>90%) or an equivalent concentration to that of the running mobile phase is required so as not to disturb the state of equilibrium of the sorbent. Clearly, acetonitrile rich injection solvents are not suitable for all analytes especially when higher sample concentrations are required due to solubility issues. An examination into the effect of injection solvent for HILIC was conducted by Veuthey *et al.* [109] and elsewhere by Grumbach *et al.* [108] concluding that compromises are required in certain circumstances, otherwise poor peak shape or losses in retention will be observed. It may be that the wider adoption of HILIC is somewhat hindered due to concerns over method robustness, however if the right precautions are taken when selecting injection solvents, these issues may be negated. The base silica of any sorbent can influence the retention behavior of a separation as has been extensively studied by Euerby and Petersson [185, 186] when classifying reversed-phase stationary phases. Clearly, the acidic nature of silica can be diverse and with many manufacturers now offering bare/naked silicas as supports for HILIC separations, it is useful to contrast these materials for method development.

The introduction of superficially porous silicas have caused much debate as to the performance gains observed with these phases, with arguments originally purporting that the improvements were based solely on the enhanced mass transfer characteristics of these supports [92]. Several benefits were reported by Petersson *et al.* [37] in that lower backpressures and equivalent or near sub-2 μm performances are afforded with superficially porous materials depending on analysis time. Several commercially available phases have been evaluated in the form of Poroshell 300Å for protein and peptide separations [187] and more recently the HALO or fused-core supra-2 μm silicas [92]. Guiochon *et al.* [188] concluded that the efficiency gains with current superficially porous materials over their modern fully porous counterparts are due to a combination of reduced *A*- and *B*-term contributions to band broadening. The narrower particle size distributions found with the superficially porous materials imply lower inter-channel velocity biases due to the more uniform packing which in turn lowers eddy diffusion characteristics i.e. the *A* term. [189]. Cabooter *et al.* [190] also found strong correlation between the particle size distribution and column performance drawing similar conclusions in that *A*-term values for superficially porous materials were lower than those found with fully porous silicas. In another article by Cabooter *et al.* [191] the difference in particle size distributions for 3.5 μm and sub-2 μm materials was compared and related to column performance, inferring the difficulty in packing particles of smaller diameter along with their wider size distribution may be accountable

for the lower than expected performances of these materials. Conversely, Tallarek *et al.* [192] argued that the narrow particle size distribution did not overly influence the eddy dispersion contribution and instead had more of an impact on bed porosity. They concluded that the low eddy diffusion term observed with shell-particles is mainly down to the goodness of packing rather than monodispersity

We have evaluated a number of modern commercially available bare silica narrow bore packed columns in terms of separation efficiency for the purposes of studying the HILIC separation of polar bases. Van Deemter experiments were performed using a range of realistic basic test solutes in order to elucidate what performances might be encountered for this common class of compounds. The aim of this study was to contribute further on the performance behavior of fully and superficially porous silica substrates and to illustrate the effectiveness of HILIC as a real alternative to reversed-phase separations. Due to the lower viscosities of the acetonitrile rich mobile phases associated with HILIC, the lack of the kinetic constraints normally imposed by most reversed-phase solvent systems results in the possibility of achieving even faster analyses highlighted using the kinetic plot method.

5.2 Experimental

5.2.1 Materials and reagents

Acetonitrile (HPLC grade), ammonium formate and formic acid (98 %) were obtained from Fisher Scientific (Loughborough, UK). Toluene, benzylamine, nortriptyline, diphenhydramine and procainamide were purchased from Sigma (Poole, UK). Water was purified by an ultra-pure water system (Millipore, UK). Ammonium formate buffer solution was prepared at 100 mM stock concentration adjusted to pH 3.0 before mixing with acetonitrile. Analyte test solutions were prepared in the mobile phase which was pre-mixed 90:10 v/v CH₃CN:10 mM Ammonium Formate pH 3.0 and remained constant throughout all experiments. The test mix consisted of nortriptyline (0.05 mg/mL), caffeine (0.05 mg/mL), benzylamine (0.5 mg/mL), procainamide (0.05 mg/mL) and diphenhydramine (0.25 mg/mL). The latter was injected separately to avoid co-elution with nortriptyline on certain phases. Toluene was used as the un-retained marker.

5.2.2 Instrumentation

Liquid chromatography was carried out on a Waters Acquity UPLC system (Waters Corp., Milford, US) which consisted of a sample manager, binary solvent delivery system and a PDA detector with a 500 nL flow cell. The acquisition rate was 40 Hz with a 50 ms time constant. The autosampler was thermostatted at 6 °C. Injections were made in duplicate and averaged for all experiments. All experiments were performed at 30 °C unless otherwise stated. Columns were connected to the injection valve using the temperature stabiliser tubing so as to ensure that adequate eluent pre-conditioning took place. All injections were of 1 µL made using a 2 µL loop in the partial loop with needle overfill mode. Empower 2 software (Waters, MA, USA) was used for data acquisition. Weak and strong needle washes were 90:10 v/v CH₃CN:H₂O and 50:50 v/v CH₃CN:H₂O respectively.

5.2.3 Flow rate study methodology

Diffusion coefficients (D_m) were measured elsewhere using the Taylor-Aris procedure (Table 5.1) taken from a previous study for reducing experimental van Deemter data to the Knox equation. All data was corrected for extra column band broadening by removing the column and replacing with a zero dead volume union. Reduced plate heights h and interstitial linear velocities u were determined by the following:

$$h = \frac{H}{d_p} \quad (5.4)$$

Where, H is the height of a theoretical plate and d_p is the particle diameter. Based on the superficial velocity (u_s) and the experimentally derived interstitial porosity (E_i) the reduced interstitial velocity (u_i) was determined using the following:

$$u_i = \frac{u_s}{E_i} \quad (5.5)$$

Where u_s is the superficial velocity based on the cross-sectional area of the empty column (A) whilst F is the volumetric flow rate u_s is then determined by:

$$u_s = \frac{F}{A} \quad (5.6)$$

The reduced interstitial velocity (v_e) is then determined by:

$$v_e = \frac{u_i d_p}{D_m} \quad (5.7)$$

All physiochemical property data for the analytes used in this study are illustrated in Table 5.1. Curve fitting was performed using Microsoft Excel and SigmaPlot, whilst construction of Kinetic plots based on Equations (5.2) and (5.3) was carried out with Kinetic Plot Creator 3.1. Mobile phase viscosity (η) was determined as 0.415 cP using the Chen and Horvath correlation [103] for binary acetonitrile-water mixtures.

Table 5.1. Physiochemical properties of test analytes. Analyte pKa values were taken from [193] and diffusion coefficients measured by McCalley [106] using the Taylor-Aris procedure.

Solute	pka	logP ^a	D_m at 30 °C ($\times 10^{-9}$ m ² /s)	D_m at 50 °C ($\times 10^{-9}$ m ² /s)
Nortriptyline	10.2	5.65	1.4	1.9
Diphenhydramin	9.2	3.66	1.4	1.9
Benzylamine	9.5	1.37	1.6	2.0
Procainamide	9.3	1.10	1.3	1.7

^a source www.chemspider.com

5.3 Results and discussion

5.3.1 Permeability and flow resistance comparison

In comparison to chromatographic systems operating reversed-phase separations, a HILIC mode offers certain kinetic advantages. Typical HILIC operation requires the use of organic rich mobile phases with low viscosity and high analyte diffusivity, usually only obtainable in reversed-phase separations using elevated temperatures. To evaluate the kinetic advantages between the stationary phases used in this study, backpressure and chromatographic efficiency were measured experimentally up to the flow and pressure limits of our chromatographic instrument. The Darcy equation (Equation 5.8) allows for the determination of flow resistance (ϕ) for each of the packed columns as a function of linear velocity (μ_o) and backpressure (ΔP) as follows:

$$\Delta P = \phi \frac{\eta L \mu_o}{d_p^2} \quad (5.8)$$

Where, η is the mobile phase viscosity and d_p is the particle diameter. In migrating to smaller particle sizes it is obvious that pressure will increase proportionally.

Figure 5.1 shows the experimentally derived plots of corrected column pressure versus linear velocity for each of the evaluated stationary phase materials. All data had linearity coefficients ≥ 0.999 . As to be expected, the highest backpressures were observed for the Fortis 1.7 μm and BEH 1.7 μm packed columns. Lower backpressures were obtained for the corresponding sub-2 μm superficially porous Kinetex materials. Data for the Fortis column above 7.1 mm/s was omitted as an increase in pressure and deviation from linearity was observed, indicating packing instability with this particular column. The Atlantis 3 μm and BEH 3.5 μm columns were not operated in excess of 180 bars due to flow rate restrictions with our instrument (≤ 2.0 mL/min). Therefore, operating at the maximum evaluated flow rate produced pressures < 180 bars

illustrating the potential for operating very long columns with these particular size particles. Operation of such phases at elevated pressures depends of course on the chromatographic hardware and mechanical stability of the packing.

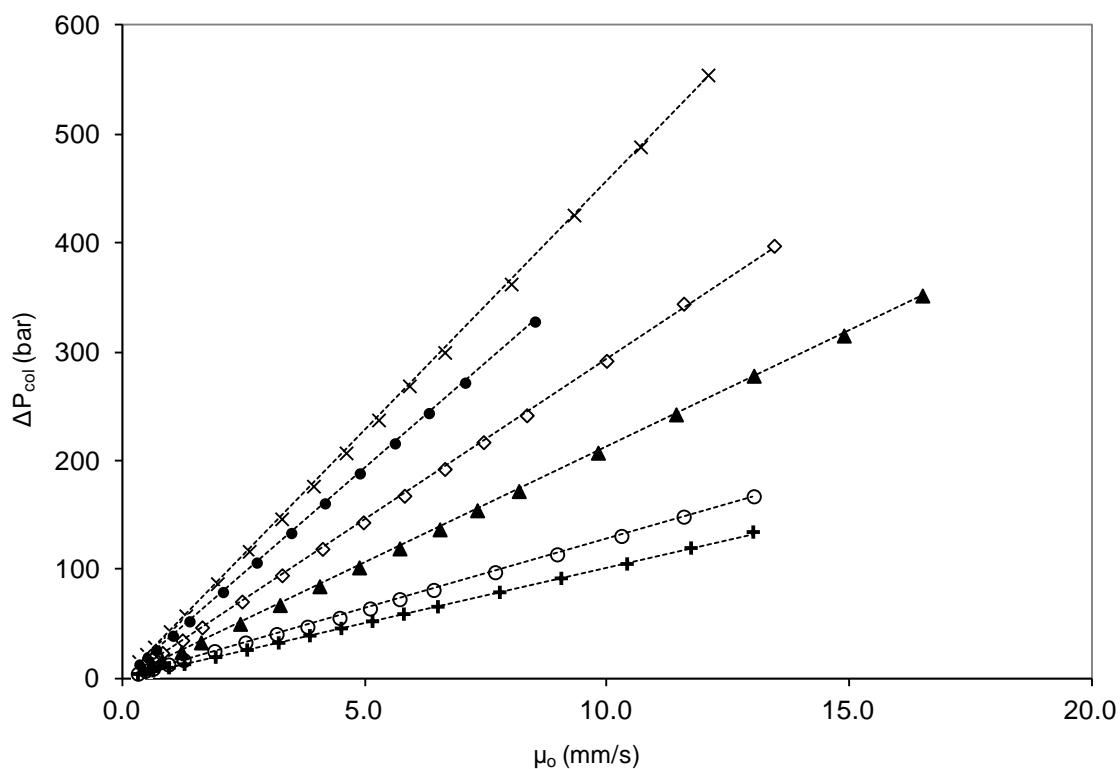


Figure 5.1. On column pressure drop versus linear velocity for the tested supports. BEH 1.7 μm ΔP_{max} 1000 bar (x), Fortis 1.7 μm , ΔP_{max} 1000 bar (●), Kinetex 1.7 μm ΔP_{max} 1000 bar (◇), Kinetex 2.6 μm ΔP_{max} 600 bar (▲), BEH 3.5 μm ΔP_{max} 400 bar (○) and Atlantis 3 μm ΔP_{max} 400 bar (+).

Table 5.2. Physical and kinetic characteristics of tested chromatographic supports.

Column ^a	Particle size (μm)	Dimensions (mm)	Type	Permeability (K_{vo}) ^b	Flow Resistance (Φ)	Pore Size (Å)	Surface Area (m ² /g)
1) Acquity BEH	1.7	2.1 x 50	Hybird, Fully porous	4.5E-15	640	130	185
2) Acquity BEH	3.5	2.1 x 50	Hybird, Fully porous	2.0E-14	610	130	185
3) Atlantis	3.0	2.1 x 50	Silica, Fully porous	1.6E-14	559	100	330
4) Fortis	1.7	2.1 x 50	Silica, Fully porous	4.4E-15	653	Unavailable	380
5) Kinetex	2.6	2.1 x 50	Silica, Superficially porous	7.0E-15	696	100	200
6) Kinetex	1.7	2.1 x 50	Silica, Superficially porous	9.7E-15	412	100	200

^a all phases are bare silica without bonded group

^b corrected for pressure drop (ΔP_{col})

As shown in Table 5.2, the two fully porous 1.7 μm materials had the lowest permeability values, characteristic for this type of particle packed column. On the other hand the larger (3.5 μm) fully porous particles had significantly higher permeabilities than their smaller (1.7 μm) particle counterparts, although interestingly the flow resistances were similar for the two BEH materials with slightly lower values obtained for the standard silica (Atlantis) variant. This may be due to similarities in packing techniques used to pack BEH particles resulting in similar bed densities. For the superficially porous Kinetex phases, the 1.7 and 2.6 μm materials were approximately 1.5 and the 2.0 times more permeable than the 1.7 μm BEH material respectively. Interestingly, flow resistance for the Kinetex 2.6 μm packing was found to be higher than all other packing materials with the corresponding 1.7 μm version having the lowest value. This is an unusual result in light of the larger solid core present in the supra-2 μm superficially porous versus the sub-2 μm version. This may be a function of the packing process, in that smaller particles are notoriously more difficult to pack than larger particles and differences in density of the packed bed may account for these observations. Similar differences in flow resistance were noted by Petersson *et al.* [37] in a previous study where higher values for the HALO versus the BEH material were obtained. Thus it is reasonable to assume that with an equivalent packing density, higher resistance to flow would be found due to the presence of a non-permeable solid-core in shell-particles when compared to their fully porous counterparts. Interstitial porosities (ϵ_i) were estimated using the Kozeny-Carmen equation for each column. For example, values of 0.3916 and 0.4395 were determined for the 2.6 μm and 1.7 μm Kinetex phases respectively. The former was lowest of all the evaluated columns in this study, which may further explain that the high flow resistance observed was due to differences in packing density. The very low flow resistance observed for the 1.7 μm Kinetex phase indicates loose packing, and we subsequently observed severe peak fronting upon conclusion of our van Deemter studies. Similar findings were noted in a separate paper by Yang *et al.* [98].

As dictated by theory, the kinetic advantages of using smaller particles are constrained by the pressure limitations required to operate at their optimal linear velocity. In the context of using HILIC mobile phases however, and with the appropriate surface chemistry to obtain adequate analyte retention, instrument pressure limitations can be somewhat overcome. Operation of sub-2 μm materials is obviously possible on conventional instrumentation, even at or near their optimum linear velocity when using organic rich mobile phases. However, as stated elsewhere

[38, 99] the optimisation of extra column system volume with such conventional systems would be essential for accommodating the inherently smaller peak volumes obtained. A recent examination by Guiochon [188] on optimising system volumes of several commercially available instruments was undertaken. It is therefore somewhat irrelevant to mention sub-2 μm HILIC based separations in the context of UHPLC with $\leq 5\text{cm}$ long columns, as this implies operation at pressures exceeding 400 bars.

5.3.2 Chromatographic performance comparison using basic solutes

5.3.2.1 Effect of flow rate on efficiency (van Deemter analysis)

Migration to smaller particle sizes brings the opportunity to achieve very efficient chromatographic separations. In order to compare the relative efficiencies of the selected columns in this study, van Deemter curves were constructed for a range of basic test solutes using toluene as a marker for the un-retained compound. As shown in Figure 5.2 data constructed for the test analyte procainamide shows an improvement in performance with decreasing particle size. Table 5.3 depicts the determined van Deemter coefficients for all the considered columns and analytes. For the three tested sub-2 μm columns the minimum plate heights achieved were comparable at approximately 4.7 μm using an optimum linear velocity between 2 and 4 mm/s. The minimum plate heights recorded here are slightly different to those reported by Veuthey *et al.* [182] for sub-2 μm bare silica phases. This is likely due to the nature of the test solutes used in this study. As stated in their findings, optimum linear velocities were lower than expected at a theoretical value of ~ 10 mm/s [36] for low viscosity eluents with small particle size packings. As also pointed out, the retention mechanism in HILIC is a combination of adsorption and partition, the contributions of which undoubtedly vary depending on the nature of the probe analyte and the chemical activity of the stationary phase. The slower retention isotherm involved with HILIC compared to reversed-phase systems may therefore be a suitable explanation for these observations. The C-term region of the van Deemter plot shows the typical upturn expected from larger diameter particles when exceeding the optimum linear velocity. Although the two fully porous materials have shallower upturns in their van Deemter curves, the

superficially porous 1.7 μm Kinetex phase showed superior behavior. A lower C-term contribution was observed for the superficially porous 1.7 μm packing indicative of the short diffusion distance with this type of particle.

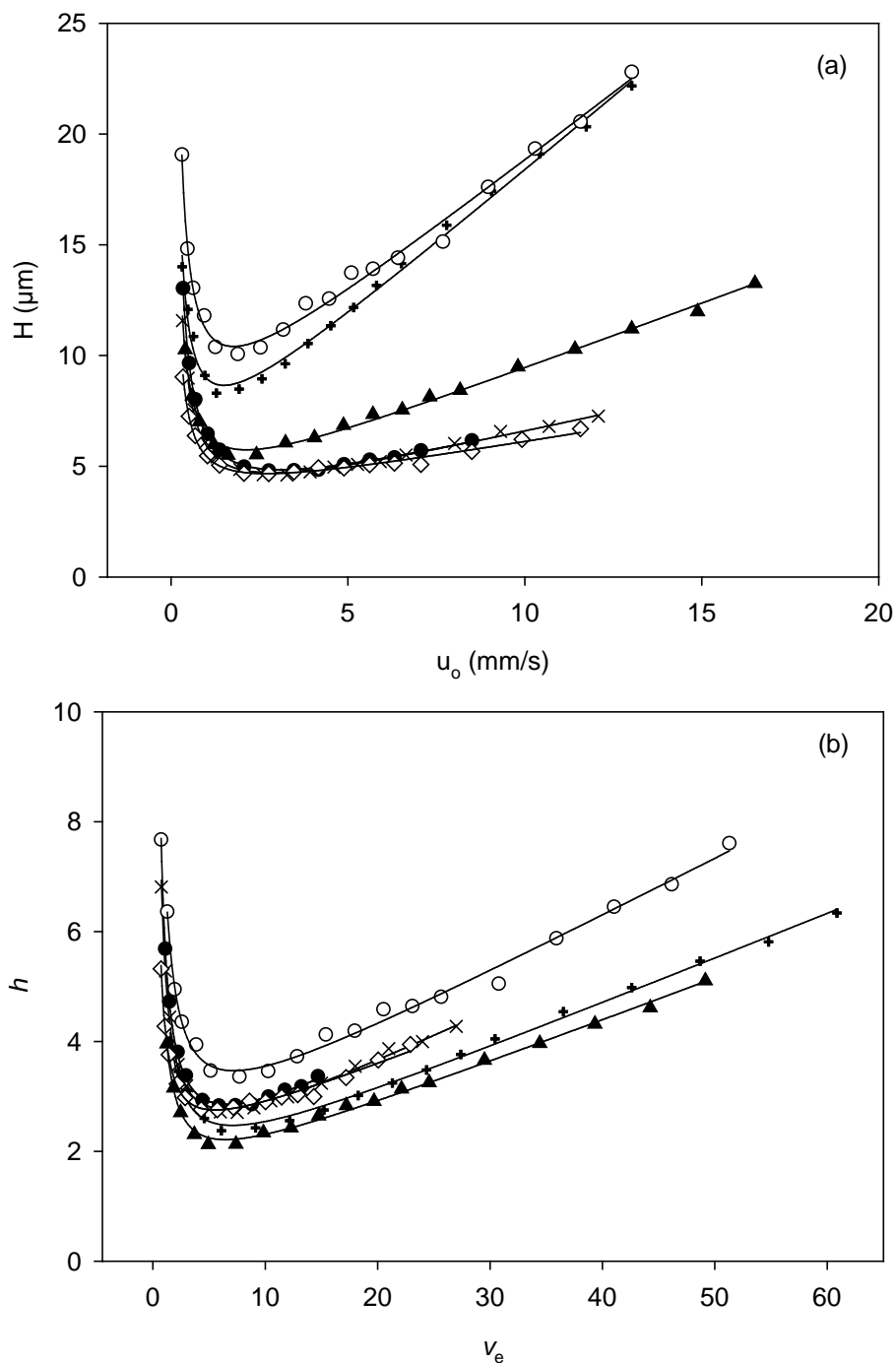


Figure 5.2. (a) van Deemter (b) Knox curves constructed for procainamide. Symbols are as for Fig. 5.1.

Table 5.3. Retention data and van Deemter curve fit coefficients.

Column ^a	Solute	k'	van Deemter coefficients			μ_{opt} (mm/s)	H_{min} (μm)
			A (μm)	B ($\times 10^{-4}$ mm ² /s)	C (ms)		
Acquity BEH (1.7 μm)	Nortriptyline	1.1	3.1	2.5	0.38	2.6	5.0
	Diphenhydramine	1.1	3.1	2.6	0.34	2.8	4.8
	Benzylamine	1.8	2.8	3.6	0.28	3.6	4.7
	Procainamide	2.6	2.7	2.9	0.37	2.8	4.6
Acquity BEH (3.5 μm)	Nortriptyline	1.0	5.8	2.6	1.23	1.5	8.8
	Diphenhydramine	1.0	5.3	2.9	1.18	1.6	8.5
	Benzylamine	1.7	4.5	4.0	1.06	1.9	8.3
	Procainamide	2.5	4.6	3.0	1.35	1.5	8.3
Atlantis (3.0 μm)	Nortriptyline	1.8	6.7	3.2	1.28	1.6	10.7
	Diphenhydramine	2.1	6.6	3.3	1.15	1.7	10.1
	Benzylamine	3.3	6.4	4.9	1.02	2.2	10.7
	Procainamide	5.5	6.0	3.9	1.24	1.8	10.1
Fortis (1.7 μm)	Nortriptyline	2.0	3.0	3.0	0.40	2.8	5.2
	Diphenhydramine	2.2	2.9	3.2	0.36	3.0	5.0
	Benzylamine	4.0	2.6	4.9	0.29	4.2	5.0
	Procainamide	6.0	2.6	3.5	0.37	3.1	4.8
Kinetex (1.7 μm)	Nortriptyline	1.2	3.8	1.6	0.31	2.3	5.2
	Diphenhydramine	1.4	3.2	1.8	0.31	2.4	4.7
	Benzylamine	2.2	3.0	2.6	0.25	3.2	4.6
	Procainamide	4.2	3.2	2.0	0.27	2.7	4.7
Kinetex (2.6 μm)	Nortriptyline	1.3	3.0	3.3	1.40	1.5	7.0
	Diphenhydramine	1.5	3.1	2.7	1.18	1.5	6.5
	Benzylamine	2.3	2.9	4.0	0.79	2.2	6.3
	Procainamide	4.2	3.2	2.7	0.60	2.1	5.5

^a all columns were 5 cm in length

As indicated previously [92], one of the benefits of using superficially porous materials is the reduced analyte diffusion distance into the core of the particle. Guiochon *et al.* [93] described the dependency on the ratio (ρ) of the overall particle diameter to that of the solid core on intraparticle diffusivity. This has been examined further by Glennon *et al.* [168] who investigated what the optimum shell thickness might be for shell-type stationary phases. Their study indicated higher C -term coefficients with phases prepared with increasing solid-core to shell thickness ratios. Overall, our study showed that the superficially porous 1.7 μm particle outperformed the fully porous phases in the C -term region of the constructed van Deemter curves. Very similar mass transfer coefficients were found between the larger fully porous particles, an unusual result considering the Atlantis is conventional silica whereas the 3.5 μm BEH is a hybrid material and that the former are usually considered to perform more efficiently. It should also be highlighted that the lack of a bonded group or polymeric coating on the surface of any of the particles examined means mass transfer should be maximised. This was referred to previously in separate publications by McCalley [183] and Hemström *et al.* [194] for the interpretation of the van Deemter behavior of polymer functionalised silica in the HILIC mode.

With regards to the determined *B*-term coefficients, the lowest overall value was found with the 1.7 μm Kinetex phase. Highest values were obtained with the silica based fully porous Atlantis and Fortis phases which are perhaps related due to their similar surface areas and pore sizes. Atlantis had the largest *B*-term coefficient, and this may be linked to it also having the lowest flow resistance and highest permeability. The Kinetex 2.6 μm phase had larger overall axial diffusion coefficients compared to the 1.7 μm material. Similar results were obtained between the BEH materials, with the larger particle substrate having higher *B*-term values. This is then perhaps due to the higher permeabilities observed with the larger particles. Notably, no significant reduction in axial-diffusion was observed with the 2.6 μm superficially porous material usually observed as a function of the low internal porosity due to the presence of the solid-core. The *B*-term is inextricably linked to the solute retention factor [195] and can only be realistically compared when similar values are obtained on each phase. It is therefore pertinent to mention the difficulty in obtaining equivalent retention factors for each test solute on each of the tested supports in the HILIC mode. In reversed-phase mode however manipulation of the mobile phase composition in order to obtain similar retention is more convenient. Hence, this study was carried out using a set of physiochemically different test analytes with varying hydrophilic character, covering a range of retention factors. The *B*-term usually increases with increasing retention factor, however this was not observed with all phases. This observation may be a function of molecular diffusion coefficient, pore exclusion or a not fully characterised axial diffusion term (i.e. insufficient data points at low linear velocities).

The *A*-terms derived for each of the evaluated columns provide an insight into the differences in Eddy diffusion behavior. However these values are practically of no use when comparing supports of different morphology, due to the proportional relationship with particle size. It is therefore more useful to compare these values independent of particle size, as is dealt with in section 5.3.2.2. Chromatograms of each column operated at their van Deemter optimum are shown in Figure 5.3.

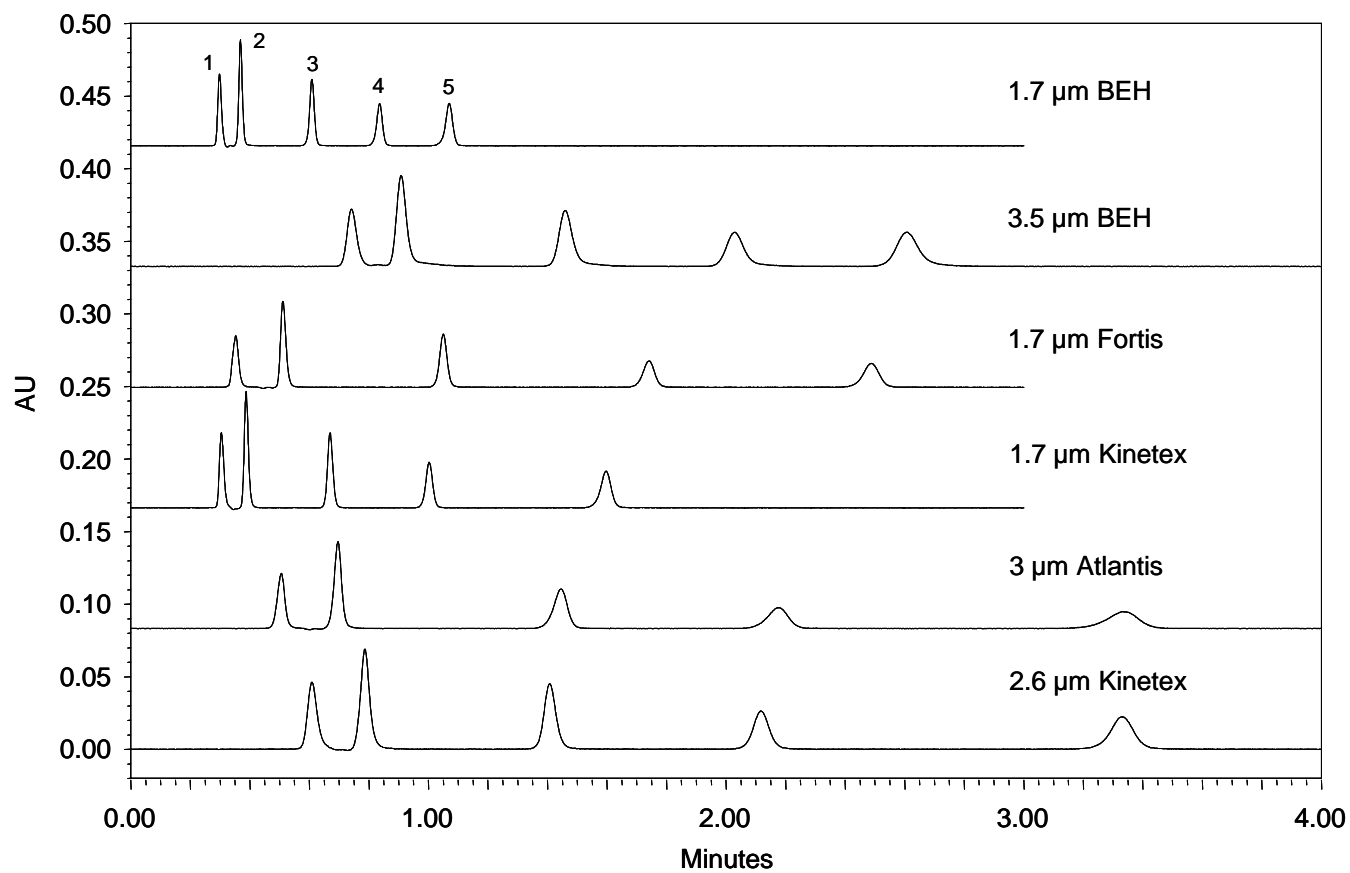


Figure 5.3. Separation of (1) toluene (2) caffeine (3) benzylamine (4) nortriptyline (5) procainamide. Order of elution identical on each column. Columns operated to yield their respective optimum plate number. Chromatographic conditions are as in section 5.2.1.

5.3.2.2 Knox plot data (ambient temperature)

Although there is a dependency on the accuracy of the mean particle size distribution when considering data fitted to the Knox equation, there is still merit in evaluating the extrapolations. This is particularly useful when comparing the performance merits of each support based on the packing quality of each column. In this particular study it was deemed necessary to utilise the reduced interstitial velocity which takes into account the space in-between the particles, and as such allows interrogation of velocity biases of particular supports. It has been suggested that when there is a homogeneous distribution of axial velocities, low Eddy diffusion values are achieved. The Knox equation is represented below using reduced plate height and linear velocity parameters:

$$h = A v^{1/3} + \frac{B}{v} + C v \quad (5.9)$$

The fitting coefficients for each column and probe analyte are shown in Table 5.4 transformed using the previously determined van Deemter data set. The Knox plot for procainamide is shown in Figure 5.2 (b). Minimum reduced plate heights were in the region of 2-3 with no anomalous results. Previous reports [188] suggest smoothness of the particle surface can somewhat influence the packing quality and also contribute to the analyte mass transfer resistance term, caused by a stagnant external film of mobile phase. The roughness of the particle surface is said to prevent slippage during bed formation which intrinsically allows for a more homogeneous packing structure. The Kinetex 2.6 μm showed the lowest overall reduced A-term coefficients (average of 1.1) indicating superior packing quality compared with the other tested columns. Improvements in packing qualities of superficially porous materials have been examined on several occasions, indicating that particle size distribution may account for the lower eddy diffusion coefficients observed. In contrast, Guiochon *et al.* [189] have reported that particle size distribution may not be the sole contributing factor to lower A-term values for shell-particle packed columns. Instead, their conclusions suggest significant reductions are realised in either or both of the trans-column and long-range inter channel-velocity biases, which are related to the structure of the packed bed.

Table 5.4. Knox curve fit coefficients.

Column ^a	Solute	Knox coefficients			V_{opt}	Calc. h_{min}	Exp. h_{min} ^b
		A	B	C			
Acquity BEH (1.7 μ m)	Nortriptyline	1.8	3.2	0.107	5.5	3.0	2.9
	Diphenhydramine	1.8	3.4	0.096	5.9	2.9	2.8
	Benzylamine	1.6	4.1	0.090	6.7	2.8	2.8
	Procainamide	1.5	4.0	0.097	6.4	2.8	2.7
Acquity BEH (3.5 μ m)	Nortriptyline	1.6	3.4	0.081	6.5	2.7	2.5
	Diphenhydramine	1.5	3.8	0.078	7.0	2.6	2.4
	Benzylamine	1.3	4.5	0.080	7.4	2.5	2.4
	Procainamide	1.3	4.1	0.083	7.1	2.5	2.4
Atlantis (3.0 μ m)	Nortriptyline	2.2	4.2	0.117	6.0	3.6	3.6
	Diphenhydramine	2.1	4.3	0.105	6.4	3.5	3.4
	Benzylamine	2.1	5.7	0.107	7.3	3.6	3.6
	Procainamide	1.9	5.5	0.106	7.2	3.5	3.4
Fortis (1.7 μ m)	Nortriptyline	1.7	3.6	0.123	5.4	3.1	3.1
	Diphenhydramine	1.7	3.9	0.109	5.9	3.0	2.9
	Benzylamine	1.5	5.1	0.099	7.2	3.0	2.9
	Procainamide	1.5	4.5	0.104	6.6	2.9	2.8
Kinetex (1.7 μ m)	Nortriptyline	2.2	1.8	0.097	4.3	3.1	3.0
	Diphenhydramine	1.9	2.0	0.091	4.7	2.8	2.8
	Benzylamine	1.8	2.6	0.087	5.5	2.7	2.7
	Procainamide	1.9	2.4	0.076	5.7	2.8	2.8
Kinetex (2.6 μ m)	Nortriptyline	1.1	3.7	0.195	4.3	2.8	2.7
	Diphenhydramine	1.1	3.0	0.164	4.3	2.5	2.5
	Benzylamine	1.1	3.8	0.125	5.5	2.4	2.4
	Procainamide	1.2	3.2	0.078	6.5	2.2	2.1

^aall columns were 5 cm in length^bcalculated based on manufacturers d_p values

The highest eddy diffusion coefficient was determined for the Atlantis silica which may be due to wider particle size distribution, possibly due to the fact that this is an 'older-type' silica material and hence results in poor packed bed homogeneity. In comparison to the values obtained by McCalley [104] using a 4.6 mm ID column packed with 5 μ m particles, as opposed to the 2.1 mm ID size used in this study, inferior van Deemter coefficients were observed. This could be ascribed to the poorer packing generally observed for microbore columns. The reduced A-term coefficients for the Kinetex 2.6 μ m resulted in remarkably low reduced plate heights for basic solutes using a microbore column (Procainamide, $h_{min} = 2.1$). However, this is still significantly below what is achievable with this type of material when packed into 4.6 mm ID columns, with the lowest reported reduced plate height being around 1.1 for a neutral compound [196]. Nevertheless, this result is promising considering the losses in performance generally reported for columns with small internal diameters packed with sub-3 μ m particles. In comparison, the Kinetex 1.7 μ m particle had significantly higher A-coefficients than the equivalent fully porous materials which are in contrast to what might be expected for monodisperse packings. Similar

findings were observed by Glennon *et al.* [168, 169] and are almost comparable to those obtained for the Atlantis silica. This is perhaps due to the density of the packing resulting in poorer bed homogeneity. Interestingly however, the *B*-coefficients were overall lower for this material (in the region of 1.8-2.4) suggesting some advantage to the solid-core in reducing axial dispersion. The 1.7 μm Kinetex particle exhibited the lowest *C*-term values of all the phases implying advantages due to the thickness of the diffusion layer, a feature not observed with the 2.6 μm material. It appears then that much of the performance gains of the sub-2 μm core-shell particles are due to enhanced mass transfer and reduced axial diffusion properties. Moreover, it could be that if *A*-term values were indeed similar to the 2.6 μm counterpart then extremely efficient separations could be achieved. It has nevertheless been suggested that the advantage of reduced diffusion paths becomes more significant for larger molecules such as proteins and peptides with increasing flow rate [197].

Surprisingly, the 3.5 μm BEH material showed superior performance in comparison to the 1.7 μm counterpart offering excellent reduced plate heights of 2.3-2.5. Much of the difference can be accounted for due to the reduced Eddy diffusion term, however their respective *C*-term behaviors differ somewhat. This difference could be ascribed to the effect of frictional heating and the low thermal conductivity of the mobile phase. Unlike what has been stated previously [182], frictional heating is very much present even when operating at low pressures, as reported by the earlier work of Poppe *et al.* [150, 153]. Recently, McCalley [179] reported that the poor thermal conductivity of acetonitrile rich mobile phases results in insufficient radial heat transport. The impact of which results in an increasing steepness in the upturn of the *C*-term region of the Knox curve, whereas in more aqueous based eluents this detrimental effect is less significant. Considering the similarities and close retention factors between the experiments regarding the BEH materials this may explain then the divergence in their apparent *C*-term values. Lower *C*-term values were observed for the superficially porous materials. This correlates with the work reported by Guiochon *et al.* [198], in that the thermal conductivity of core shell-materials was found to be superior at 0.69 W/m/K as opposed to 0.31 W/m/K for hybrid-based particles (BEH) hence assisting in favorable heat transport. The impact of this on plate height is more important across the radius of the packing rather in the longitudinal coordinate.

As discussed previously, the migration to smaller bore column formats tends to result in inferior packing reflected in the Knox *A*-term coefficients. The resulting performance losses observed (before correction of data to account for extra-column band broadening at the corresponding flow rate as per section 4.2.3) are therefore a combination of packing quality and poor system optimisation. To illustrate losses in performance due to the chromatographic system, corrected versus uncorrected data are shown in Figure 5.4 obtained at the highest achieved plate count on each column. This highlights that for analytes with low retention factors large performance losses are observed even on a modern instrument with very low extra column volume. This means that the advantages of adopting microbore column technology (≤ 2.1 mm internal diameter) may not be fully realised as predicted by theory. Until such advances are realised the use of small bore columns may not result in the theoretical performance gains. This becomes more relevant when moving to smaller particles as frictional heating effects become increasingly significant. However, this can be alleviated by moving into yet smaller bore columns as the reduced volumetric flow will lead to a diminished frictional heating.

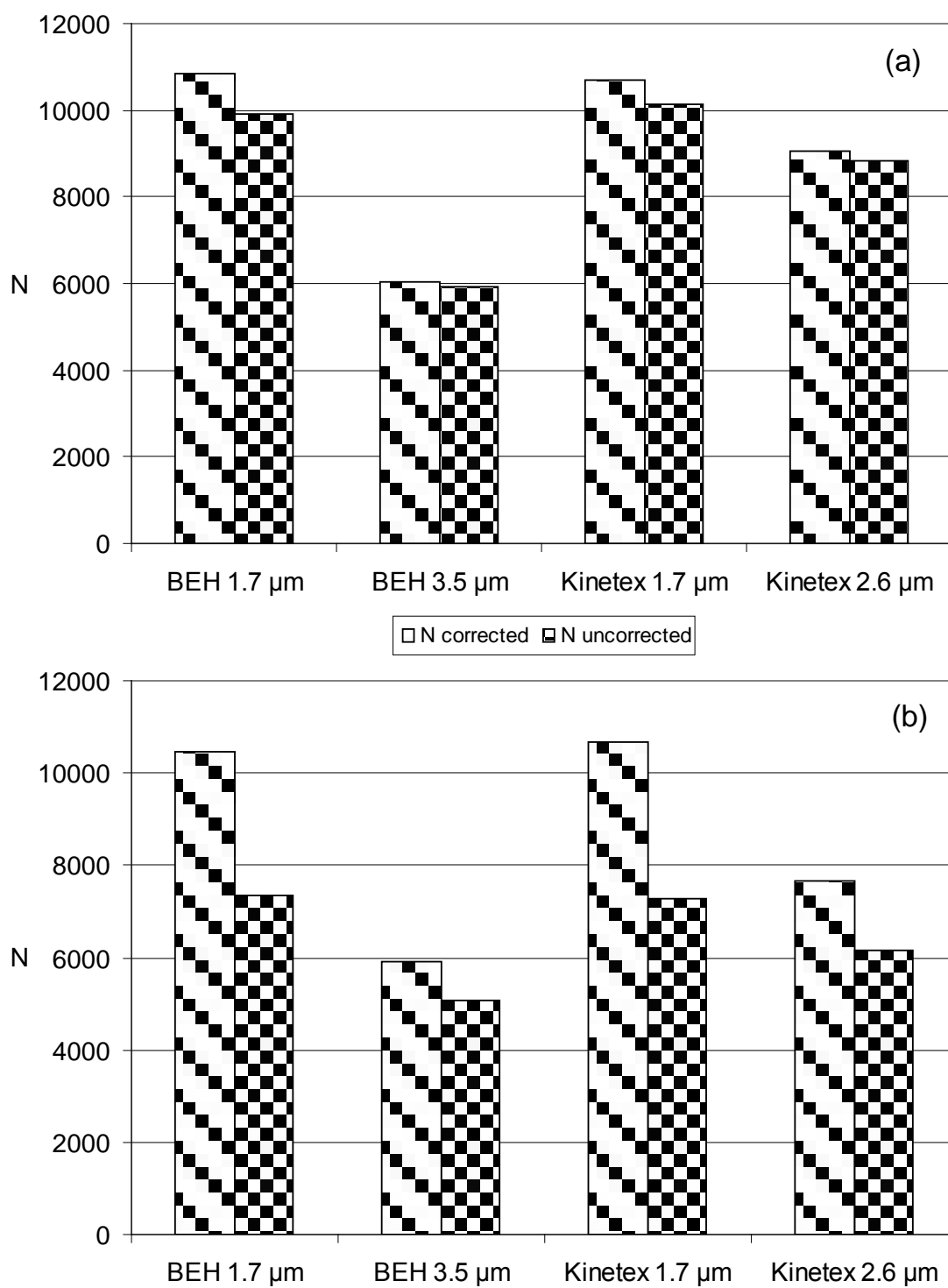


Figure 5.4. Comparison between observed and corrected column performance for (a) procainamide and (b) diphenhydramine at the optimum plate count achieved for each phase.

5.3.2.3 Operation at moderate versus ambient temperatures

Guiochon *et al.* [197] reported that when operating at elevated versus ambient temperatures a deterioration in resistance to mass transfer resulted when using core-shell materials, contrary to expectation, due to the effect of temperature on the diffusion coefficient. This work was followed up by McCalley [106] using the same column except with bare silica in the HILIC mode, who was able to reach higher reduced interstitial velocities than those reported in previous studies. No dramatic upturn in the *C*-term was observed between ambient and moderate temperatures contrary to findings from the previous report. In this study however, much higher reduced interstitial velocities were achieved due to the adoption of much smaller column formats as well as using low viscosity eluents. As discussed in a previous section, an upturn in the *C*-section of the Knox curve was observed even at ambient temperature for the supra-2 μm shell-particles, in contrast to theoretical expectation. In addition to data collected at 30 °C, the same experiment was performed at moderate (50 °C) temperatures in order to observe whether resistance to mass transfer deteriorated with the core-shell particles. This data is illustrated in Table 5.5.

Table 5.5. Knox *C*-terms determined at ambient and moderate temperatures.

Column	Temperature (°C)	Knox <i>C</i> -term (Benzylamine)	Knox <i>C</i> -term (Procainamide)
Kinetex 1.7 μm	50	0.062	0.072
	30	0.087	0.076
Kinetex 2.6 μm	50	0.133	0.085
	30	0.125	0.078
BEH 1.7 μm	50	0.088	0.098
	30	0.090	0.097
BEH 3.5 μm	50	0.084	0.089
	30	0.080	0.083

As shown in Table 5.5 and in agreement to the work of McCalley, only a slight increase in the *C*-term coefficient upon increasing temperature for the 2.6 μm Kinetex phase was observed. In contrast, the 1.7 μm material showed a small decrease in the *C*-term coefficient, in line with theoretical expectation for increased temperature operation. Very similar mass transfer

behaviors were found with the fully porous BEH materials upon increasing temperature. All analytes showed increases in their axial diffusion coefficients as would be expected, albeit to varying degrees and not in keeping with their retention factor (data not shown). This was particularly true for benzylamine, which being the simplest probe analyte is perhaps more able to interrogate the pores of the silica than procainamide which had a higher retention factor. Interestingly, with increasing temperature, solute retention factors remained similar, meaning that actual differences in mass transfer are due to the impact of reduced viscosity on diffusion coefficient alone and not due to changes in organic modifier concentration. Usually with reversed-phase optimisation, manipulation of the mobile phase is carried out in order to achieve identical retention factors. However, the resulting differences in viscosity are often ignored and the impact on the C - and B -terms can be somewhat significant and misleading, especially if kinetic plot extrapolations are derived from such data. Veuthey *et al.* [180] reported that kinetic plot predictions can be compromised depending on the column length on which the original van Deemter data was determined, due to the differences in packing qualities of columns of increasing lengths. This is dealt with in the next section.

5.3.2.4 Kinetic plot representation of data

The use of kinetic plots has gained much interest for chromatographic support evaluation, reviving the earlier work of Poppe [19]. These extrapolations are useful for determining the plate counts which may be achieved with a given support when constrained by the maximum operating pressure of the chromatographic instrumentation. Such is the trend to smaller and more sophisticated particles it has become relevant to compare chromatographic efficiencies based on the limitations which may be imposed by the equipment i.e. the maximum available operating pressure. This is becoming vastly important as operation at the optimum pressure maximises the column operating performance. Initially many kinetic plot extrapolations were made using neutral or chromatographically well behaved analytes, providing useful information as to the performance limitations of differing chromatographic materials. Basic solutes are one of the most challenging classes of analytes to chromatograph and still present problems in terms of optimising peak shape. As shown previously [104], HILIC often produces highly symmetrical peak shapes for basic compounds, which is not usually the case when using reversed-phase conditions. The kinetic plot methodology was applied to pharmaceutically relevant compounds using reversed-phase approaches as shown by Fanigliulo *et al.* [199, 200]. Having already determined van Deemter data for the four basic compounds in this study on each stationary phase, transformation into the kinetic plot representation is possible using the approach outlined by Desmet, as discussed previously. Using the kinetic plot extrapolation procedure it is possible to show the potential benefits of all the evaluated phases, including those which are recommended to be operated ≤ 400 bars at even higher pressures. Likewise it is also representative to compare performance merits at the recommended maximum operating pressure as is shown in Figure 5.5 (a). Moreover, the very low operating viscosity enjoyed with HILIC mobile phases offers kinetic advantages for analytes such as hydrophilic bases which cannot be obtained using reversed-phase i.e. using much longer columns or operation at very high flow rates.

Figure 5.5 depicts the simplest kinetic plot representation showing the achievable plate number at any given analysis time, as limited by the system operating pressure. Figure 5.5 (b) and (c) illustrate the kinetic performance extrapolated to 600 and 1000 bar for all columns. It is possible then to present the potential efficiencies at any given pressure maximum as dictated by the instrument limit and or particle mechanical stability. In a separate publication by Veuthey *et al.* [182] on HILIC column evaluation, poor curve fitting in the high efficiency or *B*-term region was noted, suggested as due to lack of experimental data. It may also be possible that the prediction of analyte diffusion coefficient may have been inaccurate since it was determined using the Wilke-Chang equation, which has been noted to be prone to error when calculated in acetonitrile rich mobile phases [17].

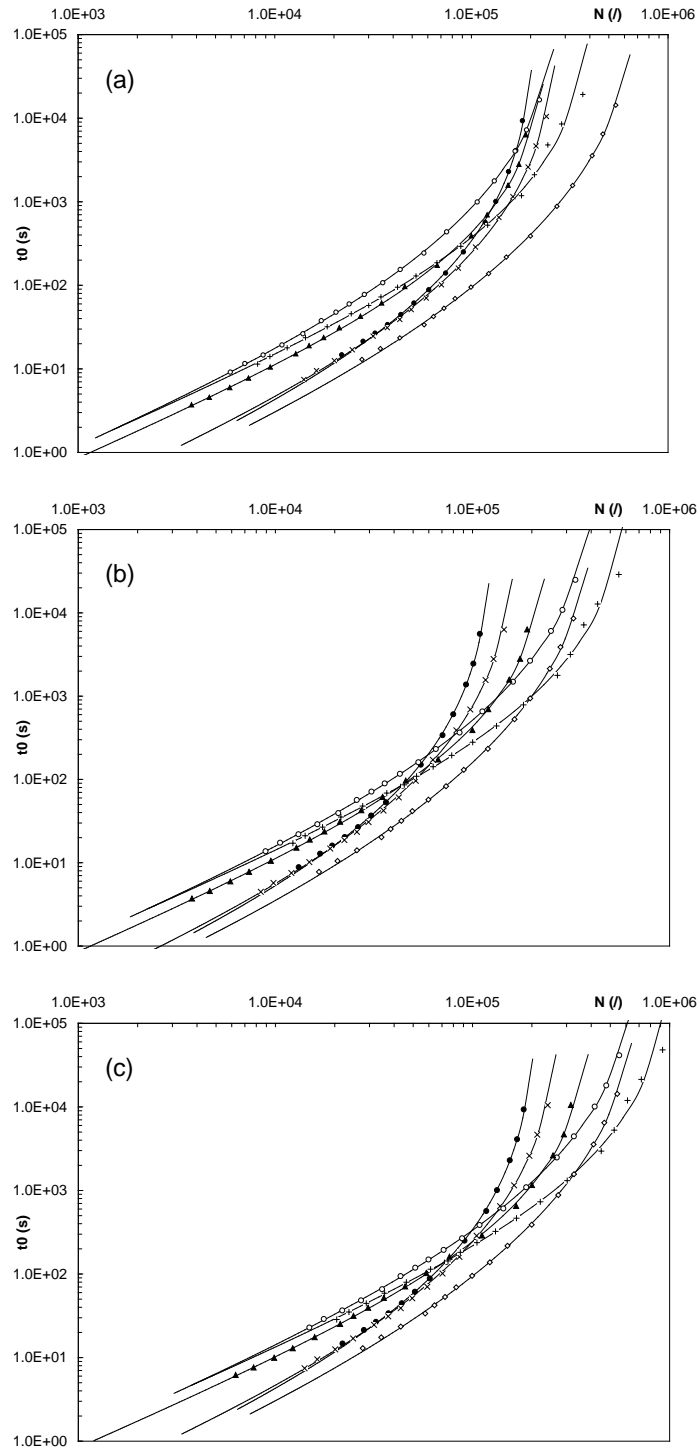


Figure 5.5. t_0 versus N kinetic plots for benzylamine. Plot (a) plotted at ΔP_{max} based on manufacturer recommendations and (b) at 600 bar ΔP_{max} and (c) 1000 bar ΔP_{max} . BEH 1.7 μm (x), Fortis 1.7 μm (●), Kinetex 1.7 μm (◇), Kinetex 2.6 μm (▲), BEH 3.5 μm (○) and Atlantis 3 μm (+).

The curve fitting performed in this study utilised diffusion coefficients determined in a previous report by McCalley [106]. As observed in both Figures 5.5 and 5.6, very acceptable fitting coefficients were determined allowing interpretation of the B -term dominant region of the kinetic plot asymptote. This corresponds to the maximum number of plates achievable with a particular support at a given operating pressure, denoted by the following [22]:

$$N_{\max} = \frac{\Delta P}{\eta} \left[\frac{K_v}{B} \right]_{\text{exp}} \quad (5.10)$$

The plot of t_0 versus N shown in Figure 5.5 is useful for comparing the achievable plate numbers for each of the investigated columns across a range of analysis times. In terms of fast and efficient analysis, the lower asymptote is regarded as the most relevant, since here the columns are operated at high flow rates. Table 5.6 shows the calculated extrapolations and the corresponding column lengths required to achieve a particular plate count at a fixed analysis time. It is clear that the larger supra-2 μm particles do not outperform the sub-2 μm phases at $t_0 \leq 10$ (s) regardless of the applied operating pressure. Conversely, if very high plate counts are required the larger particles dominate except at the expense of analysis time.

Table 5.6. Comparison of achievable plate counts at set analysis times and corresponding column length required at different maximum pressures. Column (1) BEH 1.7 μm (2) BEH 3.5 μm (3) Atlantis 3 μm (4) Fortis 1.7 μm (5) Kinetex 2.6 μm (6) Kinetex 1.7 μm .

$\Delta P_{max} = 1000 \text{ bar}$						
t_0 (s)	10		500		1000	
Column	N	L (cm)	N	L (cm)	N	L (cm)
1)	17446	10	128551	74	157011	104
2)	7653	22	174091	156	258934	220
3)	7377	20	125835	139	179524	197
4)	18072	10	111754	73	132496	103
5)	9800	13	143018	92	189554	130
6)	24600	15	218010	108	282316	153

$\Delta P_{max} = 600 \text{ bar}$						
t_0 (s)	10		500		1000	
Column	N	L (cm)	N	L (cm)	N	L (cm)
1)	14792	8	89741	57	106390	81
2)	7317	17	140784	121	200128	170
3)	6850	15	98570	108	135649	153
4)	15018	8	76303	57	88009	80
5)	9077	10	106238	71	134759	101
6)	21036	12	158848	84	199970	119

$\Delta P_{max} = 400 \text{ bar}$						
t_0 (s)	10		500		1000	
Column	N	L (cm)	N	L (cm)	N	L (cm)
1)	12752	7	66400	47	77021	66
2)	7002	14	116168	98	159275	139
3)	6387	12	79678	88	106588	125
4)	12729	7	55535	46	62805	65
5)	8428	8	81963	58	100667	82
6)	18309	10	121726	68	149891	97

For fast analyses in particular, analysis times of $t_0 \leq 10$ (s) the 2.6 μm Kinetex phase would correspond with operation at linear velocities into the C-term region which is not as flat as the corresponding sub-2 μm particles. This is better visualised in Figure 5.6 which closely resembles the curvature of the classical van Deemter plot. All supra-2 μm phases exhibit the same trend in the fast analysis region which is intrinsically linked to their C-term behavior. When operating at well above 400 bar, as is the case with the supra-2 μm materials, the vertical asymptote of the kinetic curve shifts towards higher achievable plate numbers significantly exceeding those possible with sub-2 μm particles. This is due to the higher permeabilities of larger particles allowing for much longer columns to be operated within a given maximum pressure. However, in order to achieve plate counts in the region of $\sim 500,000/\text{m}$ the predictions dictate the use of columns which are several meters in length and require prohibitively long analysis times. As shown in Table 5.6, analysis times of $t_0 = 500$ (s) and 1000 (s) column lengths in excess of 50 cm towards several meters are required in order to achieve such high plate counts. Such columns are not commercially available and must be manufactured to withstand ultra-high pressure operation. Also, such lengths of column would require very long re-equilibration times when used in gradient mode. It is also worth mentioning in the context of HILIC that acetonitrile compressibility at pressures > 400 bar may also inflict poor kinetic predictability due to changes in molecular diffusivity and viscosity [201]. Veuthey *et al.* [180] reported that extrapolations of data based on columns of different length can result in erroneous kinetic plot predictions and therefore only hold true to columns of similar packing qualities. Interestingly however, due to the low B-term values obtained for the Kinetex 1.7 μm particle this material outperformed the larger particle materials in the high plate count vertical asymptote region. As dictated by Equation 5.10 the performance gain is also related to the permeability found with this column, therefore the combination of these values resulted in overall kinetically superior performance. In the fast analysis region this column also outperforms all other sub-2 μm particles in that similar plate counts are achieved but with shorter analysis times. This is an interesting observation and correlates well with the work of Fekete *et al.* [181] in their evaluation of the same particle substrate except in reversed-phase.

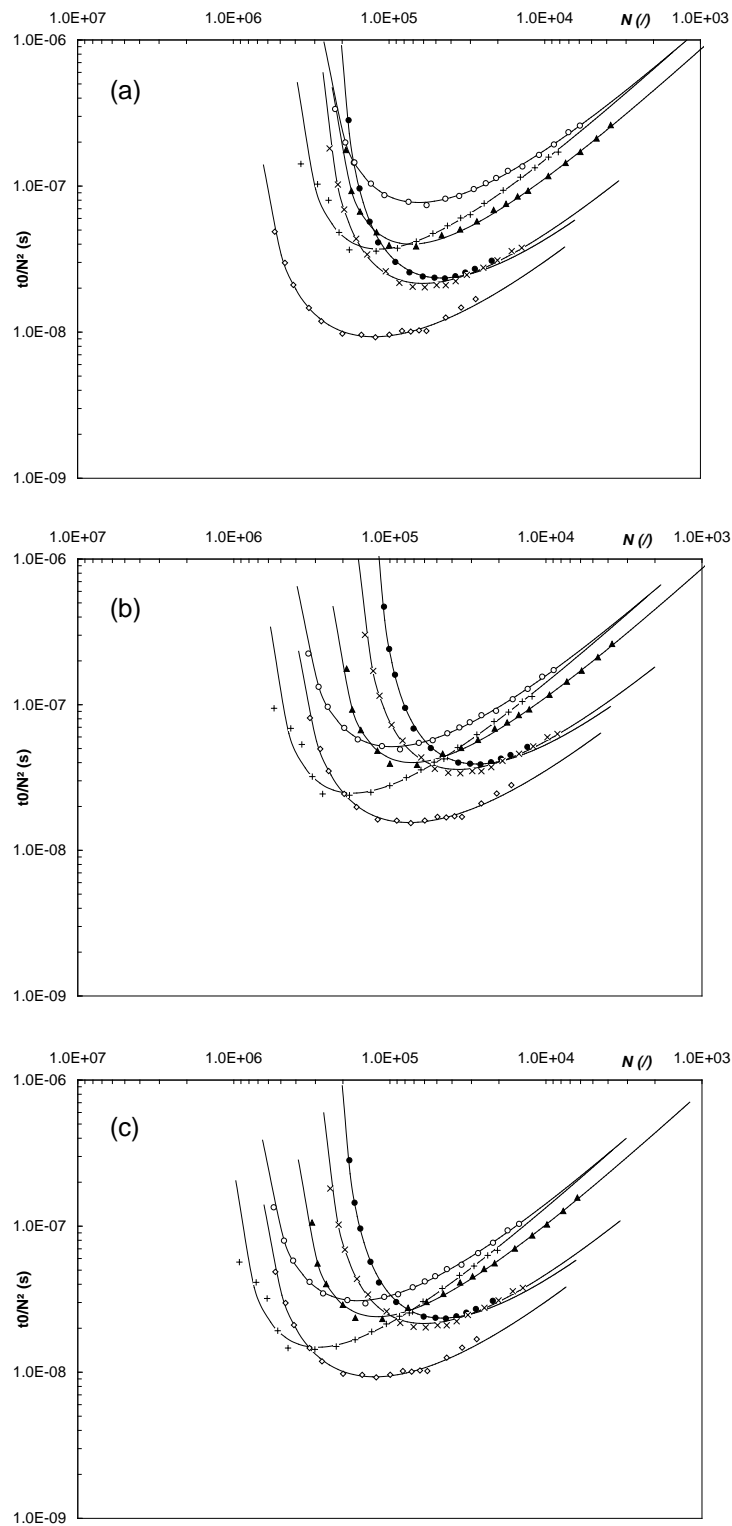


Figure 5.6. t_0/N^2 versus N kinetic plots for benzylamine. Plot (a) plotted at ΔP_{max} based on manufacturer recommendations and all at (b) 600 bar ΔP_{max} and (c) 1000 bar ΔP_{max} . Symbols as in Fig. 5.5.

Kinetic plots can also be illustrated in terms of separation impedance (t_o/N^2) versus plate count as shown in Figure 5.6 using benzylamine as the probe analyte. Here the orientations of the curves are synonymous to those of a typical van Deemter curve. The minima of each curve correspond to N_{opt} as well as the Knox-Saleem limit for each of the tested supports. Again, the Kinetex 1.7 μm yielded the most kinetically favourable performance when operated at 1000 bar. When operating at the recommended pressure maximum for each column, as in the kinetic plot in Figure 5.6 (a) with plate counts between $1.0E5$ and $1.0E4$, the sub-2 μm materials perform best due to the excessive column lengths required to achieve equivalent efficiencies with larger particles. Upon increasing pressure from 600 to 1000 bar as in Figure 5.6 (b) and (c) the curves shift down and left illustrating potential performance gains in operating at even higher pressures, particularly noticeable with the large particle materials. However, as stated previously these require potentially unrealistic column lengths and analysis times ($t_o > 8$ minutes) to be practically useful. The increasing pressure on the C-term region in Figure 5.6 (b) and (c) shows no benefit other than increased analysis speed and the advantages in using smaller particles remain apparent.

5.4 Conclusion

Short, microbore columns packed with bare silica stationary phases of varying particle diameters were compared under HILIC operating conditions using pharmaceutically relevant test probes. Various kinetic data were determined illustrating that migration to smaller particles does indeed yield the most efficient separations in the shortest amount of time, such as the adoption of sub-2 μm materials. However, significant performance losses are observed even when using a modern UHPLC instrument, especially for poorly retained solutes. In light of the low viscosity operation of HILIC it should be cautioned that the use of column formats packed with small particles on conventional systems should only be undertaken on a well optimised instrument. The migration into yet smaller bore columns will indeed become more prevalent in order to accommodate increasingly smaller particles and higher pressures, as the reduced volumetric flow will lead to diminished frictional heating which is in turn critical to preserving column performance. The kinetic advantages of sub-2 μm superficially porous particles were shown to be particularly interesting in terms of their relative permeabilities and *B*-term performance, allowing for much longer column formats than would be generally possible with the corresponding fully porous particle sizes. However, further work is necessary to elucidate whether the observations shown here are valid considering the lower than expected backpressure and flow resistance of the sample 1.7 μm Kinetex column used here. Overall, the evaluated sub-2 μm phases offered practically comparable efficiencies. In light of the kinetic extrapolations of larger particles yielding very high plate counts, it should perhaps be considered that this is not a practically viable means of achieving such efficiencies, especially when taking into account the analysis times and column lengths required.

Chapter 6

Comparison of reversed-phase and hydrophilic interaction liquid chromatography for the separation of ephedrines

Abstract

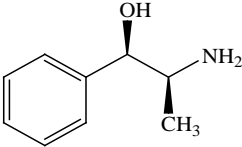
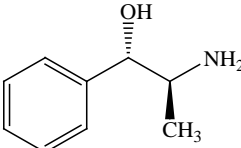
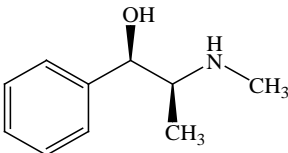
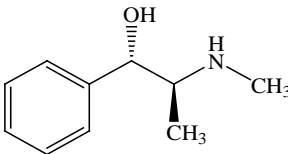
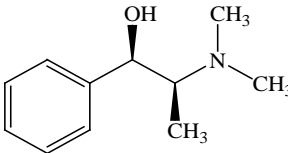
Following on from the previous chapter on the kinetic evaluation of bare silica phases an application was sought to embellish on the utility of HILIC. The separation of highly basic solutes is an ongoing challenge, especially in achieving suitable retention and peak shapes for compounds such as ephedrines that have both high pK_a values (≥ 9.3) and low lipophilicity ($\log P \leq 1.74$). In this chapter the application of HILIC as a potential alternative approach for the fast separation of the ephedrines phenylpropanolamine, cathine, ephedrine, pseudoephedrine and methylephedrine in doping control analysis was investigated. Using sub-2 μm bare silica bridged-ethylene hybrid (BEH) HILIC material, the effects of organic modifier, buffer pH and concentration and column temperature on the retention and selectivity of these compounds were evaluated. Highly symmetrical peak shapes for all ephedrines were achieved under HILIC conditions ($A_{s0.1} \leq 1.1$). Also compared was the kinetic performance of the optimised HILIC separation with a previously developed high pH reversed-phase approach. This would not realistically be possible without pH stable hybrid materials, and further demonstrates the impact of BEH particles for modern chromatography. van Deemter curves and kinetic plots for the two approaches were constructed and illustrate the kinetic benefits of HILIC over the reversed-phase approach. Improved mass transfer characteristics and enhanced diffusion with HILIC offers lower C-term coefficients of 1.46 and 5.68 for ephedrine with HILIC and RPLC, respectively.

6.1 Introduction

Achieving symmetrical peak shapes and acceptable retention factors for hydrophilic basic compounds with high performance liquid chromatography (HPLC) is challenging by traditional reversed-phase approaches. In cases where these types of solutes are also polar, such as ephedrines which are highly basic (pK_a values > 9.3) and hydrophilic ($\log P$ values < 1.74), the challenge is amplified and provokes alternative solutions for separation by LC (see Table 6.1 for analyte properties). In human sport, the World Anti-Doping Agency (WADA) prohibits the use of many of the ephedrines since they are regarded as stimulants [202]. At present, cathine (norpseudoephedrine), ephedrine, pseudoephedrine and methylephedrine are prohibited in competition above threshold concentrations. To control use, urine samples from athletes must be analysed for their presence and quantitative confirmation analyses performed where necessary [202]. Ephedrine and pseudoephedrine are diastereoisomers, as are their related demethylated substances cathine and phenylpropanolamine. Also related is the compound methylephedrine, differing only by a single methyl group from the ephedrine geometric isomers. Mass spectrometric (MS) detection is necessary for the unequivocal identification of these analytes in doping control, presenting a further challenge since the diastereoisomers share very similar fragmentation patterns, and hence each analyte must be separated chromatographically prior to detection.

Previous methods of separation have included gas chromatography coupled to either nitrogen phosphorous detection (GC-NPD) [203] or mass spectrometry (GC-MS) [204], high performance liquid chromatography coupled to ultra-violet detection (HPLC-UV) [205], where GC-MS requires derivatisation and HPLC-UV lacks the sensitivity and selectivity of MS. Hyphenation to mass spectrometry, when dealing with analytes in biological matrices, offers decidedly more information for identification and confirmation of a positive doping suspect. More recently, anti-doping drug analysis methodology is being transferred to LC-MS, offering faster analysis times and simple sample preparation, critical factors where fast turn-around times are required, as well as increased sensitivity [206-209]. However, certain approaches to achieving good retention and peak shape for basic compounds with reversed-phase (RP) LC are not amenable to MS detection, such as ion-pairing reagents and high ionic strength buffers.

Table 6.1. Properties of the compounds considered in the present study.

Compound	Structure	pK _a	logP	logD (pH 5)	logD (pH 10)
Phenylpropanolamine (Norephedrine)		9.4	0.81	-3.59	0.71
Cathine (Norpseudoephedrine)		9.4	0.81	-3.59	0.71
Ephedrine		9.6	1.05	-3.55	0.90
Pseudoephedrine		9.8	1.05	-3.75	0.84
Methylephedrine		9.3	1.74	-2.56	1.66

* pK_a values obtained from Clarke's Analysis of Drugs and Poisons

** LogP values obtained from ChemSpider

*** LogD values calculated from pK_a and logP values using the equation:

$$\text{LogD} = \log P + \log \left[\frac{1}{(1 + 10^{pK_a - pH})} \right]$$

The impact of utilising perfluorinated ion-pairing reagents for LC-MS analysis of a range of basic drugs was evaluated by Oberacher *et al.* [210] noting that under overloading conditions simple carboxylic acid additives provide much inferior peak shapes and poor retention for hydrophilic analytes such as nicotine. The use of fluorinated ion-pairing reagents were shown to significantly improve peak shape, however this was at the detriment of mass spectrometric performance. Fleiger [211] investigated the use of perfluorinated ion-pairing reagents as applied

to the reversed-phase separation of β -blockers reporting useful increases in retention and improved peak shapes when compared to acetic acid.

Stuppner *et al.* [212] utilised the ion-pairing reagent sodium dodecyl sulfate (SDS) for the separation of ephedra alkaloids in dietary supplements. Alternative solutions involve the use of highly aqueous mobile phases in order to retain these polar analytes [213, 214] but such approaches are associated with poor MS desolvation and stationary phase de-wetting. Other strategies such as the use of chaotropic salts and ionic liquids [215, 216] as mobile phase additives for the analysis of hydrophilic amines have been shown to yield highly symmetrical and efficient separations, however such approaches are unsuitable for interfacing to electrospray ionisation mass spectrometry. Suitable retention has also previously been achieved by manipulating the mobile phase so as to reduce the degree of analyte ionisation, recently made possible with high pH stable stationary phases [217], or by utilising complementary stationary phase materials such as the pentafluorophenyl variant [218, 219].

Hydrophilic interaction chromatography (HILIC) has recently become a widespread alternative to RPLC for achieving good retention and peak shapes for polar or ionisable analytes, and is also amenable to MS detection [104, 184, 220]. In addition, HILIC offers particular advantages over RPLC approaches, including lower back pressures and enhanced desolvation with electrospray ionisation (ESI) owing to the large percentage of organic modifier in the mobile phase. The resulting lower back pressures permit the use of faster flow rates for increased sample throughput, longer columns for enhanced resolution or use of sub-2 μm particle materials with traditional pumping systems, while improved desolvation with ESI mass spectrometry offers better sensitivity and lower limits of detection. Nevertheless, the technique also brings with it certain disadvantages over RPLC, in particular regarding the complex and poorly-understood retention mechanisms. Unlike the well-identified mechanisms of retention in RPLC, there are several proposed mechanisms of interaction at play in HILIC [102, 194, 221], complicating the predication of retention which is widely valued in RPLC. Nor does HILIC offer the flexibility and applicability that RPLC does, with only limited tools available to manipulate a separation, and is associated with longer re-equilibration times and problems with sample solubility.

However, where other methods cannot provide appropriate retention or peak symmetry, HILIC has been shown to be a powerful alternative for separating polar, hydrophilic compounds. Here is presented the investigation on the suitability of HILIC as an alternative to RPLC for the fast chromatographic separation of ephedrine isomers. The compounds in question are structurally similar, and without the presence of a shape selective moiety bonded to the stationary phase, as is the case with bare silica, the separation of these solutes may prove difficult. Encompassing this investigation are the effects of chromatographic parameters including the proportion of acetonitrile, buffer pH and concentration and column temperature on the HILIC separation in order to determine whether HILIC is a viable option for the retention and separation of the distinct ephedrines. With these parameters optimised, the same bridged-ethylene hybrid (BEH) material functionalised with C18 ligands was used as a comparator technique to evaluate the benefits of HILIC over RPLC. A kinetic performance comparison is presented between RPLC and HILIC as two possible approaches for the separation of ephedrines.

6.2 Experimental

6.2.1 Chemicals and reagents

Acetonitrile (HPLC grade), ammonium bicarbonate, ammonium hydroxide solution (35 %) and formic acid (98 %) were obtained from Fisher Scientific (Loughborough, UK). Ammonium acetate, ammonium formate, uracil and toluene were purchased from Sigma (Poole, UK). Norephedrine, norpseudoephedrine, ephedrine, pseudoephedrine and methylephedrine were purchased as hydrochloride salts from Sigma (Poole, UK). Water was purified by an ultra-pure water system (Millipore, UK).

6.2.2 Solutions

6.2.2.1 Reversed-phase mobile phase

Ammonium bicarbonate buffer was prepared at 10 mM in purified water and adjusted to pH 10 with ammonium hydroxide solution (35 %). The mobile phase was pre-mixed at a composition of 90:10 v/v 10 mM ammonium bicarbonate pH 10:CH₃CN by adding 100 mL of acetonitrile to 900 mL 10 mM ammonium bicarbonate pH 10.

6.2.2.2 HILIC mobile phase

Ammonium formate (pH 3 and 4) and ammonium acetate (pH 5) buffers were prepared separately at 200 mM in purified water and adjusted to the appropriate pH with formic acid (98 %). Typically, the mobile phase preparation consisted of 95:5 v/v CH₃CN:200 mM buffer prepared by taking 50 mL of the 200 mM stock buffer and adding to 950 mL acetonitrile. The pre-mixed mobile phase was then sonicated to ensure complete dissolution of the buffer salt.

6.2.2.3 Sample preparation

Stock solutions were prepared at a concentration of 1 mg/mL for norephedrine, norpseudoephedrine, ephedrine and methylephedrine and pseudoephedrine in methanol at -20 °C until required. Standard working solutions at 50 µg/mL were prepared by diluting stock solutions with the appropriate mobile phase for either HILIC or reversed-phase operations.

6.2.3 LC conditions

Liquid chromatography was carried out on a Waters Acquity UPLC[®] (Waters Corp., Milford, USA) which consisted of a sample manager, binary solvent delivery system and a PDA detector. The autosampler was thermostatted at 6 °C. All injections were made in duplicate and averaged for all experiments. For the van't Hoff experiments a Waters Xevo Q-TOF-MS (Waters Corp., Manchester, UK) was used to track the compounds of interest. The columns were connected to the injection valve using the temperature stabiliser tubing so as to ensure that adequate eluent pre-conditioning took place. For the kinetic performance experiments sample injections of 1 µL were made using a 2 µL loop in the partial loop with needle overfill mode and for the mass spectrometry experiments 5 µL injections were made using a 5 µL loop in full loop mode. Empower 2 or MassLynx V4.1 software (Waters Corp., Milford, USA) was used for data acquisition.

6.2.3.1 Reversed-phase conditions

Separations were carried out on an Acquity UPLC[®] system (Waters Corp., Milford, USA) with an Acquity BEH C₁₈ 1.7 µm, 2.1 x 50 mm column for the reversed-phase separation equipped with a 0.2 µm in-line filter. Isocratic chromatography was performed using a prefixed mobile phase of 90:10 v/v 10 mM ammonium bicarbonate pH 10:CH₃CN. The flow rate was 500 µL/min and column temperature set at 60 °C. The weak and strong needle wash lines of the Acquity UPLC[®] system were placed in 90:10 H₂O:CH₃OH (v/v) and 10:90 H₂O:CH₃OH (v/v) respectively. The

elution conditions were slightly modified from a previously reported separation of ephedrines by Gray *et al.* [217] except performed using sub-2 μm BEH C_{18} .

6.2.3.2 HILIC conditions

Acquity BEH HILIC 1.7 μm , 2.1 x 50 or 100 mm columns were used for the HILIC separation using a 0.2 μm in-line filter. The mobile phase comprised of premixed 95:5 v/v CH_3CN :200 mM buffer for the HILIC separation. Flow rate was 500 $\mu\text{L}/\text{min}$ and column temperature set at 50 $^\circ\text{C}$ unless otherwise specified. The weak and strong needle wash lines of the Acquity UPLC system were placed in 95:5 v/v CH_3CN : H_2O and 50:50 v/v CH_3CN : H_2O , respectively, so as not to cause any interference with the sample plug.

6.2.4 Detection

Analyte detection was performed using an Acquity PDA detector or a Xevo QToF mass spectrometer (Waters Corp., Milford, USA) equipped with an electrospray ionisation (ESI) source operated in positive ion mode. UV data was collected at 210 nm using a sampling rate of 40 Hz. Columns were connected to either the mass spectrometer ion source or PDA-UV detector using minimal lengths of 0.004" ID PEEK tubing.

The MS was operated in MS^{E} mode collecting two channels of data throughout the run, one with low collision energy (4 V) and one high (ramp from 10-20 V) in order to obtain both the precursor and product ions. Source conditions were optimised for each mobile phase composition and for reversed-phase separation the capillary voltage was set at 1.0 kV, the sample cone 10 V, source temperature 120 $^\circ\text{C}$, desolvation temperature 400 $^\circ\text{C}$. In HILIC the capillary voltage was set at 3.0 kV, sampling cone 20 V, source temperature was 120 $^\circ\text{C}$, desolvation temperature 350 $^\circ\text{C}$. For both LC setups the cone gas flow was set at 10 L/h and the desolvation gas was set at 800 L/h. The micro-channel plate detector was operated at 2150 V. Data were collected in centroid mode over an m/z range of 100-1000 Da with a scan time of 0.05 sec. Leucine enkephalin (5 ng/mL) was used as the accurate mass reference material,

infused through the LockSpray probe at 5 $\mu\text{L}/\text{min}$ and acquired every 20 seconds with a 0.3 sec scan time scans (3 scans were averaged).

6.2.5 Methodology for the construction of van Deemter plots

The kinetic study was performed using phenylpropanolamine, ephedrine and methylephedrine as the test solutes. Column efficiency (N_{col}) was determined from peak widths at half height for the HILIC study. The asymmetry factor (A_s) and peak widths ($w_{0.1}$) were determined at 10 % of the peak height for the reversed-phase study. All reported data were obtained after correction for extra-column band broadening (σ_{sys}^2) caused by the instrument, determined by removing the column and replacing it with a zero volume connector and injecting each solute individually in the relative mobile phase for each study.

$$N_{col} = \frac{(t_{R,total} - t_{R,sys})^2}{\sigma_{total}^2 - \sigma_{sys}^2} \quad (6.1)$$

Data was transformed into on-column plate height as follows:

$$H_{col} = \frac{L}{N_{col}} \quad (6.2)$$

Where L is the column length (m) and H_{col} is plate height (μm). Plate height data were fitted to the van Deemter equation:

$$H_{col} = A + \frac{B}{u_o} + Cu_o \quad (6.3)$$

where A, B and C are the Eddy diffusion, longitudinal dispersion and resistance to mass transfer coefficients respectively, and u_o is the mobile phase linear velocity, determined in cm/s in this

study. SigmaPlot (version 11.0, Systat Software Inc.) software was used to fit the (u_o, H) data to equation (6.3).

6.2.6 Methodology for the construction of kinetic plots

Based on experimental van Deemter data (u_o, H_{col}) and column permeability values (K_{vO}) , kinetic plots were constructed to better visualise the potential of the two analytical systems investigated, accounting for mobile phase flow rate, chromatographic efficiency, generated back pressure and column geometry. Two equations are necessary to transform this experimental data into extrapolated plots of analysis time *versus* efficiency, as outlined by Desmet *et al.* [22, 23]:

$$N = \frac{\Delta P_{\max}}{\eta} \left(\frac{K_{vO}}{\mu_o H_{col}} \right)_{\text{experimental}} \quad (6.4)$$

$$t_o = \frac{\Delta P_{\max}}{\eta} \left(\frac{K_{vO}}{\mu_o^2} \right)_{\text{experimental}} \quad (6.5)$$

Where ΔP_{\max} is the maximum allowed pressure drop with any given support material, pending also the constraints of the chromatographic apparatus, and η is the mobile phase viscosity (cP). Data was processed and curve fittings made using the Kinetic Plot Creator 3.1 (Vrije Universiteit Brussels, Belgium) for generation of kinetic plots.

6.3 Results and discussion

6.3.1 Effect of CH₃CN composition on retention of phenylpropanolamine, ephedrine and methylephedrine

Retention in HILIC is achieved through the establishment of a water rich layer immobilised on the surface of the polar stationary phase, thereby facilitating a multitude of chemical interactions. Upon increasing the concentration of acetonitrile in the mobile phase relative to the aqueous component, an increase in retention is generally observed. As illustrated by McCalley [104], it is essential to include buffer at the appropriate concentration when using HILIC as poor peak shapes are observed if only weak acids are used as mobile phase additives. It is therefore essential to employ a buffer which is soluble in the acetonitrile rich mobile phase. Ammonium acetate and ammonium formate were chosen as suitable buffers in this study, which have the added benefit of being MS compatible. Also of importance is the concentration of the buffer as long equilibration will be necessary if low concentrations are used. Whereas precipitation will occur in the organic rich mobile phase at high concentrations and contamination within the LC-MS ion source may result, causing signal suppression. In the first instance an overall concentration of 10 mM was employed, and it was noted that higher concentrations resulted in a precipitate being formed when mixed with acetonitrile. Initially, prior to attempting the separation of the geometric isomers, retention of the individual amines was established using 10 mM ammonium acetate buffer adjusted to pH 5. As observed in Figure 6.1, there was an increase in retention with increasing acetonitrile concentration for phenylpropanolamine, ephedrine and methylephedrine. Although retention was adequate at 90 % acetonitrile ($k \sim 2$) for all compounds, little or no separation was achieved between the three compounds. However, by increasing the acetonitrile content further, to 95 %, the separation of phenylpropanolamine, ephedrine and methylephedrine was achieved.

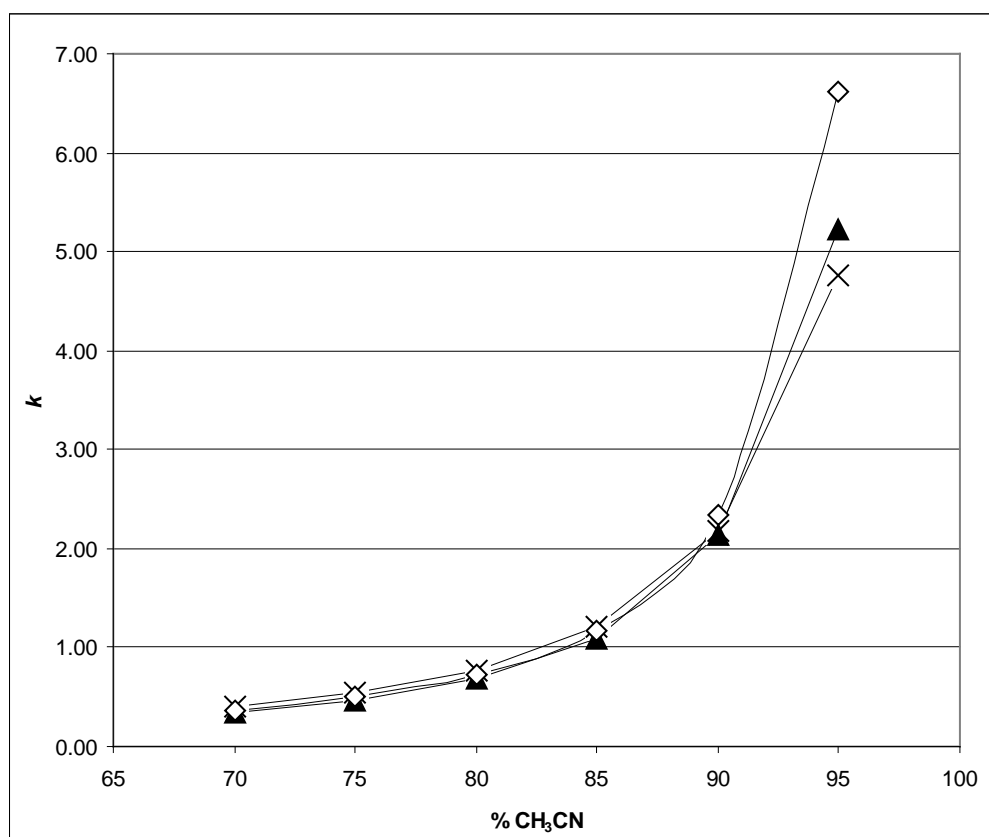


Figure 6.1. HILIC retention behaviour (k) of methylephedrine (crosses), phenylpropanolamine (triangles) and ephedrine (diamonds) at 50 °C, constant 10 mM ammonium acetate pH 5.0, as a function of percentage acetonitrile. Column was 10 cm x 2.1 mm ID, HILIC BEH 1.7 μ m operated at 500 μ L/min.

6.3.2 Dependence on retention of mobile phase pH

Residual silanols on the surface of silica are reported to have a pK_a of 7.1 ± 0.5 [222], although the bridged-ethylene hybrid (BEH) material used here has been reported to be less acidic than conventional silicas due to surface deactivation [223, 224]. According to Neue [224], the pK_a of hybrid packings decreases with increasing organic modifier concentrations by as much as 0.63 units per 30 % increase in acetonitrile content. As already shown by Grumbach [108] and McCalley [104], this further highlights the importance of pH as a variable in developing separations, especially where retention is poor and selectivity must be maximised in order to separate structurally similar compounds. In order to investigate the effect of pH so as to improve

the retention of the ephedrines, pH 3.0 and 4.0 using 10 mM ammonium formate and pH 5.0 using 10 mM ammonium acetate, measured in the aqueous phase were used. As shown in Figure 6.2, a marked change in the selectivity of these analytes is noted with increasing pH.

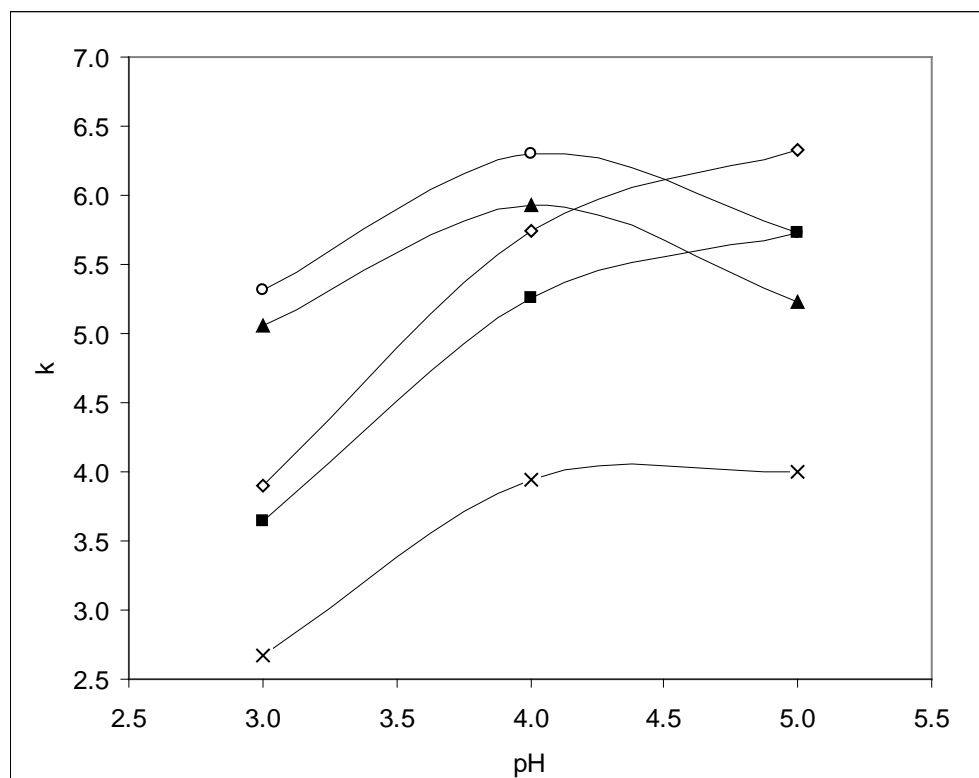


Figure 6.2. Retention factors (k) of ephedrines on a 5 cm BEH HILIC column as a function of pH at 50 °C in CH₃CN:200 mM buffer (95:5 v/v). Ephedrine (squares), phenylpropanolamine (triangles), cathine (circles), methylephedrine (crosses), pseudoephedrine (diamonds).

This may be explained by the dissociation of the silanol groups allowing for cation exchange contributions to take place with the charged basic solutes. The strongest retention of the secondary (ephedrine and pseudoephedrine) and tertiary (methylephedrine) amines was encountered at pH 5. Interestingly, the primary amines (phenylpropanolamine and cathine) slightly decreased in retention with increasing pH, which may be the result of interplay between the pK_a of the analytes and dissociation of silanol groups. It appears overall that the resolution of the ephedrine isomers is in fact improved with increasing pH on bare silica, where dissociation of silanols is clearly contributing to selectivity. Although, as seen in Figure 6.2, the

resolution of the diastereoisomeric pairs is enhanced with the change in selectivity, the co-elution of cathine and ephedrine is apparent. This was subsequently overcome by increasing the column length from 5 cm to 10 cm, offering separation of all five ephedrines. A higher pH eluent was not used since there are no MS compatible buffers in the pH region 5.5 - 7.0, and pH values above this may incur dissolution of the bare silica stationary phase, particularly at elevated temperatures.

6.3.3 Effect of increasing temperature on retention

Utilising temperature as a means of manipulating selectivity is a parameter often overlooked in method development. In this study the effect of temperature was investigated, ranging from 25 to 50 °C, on the retention of each analyte with the underivatized BEH silica, represented as $\log k$ vs $1/T$ (Figure 3). As shown in Figure 6.3, the relationship between increasing temperature and retention is non-linear and a quadratic model was required for the van't Hoff plot.

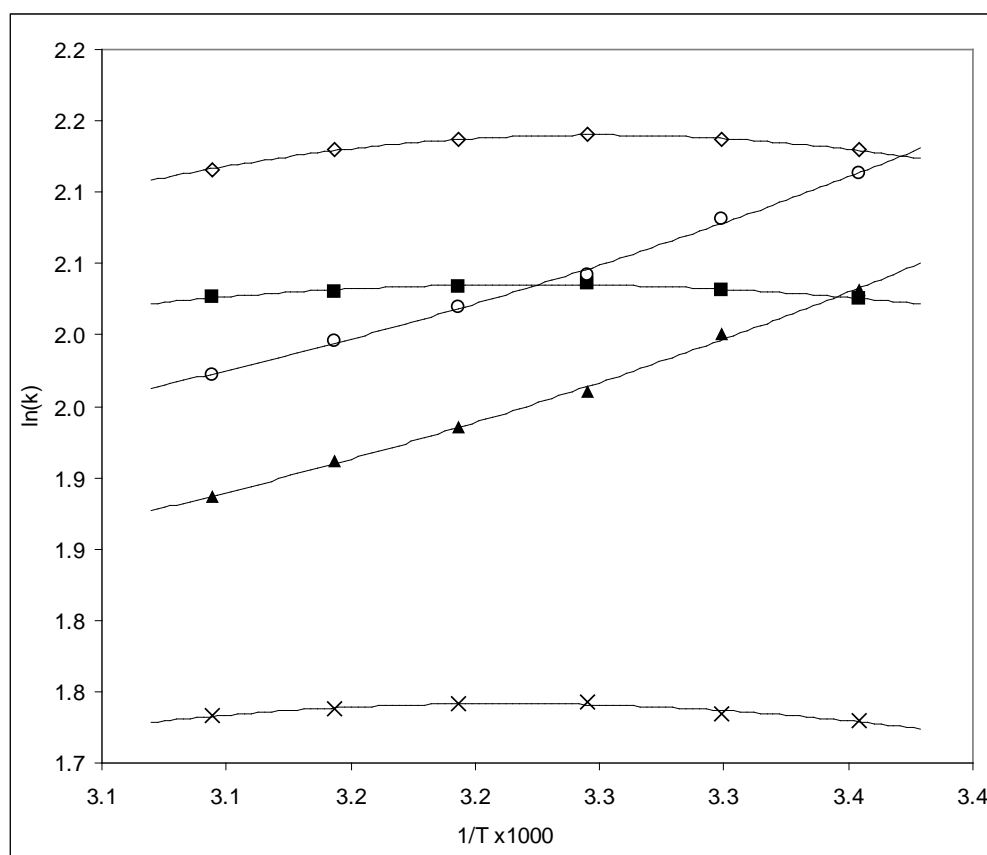


Figure 6.3. Plot of $\log k$ vs. $1/T$ using acetonitrile:200 mM ammonium acetate pH 5.0 (95:5 v/v). Compound identities as in Figure 6.2.

Interestingly, the secondary and tertiary amines experienced little change in retention as a function of temperature at pH 5, whereas the primary amines showed a decrease in retention enthalpy with increasing temperature. At 25 °C the diastereoisomeric pairs (phenylpropanolamine-cathine and ephedrine-pseudoephedrine) are resolved, however the pairs co-elute and inadequate resolution of all ephedrines is observed. As temperature is increased the primary amines lose retention, affording separation of the five ephedrines. This change in selectivity as a function of temperature between the primary amines versus the secondary and tertiary amines was shown as a useful means for achieving separation and further highlights the importance of temperature as a variable for achieving resolution.

After observing the unusual retention behaviour as a function of increasing temperature with 10 mM ammonium acetate for secondary and tertiary amines, the effect of lowering the buffer concentration to 5 mM was investigated to allow more exposure of the free silanol groups for cation exchange. An increase in retention was observed for all solutes upon decreasing the buffer concentration, which was expected due to the stronger cation exchange between the basic amines and the silanol groups. However, upon increasing the temperature, a more pronounced decrease in retention was observed for all solutes, shown in Figure 6.4.

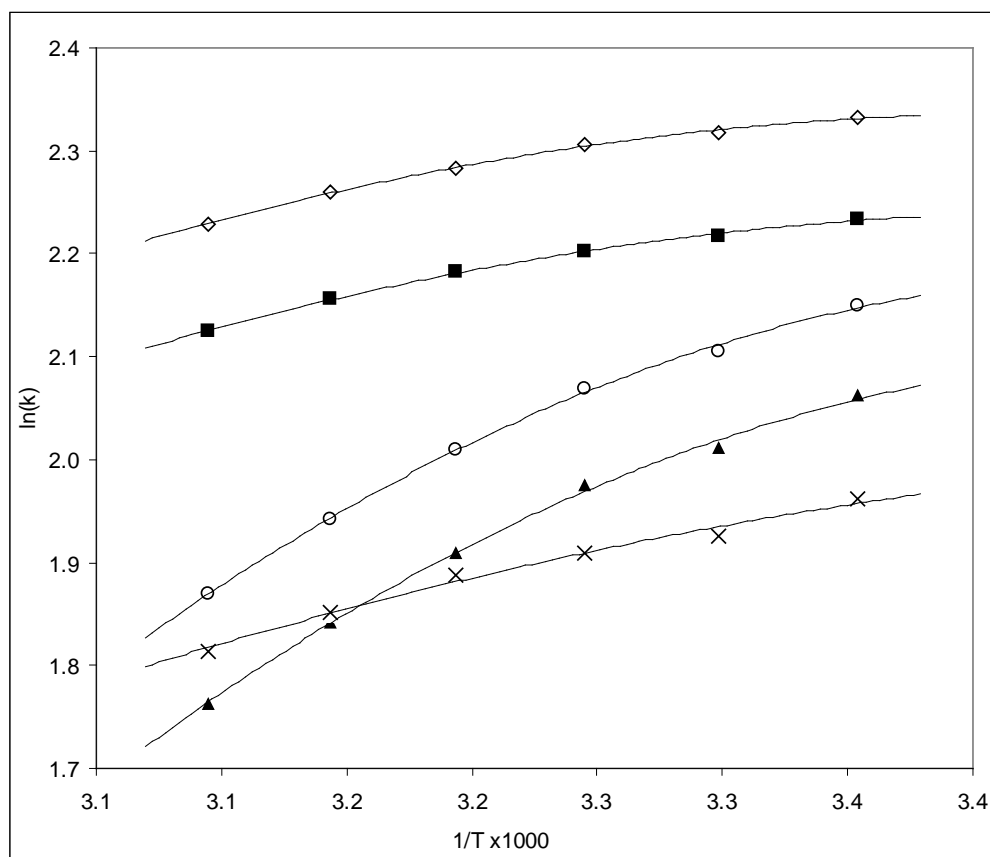


Figure 6.4. Plot of $\log k$ vs. $1/T$ using acetonitrile:100 mM ammonium acetate pH 5.0 (95:5 v/v). Compound identities as in Figure 6.2.

Again, there was a curvature of the retention van't Hoff isotherm. This implies that the enthalpy of retention is dependent on buffer concentration, and that analyte solvation is affected by increasing temperature with higher buffer concentrations. The effect of analyte solvation on retention enthalpy as a function of temperature was recently postulated by Wilson *et al.* [225] for the separation of nucleoside triphosphates. Upon increasing temperature, Buckenmaier *et al.* [59] showed pK_a decreases for a group of basic solutes, resulting in a decrease in %BH⁺ for benzylamine of 29 %. Further work by Buckenmaier and co-workers [193] investigated the influence of acetonitrile content on pK_a , showing a decrease of 0.77 units for benzylamine on going from pure water to 60 % organic fraction. Thus, there are consequently multiple features at play which are affecting the pK_a values of the ephedrine analytes, exemplified by the curvature of van't Hoff plots suggesting mixed-mode retention. Bidlingmeyer *et al.* [226] postulated that, at lower temperatures, electrostatic and adsorptive forces dominate whereas, at elevated temperatures, the former is weakened. They also indicated that the amount of

adsorbed solvent on the silica surface may also be changing thereby affecting the immobilised phase-ratio found with HILIC.

6.3.4 Performance comparison between reversed-phase and HILIC

Typically, to retain and separate ephedrine-type compounds by RPLC highly aqueous mobile phases are required, which may yield unfavorable desolvation properties and poor peak shapes making peak integration difficult. This also entails the use of comparatively high viscosity mobile phases in relation to those encountered in HILIC, and as such separation speed is restricted by the high back-pressures generated, especially with the use of sub-2 μm particles. As a comparative method, a RPLC approach modified from a previously reported one [217], which utilised a high pH mobile phase and supra-2 μm C18 BEH particles, was used.

6.3.4.1 Peak shape comparison between HILIC and reversed-phase approach

The analysis of basic solutes has been of significant interest not only academically but also in the pharmaceutical arena where many drug molecules contain amine groups, as has been recently reviewed [184]. Achieving suitable peak shapes for these molecules requires careful consideration of the chromatographic conditions, particularly where solvent systems must be compatible with MS detection. In order to investigate the column performance obtained with either HILIC or reversed-phase, van Deemter curves were constructed for each system generated using phenylpropanolamine, ephedrine and methylephedrine as test solutes. In the case of the reversed-phase separation, peak asymmetry was problematic, even at the increased temperature (60 °C) and high pH (10.0) employed. In order to ascertain an estimate of the true column efficiency, the Dorsey-Foley procedure [227] was applied where necessary to take into account the peak asymmetry when calculating performance for the reversed-phase study:

$$N_{df} = 41.7 \left(\frac{t_r}{w_{0.1}} \right)^2 / (A_s + 1.25) \quad (6.6)$$

Phenylpropanolamine and ephedrine both yield skewed peak shapes under RP conditions as a function of flow rate and peak asymmetry measured at 10 % peak height, as illustrated in Figure 6.5.

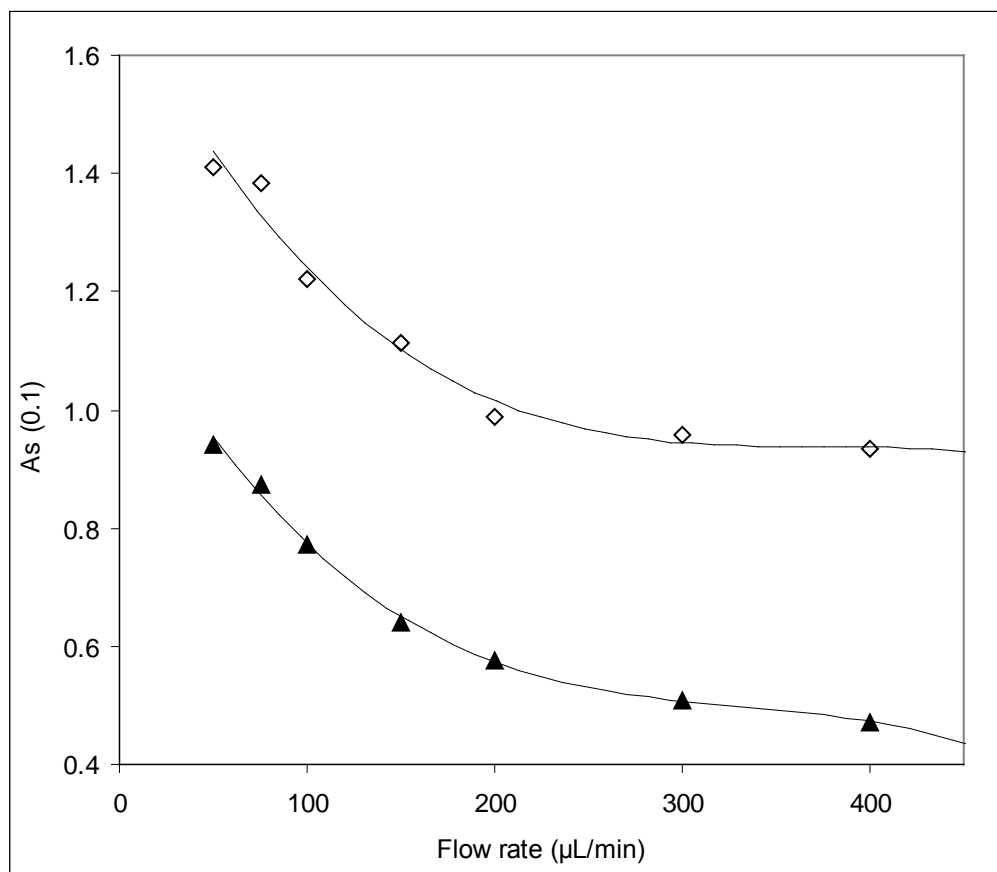


Figure 6.5. Effect of increasing flow rate on peak asymmetry (measured at 10 % peak height) for ephedrine and phenylpropanolamine using reversed-phase conditions. Compound identities as in Figure 6.2.

The peak shapes for methylephedrine were found to be similar to those found with HILIC for the flow study, possibly due to the high retention factor ($k \sim 22$) obscuring peak symmetry issues due to on column band broadening. Another possibility is the steric effect of the protecting methyl groups surrounding the tertiary amino group, affording fewer secondary interactions with acidic silanol groups as well as the combined effect of high pH and elevated temperature used here on the analyte pK_a . With increasing flow rate, the peak asymmetry of phenylpropanolamine was found to deteriorate rapidly, with severe peak fronting observed, while for ephedrine, peak tailing was reduced and excellent peak symmetry was achieved. This finding of improved peak

asymmetry with increasing flow rate for ephedrine resembles that observed by McCalley [58] for quinine and nortriptyline at intermediate pH. Peak fronting for oxycodone was investigated by Ornaf *et al.* [228] explaining that the formation of interconverting solvent adducts were involved. However, in their study, this was a temperature dependent effect. As referred to by McCalley [229], based on the work of Neue and co-workers [223] another possibility could be a partial exclusion effect taking place in the stationary phase, which is the result of residual cationic sites that remain from silica manufacture resulting in analyte repulsion. This effect is known to be more pronounced in mobile phases of lower ionic strength. Although, in their study, this was not observed for hybrid-silica packings.

6.3.4.2 van Deemter flow study to compare HILIC and reversed-phase

The mobile phase composition used for the reversed-phase approach was mainly aqueous, with 10 % CH₃CN compared to the 95 % used with HILIC. It has been suggested previously by Walters *et al.* [230] that working with highly aqueous mobile phases, below the composition used here, can cause de-wetting of C18 stationary phases resulting in retention losses. Due to the hydrophilicity of the ephedrine alkaloids, this approach was essential for adequate retention and a high pH mobile phase was also necessary to improve peak shape and resolution as reported previously [217]. In contrast, with the HILIC retention mechanism, superior peak shapes and performance for all analytes were observed. As seen in Figure 6.6 (a), the deterioration in column performance for phenylpropanolamine is inherently linked to the effect of flow rate on peak asymmetry and hence poor efficiency ($H_{\min} = 12 \mu\text{m}$) was observed for this analyte. The low $\log P$ and $\log D$ values (Table 6.1) for this compound, in comparison to the secondary and tertiary amino containing solutes, can somewhat explain the poor mass transfer properties observed. This low efficiency is not due to the effect of system dead volume as the solute k is 3.5 and losses in performance were calculated to be only 1-2 % when correcting for extra-column band broadening.

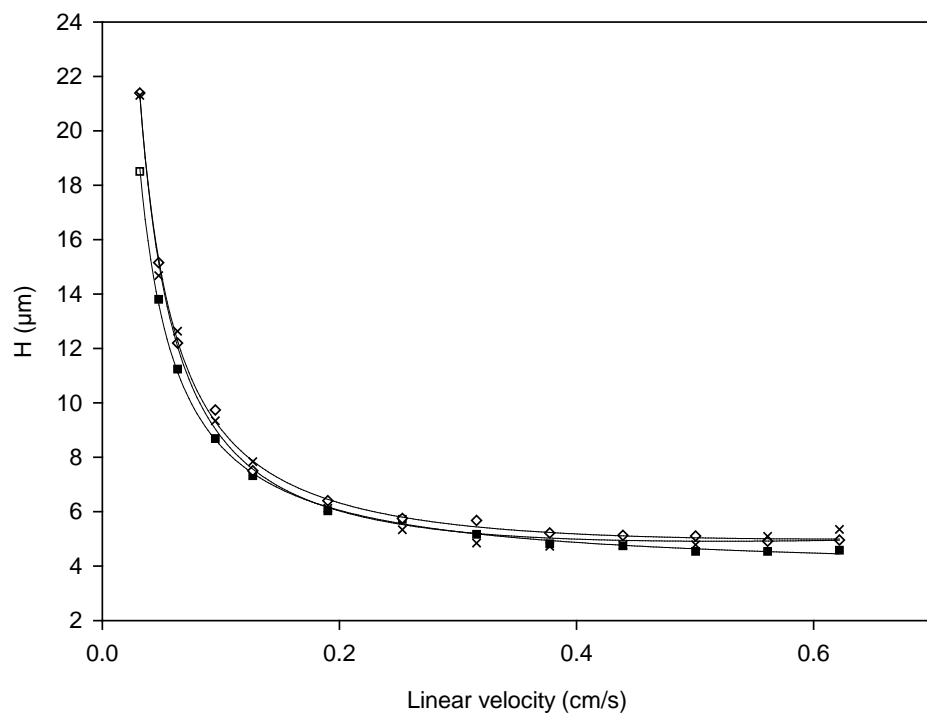
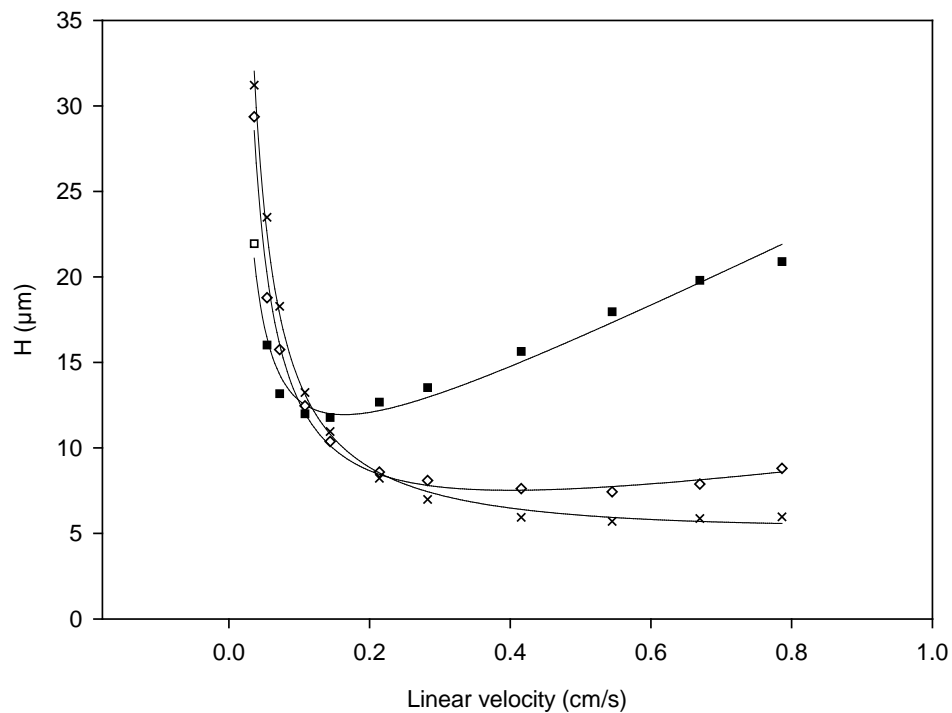


Figure 6.6. van Deemter curves for reversed-phase (a) and HILIC (b) phenylpropanolamine (squares), ephedrine (diamonds) and methylephedrine (crosses).

For ephedrine and methylephedrine the benefits of using sub-2 μm stationary phases are apparent due to the *C*-term flattening of their respective van Deemter curves. The Dorsey-Foley correction was applied to the former due to peak tailing at low flow rate, as alluded to previously. Figure 6.6 (b), in comparison, shows the van Deemter curve for phenylpropanolamine, ephedrine and methylephedrine under HILIC conditions, where similar column performance is achieved for each compound, approximately 200,000 plates per meter. Table 6.2 shows the van Deemter coefficients from curve fitting for the RPLC and HILIC approaches.

Table 6.2. Van Deemter coefficients determined for HILIC and reversed-phase conditions.

Analyte	<i>k</i>	A (μm)	B ($\times 10^{-5} \text{ cm}^2/\text{s}$)	C (ms)	u_{opt} (cm/s)	HETP _{min} (μm)
HILIC (95% CH₃CN)						
Phenylpropanolamine	5.6	3.7	0.47	0.02	0.4	4.7
Ephedrine	6.9	3.2	0.57	1.46	0.6	4.9
Methylephedrine	5.1	2.6	0.59	2.19	0.4	4.7
Reversed-Phase (10% CH₃CN)						
Phenylpropanolamine	3.5	5.3	0.54	20.2	0.1	11.8
Ephedrine	8.1	3.0	0.91	5.68	0.5	7.4
Methylephedrine	22.6	3.6	1.02	0.91	0.5	5.7

As stated elsewhere [195], the retention factor has an impact on the *B*-term and therefore this coefficient cannot be fairly compared unless similar retention factors are obtained on the two chromatographic systems due to the impact of viscosity and therefore solute diffusivity. Larger *B*-terms were found for the reversed-phase conditions in all cases, and it is noteworthy that there is a 10 °C difference in column temperature between the evaluations which also contributes to the aforementioned longitudinal band broadening. Clearly, the *C*-term for phenylpropanolamine under RPLC conditions was much larger than that under HILIC conditions. The fairest comparison for *C*-term values would be the relative performances of ephedrine since the retention factors are similar on both systems, found to be 1.46 for HILIC and 5.68 for reversed-phase. Overall, *A*-term coefficients were in the range of 2.5 – 5 for both columns, with the exception of phenylpropanolamine, suggesting similar packing qualities.

6.3.4.3 Kinetic plots of HILIC and reversed-phase

As shown in Table 6.3, the viscosity of the organic rich mobile phase used in HILIC, 0.32 cP, was far lower than that of the reversed-phase eluent, 0.51 cP. This affords faster analyte diffusivity in the mobile phase, enhancing solute mass transfer and thereby preserving column efficiency when higher flow rates are desired for high throughput analyses. For this reason, the kinetic benefits of the HILIC approach are unparalleled, since instrument pressure limitations restrict high flow rates in RPLC due to the large back pressures generated, a function of packing particle diameter, column length and bed permeability. The latter is denoted by:

$$K_{vO} = \frac{\mu_o \eta L}{\Delta P_{col}} \quad (6.7)$$

Where u_o is the linear velocity (m/s), η is viscosity (cP), L is column length (m) and ΔP_{col} is the system corrected pressure drop (Pascal). Using eluents of lower viscosity affords the chromatographer to use longer columns than those limited by higher viscosity operations resulting in enhanced resolution, or faster flow rates for reduced analysis time. This concept was shown by McCalley [106] using conventional pressures (280 bar) with long columns (45 cm) packed with 2.7 μm superficially porous particles yielding 100,000 plates with analysis times between 7.5 and 15 minutes. Using the approach of Desmet *et al.* [22, 23] kinetic plots based on the experimental data generated for the van Deemter flow study were constructed.

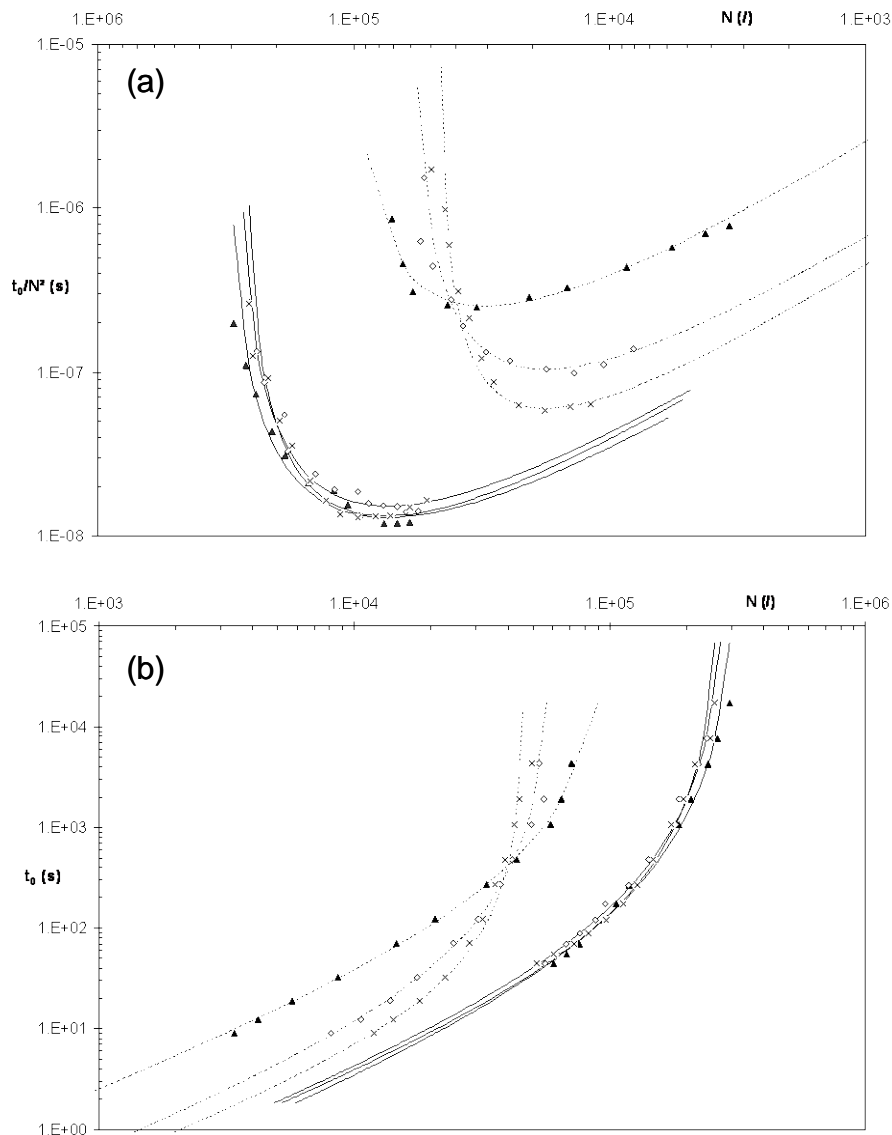


Figure 6.7. Kinetic plot representation of pressure drop limited plate number based on van Deemter data were (a) impedance and (b) are plate time dependent. Dotted and full lines represent the reversed-phase and HILIC systems, respectively. Data points are as in Figure 6.6.

Figures 6.7 (a) and (b) represent kinetic plots for phenylpropanolamine, ephedrine and methylephedrine generated under HILIC and reversed-phase conditions. As shown in Figure 6.7 (b), significant gains in plate number *versus* analysis time can be realised using HILIC conditions. For example, at a t_0 value of 100 seconds approximately 100,000 theoretical plates per meter are generated, whereas the corresponding reversed-phase system generates around 20,000 for phenylpropanolamine or 30,000 for ephedrine and methylephedrine. This clearly demonstrates the kinetic benefits of performing HILIC for this solute type, and is further

emphasised in Figure 6.7 (a) which fundamentally represents a plot of separation impedance *versus* theoretical plate number. The contrast in separation performance is essentially a function of eluent viscosity, dictated by column permeability, since not only are higher plate numbers achievable using HILIC, but this can be performed at lower pressures using equivalent particle sizes. It is therefore possible to accommodate sub-2 μm materials in the HILIC mode using conventional instruments, however the advantages would only be preserved using well optimised equipment as previously highlighted [38, 99]. Column permeability using the HILIC conditions was found to be double that of reversed-phase, reflected in the 50 % lower flow resistance, shown in Table 6.3. Minimum separation impedances (E) for ephedrine under HILIC conditions were found to be < 5000 for the three probe solutes, compared to 12,000 to 50,000 for RPLC yielding significantly lower plate numbers.

Table 6.3. Kinetic plot parameters determined for HILIC and reversed-phase systems. Viscosity (η) was calculated using the Chen-Horvath correlation [103].

Kinetic parameter	HILIC (50 °C)	Reversed-phase (60 °C)
Permeability, K_{vo} (m^2)	5.50E-15	2.83E-15
Viscosity, η (cP)	0.318	0.506
Flow resistance, Φ	526	1020
Max. ΔP (bar)	564	702

6.3.5 Application: Analysis of ephedrines by LC-Q-TOF-MS

The final separation of structurally related hydrophilic ephedrine solutes is shown in Figure 6.8 as by the overlaid extracted ion chromatograms obtained by interfacing with a fast scanning Q-TOF mass spectrometer. Our separation compares very favorably to previously reported methodologies for the analysis of ephedrines, using mobile phase eluents and flow rates (typically $\leq 500 \mu\text{L}/\text{min}$) amenable to mass spectrometry. The five compounds can be separated by HILIC in under 5 minutes with high column efficiency ($\sim 20,000$ plates on column) and excellent peak shapes ($A_{s0.1} \leq 1.1$) with WADA acceptable retention factors (Table 6.2).

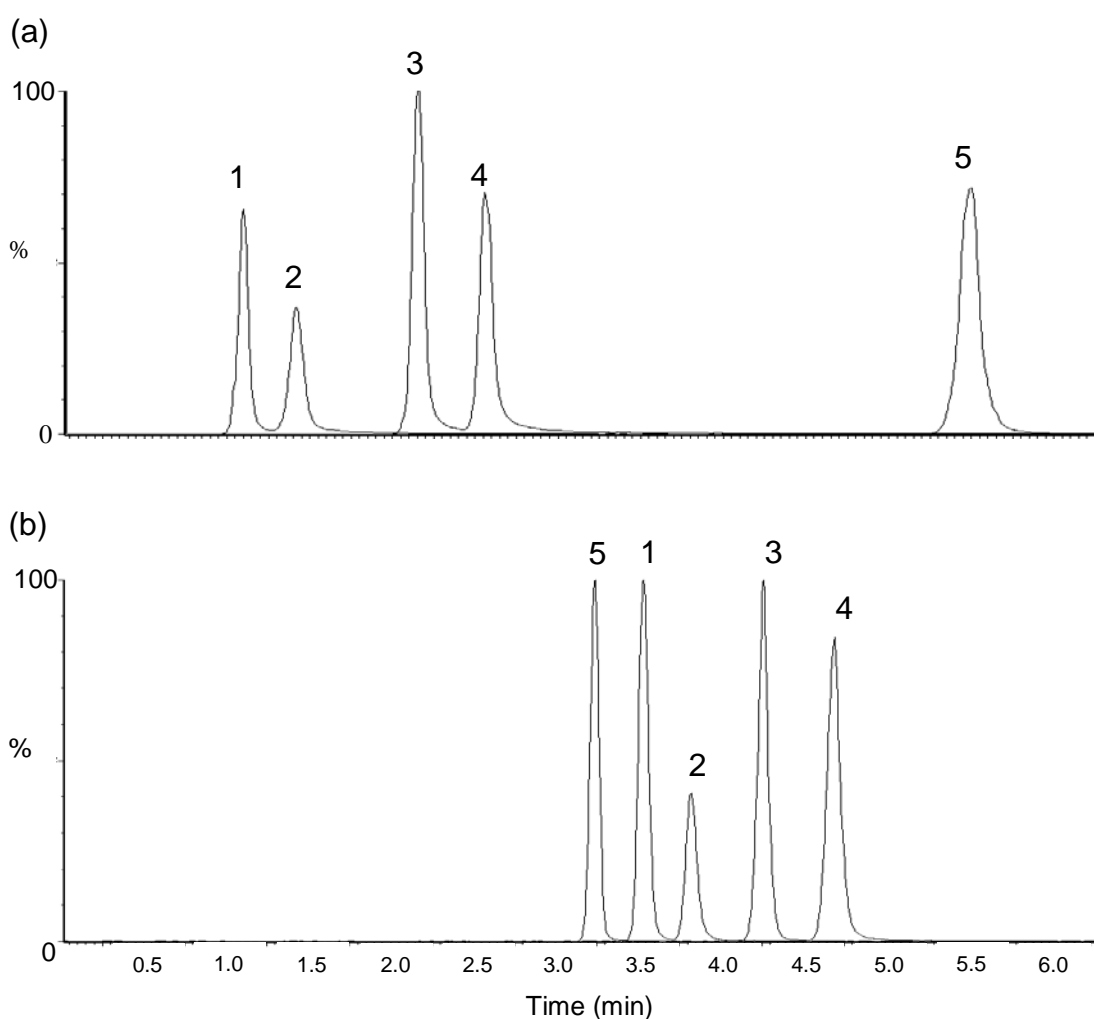


Figure 6.8. Chromatograms illustrating the separation of phenylpropanolamine (1), cathine (2), ephedrine (3), pseudoephedrine (4) and methylephedrine (5) under the reversed-phase conditions as in 6.2.3.1 (a) and HILIC conditions (b). HILIC was performed using 95:5 v/v CH_3CN :200 mM ammonium acetate pH 5, 100 x 2.1 mm ID Acquity BEH HILIC 1.7 μm , column temperature 50 $^\circ\text{C}$. Flow rate for both separations was 500 $\mu\text{L}/\text{min}$.

6.4 Conclusions

The advantage of HILIC as an attractive alternative to RPLC for the separation of hydrophilic ephedrines has been demonstrated. This study highlights the ability of pH and temperature to manipulate the separation of critical pairs, particularly where analytes are structurally similar. Superior peak shapes are obtained under HILIC conditions compared to the tailing peaks inherently observed with basic compounds under reversed-phase conditions. The HILIC separation also affords significantly lower mobile phase viscosity and higher solute diffusivity allowing yet faster separations without the expense of column performance.

It is the intention elsewhere in further studies to compare a quantitative method between the two techniques encompassing typical validation parameters, since it is proposed that HILIC will provide enhanced sensitivity owing to improved desolvation of the organic rich mobile phase with ESI. This additional advantage will be of particular significance for analytes where sensitivity is problematic and lower limits of detection are required, and may also permit the use of small sample volumes and reduced sample preparation efforts, such as direct dilution and injection of a sample. The HILIC approach must also be assessed for repeatability and robustness to ensure suitability as a routine technique. This would then allow for full comparison of the technologies evaluated herein to be realised.

Chapter 7

Systematic evaluation of Acetone and Acetonitrile for use in HILIC Coupled with ESI Mass Spectrometry of Basic Small Molecules

Abstract

This chapter deals with the limitation of HILIC in that reliance on acetonitrile rich mobile phases can be potentially inhibitory should supplies of the latter fall short of demand. In comparison to reversed-phase, where many water soluble solvents are available, reliance on the aprotic solvent acetonitrile for HILIC inhibits the extent to which solvent selectivity can be used in method development. Sub-2 μm particle size hydrophilic interaction liquid chromatography [HILIC] combined with mass spectrometry has been increasing in popularity as a complementary technique to reversed-phase LC for the analysis of polar analytes. The organic-rich mobile phase associated with HILIC techniques provides increases in compound ionization, due to increased desolvation efficiency during electrospray MS analysis. Although recent publications illustrated selectivity and response comparisons between reversed-phase LC/MS and HILIC LC/MS, there are limited discussions evaluating the optimisation of the mass spectrometry parameters regarding analytes and alternative mobile phases. The use of acetone as an alternative organic modifier in HILIC has been investigated with respect to signal-to-noise in ESI-MS for a variety of polar analytes. Analyte responses were measured based on a variety of cone and capillary voltages at low and high pH in both acetone and acetonitrile. In order to visualise compound behaviour in the ESI source, surface plots were constructed to assist in interpreting the observed results. The use of acetone in ESI is complicated at low m/z due to the formation of condensation products. Favorable responses were observed for certain analytes and the work here envisages offering an insight into the use of acetone as an alternative to acetonitrile under certain analytical conditions. This is particularly useful with respect to different compound classifications in the area of small molecule LC/MS analysis. Highlighted is the importance of optimising source voltages in order to obtain the maximum signal stability and sensitivity, which are invariably, highly solvent composition dependent parameters.

7.1 Introduction

Reversed-phase chromatography is, in many cases, an unsuitable mode of retention for polar, hydrophilic compounds and notably undesirable peak shapes are observed with highly basic solutes under acidic conditions making peak integration more difficult whilst leading to low column efficiencies. As was shown in Chapter 6 this is certainly true. Furthermore, this mode of chromatography may not be suitable in certain circumstances, in particular when hyphenation to mass spectrometry is required. For instance, the use of triethylamine competing base [231] in the mobile phase or an ion-pairing [232] approach may invariably render the hyphenation of separations to mass spectrometry redundant or undesirable due to ion suppression. For analytical scale liquid chromatographic separations of hydrophilic polar compounds few alternatives arise, where normal-phase isn't considered to be environmentally friendly due to the toxicity of the eluents used and at present supercritical fluid chromatography (SFC) isn't widely accessible.

The term hydrophilic interaction chromatography (HILIC) was first proposed by Alpert [101] for the separation of polar biological solutes, and was followed up with further work on the separation of complex carbohydrates [233] and the development of an assay for tyrosine protein kinase activity [234] in the early 1990s. Retention was initially thought to be attributed to the partitioning of a solute between an immobilised layer of water on the stationary phase and the bulk organic-rich mobile phase, however recent studies suggest a more complex scenario is taking place comprising of multiple solute-stationary phase interactions. As proposed by Pesek *et al.* [235] and McCalley [104], HILIC should arguably be termed aqueous normal phase chromatography (ANP) due to the polar nature of the stationary phase and the relative low polarity of the corresponding eluent. The utility of aqueous-organic mobile phases on bare silica was exploited in an earlier quantitative LC-MS/MS application for the separation of morphine and its related glucuronides [236] and was shown to be a robust and sensitive approach. A review by Hemström and Irgum [194] has summarised many of these interactions concluding that coulombic, hydrogen-bonding and liquid-liquid partitioning are all taking place to different degrees. As illustrated recently by McCalley [183], the HILIC retention mechanism is highly

dependent on the presence of a bonded group on the stationary phase surface as the introduction of polar groups results in dramatic changes in selectivity for methods development.

The other benefit of HILIC is the by-product of using organic-rich mobile phases, in that eluent desolvation is achieved more efficiently due to the lower viscosity and surface tension properties enhancing sensitivity for electrospray ionization mass spectrometry [108, 237, 238]. Many of the reported uses of HILIC are accompanied significantly by hyphenation to mass spectrometry in comparison to UV detection and or other detection systems such as ELSD or CAD. Obviously, the use of acetone in analytical separations is restricted by the strong adsorption of the carbonyl group when utilising UV detection at wavelengths < 330 nm, however few evaluations have been carried out regarding this polar aprotic solvent as an alternative to acetonitrile when using a mass spectrometer as a means of detection for small molecule analysis. Therefore, the use of acetone as the weak organic modifier for HILIC separations requires further evaluation, being that it is an aprotic polar solvent with similar properties to acetonitrile; it is necessary that the immobilised water layer on the surface of the stationary phase is not disrupted by protic solvents such as methanol for the "pure HILIC" contribution of the retention mechanism to become established. We define the term "pure HILIC" in the sense that an immobilized layer of water on the surface of the stationary phase is present which is otherwise not part of an extensively hydrogen bonded solvent system i.e. water-methanol mixtures.

There have already been reports on the use of acetone for reversed-phase LC-MS applications. The first such investigation being conducted by Fritz and co-workers [239] for peptide analysis by directly comparing acetone, acetonitrile and methanol. They reported sharper peaks, most likely due to enhanced diffusivity as a function of reduced viscosity in using acetone, shorter run times and overall superior separations with this organic modifier. More recently, Keppel and co-workers [240] further evaluated acetone for RPLC-MS for a similar application involving peptide analysis. The authors discussed chemical noise and ionization efficiency as well as column performance features of acetone, concluding in some cases this solvent to be inferior to acetonitrile. Duderstadt *et al.* [241] investigated the utility of acetone as a post-column additive for the analysis of polyalkenes using APCI and APPI for promoting gas-phase proton transfer as a means of protonation using photoionization. Their findings suggested that the use of acetone as an ionization dopant showed limited signal enhancements to only a few of their evaluated

analytes. Fountain *et al.* [116] discussed the use of acetone with HILIC-MS noting poor signal intensities for basic compounds in comparison to acetonitrile suggesting the presence of solvent condensation products and adduct formation. The aim of the work presented here was to investigate further the discrepancies in signal intensity observed previously when comparing acetone and acetonitrile for HILIC-ESI-MS by comprehensive optimisation of source voltages in order to maximise the signal-to-noise values for a set of hydrophilic and basic analytes. The two parameters deemed most important for systematic adjustment being the electrospray capillary and cone voltages once the appropriate desolvation temperature and gas flows had been optimised to accommodate the interfaced chromatography. Highlighted is the importance in applying the optimal source voltages for achieving both the most stable, reproducible electrospray conditions and also in achieving the highest analyte signal-to-noise ratio. The purpose of the work in this chapter is to emphasise on the dependence of ESI source conditions in order to achieve optimum sensitivity and stability as a function of solvent type and composition for typical pharmaceutically relevant basic solutes. We also feel HILIC is limited in solvent selection due to its dependence on aprotic solvents in comparison to its reversed-phase counterpart when using bare silica stationary phases. We show that acetone is perhaps an unfavourable alternative to acetonitrile in the context of hydrophilic and basic solute analysis using HILIC with ESI-MS.

7.2 Experimental

7.2.1 Chemicals

The organic solvents acetonitrile (CH_3CN) and 2-propanol (IPA) were optima grade whilst acetone ($(\text{CH}_3)_2\text{CO}$) was HPLC grade and were supplied by ThermoFisher Scientific (Fair Lawn, NJ, USA). Water (18.2M Ω cm, 5ppb TOC) was purified using a Milli-Q Advantage A10. The following analyte test probes were purchased from Sigma-Aldrich (St. Louis, MO, USA): cytosine (99%), adenine (99%), caffeine (meets USP specifications, anhydrous), procainamide hydrochloride, nicotine (hydrogen tartrate salt), nortriptyline hydrochloride (>98%), and diphenhydramine hydrochloride (analytical standard). The physicochemical properties of the test probes and the solvents are given in Tables 7.1 and 7.2, respectively. Buffer reagents ammonium acetate (puriss), ammonium formate (puriss), ammonium hydroxide (>25% solution in water), and formic acid (eluent additive for LC-MS) were supplied by Fluka (distributed by Sigma-Aldrich, Allentown, PA, USA).

Table 7.1. Physicochemical properties of hydrophilic test probes from www.chemspider.com

Compound	MW (g mol^{-1})	pKa	logP
Adenine	135.1	4.2, 9.9	-
Cytosine	111.1	4.2	-
Caffeine	194.2	14	-0.07
Procainamide	271.8	9.2	0.9
Nicotine	162.3	3.2, 7.9	1.2
Nortriptyline	263.4	9.7	1.7
Diphenhydramine	255.1	9	3.3

Table 7.2. Solvent physicochemical properties modified from reference [242].

	H_2O	CH_3CN	$(\text{CH}_3)_2\text{CO}$
ϵ	80.4	36.1	20.1
η (10^5 .poises)	1004	383	327
Vapor Pressure (Torr) at 25°C	24	90	203
Proton affinity (kcal/mol)	165	186.2	194

7.2.2 Preparation of solutions

The aqueous mobile phase component consisted of either 100 mM ammonium acetate or 100 mM ammonium formate prepared in H₂O and adjusted to either pH 9 or 3 with ammonium hydroxide or formic acid, respectively. The stock solutions were blended via the on-line fluidics to achieve 90:10 v/v organic modifier:100 mM buffer in order to maintain a constant ionic strength of 10 mM buffer during the experimental process. The needle wash solvent and seal wash solvent were prepared with a ratio 80:20 v/v of 2-propanol and water, respectively.

7.2.3 Sample Preparations

The probe solutes adenine, cytosine, caffeine, procainamide, nicotine, nortriptyline and diphenhydramine were prepared at a stock concentration of 1 mg/mL in 75:25 v/v (CH₃CN:MeOH). Dilutions were performed to yield working standard concentrations of 1 µg/mL in 95:5 v/v (CH₃CN/H₂O) for injection into the LC-MS instrument.

7.2.4 Chromatographic Conditions

Separations were performed on a Waters ACQUITY H-Class UPLC (Waters Corp., MA, USA) with quaternary solvent delivery system. The ACQUITY H-Class system was modified by installing the hexane/THF compatibility kit. All data was collected using Empower 2 chromatography data system (Waters Corp., MA, USA). The chromatography was performed on a (2.1 mm x 100 mm, 1.7 µm) Waters BEH (Bridged-Ethylene Hybrid) bare silica HILIC column operated at a flow rate of 800 µL/min and the column temperature maintained at 30 °C for all analysis. No post-column splitting of eluents was carried out with direct interfacing of the column to the electrospray source. All analyte solutions were injected separately to avoid a competing ion effect of co-eluted species.

7.2.5 Mass spectrometry conditions

In order to investigate the effect of electrospray conditions on the signal-to-noise ratio of the selected test probes under different eluotropic conditions, capillary voltages were varied from 0.5 to 3.5 kV in 0.5 kV steps. At each capillary voltage a concomitant cone voltage (Declustering potential on certain instruments) from 10 to 30 eV was applied and increased stepwise by 5 eV. The mass spectrometer used for this work was a Waters SQD detector (Waters Corp., Manchester, UK) equipped with an ESI source operated in positive ion mode. The respective cone and desolvation temperatures were 150 °C and 550 °C. The cone and desolvation gas flows were 10 and 900 L/min respectively. Source temperatures and flow rates were maintained during all experiments unless otherwise stated. Mass spectral data was determined and extracted using Empower 2 chromatography data system (Waters Corp., MA, USA). The mass range investigated was 100-600 Daltons operated at a scan speed of 5000 Daltons per second. Noise was determined using the average peak-to-peak processing algorithm within Empower 2. Measurements were made over 1 minute using a segment width of 20 seconds averaged from the EIC at times when the analyte of interest was not eluting. Data treatment was performed using Microsoft Excel 2007 and SimcaP (Umea, Sweden).

7.3 Results and discussion

7.3.1 Optimisation of source parameters

To investigate the use of acetone for HILIC-MS of basic compounds experiments were performed whereby a response surface of signal-to-noise was constructed for each of the probe solutes in order to determine the optimum source conditions. The positive ion electrospray ionization conditions were optimised as a function of capillary and cone voltages in full scan mode and the extracted ion was smoothed with a 9 point mean filter and baseline corrected to filter noise ions for each analyte and this data was used for the construction of the response surfaces. Figure 7.1 shows the influence of varying cone and capillary voltages for two different analytes (a) diphenhydramine, a hydrophobic ($\log P$ 3.3) tertiary amine and the hydrophilic analyte (b) cytosine. For diphenhydramine, high capillary and cone voltages were required for effective protonation under the applied eluotropic conditions ($(\text{CH}_3)_2\text{CO}$, low pH) with almost no signal detected at lower voltage potentials.

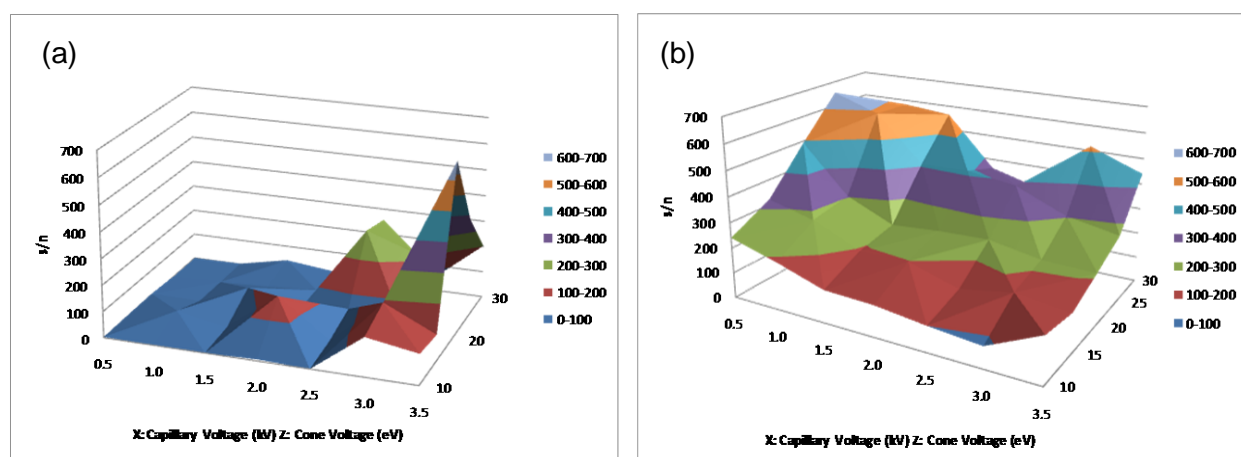


Figure 7.1. Signal-to-noise surface plots of cone vs. capillary voltage for (a) diphenhydramine determined with 90:10 $(\text{CH}_3)_2\text{CO}$:10 mM ammonium formate, pH 3.0) and (b) cytosine determined with 90:10 CH_3CN :10 mM ammonium formate, pH 9.0). The x-, y- and z- axis represent capillary voltage (kV), cone voltage (eV) and signal-to-noise respectively.

Cytosine showed different source behaviour in comparison and could be successfully protonated at lower capillary voltages, however higher cone voltages were required for achieving optimal signal-to-noise values. Optimum source conditions were found to be similar for the other nucleobase adenine (Table 7.3). The difficulties in protonating nucleobases with a $pK_a > 3$ through gas-phase proton transfer reactions with ammonium cations in electrospray were evaluated by Charles and co-workers [243]. In the context of this work, adenine and cytosine have similar pK_a values of 4.2 and that any contributions to protonation via gas-phase ammonium cations is perhaps less likely. Furthermore, the presence of acetone (194 kcal/mol) with a higher proton affinity than acetonitrile (186.2 kcal/mol) suggests it may be competing more effectively for protonating hydrogen atoms, hence the poor signal-to-noise observed for the nucleobases and indeed also for caffeine in this study.

Adenine and cytosine have low pK_a values (Table 7.1) and are considered non-ionised under the conditions evaluated herein. In comparison to the other evaluated basic compounds, the removal of aqueous solvation in the desolvation process make compounds such as nucleobases more difficult to protonate. Caffeine is very weakly basic and overall shows difficulty in achieving effective protonation apart from when using acetonitrile at high pH, shown later in Tables 7.4 and 7.5. This observation correlates well with Zhou [138] in that solution-phase protonation is unlikely and instead either a gas phase-ion molecule interaction or collision induced dissociation of the ammonium cations and the analyte is taking place. Clearly, without any obvious basic centre for protonation adenine, cytosine and caffeine illustrate the complex ionization process involved with improving the response of these effectively neutral analytes, and that serious consideration in attenuating the interplay between eluent and source conditions are essential for improving sensitivity.

Compound	$(\text{CH}_3)_2\text{CO}$		CH_3CN	
	Capillary Voltage (kV)	Cone Voltage (eV)	Capillary Voltage (kV)	Cone Voltage (eV)
pH 3.0				
Cytosine	3.5	30	3.5	30
Adenine	3.5	25	3.5	30
Caffeine	2.0	10	2.0	15
Procainamide	0.5	25	2.0	25
Nicotine	0.5	10	2.5	20
Nortriptyline	0.5	25	2.5	25
Diphenhydramine	0.5	20	3.5	20
pH 9.0				
Cytosine	0.5	20	0.5	25
Adenine	2.0	30	0.5	25
Caffeine	n.d.	n.d.	3.0	20
Procainamide	0.5	30	1.5	15
Nicotine	1.0	10	3.0	25
Nortriptyline	0.5	30	2.0	30
Diphenhydramine	1.0	20	3.0	10

Table 7.3. Optimal source voltages determined for each compound based on surface response plots determined by extracted ion data. Data based on extracted $[\text{M}+\text{H}]^+$ ions for each compound.

Table 7.3 indicates the optimally determined source voltages for each analyte based on the systematic variation of capillary and cone voltages. With the exception of the nucleobases and caffeine, the same optimum capillary voltages using acetone at pH 3 were determined for all other probe compounds. In contrast, higher voltages were required when using acetonitrile for all analytes under acidic conditions. Interestingly, in several instances optimal signal-to-noise was obtained for some of the analytes at low capillary voltages suggesting that perhaps thermally assisted ionization is the dominant mechanism. The earlier work of Vestal *et al.* [119, 120] on thermospray ionization noted that under certain conditions molecular ions were produced when the hot filament used to ionize compounds emerging from the vapor jet was turned off, reporting substantially lower detection limits as a result. It was observed previously in Chapter 2 [244] that low optimal capillary voltages (0.8 kV) for the UPLC-MS/MS analysis of the basic solutes quinine and its major metabolite 3(S)-3-hydroxyquinine, using an instrument with a similar source design to the one in the present study. This observation may also be related to the work of Langley *et al.* [245] noting increased signal in the absence of high voltage using SFC-MS, termed novo-spray. However, in their study the definitive ionization mechanism responsible for affording increased signal was not elucidated. Nevertheless, the precision values obtained here at these lower voltages were remarkably stable and not indicative of

thermospray alone, which is typically not as reproducible as electrospray ionization. It is likely then that the dominant ionization mechanism is thermospray, with protonation occurring mainly through abstraction of protons from ammonium cations in the gas phase. The data reported here may therefore be termed electrically stabilized thermospray. Clearly, these findings warrant further investigation elsewhere. Particularly, as most modern electrospray ionization mass spectrometers are now able to operate with high desolvation temperatures and gas flow rates, just as was decided to use here in order to accommodate the higher chromatographic inlet flows in this study.

When at high pH using acetone, the overall signal-to-noise values were much lower and suppression of the responses obtained for the strongly basic solutes was impaired dramatically than those determined using the same solvent under acidic conditions. This can perhaps be related to the reactivity of acetone which exists as an enolate in aqueous basic conditions which can then result in the formation of analyte adducts and or diacetone, triacetone and higher condensation products as observed by Keppel *et al.* [240] and Fountain and co-workers [116]. It is also known that in solution chemistry tertiary amines do not react with carbonyl groups suggesting that only weakly dissociative analyte-solvent interactions are taking place. Figure 7.2 shows the presence of high intensity diacetone and triacetone condensation products in the extracted ion spectra from an injection of cytosine. The signal intensity for cytosine is in the order of 1.5×10^7 whereas the corresponding signals for diacetone and triacetone are 2×10^7 and 6.5×10^7 respectively. The observed adduct formation can be related to the work of O'Hair *et al.* [246] on glycine residue reactivity towards acetone in the gas phase, however we did not see any ions of + 40 m/z which would be consistent with the $[M + H + (CH_3)_2CO - H_2O]^+$ product.

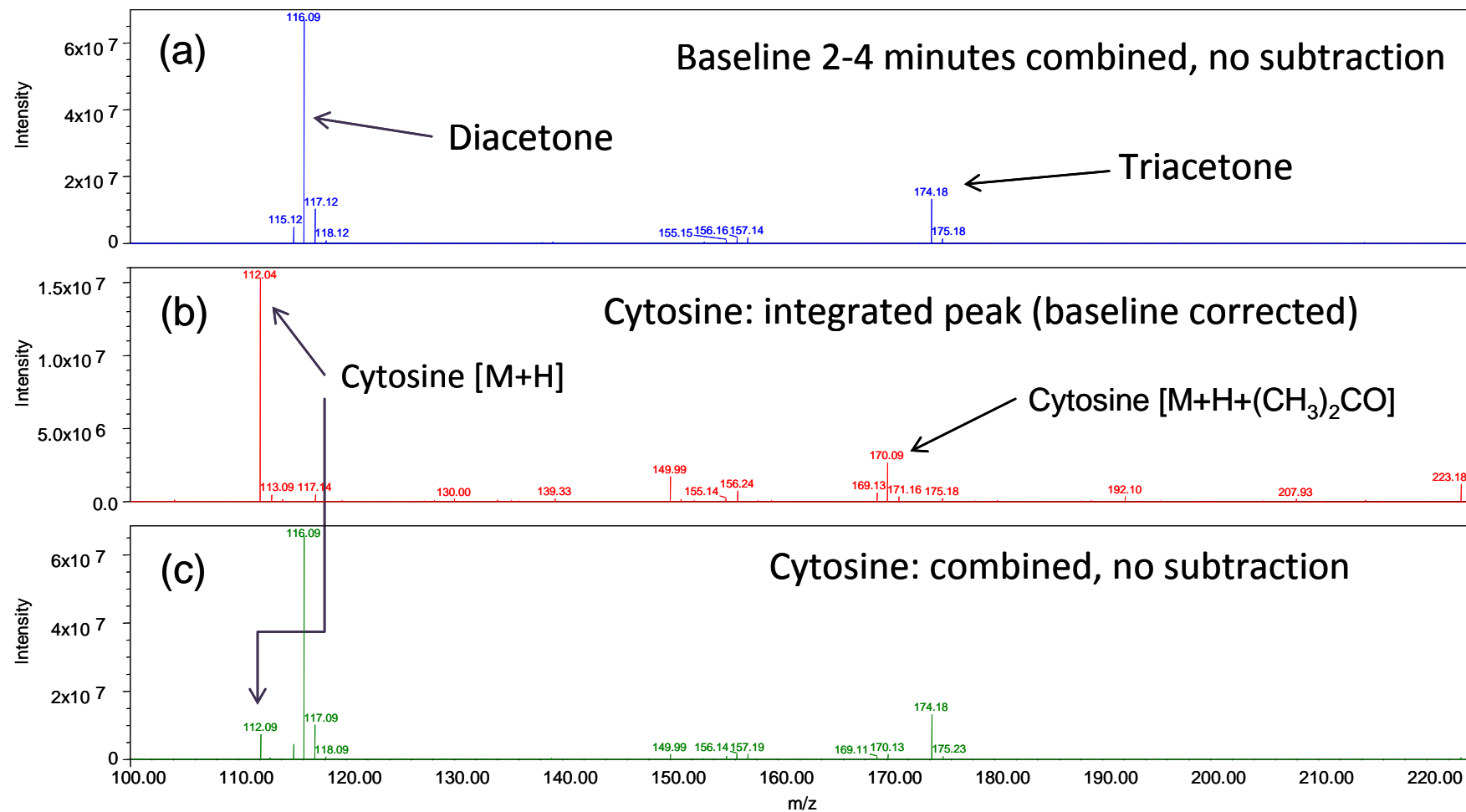


Figure 7.2. (a) combined overlay of acetone background over 2 minutes (b) cytosine spectra as result of peak integration in Empower 2 CDS undergoing baseline correction and (c) cytosine spectra combined at the baseline of the peak without baseline noise subtraction.

In an attempt to improve the undesirable signal-to-noise values observed when using acetone, the effect of increasing cone gas flow (Figure 3) was evaluated as depicted by monitoring the 116 m/z ion (diacetone). By applying values up to 200 L/min and at intermediate flow rates ranging from zero cone gas, minor signal decreases were observed on the disruption of the acetone condensation products. A slight decrease in the signal for diacetone was observed compared to the response found without application of cone gas, however this was not appreciably effective in reducing the contribution to noise when using this solvent. Disruption of the acetone-analyte interaction was not achievable using higher cone voltages or increases in cone gas (Figure 7.3) to improve signal-to-noise values. This is not surprising since diacetone and triacetone are condensation products of acetone and increased gas flows would not disrupt these covalent ions. The purpose of increasing cone gas flow was to try and inhibit the entrance of these acetone product ions into the ion source in order to improve signal-to-noise values using cytosine as a model test compound.

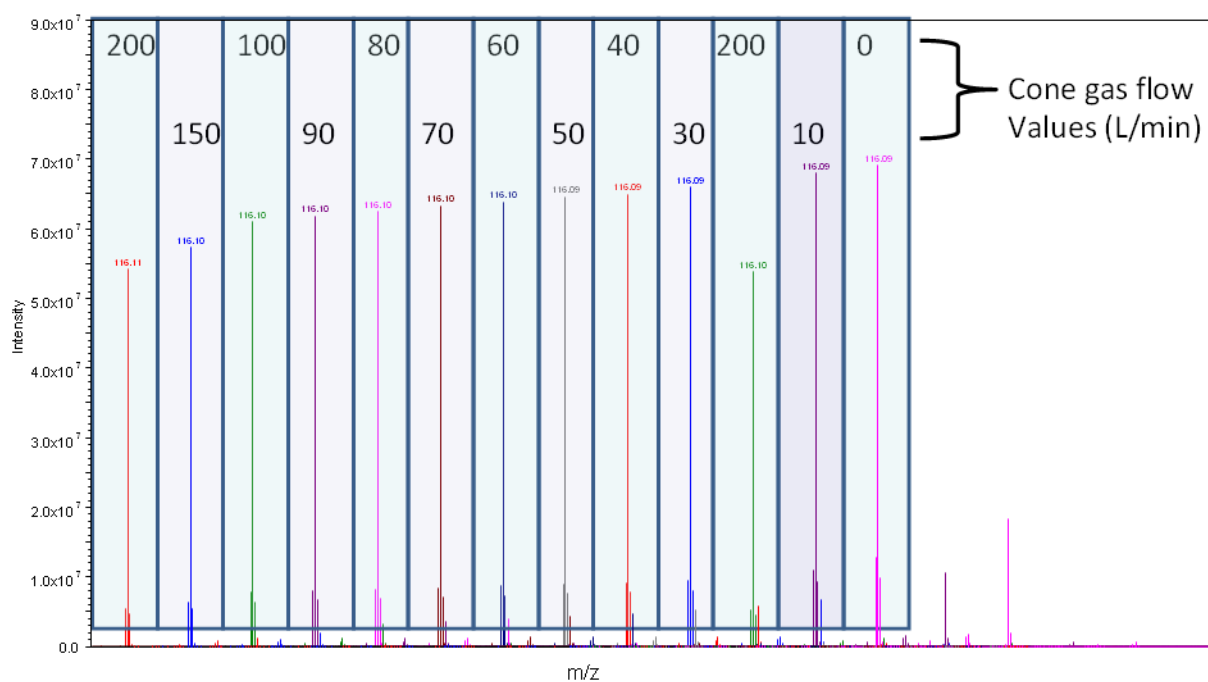


Figure 7.3. Diacetone ion at 116 m/z monitored using various cone gas flow rates with a mobile phase at pH 9.0 (200 L/min was tested twice at random to verify observations).

From the determined optimum source voltages, analyte reproducibility was determined for signal-to-noise, signal intensity and peak area as shown in Tables 4 and 5 for each of the solvent systems. Using these conditions ionization efficiency should be optimal as indicated by the precision determined for peak areas measured for ten consecutive injections of each test solute; overall < 20% RSD for each analyte determined in all solvent systems. Notably, much more stable measurements for the acetone experiments at both pH 3 and pH 9 in comparison to acetonitrile for peak area (< 10%, $(\text{CH}_3)_2\text{CO}$) were observed. Peak area reproducibility for adenine (15.2%) was poor using acetone at pH 9 and is likely to be attributed to the difficulty in protonation of this compound. On the contrary, under the same conditions nicotine showed lower signal-to-noise except the peak area precision (6.7%) was superior. Overall, peak area and signal-to-noise precision was found to be superior for acetone versus acetonitrile under both pH conditions investigated. This may be a consequence of solvent cleanliness as fewer extraneous ions were observed when using acetone, although overall higher background chemical noise was observed due to the previously discussed condensation products. Figure 7.4 shows the signal intensity values for each of the evaluated solvent systems at low and high pH, the % RSD values for ten replicate injections are shown in Tables 7.4 and 7.5. For practical purposes it is of more interest to report signal-to-noise values since this provides a more quantitative measure for determining the relative sensitivity, or limit of detection for each analyte.

Table 7.4. Comparison between acetonitrile and acetone at pH 3.0 determined at optimum source voltages (n = 10).

Compound	$(\text{CH}_3)_2\text{CO}$ (s/n) Mean	% R.S.D.			CH_3CN (s/n) Mean	% R.S.D.		
		s/n	Signal Intensity	Peak Area		s/n	Signal Intensity	Peak Area
Cytosine	34	20.5	5.6	6.1	82	31.0	11.5	11.7
Adenine	33	13.7	5.9	7.5	174	42.8	12.4	11.3
Caffeine	n.d.	n.d.	n.d.	n.d.	9	33.3	20.2	16.9
Procainamide	483	13.1	1.5	4.2	664	13.5	2.5	3.0
Nicotine	125	12.1	3.9	4.0	342	19.8	4.8	3.7
Nortriptyline	293	12.5	1.9	1.9	686	13.1	3.1	3.0
Diphenhydramine	1386	14.3	1.2	1.2	2242	23.3	1.2	1.4

Table 7.5. Comparison between acetonitrile and acetone at pH 9.0 determined at optimum source voltages (n = 10).

Compound	$(\text{CH}_3)_2\text{CO}$ (s/n) Mean	% R.S.D.			CH_3CN (s/n) Mean	% R.S.D.		
		s/n	Signal Intensity	Peak Area		s/n	Signal Intensity	Peak Area
Cytosine	217	9.0	4.4	5.3	602	11.2	4.6	5.7
Adenine	77	19.8	15.4	15.2	613	14.6	5.7	7.9
Caffeine	n.d.	n.d.	n.d.	n.d.	62	58.7	13.7	16.1
Procainamide	325	17.9	3.9	3.7	673	20.7	5.7	4.2
Nicotine	75	11.7	7.9	6.7	373	23.7	16.3	16.5
Nortriptyline	379	20.3	2.9	3.1	1582	31.3	12.3	12.3
Diphenhydramine	303	20.5	4.3	4.4	1920	16.7	2.1	2.4

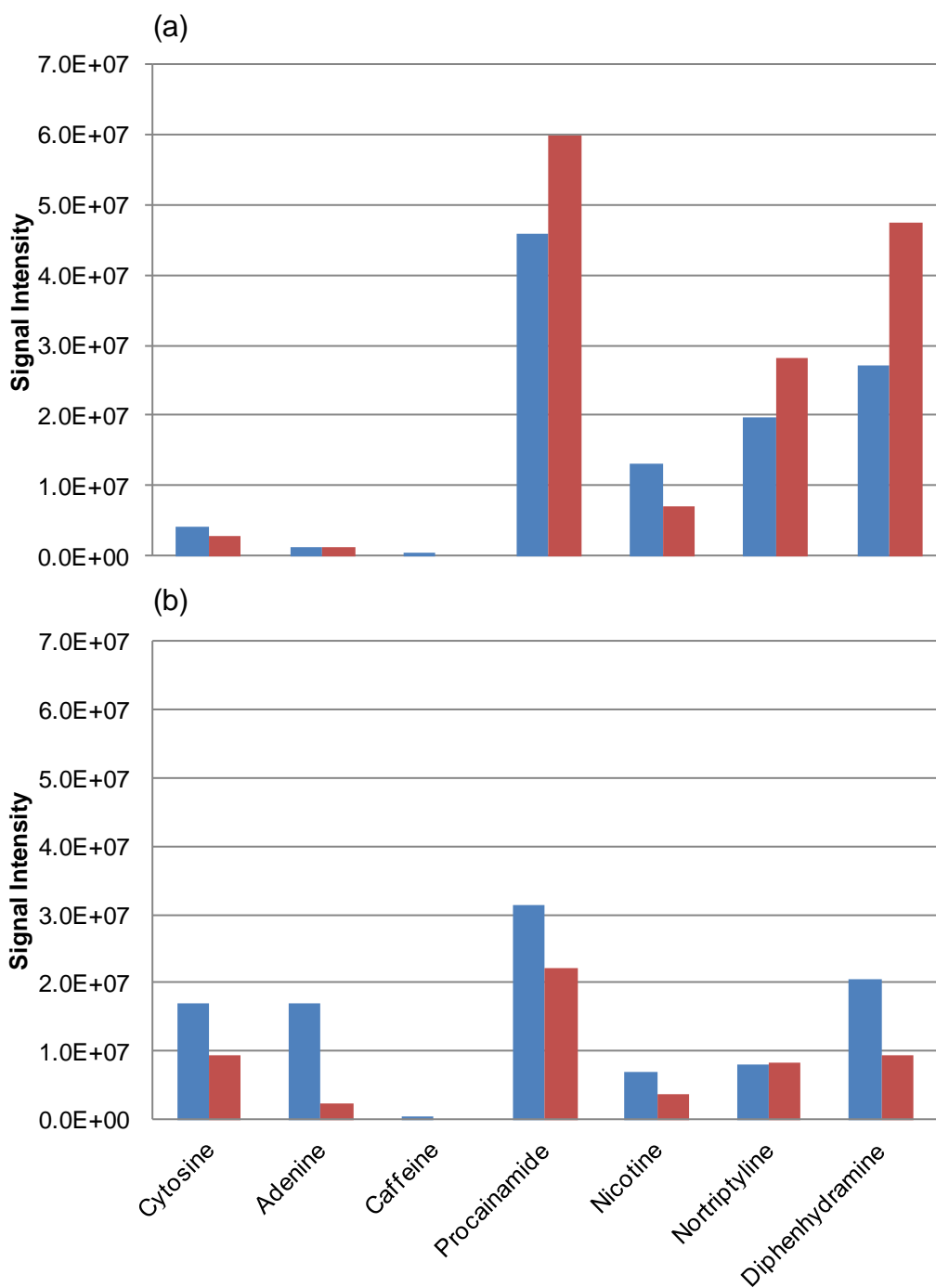


Figure 7.4. Mean signal intensity data based on n=10 injections. Where (a) is pH 3 data and (b) is pH 9 data. Blue and red are acetonitrile and acetone respectively.

The vapor pressure for acetone (Table 7.2) is higher than acetonitrile and this should facilitate more efficient desolvation due to reduced surface tension of the droplets. However, the presence of acetone condensation products and adduct formation results in inferior use of this solvent for positive ion electrospray in the lower mass range (< 300 Da). For analytes with the lowest signal-to-noise values (i.e. Adenine, Cytosine and Caffeine) observed in the full scan extracted ion experiments, a comparison was made with selected ion monitoring (SIM) so as to ascertain the extent of the background noise, acetone related chemical noise and adduct formation. Here the quadrupole was set to each ion separately, representing the protonated molecule of interest (e.g. 136.1 [M+H]⁺ for adenine) and as a result, interference was somewhat filtered out resulting in increased observed signal-to-noise values. The results of which are shown in Figure 7.5 from 10 injections of each analyte under the stated chromatographic conditions.

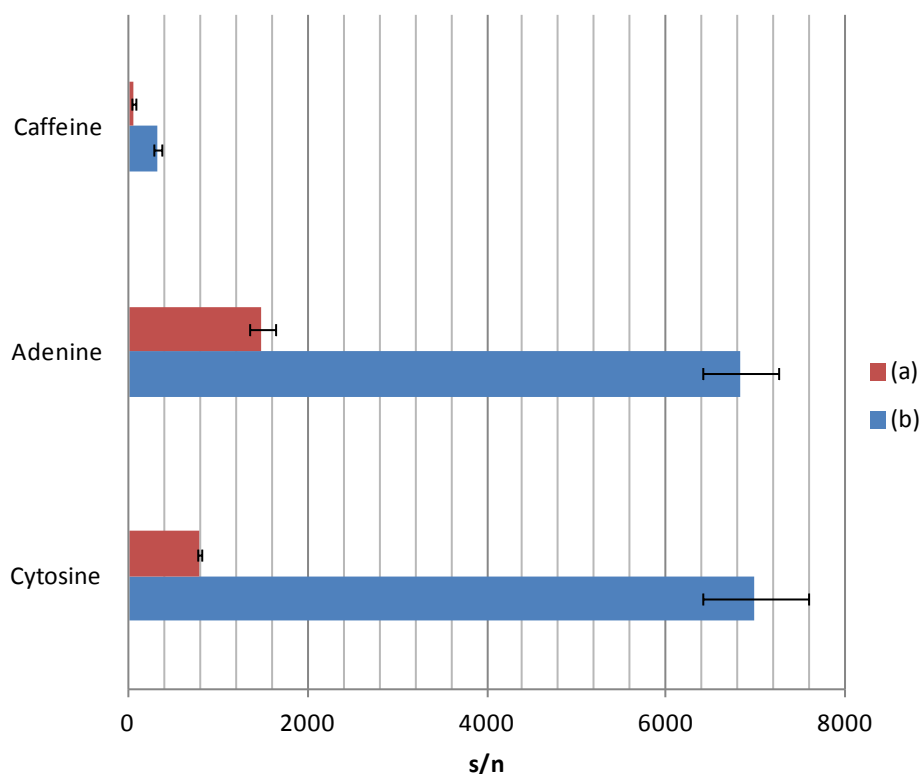


Figure 7.5. Comparison between (a) $(\text{CH}_3)_2\text{CO}$ and (b) CH_3CN at pH 9.0 using SIM for test solutes (n = 10).

This observation is in agreement with any selected ion mass spectrometry and indicates that when using acetone as an eluent for HILIC, major improvements in signal-to-noise can be achieved in comparison to when data is acquired in a full scan mode. The use of the quadrupole to select the ions of interest is acting to reduce the contribution of noise to the analyte signal. There is an improvement when using acetone under these conditions, however, the use of acetonitrile is far superior in comparison and should be the preferred solvent when maximum sensitivity is required.

Summarised statistical data treatment of the source voltage optimisation process and the resulting optimum values for each solvent at low and high pH are shown in Figure 7.6. The analytes are grouped into sets of conditions and the most favourable solvent system is highlighted as using acetonitrile at high pH determined as the highest signal-to-noise value. This is consistent with observations by Peng [135] and Delatour [247] on the uses of basic mobile phases with positive ion electrospray where higher sensitivity was reported in comparison to acidic conditions. The optimal signal-to-noise for adenine and cytosine was also found using acetonitrile at high pH. The least favourable data was the pH 9.0 buffer with acetone, also highlighted, yielding the overall poorest results for all analytes.

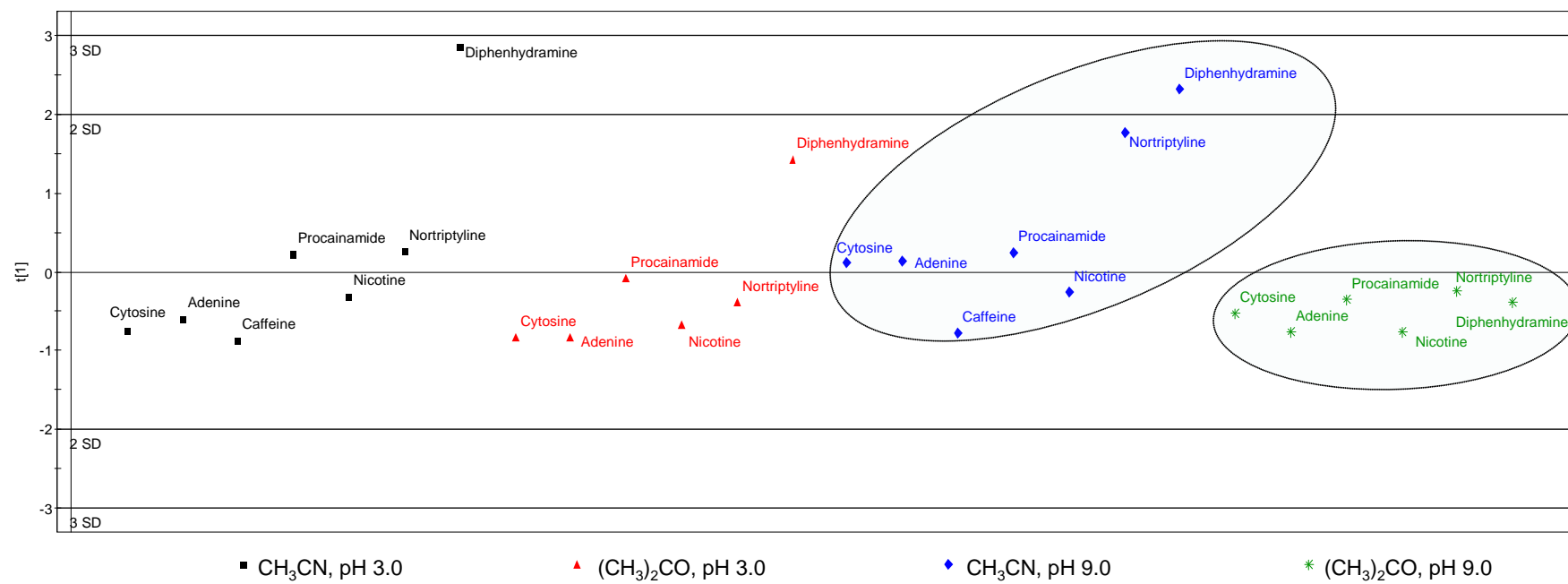


Figure 7.6. Scatter plot encompassing mean signal-to-noise values for overall sample set.

7.3.2 Influence of acetone organic modifier on retention

As already indicated by several workers [248-250] underivatized silica has been shown to be beneficial for the analysis of cationic drugs by ion exchange retention mechanisms. In terms of HILIC, there is a limited range of solvents that can be incorporated into the methods development process compared to reversed-phase LC. Spiraling costs due to shortages of acetonitrile supplies can also be troublesome as recent history has highlighted. Consequently, running costs for HILIC based separations have spiraled resulting in poor economical return in implementing this mode of chromatography. Figure 7.7 illustrates the selectivity differences between acetonitrile and acetone at pH 3. Clearly there are dramatic shifts in retention for certain analytes and in particular for nicotine, which had approximately twice the retention time in acetonitrile compared to acetone. Slight decreases in retention were observed for all analytes using acetone which is considered as a weaker solvent than acetonitrile for HILIC. Interestingly, although this evaluation was carried out only using a model test mix, superior selectivity between analytes was achieved using acetone compared with acetonitrile for the other compounds in our study. Clearly, more work needs to be invested into investigating the selectivity merits of acetone for HILIC as overall we found this solvent to result in reduced retention of our analytes, apart from nicotine. This is likely due to acetone behaving as a hydrogen bond acceptor interacting with ionised sites on the probe analytes, this may also explain the improved selectivity observed compared with acetonitrile. Therefore it can be suggested for method development purposes, and where sensitive positive ion electrospray work isn't required, that acetone could have utility for HILIC interfaced to ESI-MS or other alternative detectors to ultraviolet.

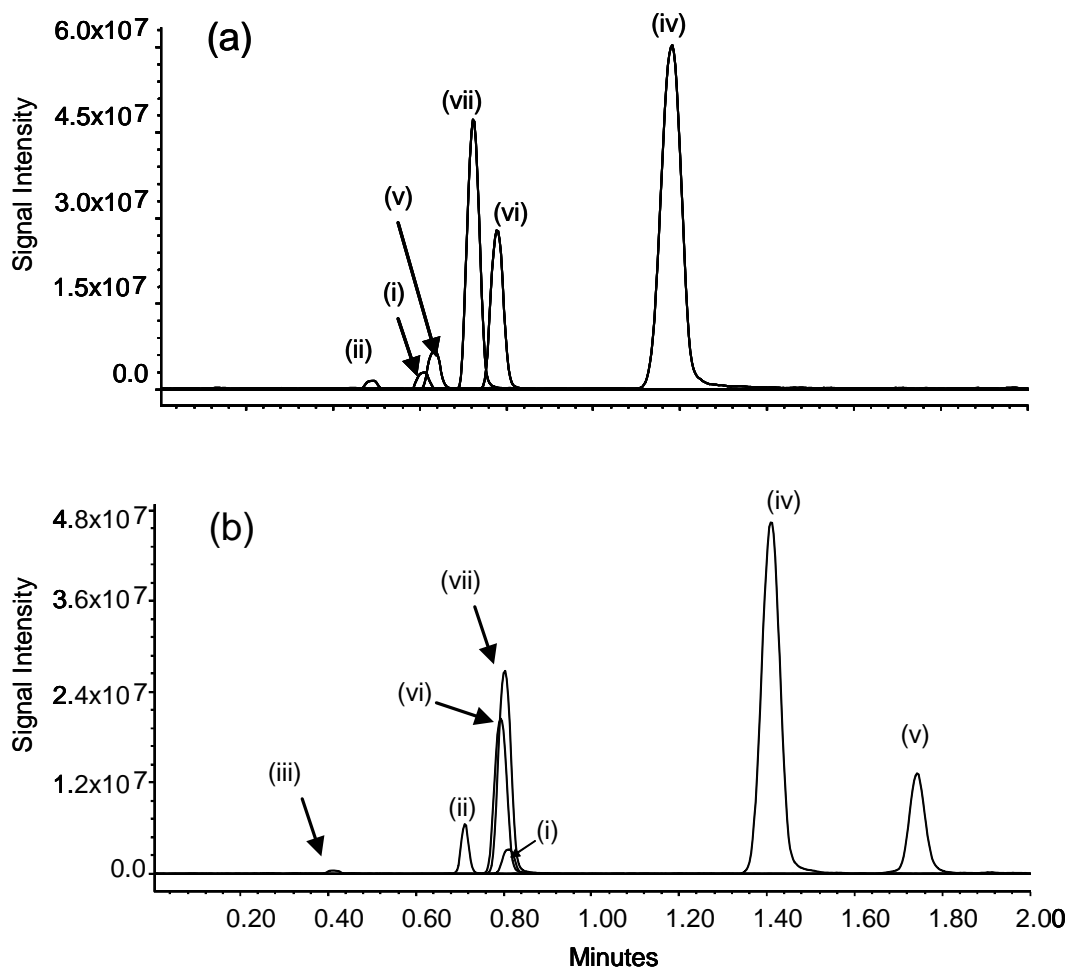


Figure 7.7. (a) $(\text{CH}_3)_2\text{CO}$, pH 3.0 and (b) CH_3CN , pH 3.0. Composition of solvent-buffer (90:10, v/v). Analytes: (i) cytosine (ii) adenine (iii) caffeine (iv) procainamide (v) nicotine (vi) nortriptyline (vii) diphenhydramine.

7.3.3 Column robustness metrics

The experimental process in generating the results presented here utilised 3 columns accounting for approximately 8500 injections. Each column lasted on average around 3000 injections before deteriorating, seen typically in the form of peak broadening and tailing. The maximum pressure the column experienced was less than 7000 psi and a maximum temperature of 30 °C throughout all analyses. All columns were subjected to high and low pH switching with water rinses prior to switching, organic solvent switching, constant ionic strength blending, and non-constant use over the span of the column life. "Non-constant" use is defined in this context as the column in use for 24 hours for multiple days but placed in shutdown with zero flow until next used. Columns were not stored when not in use and remained on the system until additional experiments were deemed necessary. The remarkable stability of these bare BEH-silica columns should be mentioned consequentially as a derivative to this investigation, adding confidence that this support can be routinely used.

7.4 Conclusions

Although clearly problematic for positive ion electrospray, acetone offers complementary selectivity to acetonitrile which is important for method development using HILIC separations. Our objective was not to embellish or question the mechanisms of electrospray ionisation but rather offer an objective measure of solvent compatibility with this mode of chromatography. The chemical noise observed when using acetone instead of acetonitrile was evaluated. This is important to measure in order to reveal more clearly the LOD for particular analytes, which is essential when sensitivity is required to be maximised. The work presented here has contributed further evidence on the use of basic mobile phases in order to achieve maximum signal-to-noise of basic solutes with positive ion ESI mass spectrometry. Acetone condensation product formation and high average peak-to-peak noise was observed in the low molecular weight region, which may inhibit LLOQ of particular classes of analytes, especially those which do not ionise efficiently as is the case for nucleobases. The systematic optimisation approach shown here has highlighted some important variables for method development in the HILIC-MS arena. Further work is under way elsewhere with regards to the use of acetone as a strong solvent for use with RPLC and for HILIC interfaced with APCI-MS for small molecule work.

Chapter 8.

Conclusion and further work.

In less than a decade liquid chromatography has been revolutionised since the introduction of ultra high pressure chromatographs and the corresponding sub-2 μm particle packed columns. Albeit with the assistance of a triple quadrupole mass spectrometer, these advances were applied in Chapter 2. Significant gains in throughput were realised using these technologies in comparison to previously reported conventional HPLC based methodologies. Undoubtedly, one of the major breakthroughs has been also in the development of bridged-ethylene hybrid (BEH) silica particles. Columns packed with these phases have been utilised extensively throughout this thesis and in several chemistry formats. These being, use at pH 10 for an extended period of time, operation at elevated temperatures (130 $^{\circ}\text{C}$) for reversed-phase separations and in the HILIC mode without the presence of a bonded group. In order to extend the capability of UHPLC the introduction of elevated temperatures was envisaged through the integration of a dedicated forced-air thermostat.

Chapter 3 dealt with an evaluation of this apparatus and several key functions pertinent to obtaining the maximum possible efficiency of sub-2 μm packed columns. In addition, the importance of the thermal environment a column operates in and the formation of radial temperature gradients were interesting challenges, as well as minimisation of extra-column volume effects. An interesting concept was devised by which to reduce heat transfer from the column to the surroundings of the forced-air thermostatic device. Using columns with thin walls was evaluated, however the results of which indicate much further work is required to elucidate whether this is a viable means of reducing the effects of radial temperature gradients.

Novel applications and evaluations have been made using predominantly the BEH material throughout this thesis. Particularly, for the efficient separation of anabolic steroids using elevated temperature as shown in Chapter 4. An extensive investigation comparing the kinetic performances of sub-2 μm BEH versus superficially porous particles was also carried out in the same study. This led on to the comparison of similar particle packed columns, except in the

bare silica format for the analysis of basic solutes. These are known to be problematic by conventional reversed-phase techniques, so it was of interest to compare the kinetic performances of several commercially available bare silica phases. It was decided to carry out an investigation concerning the kinetic performance of these phases for the analysis of amino pharmaceutical substances as shown in Chapter 5. Leading on from this study, the separation of diastereomeric ephedrine substances was the subject of an investigation using bare silica BEH packed columns, as shown in Chapter 6. This was the first reported separation of its kind for these substances using the HILIC technique, and explored the use of temperature as a means to optimise resolution. By way of comparison, an already reported reversed-phase separation at high pH was used as a kinetic benchmark. It was shown that the HILIC technique was not only superior in terms of kinetic performance but also in obtaining highly symmetrical peak shapes. One of the major limitations in adopting the HILIC approach is the reliance on acetonitrile-rich mobile phases. The use of acetone as an alternative organic modifier to acetonitrile in HILIC was investigated except with the hyphenation to electrospray ionisation mass spectrometry. This work showed that perhaps acetone is an unsuitable modifier due to the high background noise observed. The limitation being that sensitivity as well as effective ionisation was the major disadvantage for several of the evaluated analytes.

There are several future studies which could be carried out. Firstly, there still remains much conjecture in the scientific literature as to the advantages and disadvantages on the use of fully versus superficially porous particles. It should be pertinent to evaluate such materials based on the combination of a statistically significant sample set of columns. This would provide unambiguous data, on the goodness of packing for instance between manufacturers columns, which is highly debated and often conflicting in the literature. It would also be useful to introduce a standard protocol across laboratories for evaluating column performance. This might contribute to limiting broad conclusions drawn on the goodness of one column versus another reported in literature. Likewise, the drive to yet more sophisticated particle technologies is obscured by the poorness of packing 2.1 versus 4.6 mm ID columns for instance. This is a major challenge, as undoubtedly the next generation of yet smaller particle packed and higher inlet pressure operated systems would have to address the effects of viscous frictional heating. The obvious solution being to reduce the column internal diameter. However, this not only

challenges the packing technology required but also impacts on the design of instruments which would have to be devoid of extra-column volume.

It would also have been interesting to expand studies involving use of the UPLC Q-TOF-MS in order to identify novel metabolites of quinine. Although this is a well understood medicine, there are few reports on the isolation and identification of metabolites of quinine. Particularly, with respect to Phase I and Phase II O-conjugate transformations. Furthermore, it would have rounded the study to confirm and present high mass accuracy fragmentation data on the other metabolites. This could be done by scouring the post-dose urine and comparing with microsomal incubations of deuterated-quinine in order to yield the corresponding deuterium labelled metabolites. Unfortunately such a study was outside the scope of this project, and this would nevertheless provide more analytical challenges. It would be interesting to apply the HILIC approach to any further studies involving quinine metabolism, particularly as metabolites are typically more polar than their parent compound.

Investigating the use of forced-air thermostats is perhaps not an ideal approach when using ultra-high pressure chromatography. However, due to the potential impact of column hardware on heat flux and subsequent influence of performance should be revisited. It would be interesting to design column housings which have small surface areas, as this essentially results in an insulating-like effect. Obviously, this would be at the mercy of burst pressures. Nevertheless, the use of lower amounts of steel used as column hardware could impact on the cost of manufacture. Any further studies should entail the use of sensitive thermocouples or thermal imaging to accurately and precisely measure the thermodynamic behaviour of such columns in operation. Furthermore, it could be envisaged that thin wall column hardware would be more responsive to temperature programmed elution methodology.

List of Abbreviations

UHPLC	Ultra High Pressure Liquid Chromatography
HPLC	High Performance/Pressure Liquid Chromatography
UPLC	Ultra Performance Liquid Chromatography
MS	Mass Spectrometry
MS/MS	Tandem Mass Spectrometry
ESI	Electrospray ionisation
ACO	Acquity Column Oven
HILIC	Hydrophilic Interaction Chromatography
BEH	Bridged-Ethylene Hybrid
RP	Reversed-Phase
HETP	Height Equivalent to a Theoretical Plate
LC-MS	Liquid Chromatography-Mass Spectrometry
SPE	Solid Phase Extraction
LLE	Liquid-Liquid Extraction
SRM	Selected Reaction Monitoring
Q-TOF-MS	Quadrupole-Time Of Flight-Mass Spectrometry
PLUNO	Partial Loop Needle Overfill
WADA	World Anti-Doping Agency
ACN	Acetonitrile
IPA	Isopropyl Alcohol
ELSD	Evaporative Light Scattering Detector
CAD	Charged Aerosol Detector
UV	Ultra Violet
APCI	Atmospheric Pressure Chemical Ionisation
APPI	Atmospheric Pressure Photo Ionisation
LOD	Limit Of Detection
LLOQ	Lowest Limit Of Quantification
ULOQ	Upper Limit Of Quantification

Bibliography

Heaton J, Jones MD, Legido-Quigley C, Plumb RS, Smith NW. Systematic evaluation of Acetone and Acetonitrile for use in HILIC Coupled with ESI Mass Spectrometry of Basic Small Molecules. *Rapid Commun Mass Spec*. DOI: 10.1002/rcm.5271

Heaton J, Gray N, Cowan DA, Plumb RS, Legido-Quigley C, Smith NW. Comparison of reversed-phase and hydrophilic interaction liquid chromatography for the separation of ephedrines. *J Chromatogr A*. DOI:10.1016/j.chroma.2011.09.026

Rahmioglu N, Heaton J, Yong M, Hider RC, Smith NW, Ahmadi KR. Genetic Epidemiology of Induced CYP3A4 Activity. *Pharmacogenetics and Genomics*. 2011 Oct;21(10):642-51.

Rahmioglu N, Le Gall G, Heaton J, Kay KL, Smith NW, Colquhoun IJ, Ahmadi KR, Kemsley FK. Prediction of variability in CYP3A4 induction through an integrative 1H NMR metabolomics approach. *Journal of Proteome Research*. 2011 Jun 3;10(6):2807-16.

Heaton J, Rahmioglu N, Ahmadi KR, Legido-Quigley C, Smith NW. Rapid quantification of quinine and its major metabolite (3S)-3-hydroxyquinine in diluted urine by UPLC-MS/MS. *Journal of Pharmaceutical & Biomedical Analysis*. 2011 Jun 1;55(3):494-9.

Presentations

Posters:

HTC-2010 (Bruges), HPLC 2010 (Boston)

Speaker invitations:

The opening of the Waters 'Centers of Innovation program' at KCL:

Advances in separation science for pharmaceutical and sports medicine analysis

ChromSoc Spring Symposium May 2011 held at Novartis, Horsham

Biomedical Chromatography, Royal Society of Chemistry Separation Science Group, The Wellcome Centre, London, Nov 2011

References

- [1] M.S. Tswett, *Ber Dtsch Bot ges*, 24 (1906) 384.
- [2] A.J. Martin, R.L. Synge, *Biochem J*, 35 (1941) 1358-1368.
- [3] L.R. Snyder, J.J. Kirkland, *Introduction to modern liquid chromatography*, 2d ed., Wiley, New York, 1979.
- [4] U.D. Neue, *HPLC columns : theory, technology, and practice*, Wiley-VCH, New York, 1997.
- [5] J.H. Purnell, *Nature*, 184 (1959) 2009-2009.
- [6] U.F.a.D. Administration, in, 1994.
- [7] U.D. Neue, J.E. O'Gara, A. Méndez, *Journal of Chromatography A*, 1127 (2006) 161-174.
- [8] L.R. Snyder, J.J. Kirkland, J.L. Glajch, *Practical HPLC method development*, 2nd ed., Wiley, New York, 1997.
- [9] J.J. van Deemter, F.J. Zuiderweg, A. Klinkenberg, *Chemical Engineering Science*, 5 (1956) 271-289.
- [10] J.H. Knox, *Journal of Chromatography A*, 831 (1999) 3-15.
- [11] Waters, *Acquity UPLC for Laboratory Practitioners Training Manual*.
- [12] M.J.E. Golay, *Journal of Chromatography*, 186 (1979) 341-351.
- [13] C.R. Wilke, P. Chang, *Am. Inst. Chem. Eng. J.*, 1 (1955) 264-270.
- [14] J.C. Giddings, *Dynamics of Chromatography. Part 1*, Marcel, Dekker, New York, 1965.
- [15] P. Bristow, J. Knox, *Chromatographia*, 10 (1977) 279-289.
- [16] T.J. Kaiser, J.W. Thompson, J.S. Mellors, J.W. Jorgenson, *Analytical Chemistry*, 81 (2009) 2860-2868.
- [17] J. Li, P.W. Carr, *Analytical Chemistry*, 69 (1997) 2530-2536.
- [18] J.C. Giddings, *Analytical Chemistry*, 37 (1965) 60-63.
- [19] H. Poppe, *Journal of Chromatography A*, 778 (1997) 3-21.
- [20] N. Tanaka, H. Kobayashi, N. Ishizuka, H. Minakuchi, K. Nakanishi, K. Hosoya, T. Ikegami, *Journal of Chromatography A*, 965 (2002) 35-49.
- [21] S.-T. Popovici, P.J. Schoenmakers, *Journal of Chromatography A*, 1073 (2005) 87-91.
- [22] G. Desmet, D. Clicq, P. Gzil, *Analytical Chemistry*, 77 (2005) 4058-4070.
- [23] G. Desmet, D. Clicq, D.T. Nguyen, D. Guillarme, S. Rudaz, J.L. Veuthey, N. Vervoort, G. Torok, D. Cabooter, P. Gzil, *Analytical Chemistry*, 78 (2006) 2150-2162.

- [24] C. Cramers, J. Rijks, C. Schutjes, *Chromatographia*, 14 (1981) 439-444.
- [25] D. Cabooter, F. Lestremau, A. de Villiers, K. Broeckhoven, F. Lynen, P. Sandra, G. Desmet, *Journal of Chromatography A*, 1216 (2009) 3895-3903.
- [26] G. Desmet, in: <http://www.vub.ac.be/CHIS/Research/kp.html>, 2011.
- [27] S. Eeltink, P. Gzil, W.T. Kok, P.J. Schoenmakers, G. Desmet, *Journal of Chromatography A*, 1130 (2006) 108-114.
- [28] D.V. McCalley, *Journal of Chromatography A*, 965 (2002) 51-64.
- [29] G. Guiochon, *Journal of Chromatography A*, 1168 (2007) 101-168.
- [30] F. Gritti, G. Guiochon, *Journal of Chromatography A*, 1218 (2011) 5216-5227.
- [31] D. Cabooter, A. de Villiers, D. Clicq, R. Szucs, P. Sandra, G. Desmet, *Journal of Chromatography A*, 1147 (2007) 183-191.
- [32] F. Lestremau, A. Cooper, R. Szucs, F. David, P. Sandra, *Journal of Chromatography A*, 1109 (2006) 191-196.
- [33] F. Lestremau, A. de Villiers, F. Lynen, A. Cooper, R. Szucs, P. Sandra, *Journal of Chromatography A*, 1138 (2007) 120-131.
- [34] D. Cabooter, F. Lestremau, F. Lynen, P. Sandra, G. Desmet, *Journal of Chromatography A*, 1212 (2008) 23-34.
- [35] D.T.T. Nguyen, D. Guillarme, S. Rudaz, J.-L. Veuthey, *Journal of Chromatography A*, 1128 (2006) 105-113.
- [36] D.T. Nguyen, D. Guillarme, S. Heinisch, M.P. Barrioulet, J.L. Rocca, S. Rudaz, J.L. Veuthey, *Journal of Chromatography A*, 1167 (2007) 76-84.
- [37] Y. Zhang, X. Wang, P. Mukherjee, P. Petersson, *Journal of Chromatography A*, 1216 (2009) 4597-4605.
- [38] K.J. Fountain, U.D. Neue, E.S. Grumbach, D.M. Diehl, *Journal of Chromatography A*, 1216 (2009) 5979-5988.
- [39] S. Fekete, J. Fekete, K. Ganzler, *Journal of Pharmaceutical and Biomedical Analysis*, 50 (2009) 703-709.
- [40] Y. Liu, J. Zhang, X. Xu, M.K. Zhao, A.M. Andrews, S.G. Weber, *Analytical Chemistry*, 82 (2010) 9611-9616.
- [41] H. Claessens, C. Cramers, M. Kuyken, *Chromatographia*, 23 (1987) 189-194.
- [42] J.W. Dolan, L.R. Snyder, *Troubleshooting LC systems : a comprehensive approach to troubleshooting LC equipment and separations*, Humana Press, Clifton, N.J., 1989.

- [43] K.J. Fountain, E.S. Grumbach, U.D. Neue, D.M. Diehl, Waters Application Notes, 720002793en (2008).
- [44] J.C. Giddings, *Analytical Chemistry*, 39 (1967) 1027-1028.
- [45] J.W. Dolan, L.R. Snyder, N.M. Djordjevic, D.W. Hill, T.J. Waeghe, *Journal of Chromatography A*, 857 (1999) 1-20.
- [46] J.W. Dolan, J.R. Gant, L.R. Snyder, *Journal of Chromatography A*, 165 (1979) 31-58.
- [47] L.R. Snyder, J.W. Dolan, J.R. Gant, *Journal of Chromatography A*, 165 (1979) 3-30.
- [48] L.R. Snyder, M. Stadalius, M.A. Quarry, *Analytical Chemistry*, 55 (1983) 1412A-1430.
- [49] J.W. Dolan, D.C. Lommen, L.R. Snyder, *Journal of Chromatography A*, 485 (1989) 91-112.
- [50] J.W. Dolan, L.R. Snyder, N.M. Djordjevic, D.W. Hill, T.J. Waeghe, *Journal of Chromatography A*, 857 (1999) 21-39.
- [51] J.W. Dolan, L.R. Snyder, R.G. Wolcott, P. Haber, T. Baczek, R. Kaliszan, L.C. Sander, *Journal of Chromatography A*, 857 (1999) 41-68.
- [52] P.L. Zhu, L.R. Snyder, J.W. Dolan, N.M. Djordjevic, D.W. Hill, L.C. Sander, T.J. Waeghe, *Journal of Chromatography A*, 756 (1996) 21-39.
- [53] U.D. Neue, *J Chromatogr A*, 1079 (2005) 153-161.
- [54] U.D. Neue, J.L. Carmody, Y.F. Cheng, Z. Lu, C.H. Phoebe, T.E. Wheat, *Adv Chromatogr*, 41 (2001) 93-136.
- [55] J.W. Dolan, *Journal of Chromatography A*, 965 (2002) 195-205.
- [56] M.H. Chen, C. Horvath, *J Chromatogr A*, 788 (1997) 51-61.
- [57] J.W. Dolan, in: *LCGC Europe*, 2007.
- [58] D.V. McCalley, *J Chromatogr A*, 902 (2000) 311-321.
- [59] S.M. Buckenmaier, D.V. McCalley, M.R. Euerby, *Journal of Chromatography A*, 1060 (2004) 117-126.
- [60] A.H. Schmidt, I. Molnar, *Journal of Chromatography A*, 948 (2002) 51-63.
- [61] A.M. Edge, S. Shillingford, C. Smith, R. Payne, I.D. Wilson, *Journal of Chromatography A*, 1132 (2006) 206-210.
- [62] R.M. Smith, *Journal of Chromatography A*, 1184 (2008) 441-455.
- [63] R. Plumb, J.R. Mazzeo, E.S. Grumbach, P. Rainville, M. Jones, T. Wheat, U.D. Neue, B. Smith, K.A. Johnson, *J Sep Sci*, 30 (2007) 1158-1166.
- [64] G. Vanhoenacker, P. Sandra, *Anal Bioanal Chem*, 390 (2008) 245-248.

- [65] Y. Xiang, B. Yan, B. Yue, C.V. McNeff, P.W. Carr, M.L. Lee, *Journal of Chromatography A*, 983 (2003) 83-89.
- [66] Y. Xiang, Y. Liu, M.L. Lee, *Journal of Chromatography A*, 1104 (2006) 198-202.
- [67] J.D. Thompson, P.W. Carr, *Analytical Chemistry*, 74 (2002) 4150-4159.
- [68] T. Teutenberg, K. Hollebekkers, S. Wiese, A. Boergers, *Journal of Separation Science*, 32 (2009) 1262-1274.
- [69] M. Albert, G. Cretier, D. Guillarme, S. Heinisch, J. Rocca, *Journal of Separation Science*, 28 (2005) 1803-1811.
- [70] G. Vanhoenacker, P. Sandra, *J Sep Sci*, 29 (2006) 1822-1835.
- [71] J.D. Thompson, J.S. Brown, P.W. Carr, *Analytical Chemistry*, 73 (2001) 3340-3347.
- [72] T. Teutenberg, H.J. Goetze, J. Tuerk, J. Ploeger, T.K. Kiffmeyer, K.G. Schmidt, W.g. Kohorst, T. Rohe, H.D. Jansen, H. Weber, *Journal of Chromatography A*, 1114 (2006) 89-96.
- [73] L. Al-Khateeb, R.M. Smith, *J Chromatogr A*, 1201 (2008) 61-64.
- [74] H.G. Gika, G. Theodoridis, J. Extance, A.M. Edge, I.D. Wilson, *Journal of Chromatography B*, 871 (2008) 279-287.
- [75] A. Edge, I. Wilson, S. Shillingford, *Chromatographia*, 66 (2007) 831-836.
- [76] C. Smith, S. Shillingford, A. Edge, C. Bailey, I. Wilson, *Chromatographia*, 67 (2008) 673-678.
- [77] S. Shillingford, L. Bishop, C. Smith, R. Payne, I. Wilson, A. Edge, *Chromatographia*, 70 (2009) 37-44.
- [78] C.V. McNeff, B. Yan, D.R. Stoll, R.A. Henry, *J Sep Sci*, 30 (2007) 1672-1685.
- [79] L. Nováková, L. Matysová, P. Solich, *Talanta*, 68 (2006) 908-918.
- [80] J.E. MacNair, K.C. Lewis, J.W. Jorgenson, *Anal Chem*, 69 (1997) 983-989.
- [81] J.E. MacNair, K.D. Patel, J.W. Jorgenson, *Anal Chem*, 71 (1999) 700-708.
- [82] M.A. Stadalius, H.S. Gold, L.R. Snyder, *Journal of Chromatography A*, 327 (1985) 27-45.
- [83] K.D. Wyndham, J.E. O'Gara, T.H. Walter, K.H. Glose, N.L. Lawrence, B.A. Alden, G.S. Izzo, C.J. Hudalla, P.C. Iraneta, *Anal Chem*, 75 (2003) 6781-6788.
- [84] J.S. Mellors, J.W. Jorgenson, *Anal Chem*, 76 (2004) 5441-5450.
- [85] N. Wu, J.A. Lippert, M.L. Lee, *J Chromatogr A*, 911 (2001) 1-12.
- [86] M.E. Swartz, *Journal of Liquid Chromatography & Related Technologies*, 28 (2005) 1253-1263.
- [87] S.A. Wren, *J Pharm Biomed Anal*, 38 (2005) 337-343.

- [88] S.A. Wren, P. Tchelitcheff, *J Chromatogr A*, 1119 (2006) 140-146.
- [89] C.G. Horvath, S.R. Lipsky, *Analytical Chemistry*, 41 (1969) 1227-1234.
- [90] C.G. Horvath, B.A. Preiss, S.R. Lipsky, *Analytical Chemistry*, 39 (1967) 1422-1428.
- [91] J.J. Kirkland, *Analytical Chemistry*, 41 (1969) 218-220.
- [92] J.J. Destefano, T.J. Langlois, J.J. Kirkland, *J Chromatogr Sci*, 46 (2008) 254-260.
- [93] K. Kaczmarek, G. Guiochon, *Anal Chem*, 79 (2007) 4648-4656.
- [94] X. Wang, W.E. Barber, P.W. Carr, *Journal of Chromatography A*, 1107 (2006) 139-151.
- [95] Y. Hsieh, C.J.G. Duncan, J.-M. Brisson, *Analytical Chemistry*, 79 (2007) 5668-5673.
- [96] J.M. Cunliffe, T.D. Maloney, *Journal of Separation Science*, 30 (2007) 3104-3109.
- [97] D.N. Mallett, C. Ramirez-Molina, *J Pharm Biomed Anal*, 49 (2009) 100-107.
- [98] P. Yang, T. McCabe, M. Pursch, *Journal of Separation Science*, 34 (2011) 2975-2982.
- [99] D.V. McCalley, *Journal of Chromatography A*, 1217 (2010) 4561-4567.
- [100] A.J. Alexander, T.J. Waeghe, K.W. Himes, F.P. Tomasella, T.F. Hooker, *Journal of Chromatography A*, 1218 (2011) 5456-5469.
- [101] A.J. Alpert, *Journal of Chromatography A*, 499 (1990) 177-196.
- [102] D.V. McCalley, U.D. Neue, *Journal of Chromatography A*, 1192 (2008) 225-229.
- [103] H. Chen, C. Horvath, *Anal. Methods Instrum.*, 1993.
- [104] D.V. McCalley, *Journal of Chromatography A*, 1171 (2007) 46-55.
- [105] P. Appelblad, T. Jonsson, W. Jiang, K. Irgum, *Journal of Separation Science*, 31 (2008) 1529-1536.
- [106] D.V. McCalley, *Journal of Chromatography A*, 1193 (2008) 85-91.
- [107] S. Louw, F. Lynen, M. Hanna-Brown, P. Sandra, *Journal of Chromatography A*, 1217 (2010) 514-521.
- [108] E.S. Grumbach, D.M. Diehl, U.D. Neue, *Journal of Separation Science*, 31 (2008) 1511-1518.
- [109] J. Ruta, S. Rudaz, D.V. McCalley, J.L. Veuthey, D. Guillarme, *Journal of Chromatography A*, 1217 (2010) 8230-8240.
- [110] Y. Hsieh, *Journal of Separation Science*, 31 (2008) 1481-1491.
- [111] M. Kolmonen, A. Leinonen, T. Kuuranne, A. Pelander, I. Ojanperä, *Journal of Chromatography B*, 878 (2010) 2959-2966.
- [112] K.J. Fountain, Z. Yin, D.M. Diehl, *Journal of Separation Science*, 32 (2009) 2319-2326.

- [113] R.S. Jansen, H. Rosing, J.H.M. Schellens, J.H. Beijnen, *Mass Spectrometry Reviews*, 30 (2010) 321-343.
- [114] C.R. Mitchell, Y. Bao, N.J. Benz, S. Zhang, *Journal of Chromatography B*, 877 (2009) 4133-4139.
- [115] A. dos Santos Pereira, F. David, G. Vanhoenacker, P. Sandra, *Journal of Separation Science*, 32 (2009) 2001-2007.
- [116] K.J. Fountain, J. Xu, D.M. Diehl, D. Morrison, *Journal of Separation Science*, 33 (2010) 740-751.
- [117] M. Dole, L.L. Mack, R.L. Hines, R.C. Mobley, L.D. Ferguson, M.B. Alice, *The Journal of Chemical Physics*, 49 (1968) 2240-2249.
- [118] J.B. Fenn, M. Mann, C.K. Meng, S.F. Wong, C.M. Whitehouse, *Science*, 246 (1989) 64-71.
- [119] C.R. Blakley, J.J. Carmody, M.L. Vestal, *Journal of the American Chemical Society*, 102 (1980) 5931-5933.
- [120] C.R. Blakley, M.L. Vestal, *Analytical Chemistry*, 55 (1983) 750-754.
- [121] R.B. Cole, *Electrospray Ionization Mass Spectrometry: Fundamentals, Instrumentation & Applications*, Wiley-Interscience, 1997.
- [122] J.V. Iribarne, B.A. Thomson, *The Journal of Chemical Physics*, 64 (1976) 2287-2294.
- [123] L.L. Mack, P. Kralik, A. Rheude, M. Dole, *The Journal of Chemical Physics*, 52 (1970) 4977-4986.
- [124] Waters, Quattro Premier, Operation and Maintenance Training Manual.
- [125] R. King, R. Bonfiglio, C. Fernandez-Metzler, C. Miller-Stein, T. Olah, *Journal of the American Society for Mass Spectrometry*, 11 (2000) 942-950.
- [126] R.A. Mirghani, U. Hellgren, L. Bertilsson, L.L. Gustafsson, O. Ericsson, *Eur J Clin Pharmacol*, 59 (2003) 423-427.
- [127] R.A. Mirghani, U. Hellgren, P.A. Westerberg, O. Ericsson, L. Bertilsson, L.L. Gustafsson, *Clin Pharmacol Ther*, 66 (1999) 454-460.
- [128] P. Anzenbacher, E. Anzenbacherová, *Cellular and Molecular Life Sciences*, 58 (2001) 737-747.
- [129] P. Bannon, P. Yu, J.M. Cook, L. Roy, J.P. Villeneuve, *J Chromatogr B Biomed Sci Appl*, 715 (1998) 387-393.
- [130] R.A. Mirghani, O. Ericsson, J. Cook, P. Yu, L.L. Gustafsson, *J Chromatogr B Biomed Sci Appl*, 754 (2001) 57-64.

- [131] R.A. Mirghani, O. Ericsson, L.L. Gustafsson, *J Chromatogr B Biomed Sci Appl*, 708 (1998) 209-216.
- [132] J.O. Soyinka, C.O. Onyeji, S.I. Omoruyi, *Journal of Chromatography B*, 877 (2009) 441-445.
- [133] S. Abdulrahman, M.E. Harrison, K.J. Welham, M.A. Baldwin, J.D. Phillipson, M.F. Roberts, *Journal of Chromatography B: Biomedical Sciences and Applications*, 562 (1991) 713-721.
- [134] D.V. McCalley, *J Chromatogr A*, 967 (2002) 1-19.
- [135] L. Peng, T. Farkas, *J Chromatogr A*, 1179 (2008) 131-144.
- [136] J. Mather, P.D. Rainville, W.B. Potts, N.W. Smith, R.S. Plumb, *Drug Testing and Analysis*, 2 (2010) 11-18.
- [137] T. Berg, E. Lundanes, A.S. Christophersen, D.H. Strand, *Journal of Chromatography B*, 877 (2009) 421-432.
- [138] S. Zhou, K.D. Cook, *J Am Soc Mass Spectrom*, 11 (2000) 961-966.
- [139] P.V. Srirama Sarma, D. Han, J.R. Deschamps, J.M. Cook, *J Nat Prod*, 68 (2005) 942-944.
- [140] E. Chambers, D.M. Wagrowski-Diehl, Z. Lu, J.R. Mazzeo, *J Chromatogr B Analyt Technol Biomed Life Sci*, 852 (2007) 22-34.
- [141] T. Bartók, G. Szöllösi, K. Felföldi, M. Bartók, J. Thiel, *Journal of Mass Spectrometry*, 35 (2000) 711-717.
- [142] H. Fujiwara, A. Kato, I. Okabayashi, *JMSSJ*, 35 (1987) 8.
- [143] G. Mitulovic, C. Stingl, I. Steinmacher, O. Hudecz, J.R.A. Hutchins, J.-M. Peters, K. Mechtler, *Analytical Chemistry*, 81 (2009) 5955-5960.
- [144] P.R. Tiller, L.A. Romanyshyn, U.D. Neue, *Anal Bioanal Chem*, 377 (2003) 788-802.
- [145] N. Rahmioglu, G.n.l. Le Gall, J. Heaton, K.L. Kay, N.W. Smith, I.J. Colquhoun, K.R. Ahmadi, E.K. Kemsley, *Journal of Proteome Research*, 10 (2011) 2807-2816.
- [146] J.R. Mazzeo, U. D. Neue, M. Kele, R.S. Plumb, *Analytical Chemistry*, 77 (2005) 460 A-467 A.
- [147] J.H. Knox, M. Saleem, *J. Chromatogr. Sci.*, 7 (1969) 614-622.
- [148] I. Halász, R. Endeke, J. Asshauer, *Journal of Chromatography A*, 112 (1975) 37-60.
- [149] F. Gritti, G. Guiochon, *Anal Chem*, 80 (2008) 5009-5020.
- [150] H. Poppe, J.C. Kraak, J.F.K. Huber, J.H.M. Vandenberg, *Chromatographia*, 14 (1981) 515-523.
- [151] F. Gritti, G. Guiochon, *J Chromatogr A*, 1138 (2007) 141-157.

- [152] H.-j. Lin, S. Horváth, *Chemical Engineering Science*, 36 (1981) 47-55.
- [153] H. Poppe, J.C. Kraak, *Journal of Chromatography A*, 282 (1983) 399-412.
- [154] A. de Villiers, H. Lauer, R. Szucs, S. Goodall, P. Sandra, *J Chromatogr A*, 1113 (2006) 84-91.
- [155] M.M. Fallas, M.R. Hadley, D.V. McCalley, *J Chromatogr A*, 1216 (2009) 3961-3969.
- [156] F. Gritti, G. Guiochon, *J Chromatogr A*, 1216 (2009) 1353-1362.
- [157] R.S. Plumb, P. Rainville, B.W. Smith, K.A. Johnson, J. Castro-Perez, I.D. Wilson, J.K. Nicholson, *Analytical Chemistry*, 78 (2006) 7278-7283.
- [158] L.A. Colon, J.M. Cintron, J.A. Anspach, A.M. Fermier, K.A. Swinney, *Analyst*, 129 (2004) 503-504.
- [159] J. Li, P.W. Carr, *Analytical Chemistry*, 69 (1997) 837-843.
- [160] K. Kaczmarski, F. Gritti, J. Kostka, G. Guiochon, *J Chromatogr A*, 1216 (2009) 6575-6586.
- [161] M. Thirumaleshwar, *Fundamentals of Heat and Mass Transfer*, Dorling Kindersely, 2006.
- [162] M.M. Fallas, U.D. Neue, M.R. Hadley, D.V. McCalley, *J Chromatogr A*, 1217 (2010) 276-284.
- [163] M.M. Fallas, U.D. Neue, M.R. Hadley, D.V. McCalley, *J Chromatogr A*, 1209 (2008) 195-205.
- [164] F. Lestremau, D. Wu, R. Szucs, *J Chromatogr A*, 1217 4925-4933.
- [165] K. Broeckhoven, J. Billen, M. Verstraeten, K. Choikhet, M. Dittmann, G. Rozing, G. Desmet, *J Chromatogr A*, 1217 (2010) 2022-2031.
- [166] F. Gritti, G. Guiochon, *J Chromatogr A*, O 1206 (2008) 113-122.
- [167] F. Gritti, G. Guiochon, *Journal of Chromatography A*, 1218 (2011) 4632-4648.
- [168] J.O. Omamogho, J.P. Hanrahan, J. Tobin, J.D. Glennon, *Journal of Chromatography A*, 1218 (2011) 1942-1953.
- [169] J.O. Omamogho, J.D. Glennon, *Analytical Chemistry*, 83 (2011) 1547-1556.
- [170] G. Guiochon, F. Gritti, *Journal of Chromatography A*, 1218 (2011) 1915-1938.
- [171] F.D. Antia, C.S. Horváth, *Journal of Chromatography A*, 435 (1988) 1-15.
- [172] D. Guillarme, S. Heinisch, J.L. Rocca, *Journal of Chromatography A*, 1052 (2004) 39-51.
- [173] L. Al-Khateeb, R. Smith, *Analytical and Bioanalytical Chemistry*, 394 (2009) 1255-1260.
- [174] A. de Villiers, D. Cabooter, F. Lynen, G. Desmet, P. Sandra, *Journal of Chromatography A*, 1216 (2009) 3270-3279.
- [175] J. Clark, *Pharmaceutical Technology Europe*, 16 (2004) 41-46.

- [176] Y. Liu, N. Grinberg, K.C. Thompson, R.M. Wenslow, U.D. Neue, D. Morrison, T.H. Walter, J.E. O'Gara, K.D. Wyndham, *Analytica Chimica Acta*, 554 (2005) 144-151.
- [177] A. Martin, P.L. Wu, A. Adjei, M. Mehdizadeh, K.C. James, C. Metzler, *Journal of Pharmaceutical Sciences*, 71 (1982) 1334-1340.
- [178] F. Gritti, G. Guiochon, *Journal of Chromatography A*, 1217 (2010) 5069-5083.
- [179] D.V. McCalley, *Journal of Chromatography A*, 1218 (2011) 2887-2897.
- [180] J. Ruta, D. Zurlino, C. Grivel, S. Heinisch, J.L. Veuthey, D. Guillarme, *Journal of Chromatography A*, 1228 (2012) 221-231.
- [181] S. Fekete, E. Olah, J. Fekete, *Journal of Chromatography A*, 1228 (2012) 57-71.
- [182] B. Chauve, D. Guillarme, P. Cleon, J.L. Veuthey, *J Sep Sci*, 33 (2010) 752-764.
- [183] D.V. McCalley, *J Chromatogr A*, 1217 (2010) 3408-3417.
- [184] D.V. McCalley, *J Chromatogr A*, 1217 (2010) 858-880.
- [185] P. Petersson, M.R. Euerby, *J Sep Sci*, 30 (2007) 2012-2024.
- [186] M.R. Euerby, P. Petersson, *J Chromatogr A*, 994 (2003) 13-36.
- [187] J.J. Kirkland, F.A. Truszkowski, C.H. Dilks, Jr., G.S. Engel, *J Chromatogr A*, 890 (2000) 3-13.
- [188] F. Gritti, G. Guiochon, *J Chromatogr A*, 1166 (2007) 30-46.
- [189] F. Gritti, G. Guiochon, *Journal of Chromatography A*, 1217 (2010) 8167-8180.
- [190] D. Cabooter, A. Fanigliulo, G. Bellazzi, B. Allieri, A. Rottigni, G. Desmet, *J Chromatogr A*, 1217 (2010) 7074-7081.
- [191] D. Cabooter, J. Billen, H. Terryn, F. Lynen, P. Sandra, G. Desmet, *J Chromatogr A*, 1204 (2008) 1-10.
- [192] A. Daneyko, A. Holtzel, S. Khirevich, U. Tallarek, *Analytical Chemistry*, 83 (2011) 3903-3910.
- [193] S.M. Buckenmaier, D.V. McCalley, M.R. Euerby, *Journal of Chromatography A*, 1004 (2003) 71-79.
- [194] P. Hemstrom, K. Irgum, *J Sep Sci*, 29 (2006) 1784-1821.
- [195] R.W. Stout, J.J. DeStefano, L.R. Snyder, *Journal of Chromatography A*, 282 (1983) 263-286.
- [196] F. Gritti, I. Leonardis, D. Shock, P. Stevenson, A. Shalliker, G. Guiochon, *J Chromatogr A*, 1217 (2010) 1589-1603.
- [197] F. Gritti, A. Cavazzini, N. Marchetti, G. Guiochon, *J Chromatogr A*, 1157 (2007) 289-303.

- [198] F. Gritti, G. Guiochon, *Chemical Engineering Science*, 65 (2010) 6310-6319.
- [199] A. Fanigliulo, D. Cabooter, G. Bellazzi, B. Allieri, A. Rottigni, G. Desmet, *J Chromatogr A*, (2011).
- [200] A. Fanigliulo, D. Cabooter, G. Bellazzi, D. Tramarin, B. Allieri, A. Rottigni, G. Desmet, *J Sep Sci*, 33 (2010) 3655-3665.
- [201] K.D. Patel, A.D. Jerkovich, J.C. Link, J.W. Jorgenson, *Analytical Chemistry*, 76 (2004) 5777-5786.
- [202] World Anti-Doping Agency, in, *World Anti-Doping Agency: Montreal, Canada*, 2010. Available: <http://www.wada-ama.org>, 2010.
- [203] P. Van Eenoo, F.T. Delbeke, K. Roels, P. De Backer, *J Chromatogr B Biomed Sci Appl*, 760 (2001) 255-261.
- [204] M.H. Spyridaki, C.J. Tsitsimpikou, P.A. Siskos, C.G. Georgakopoulos, *J Chromatogr B Biomed Sci Appl*, 758 (2001) 311-314.
- [205] P.J. van der Merwe, L.W. Brown, S.E. Hendrikz, *J Chromatogr B Biomed Appl*, 661 (1994) 357-361.
- [206] M. Kolmonen, A. Leinonen, A. Pelander, I. Ojanperä, *Anal Chim Acta*, 585 (2007) 94-102.
- [207] M.H. Spyridaki, P. Kioussi, A. Vonaparti, P. Valavani, V. Zonaras, M. Zahariou, E. Sianos, G. Tsoupras, C. Georgakopoulos, *Anal Chim Acta*, 573-574 (2006) 242-249.
- [208] J.-O. Thörngren, F. Östervall, M. Garle, *J Mass Spectrom*, 43 (2008) 980-992.
- [209] M. Mazzarino, X. de la Torre, F. Botrè, N. Gray, D. Cowan, *Drug Test Anal*, 2 (2010) 311-322.
- [210] B. Schubert, H. Oberacher, *Journal of Chromatography A*, 1218 (2011) 3413-3422.
- [211] J. Flieger, *Journal of Chromatography A*, 1217 (2010) 540-549.
- [212] M. Ganzera, C. Lanser, H. Stuppner, *Talanta*, 66 (2005) 889-894.
- [213] K. Deventer, O.J. Pozo, P. Van Eenoo, F.T. Delbeke, *J Chromatogr B*, 877 (2009) 369-374.
- [214] F. Badoud, E. Grata, L. Perrenoud, M. Saugy, S. Rudaz, J.L. Veuthey, *J Chromatogr A*, 1217 (2010) 4109-4119.
- [215] J. Flieger, A. Czajkowska-Żelazko, *Journal of Separation Science*, 34 (2011) 733-739.
- [216] L. Pan, R. LoBrutto, Y.V. Kazakevich, R. Thompson, *Journal of Chromatography A*, 1049 (2004) 63-73.

- [217] N. Gray, A. Musenga, D.A. Cowan, R. Plumb, N.W. Smith, *J Chromatogr A*, 1218 (2011) 2098-2105.
- [218] D.S. Bell, H.M. Cramer, A.D. Jones, *J Chromatogr A*, 1095 (2005) 113-118.
- [219] F. Pellati, S. Benvenuti, *J Pharmaceut Biomed*, 48 (2008) 254-263.
- [220] Z. Aturki, G. D'Orazio, A. Rocco, K. Si-Ahmed, S. Fanali, *Anal Chim Acta*, 685 (2011) 103-110.
- [221] A.E. Karatapanis, Y.C. Fiamegos, C.D. Stalikas, *J Chromatogr A*, 1218 (2011) 2871-2879.
- [222] J. Nawrocki, *J Chromatogr A*, 779 (1997) 29-71.
- [223] A. Mendez, E. Bosch, M. Roses, U.D. Neue, *J Chromatogr A*, 986 (2003) 33-44.
- [224] U.D. Neue, C.H. Phoebe, K. Tran, Y.F. Cheng, Z. Lu, *J Chromatogr A*, 925 (2001) 49-67.
- [225] E. Johnsen, S.R. Wilson, I. Odsbu, A. Krapp, H. Malerod, K. Skarstad, E. Lundanes, *J Chromatogr A*, 1218 (2011) 5981-5986.
- [226] B.A. Bidlingmeyer, J. Henderson, *J Chromatogr A*, 1060 (2004) 187-193.
- [227] J.P. Foley, J.G. Dorsey, *Anal Chem*, 55 (1983) 730-737.
- [228] K. Broglé, R.M. Ornaf, D. Wu, P.J. Palermo, *J Pharmaceut Biomed*, 19 (1999) 669-678.
- [229] D.V. McCalley, *J Chromatogr A*, 987 (2003) 17-28.
- [230] T.H. Walter, P. Iraneta, M. Capparella, *J Chromatogr A*, 1075 (2005) 177-183.
- [231] R.W. Roos, C.A. Lau-Cam, *Journal of Chromatography A*, 370 (1986) 403-418.
- [232] S.Å. Gustavsson, J. Samskog, K.E. Markides, B. Långström, *Journal of Chromatography A*, 937 (2001) 41-47.
- [233] A.J. Alpert, M. Shukla, A.K. Shukla, L.R. Zieske, S.W. Yuen, M.A. Ferguson, A. Mehlert, M. Pauly, R. Orlando, *J Chromatogr A*, 676 (1994) 191-122.
- [234] J.A. Boutin, A.P. Ernould, G. Ferry, A. Genton, A.J. Alpert, *J Chromatogr*, 583 (1992) 137-143.
- [235] J.J. Pesek, M.T. Matyska, S. Larrabee, *J Sep Sci*, 30 (2007) 637-647.
- [236] W. Naidong, J.W. Lee, X. Jiang, M. Wehling, J.D. Hulse, P.P. Lin, *Journal of Chromatography B: Biomedical Sciences and Applications*, 735 (1999) 255-269.
- [237] H.P. Nguyen, K.A. Schug, *Journal of Separation Science*, 31 (2008) 1465-1480.
- [238] S.R. Needham, P.R. Brown, K. Duff, D. Bell, *J Chromatogr A*, 869 (2000) 159-170.
- [239] R. Fritz, W. Ruth, U. Kragl, *Rapid Communications in Mass Spectrometry*, 23 (2009) 2139-2145.
- [240] T.R. Keppel, M.E. Jacques, D.D. Weis, *Rapid Commun Mass Spectrom*, 24 (2010) 6-10.

- [241] R.E. Duderstadt, S.M. Fischer, *Journal of Chromatography A*, 1193 (2008) 70-78.
- [242] L. Charles, D. Pépin, F. Gonnet, J.-C. Tabet, *Journal of the American Society for Mass Spectrometry*, 12 (2001) 1077-1084.
- [243] T.-Y. Yen, M. Judith Charles, R.D. Voyksner, *Journal of the American Society for Mass Spectrometry*, 7 (1996) 1106-1108.
- [244] J. Heaton, N. Rahmioglu, K.R. Ahmadi, C. Legido-Quigley, N.W. Smith, *J Pharm Biomed Anal*, 55 (2011) 494-499.
- [245] M.A. Thite, R. Boughtflower, J. Caldwell, L. Hitzel, C. Holyoak, S.J. Lane, P. Oakley, F.S. Pullen, S. Richardson, G.J. Langley, *Rapid Communications in Mass Spectrometry*, 22 (2008) 3673-3682.
- [246] R.A. O'Hair, G.E. Reid, *J Am Soc Mass Spectrom*, 11 (2000) 244-256.
- [247] C. Delatour, L. Leclercq, *Rapid Communications in Mass Spectrometry*, 19 (2005) 1359-1362.
- [248] R.J. Flanagan, I. Jane, *Journal of Chromatography A*, 323 (1985) 173-189.
- [249] R.M. Smith, J.P. Westlake, R. Gill, M. David Osselton, *Journal of Chromatography A*, 514 (1990) 97-109.
- [250] R.J. Flanagan, G.C.A. Storey, R.K. Bhamra, I. Jane, *Journal of Chromatography A*, 247 (1982) 15-37.